DOCTOR OF PHILOSOPHY

Investigation of the interface shearing resistance of steel and concrete on different rocks for renewable energy gravity foundation applications

Ziogos, Andreas

Award date:
2020

University of Dundee

School of Science and Engineering
Department of Civil Engineering

Investigation of the interface shearing resistance of steel and concrete on different rocks for renewable energy gravity foundation applications

Andreas Ziogos

A dissertation submitted for the
degree of Doctor of Philosophy
to the University of Dundee
March 2020

Declaration

This is to certify that, except where specific reference to other investigation is made, the work described in this dissertation is the result of the investigation of the candidate. Neither this dissertation, nor any part of it, has been presented or is currently submitted in candidature for any degree at any other university.

Andreas Ziogos (candidate)

Dr. Michael Brown (supervisor)

Acknowledgements

Firstly, I would like to acknowledge my project supervisor Dr. Michael Brown. I am grateful to Mike for his continued and tireless support and encouragement throughout the duration of the project. He has always been willing to offer assistance in matters of academic, professional or personal nature. Mike has been an ideal supervisor and mentor.

I am grateful to the Energy Technology Partnership (ETP) and Lloyd's Register EMEA for the funding of this project. I am also grateful to Dr. Neil Morgan and Prof. Ana Ivanovic for co-supervising the project.

I would like to thank the members of the geotechnical research group at the University of Dundee who have offered assistance regarding the project over the years.

I would like to thank the members of the technical team within the Department of Civil Engineering of the University of Dundee for their help in the soils lab and in the workshop.

I would like to take the opportunity to thank my family for their continued love and support without which I could not have completed the work. It is my family this thesis is dedicated to.

I would also like to thank my friends who have supported and encouraged me throughout the project.

Last but not least, I would like to thank my partner for her unconditional support and understanding, without which I would have never completed this thesis.

Abstract

Tidal stream energy is a form of marine energy with significant advantages compared to other types of offshore renewables, albeit the levelised cost of energy is relatively high. Various types of foundations have been considered for prototype tidal stream generators, however the utilisation of Gravity Based Structures (GBS) seems like a promising approach to achieve cost reduction and increase the financial viability for commercial deployments.

The generators are expected to be deployed onto rocky seabeds and the GBS (made of steel or concrete) need to ensure the overall stability of the structures. This research focuses on the investigation of the shearing resistance of the foundation – seabed interface materials by means of laboratory element testing.

Interface tests of five different rock types (representative of sites with tidal energy potential around the U.K.) on steel and concrete were carried out under a range of normal stresses. The different properties of the counterface materials (i.e. steel, rock, concrete) allowed the investigation of the controlling parameters on the shearing resistance of steel on rock and concrete on rock interfaces.

Tests results were interpreted to determine the effect of the applied normal stress, surface roughness, hardness and rock strength (UCS) on the shearing resistance of the interfaces. It was found that the relative ratios of some counterface properties (e.g. roughness, hardness) can be utilised to explain the interface shearing behaviour. A framework described by a power function has been developed to estimate the shearing resistance of rock on steel and rock on concrete interfaces, incorporating the effect of these counterface material properties.

Keywords: interface shear testing, rock, steel, concrete, tidal stream energy, gravity based foundations

Table of Contents

1 Introduction 1

1.1 Preface 1

1.1.1 Laboratory interface shear testing 2

1.1.2 Field visits 2

1.2 Aims and objectives 3

1.3 Structure of thesis 4

2 Literature review 6

2.1 Marine energy 6

2.1.1 Introduction 6

2.2 Tidal resources around the UK 7

2.3 Geology at sites with significant tidal resources 11

2.4 Tidal energy generators 12

2.4.1 Foundation types for tidal stream energy generators 12

2.4.2 Tidal stream generators with GBS 14

2.4.3 Considerations for tidal stream generator design 18

2.5 Shear strength of the rock mass discontinuities 19

2.5.1 Introduction 19

2.5.2 Failure criteria for rock mass discontinuities 20

2.5.3 Effect of roughness on shear strength of rock mass discontinuities 22

2.6 Shearing behaviour of interfaces 24

2.6.1 Soil sheared against manufactured material interfaces 24

2.6.2 Roughness and waviness 28

2.6.3 Rock – concrete interfaces 30

2.6.4 Rock – steel interfaces 35

2.7 Hardness 36

2.8 Important findings from literature review 39
3 Methodology 41
3.1 Introduction 41
3.2 Testing equipment and procedures 42
3.2.1 Direct shear box testing 42
3.2.2 Tilt table 46
3.2.3 Interface Shear Tester (IST) 49
3.3 Rock samples 55
3.3.1 Sandstone 56
3.3.2 Flagstone 58
3.3.3 Limestone 59
3.3.4 Andesite 60
3.3.5 Chalk 61
3.3.6 In-situ determination of UCS for rock samples 63
3.3.7 Determination of UCS in the laboratory 65
3.4 Materials and preparation techniques 67
3.4.1 Cement mortar 67
3.4.2 Steel 69
3.4.3 Concrete 71
3.4.4 Sand 73
3.4.5 Coring and saw cutting of rock and concrete samples 74
3.5 Surface roughness characterisation 74
3.5.1 Methods of surface roughness measurement 74
3.5.2 Determination of roughness parameters 77
3.6 Mohs hardness measurement 78
3.7 High level summary of testing undertaken 79
4 Direct shear box interface testing 81

4.1 Introduction 81
4.2 Direct shear box interface testing of rock analogues 82
4.2.1 Determination of data points comparison 82
4.2.2 Effect of rock analogue UCS 84
4.2.3 The effect of steel roughness on shearing behaviour 89
4.2.4 Alpha (α) factor approach 96
4.3 Shear box interface testing with rock samples 100
4.3.1 Results and discussion 100
4.3.2 Alpha factor considering results from rock samples 106
4.4 Summary 108
5 Advanced rock – steel interface testing using the IST 109
5.1 Introduction 109
5.2 General results from rock-steel testing 110
5.2.1 Results for fixed steel roughness 115
5.3 Effect of normal stress on the shear behaviour 117
5.3.1 Behaviour of Sandstone and Andesite interfaces 125
5.3.2 Behaviour of Flagstone and Limestone interfaces 127
5.3.3 Effect of relative hardness 129
5.4 Failure envelopes 133
5.5 Final stage of alpha factor analysis 135
5.5.1 Simplified equations 137
5.5.2 Comparison of test data and alpha factor approach data 143
5.6 Summary 146
6 Special cases of interface testing 148
6.1 Rock – concrete interface tests 148
6.1.1 Results 149
6.1.2 Effect of relative roughness and hardness ratios 151

6.1.3 Alpha factor design approach 156
6.1.4 Comparison of rock – concrete and rock - steel interfaces 159
6.2 Testing to simulate the presence of granular sediment at the interface 166
6.2.1 Rock – sand – steel interfaces 166
6.3 Summary 177
7 Chalk interface testing 179
7.1 Results from Chalk – steel interface testing 180
7.2 Comparison of Chalk and Sandstone interfaces 188
7.3 Extended deformation tests 189
7.4 Results from Chalk – concrete interface testing 191
7.5 Alpha factor design approach for Chalk interfaces 198
7.6 Summary 200
8 Implications for industrial practice 202
8.1 Potential deployment issues 202
8.2 Effect of weathering on UCS 203
8.3 Design Framework 205
8.4 Utilisation of tilt table for simple interface characterisation 209
8.5 Summary 214
9 Conclusions and recommendations for further work 215
9.1 Introduction 215
9.2 Rock – steel and rock – concrete interfaces 215
9.3 Chalk - steel and Chalk – concrete interfaces 218
9.4 Considerations for design 219
9.5 Recommendations for further work 220
References 223

List of Figures

Figure 2-1. Proposed UK Tidal Stream Power Sites, (Source: Carbon Trust, 2005) 8

Figure 2-2. Areas with significant tidal resources around the UK (Source of underlying map: http://www.lsamoforumuk.scot.nhs.uk/) 9

Figure 2-3. Different configurations of foundations for tidal energy generators (Fraenkel, 2002) 14

Figure 2-4. (a) Atlantis AK-1000 (Source: news.cnet.com), (b) Atlantis AK-1000 (Source: EMEC Decommissioning Programme) 15

Figure 2-5. Tidal Energy Ltd. Deltastream source: http://www.tidalenergyltd.com/?page_id=640) 16

Figure 2-6. Tidal Energy Ltd Deltastream Rock Foot Detail (Source: Deltastream White Paper 2012) 17

Figure 2-7. Voith Hydro Tidal Turbine's Concrete Gravity Foundation (Source: STRABAG Offshore Wind GmbH) 18

Figure 2-8. Typical approximate bilinear and real curvi-linear failure envelopes for modelled discontinuous rock (Source: Engineering and Design Rock Foundations, U.S. Army Corps of Engineers, 1994) 21

Figure 2-9. Measurement of roughness angles i for first and second order asperities on rough rock surfaces (after Patton, 1966) 23

Figure 2-10. Summary of δ' values from parametric study, $\sigma' n$~100kPa, after Jardine et. al 1993 25

Figure 2-11. Variation of δ vs Relative roughness for concrete sand interfaces (from Barmpopoulos et al., 2010) 26

Figure 2-12. Horizontal Displacement – Interface stress curves of concrete against (a) FA: (b) FAC10: (C) FAC20 group pellets (Source: Danyildiz and Baykal 2008) 27

Figure 2-13. Calculation of the average roughness value R_a 29

Figure 2-14. Description of roughness and waviness,(source: http://www.mahr.com/index.php?print=1&NodeID=14676&ContentID=15099&Overview=1&ActionID=0&view=1&nl=-1&nld=-1&year=-1) 30

Figure 2-15. Application of forces during the test (Source: Ghosh 2010) 31

Figure 2-16. Shear stress vs shear displacement of concrete - outcrop interfaces from Ghosh 2010 32
Figure 2-17. Test Results for Clean Sockets with different degrees of sidewall roughness (Source: Pells et al., 1980) 33
Figure 2-18. Constant normal stiffness conditions (Source: Xue et. al. 2003) 34
Figure 2-19. Roughness profiles used in tests (from Xue et al., 2003) 34
Figure 2-20. Friction between a metal point and a metal sheet of varying hardness after Bowden & Tabor, 1964. (image take from Engelder and Scholz 1976) 37
Figure 2-21. Strength Envelopes from Interface Shear Tests on Smooth Geomembrane (from Dove and Frost, 1999) 38
Figure 2-22. Relation between surface hardness and coefficient of friction (from Abuel Naga et. al., 2018) 39
Figure 3-1. Steel block in the bottom half of the shear box, arrows indicating the edges where the cement block can be snagged 43
Figure 3-2. Shear stress vs horizontal displacement data for a cement – steel interface.. Spikes due to cement snagging are apparent 44
Figure 3-3. Steel block, used instead of bottom half of the shear box 44
Figure 3-4. Fitting assembly used to accommodate cylindrical samples for shear box testing 45
Figure 3-5. Tilt table apparatus 47
Figure 3-6. Rotational failure during a tilt test (after Alejano et al., 2012) 48
Figure 3-7. (a) Basic friction angle test configuration (sandstone samples), (b) sandstone-steel interface test configuration 49
Figure 3-8. (a) Photograph of the Interface Shear Tester, (b) detailed view of the Interface Shear Tester sample mounting arrangement 51
Figure 3-9. Foundation analogue with “single grain thick” sand layer, prior to testing 53
Figure 3-10. Detailed view of Perspex bath used for saturated testing 54
Figure 3-11. Disused sandstone quarry (ND37150 70138), near John O’ Groats 56

Figure 3-12. Wave cut platform at John O' Groats, repeating stratigraphy leading edges in the sandstone strata can be seen (ND38299 73382). The Island of Stroma is visible on the horizon (subfigure a) 57
Figure 3-13. (a) Sandstone block after coring, (b) typical Old Red Sandstone sample. 57
Figure 3-14. (a) Caithness Flagstone wave cut platform at Castletown (ND19305 68858), UK. Line displays saw-blade type structure, (b) Achscrabster Caithness flagstone quarry (ND07829 63333) 58
Figure 3-15. Typical Caithness Flagstone sample 59
Figure 3-16. (a) Lower Skateraw Limestone formations at Dunbar wave cut platform, (b) Middle Skateraw Limestone sample 60
Figure 3-17. Andesite sample 61
Figure 3-18. Stress vs strain curve from a UCS test on a dry Chalk sample 63
Figure 3-19. In-situ recording of the rebound hardness number (N) using an L-type Schmidt Hammer. (a) Caithness Flagstone (ND07829 63333), (b) John O'Groats Sandstone (ND37150 70138) 64
Figure 3-20. (a) Principles of Brazilian test, (b) sandstone disc after failure where tensile cracking is apparent 66
Figure 3-21. Mould used for preparation of rock analogues 68
Figure 3-22. Variation of unconfined compressive strength of cement mortar samples with respect to preparation and curing process 69
Figure 3-23. Mortar sample used as rock analogue 69
Figure 3-24. (a) polished R_a=0.4 μm, (b) machined R_a=7.2 μm, (c) machined R_a=34.0 μm 71
Figure 3-25. (a) mould used to cast concrete cylinders, (b) concrete disc used for interface testing 72
Figure 3-26. (a) rock coring drill, (b) tile masonry saw 74
Figure 3-27. Taylor-Hobson Talysurf series 2 stylus profilometer (Source: Iscimen and Frost 2008) 75
Figure 3-28. (a) typical arrangement for pipe surface profile testing, (b) material during surface characterization, (Source: Staheli et al., 2006) 76
Figure 3-29. Roland 3D Laser scanner at the University of Hong Kong (Source: Tam et. al, 2008) 76

Figure 3-30. Taylor Hobson Surtronic Duo stylus contact profilometer 77
Figure 3-31. Measurement pattern used for (a) rock analogue and steel samples, (b) rock and concrete samples. The straight lines indicate the position of measurement. 78
Figure 4-1. Typical shear stress vs horizontal displacement from smooth steel - cement mortar interface testing at a normal stress of 200 kPa and cement mortar with UCS = 65 MPa. (Steel R_a = 0.4 μm, Cement mortar R_a = 2.4 μm) 83
Figure 4-2. Typical shear stress vs horizontal displacement graph from steel - smooth cement interface testing at normal stress of 100 kPa and cement mortar with UCS = 35 MPa (Medium Strong) (Cement R_a = 2.4 μm) 83
Figure 4-3. Relationship between peak shear stress and UCS for rock analogues against smooth steel with R_a=0.4μm. Dashed line indicates the transition points contour 84
Figure 4-4. Coefficient of friction μ considering peak values vs UCS for rock analogues against smooth steel with R_a=0.4μm at four normal stress levels 85
Figure 4-5. Relationship between ultimate shear stress and UCS for rock analogues against smooth steel with R_a=0.4μm. 86
Figure 4-6. Coefficient of friction μ considering ultimate values vs UCS for rock analogues against smooth steel with R_a=0.4μm 87
Figure 4-7. Failure envelopes for rock analogue (of varying UCS) – steel (R_a = 0.4 μm) interfaces 88
Figure 4-8. Summary of δ' values from parametric study, $\sigma'n$~100kPa, after Jardine et. al 1993 90
Figure 4-9. Relationship between peak shear stress and relative roughness for strong rock analogues (UCS = 65 MPa), rock analogue R_a = 2.4 μm 91
Figure 4-10. Interface friction angle δ considering peak values vs steel R_a for strong rock analogues (UCS = 65 MPa), rock analogue R_a = 2.4 μm 91
Figure 4-11. Relationship between ultimate shear stress and relative roughness for strong rock analogues (UCS = 65 MPa), rock analogue R_a = 2.4 μm 93

Figure 4-12. Coefficient of friction μ considering ultimate values vs steel R_a for strong rock analogues (UCS = 65 MPa), dashed line indicates rock analogue R_a = 2.4 µm 93
Figure 4-13. Rock analogues after shearing against steel plate with R_a = 34 µm at normal stress of (a) 10 kPa, (b) 50 kPa, (c) 100 kPa and (d) 200 kPa 95
Figure 4-14. Rock socket skin friction related to the uniaxial compression strength of intact rock (Source: Tomlinson 2001) 96
Figure 4-15. Alpha factor α vs normalised UCS of rock analogue (R_a = 2.4 µm), considering peak values 98
Figure 4-16. Alpha factor α vs normalised UCS of rock analogue (R_a = 2.4 µm), considering ultimate values 98
Figure 4-17. Alpha factor vs normalised UCS of rock analogue (R_a = 2.4 µm) for varying steel roughness, considering peak values 99
Figure 4-18. Alpha factor vs normalised UCS of rock analogue (R_a = 2.4 µm) for varying steel roughness, considering ultimate values 99
Figure 4-19. Shear stress vs horizontal displacement graph from machined steel (R_a = 7.2 µm) - Sandstone (R_a = 19 µm) interface testing at four normal stress levels 101
Figure 4-20. Typical shear stress vs horizontal displacement graph for four different rock types against machined steel (R_a = 7.2 µm) 101
Figure 4-21. Interface friction angle δ considering peak values vs UCS for rock samples against smooth steel with R_a = 0.4 µm 102
Figure 4-22. Interface friction angle δ considering peak values vs UCS for rock samples against machined steel with R_a = 7.2 µm 103
Figure 4-23. Alpha factors for rock – steel interfaces (shearbox), considering peak values 107
Figure 4-24. Alpha factors for rock – steel interfaces (shear box), considering ultimate values 107
Figure 5-1. Coefficient of friction μ vs horizontal displacement for Sandstone samples against steel R_a = 0.4 µm 111
Figure 5-2. Coefficient of friction μ vs horizontal displacement for Flagstone samples against steel R_a = 7.2 µm 111

Figure 5-3. Coefficient of friction μ vs horizontal displacement for Andesite samples against steel R_a = 0.4 μm 112
Figure 5-4. Coefficient of friction μ vs horizontal displacement for Limestone samples against steel R_a = 34.0 μm 112
Figure 5-5. Comparison of $\delta peak$ from interface testing of four rock types against steel with R_a = 0.4 μm 115
Figure 5-6. Comparison of $\delta peak$ from interface testing of four rock types against steel with R_a = 7.2 μm 116
Figure 5-7. Comparison of $\delta peak$ from interface testing of four rock types against steel with R_a = 34 μm 116
Figure 5-8. Variation of peak interface friction angle for Sandstone-steel interfaces of varying roughness, Sandstone R_a = 19 μm 118
Figure 5-9. Variation of ultimate interface friction angle for Sandstone-steel interfaces of varying roughness, Sandstone R_a = 19 μm 118
Figure 5-10. Variation of peak interface friction angle for Flagstone-steel interfaces of varying roughness, Flagstone R_a = 5.5 μm 119
Figure 5-11. Variation of ultimate interface friction angle for Flagstone-steel interfaces of varying roughness, Flagstone R_a = 5.5 μm 119
Figure 5-12. Variation of peak interface friction angle for Andesite-steel interfaces of varying roughness, Andesite R_a = 5.8 μm 120
Figure 5-13. Variation of ultimate interface friction angle for Andesite-steel interfaces of varying roughness, Andesite R_a = 5.8 μm 120
Figure 5-14. Variation of peak interface friction angle for Limestone-steel interfaces of varying roughness, Limestone R_a = 2.7 μm 121
Figure 5-15. Variation of ultimate interface friction angle for Limestone-steel interfaces of varying roughness, Limestone R_a = 2.7 μm 121
Figure 5-16. Effect of normal stress on interface friction angle of continuum material – sand interfaces. Modified from Abu Haga et al. (2018) 122
Figure 5-17. Interface friction angle vs relative roughness ratio R, considering average peak values of rock – steel interfaces at 159 and 316 kPa 124

Figure 5-18. Interface friction angle vs relative roughness ratio R, considering average ultimate values of rock – steel interfaces at 159 and 316 kPa 124
Figure 5-19. Normal displacement vs shear displacement for Sandstone and Andesite against steel of R_a = 0.4 and 34 μm 126
Figure 5-20. Normal displacement vs shear displacement for Flagstone and Limestone against steel R_a = 0.4 and 34 μm 128
Figure 5-21. Interface friction angle δ vs relative hardness ratio M, considering average peak values of tests at 159 and 316 kPa 129
Figure 5-22. Interface friction angle δ vs relative hardness ratio M, considering average ultimate values of tests at 159 and 316 kPa 130
Figure 5-23. Interface friction angle δ vs relative hardness ratio M, considering average ultimate values of tests at 159 and 316 kPa, considering data from selected tests with comparable roughness ratio R 132
Figure 5-24. Failure envelopes for Sandstone –steel interfaces 133
Figure 5-25. Failure envelopes for Flagstone – steel interfaces 133
Figure 5-26. Failure envelopes for Andesite –steel interfaces 134
Figure 5-27. Failure envelopes for Limestone – steel interfaces 134
Figure 5-28. Alpha factors for rock – steel interfaces (IST), considering peak values 135
Figure 5-29. Alpha factors for rock – steel interfaces (IST), considering ultimate values 136
Figure 5-30. Variation of fitting parameter b with relative roughness of the interface (considering peak values of all the rock types combined) 138
Figure 5-31. Variation of fitting parameter b with relative roughness of the interface (considering ultimate values of all the rock types combined) 138
Figure 5-32. Variation of fitting parameter b with relative roughness of the interface (considering peak values of Sandstone and Andesite interfaces) 139
Figure 5-33. Variation of fitting parameter b with relative roughness of the interface (considering ultimate values of Sandstone and Andesite interfaces) 140

Figure 5-34. Variation of fitting parameter b with relative roughness of the interface (considering peak values of Flagstone and Limestone interfaces) 141
Figure 5-35. Variation of fitting parameter b with relative roughness of the interface (considering ultimate values of Flagstone and Limestone interfaces). 141
Figure 5-36. Comparison of calculated data and test data from all the normal stress levels used (i.e. 16 – 316kPa), considering peak values 144
Figure 5-37. Comparison of calculated data and test data from the normal stress levels of 159 and 316 kPa, considering peak values 145
Figure 5-38. Comparison of calculated data and test data from the normal stress levels of 159 and 316 kPa, considering ultimate values 145
Figure 6-1. Comparison of $\delta peak$ from interface testing of four rock types against concrete 149
Figure 6-2. Comparison of δult from interface testing of four rock types against concrete 150
Figure 6-3. Average interface friction angle vs relative roughness ratio R, for rock – concrete interfaces 151
Figure 6-4. Average interface friction angle vs relative hardness ratio M, for rock – concrete interfaces 152
Figure 6-5. Schematic representation of variation of average interface friction angle in the R – M space 153
Figure 6-6. Average interface friction angle vs relative UCS ratio U, for rock – concrete interfaces 154
Figure 6-7. Normal displacement vs shear displacement for rock – concrete interfaces at normal stress of 316 kPa 155
Figure 6-8. Alpha factors for rock – concrete interfaces (IST), considering peak values 156
Figure 6-9. Alpha factors for rock – concrete interfaces (IST), considering ultimate values 157
Figure 6-10. Alpha factors for rock – concrete interfaces (IST), considering peak values at normal stress of 159 and 316 kPa 158

Figure 6-11. Alpha factors for rock – concrete interfaces (IST), considering ultimate values at normal stress of 159 and 316 kPa 159
Figure 6-12. Interface friction angle vs relative hardness ratio M, for rock – concrete and rock – steel interfaces, considering peak values 160
Figure 6-13. Normalised interface friction angles for rock concrete interfaces over rock steel (R_a = 34 μm) interfaces, considering peak values 161
Figure 6-14. Normalised interface friction angles for rock concrete interfaces over rock steel (R_a = 34 μm) interfaces, considering ultimate values 161
Figure 6-15. Alpha factor of rock – concrete interfaces compared with contours from rock – steel interfaces (IST), considering peak values 164
Figure 6-16. Alpha factor of rock – concrete interfaces compared with contours from rock – steel interfaces (IST), considering ultimate values 165
Figure 6-17. Coefficient of friction μ vs horizontal displacement for Sandstone - sand – steel interfaces (steel R_a = 0.4 μm) 167
Figure 6-18. Coefficient of friction μ vs horizontal displacement for Flagstone - sand – steel interfaces (steel R_a = 0.4 μm) 167
Figure 6-19. Coefficient of friction μ vs horizontal displacement for Andesite - sand – steel interfaces (steel R_a = 0.4 μm) 168
Figure 6-20. Coefficient of friction μ vs horizontal displacement for Limestone - sand – steel interfaces (steel R_a = 0.4 μm) 168
Figure 6-21. Normalised interface friction angles for Sandstone – sand – steel interfaces, considering peak and ultimate values 170
Figure 6-22. Normalised interface friction angles for Flagstone – sand –steel interfaces, considering peak and ultimate values 171
Figure 6-23. Normalised interface friction angles for Andesite – sand –steel interfaces, considering peak and ultimate values 172
Figure 6-24. Normalised interface friction angles for Limestone – sand –steel interfaces, considering peak and ultimate values 173
Figure 6-25. Interface friction angle δ vs relative roughness ratio R_s for rock – sand – steel interfaces, considering peak values 175
Figure 6-26. Interface friction angle δ vs relative roughness ratio R_s for rock – sand – steel interfaces, considering ultimate values 176

Figure 7-1. Normalised shear stress plotted against horizontal displacement for saturated Chalk samples against steel R_a = 0.4 μm 181
Figure 7-2. Normalised shear stress plotted against horizontal displacement for saturated Chalk samples against steel R_a = 7.2 μm 181
Figure 7-3. Normalised shear stress plotted against horizontal displacement for saturated Chalk samples against steel R_a = 34 μm 182
Figure 7-4. Normalised shear stress plotted against horizontal displacement for Sandstone samples against steel R_a = 7.2 μm 184
Figure 7-5. Variation of interface friction angle and coefficient of friction for Chalk–steel interface test for steel with R_a= 0·4 μm against (a) dry and (b) saturated Chalk 185
Figure 7-6. Variation of interface friction angle and coefficient of friction for Chalk–steel interface test for steel with R_a= 7·2 μm against (a) dry and (b) saturated Chalk 185
Figure 7-7. Variation of interface friction angle and coefficient of friction for Chalk–steel interface test for steel with R_a=34 μm against (a) dry and (b) saturated Chalk 186
Figure 7-8. Tensile failure of a dry Chalk sample sheared at 1000 kPa 188
Figure 7-9. Variation of normalised friction angle with increasing steel roughness, for saturated Chalk samples and dry Sandstone 189
Figure 7-10. Interface friction angle plotted against horizontal displacement for saturated Chalk samples 190
Figure 7-11. Results of IST testing Chalk-concrete interface for dry Chalk192
Figure 7-12. Results of IST testing Chalk-concrete interface for saturated Chalk 192
Figure 7-13. Summary of results for Chalk-concrete interface for dry Chalk 193
Figure 7-14. Summary of results for Chalk-concrete interface for saturated Chalk 194
Figure 7-15. Normalised interface friction angles for Chalk - concrete interfaces over Chalk - steel (R_a = 34 μm) interfaces, considering dry samples 196

Figure 7-16. Normalised interface friction angles for Chalk - concrete interfaces over Chalk - steel (R_a = 34 μm) interfaces, considering dry samples 197
Figure 7-17. Alpha factors for Chalk-concrete compared with Chalk-steel and contours from data from rock –steel testing 198
Figure 7-18. Alpha factors for Chalk-concrete compared with Chalk-steel and Sandstone-steel and contours from contours from data from rock –steel testing. (modified from Ziogos et al., 2017and Ziogos et al., 2018) 199
Figure 8-1. Old Red Sandstone wave cut platform at John O' Groats, UK. Zigzag line displays saw blade structure 203
Figure 8-2. Flowchart for the estimation of the shear resistance of steel foundation – seabed interface. The flowchart shall not be used for values of M < 0.57 or M > 1.33 208

List of Tables

Table 2-1. Selective summary of interface friction tests found in the literature 28
Table 3-1. Level of saturation of Chalk samples 55
Table 3-2. Summary of key Index properties for the Chalk samples 62
Table 3-3. UCS determined in-situ at visited locations. 65
Table 3-4. UCS values obtained from unconfined compression test (direct method). 66
Table 3-5. UCS values obtained from Brazilian test. 67
Table 3-6. Surface properties of steel plates 71
Table 3-7. Concrete mix proportions 72
Table 3-8. UCS of concrete samples 73
Table 3-9. Physical properties of HST 95 sand 73
Table 3-10. Mohs hardness values of samples used for interface testing. 79
Table 3-11. Summary of interface testing to be carried out 79
Table 4-1. Rock analogue with varying strength (UCS = 15, 35 and 65 MPa) – smooth steel (R_a = 0.4 μm). 88
Table 4-2. Summary table of interface friction angles recorded for all the rock analogue – steel interface combinations 89
Table 4-3. Sandstone (R_a = 19 μm) – steel interface testing summary results 105
Table 4-4. Flagstone (R_a = 5.5 μm) – steel interface testing summary results 105
Table 4-5. Andesite (R_a = 5.8 μm) – steel interface testing summary results 106
Table 4-6. Limestone (R_a = 2.7 μm) – steel interface testing summary results 106
Table 5-1. Summary of results from rock – steel interface testing 114
Table 5-2. Relative roughness ratio R for various rock – steel interfaces 115
Table 5-3. Values of relative roughness ratio R, considered for data shown in Figure 5-31 132
Table 5-4. Summary table of arithmetic fitting constats b and c. 136

Table 6-1. Arithmetic fitting constants considering alpha type approach for peak and ultimate values of rock – concrete interfaces 157
Table 6-2. Arithmetic fitting constants considering alpha type approach for peak and ultimate values of rock – concrete interfaces at normal stress of 159 and 316 kPa 159
Table 6-3. Summary table of relative roughness and relative hardness ratios for rock – steel and rock – concrete interfaces 164
Table 6-4. Summary of results from rock – sand - steel interface testing 169
Table 7-1. Summary of results from interface testing of Chalk-steel interface 183
Table 7-2. Summary of Chalk - concrete testing results 195
Table 8-1. UCS values (determined in-situ) at various locations (modified Table 3-2) 204
Table 8-2. Comparison of results of Sandstone - steel interface testing utilising the tilt table and the IST device 209
Table 8-3. Comparison of results of Flagstone - steel interface testing utilising the tilt table and the IST device 210
Table 8-4. Comparison of results of Andesite - steel interface testing utilising the tilt table and the IST device 211
Table 8-5. Comparison of results of Limestone - steel interface testing utilising the tilt table and the IST device 212
Table 8-6. Comparison of results of Chalk - steel interface testing utilising the tilt table and the IST device 213

Notation

d	linear displacement
d_{10}, d_{50} etc	particle size characteristics
e_{max}	maximum void ratio
e_{min}	minimum void ratio
G_s	specific gravity
M	relative hardness ratio
m_{sat}	saturated moisture content
n	porosity
r	rock sample radius
P	interface friction angle ratio (δ_s/δ_{st})
R	relative roughness ratio
R_a	average centre line roughness
R_s	sand – steel relative roughness ratio
R_t	maximum profile height
R_z	average distance between the highest peak and lowest valley
T	torque
T_0	tensile strength
U	relative UCS ratio
α	alpha factor
δ	interface friction angle
δ_c	interface friction angle of rock – concrete interfaces
δ_{cv}	critical state interface friction angle
δ_{lim}	limiting value of interface friction angle
δ_{peak}	peak interface friction angle
δ_{res}	residual interface friction angle
δ_s	interface friction angle of rock – sand – steel interfaces
δ_{st}	interface friction angle of rock – steel interfaces
δ_{ult}	ultimate interface friction angle
φ_{crit}	critical state angle of internal friction
φ_b	basic friction angle
θ	rotational displacement
μ	coefficient of friction
ρ_d	dry density
σ_n	normal stress
τ	shear stress

w	moisture content
w_s	saturation moisture content

Abbreviations

CNL	Constant Normal Load
CNS	Constant Normal Stiffness
DNA	(American) Defence Nuclear Agency
GBS	Gravity Based Structure
IST	Interface Shear Tester
LVDT	Linear Variable Differential Transformer
SSSI	Site of Special Scientific Interest
UCS	unconfined compressive strength of rock
USBR	United States Bureau of Reclamation

Chapter 1

1 Introduction

1.1 Preface

Marine energy generators (e.g. tidal stream and wave bobbing units) are relatively new technologies aiming to harness the oceans energy. A cost analysis of marine generators reveals that foundation installation may make up 1/3 of the total devices' installation cost (Carbon Trust 2011). This cost would be an ideal element to try and reduce in order to increase the financial viability of marine energy.

Tidal stream generators are typically deployed where fast flowing tidal currents exist (e.g. Pentland Firth, Islay sound in Scotland, U.K.). That means that generators have to be installed under difficult environmental and seabed conditions. Most current devices are permanently anchored to the seabed (using bespoke foundation solutions), making their recovery for maintenance difficult and installation expensive. In addition, the whole offshore/nearshore, installation operation may last several days utilising vessels and divers (if they can be deployed due to currents) resulting in very high cost. In order to reduce the cost, installation operations should be as short duration as possible and ideally reproducible over a farm type development that may have variable seabed conditions across the farm yet using a single foundation solution.

Utilisation of simple gravity based structures (GBS) can be an alternative way of generator installation. These foundations can be made of steel or concrete onshore and be deployed offshore in a relatively narrow time window. GBS maintain stability due to their mass and their interface frictional properties. There is no need for permanent anchoring, so the recovery is easier and the cost diminishes. The foundation structures themselves could also remain on

the seabed with separate recovery of the generator device to aid fast and economical inspection, servicing and maintenance.

Strong tidal currents often wash out the sediments so generators may have to be mounted on exposed rock (or thin soil layers over rock) (Small et al., 2014). Although, significant research has been undertaken on shearing of interfaces under constant normal stiffness conditions (e.g. rock socket piles and rock bolts) to date; very little research has been undertaken to assess the frictional properties of steel on rock and concrete on rock interfaces for GBS applications (i.e. shearing under constant normal load conditions, at low stress levels when compared to say pile rock sockets, unbonded interfaces etc.).

In order to bridge some of this knowledge gap and to provide better understanding of the behaviour of GBS with rock foundation interfaces for marine energy generators, this research project was carried out by University of Dundee in collaboration with Lloyd's Register EMEA and University of Aberdeen. The project was funded by the Energy Technology Partnership (ETP) and Lloyd's Register EMEA.

1.1.1 Laboratory interface shear testing

Interface friction properties and insights on the shearing behaviour of various foundation – seabed interfaces have been obtained via laboratory interface testing. The controlled laboratory environment, allowed the investigation of the possible individual controlling factors (e.g. normal stress, surface roughness etc.) and the results were used to develop a design framework for the calculation of the shearing resistance of Gravity Based Structure (GBS) on rock. A modified direct shear box, a bespoke Interface Shear Tester (IST) and a tilt table were used during the project.

1.1.2 Field visits

Field visits at wave cut platforms and quarries at the north of U.K. were carried out during the project. This offered insights on challenges that might be posed during the deployment of the GBS and allowed the recovery of rock samples for laboratory testing. In-situ strength tests revealed the effect of weathering

on the unconfined compressive strength (UCS) of the rock which was analysed and discussed further.

1.2 Aims and objectives

The broader scope of this project was to achieve a better understanding of the underlying factors that determine the interface behaviour between rock and foundation materials at stress levels associated with gravity or self-weight foundations.

The aims of the project:

1. Improve the understanding of rock - steel and rock – concrete interface behaviour at stress levels associated with shallow foundations

2. Develop a database of rock/foundation interface properties and investigate the underlying controls on the interface behaviour.

3. Provide guidance that will help to achieve a less conservative design for marine energy generators.

To achieve these aims, the following objectives were formed.

1. Carry out interface testing to gather interface properties of various interface combinations with rock types from areas of high tidal stream potential in the U.K.

2. Analyse the results to determine the parameters that influence the shear behaviour of the interfaces.

3. Develop relationships between material properties and interface shear strength.

4. Develop a design framework that allows the estimation of the shear strength of the interface based on the characteristics of the interface materials.

5. Combine data gathered from field visits and laboratory testing to provide guidance for less conservative design.

1.3 Structure of thesis

The thesis consists of nine chapters.

Chapter 2 provides a review of the tidal stream energy technology (e.g. types of generators, foundations etc.) a and reveals that limited information is available on constant normal load rock – steel and rock – concrete interface testing. Factors that could potentially affect the shear behaviour of interfaces are identified in order to direct the research plan.

Chapter 3 describes the experimental methods used to carry out this study. Three types of interface testing are presented including: direct shear box, tilt table and Interface Shear Tester (IST). Material characterisation methods applied to the samples both in-situ and in the laboratory are also described.

Chapters 4, 5, 6 and 7 contain results and discussion from the different types of interface testing. Data from early stage shear box testing are analysed in Chapter 4 leading to the primary stage of the proposed design framework (alpha factor design). Chapter 5, Chapter 6 and Chapter 7 contain the main volume of interface testing (carried out using the IST) including: rock – steel, rock – sand – steel and rock – concrete testing over a wide range of material properties. Analysis of this data resulted in the development of the alpha factor power functions (shaping factors) that describe the shear strength of the interface based on inherent material properties.

Considerations that arose from field study visits along with evaluation of the different methods of interface testing are presented in Chapter 8, leading to suggestions that could be taken into account during the design process.

The findings from all the previous chapters are summarised in chapter 9. Through the progress of this study, various potential research routes have been identified and are presented as suggestions for future research.

Chapter 2

2 Literature review

2.1 Marine energy

The term marine energy refers to the energy that is carried by the ocean waves, the tides the temperature difference of the ocean water and the salinity. Tidal energy is divided in two categories, the tidal stream and the tidal range. Prior to 2010 only small pilot marine energy generator programmes existed. In 2011 the worldwide total capacity of energy generated by these means almost doubled and by the end of 2011 it was responsible for 527 MW (REN 21, 2012). Comparing the total capacity to other types of renewable energy (e.g. wind energy had 238 GW of total installed capacity by the end of 2011), marine energy is at a very early stage of development and there is significant potential for development and increased output. According to Stegman et al. (2017), 2.5 GW of tidal stream energy could be deployed by 2050, if the overall levelised cost of energy is reduced. Up to 2015, 2.1 MW of tidal stream energy were installed in the U.K. (OES, 2015).

2.1.1 Introduction

Tide is the change in the sea level resulting from the interaction of the sun and moon's gravitational forces on the earth. Large water masses are moved every day forming currents. The kinetic energy from these currents is converted to electricity through tidal stream energy generators.

The power of a tidal current can be calculated by Equation 2-1 (Carbon Trust, 2005).

$Power = \frac{1}{2} ApV^3$ (W) Equation 2-1

where:

A = the swept area of the rotor in m^2

ρ = the density of water e.g. kg/m^3

V = instantaneous current velocity in m/s

From equation 2.1 it can be easily understood that water current velocity is a significant factor in the assessment of an areas' resource potential, and typically generators are deployed in peak current velocities of 2-3 m/s (or more) at locations of interest for energy generation and significant horizontal forces are imposed on the structure making sliding capacity more critical than bearing (Newson et al., 2011).

One major advantage that tidal energy has over other types of renewable energy (solar, wind) is predictability for many years in advance. Also water is much denser than air (over 800 times), thus a significantly smaller tidal turbine can produce the same amount of electricity as a much bigger wind turbine. During the last few years a significant amount of research has been carried out to exploit this energy (Bryden and Scott, 2006, Johnstone et al., 2006) but the manufacture and development of tidal energy generators is still at a stage where it is difficult to establish a clearly dominant technology.

2.2 Tidal resources around the UK

The Carbon Trust examined 36 sites around the UK, which have 99.5% of the U.K.'s identified tidal current resource (Carbon Trust, 2005). These sites belong to five broader areas (Northern Isles Region, Pentland Region, North West Region, South West Region & Channel Isle Region) as seen in Figure 2-1.

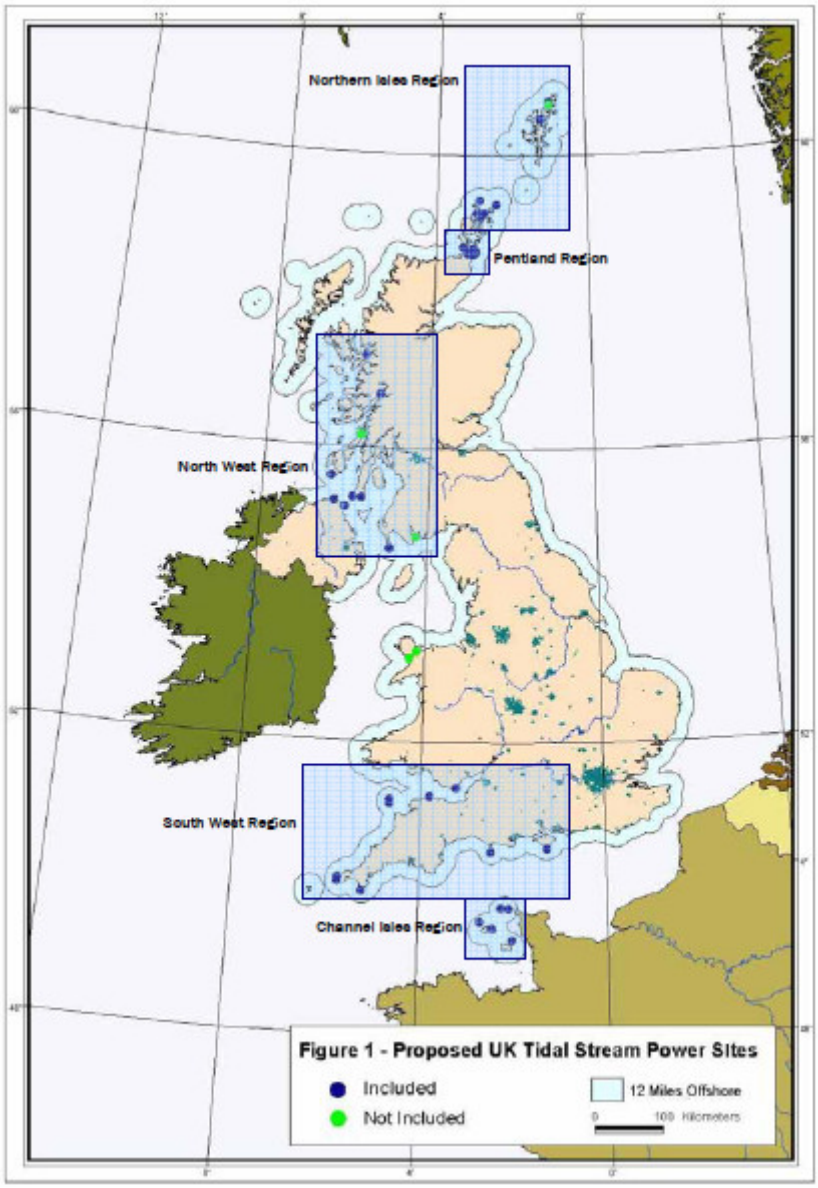

Figure 2-1. Proposed UK Tidal Stream Power Sites, (Source: Carbon Trust, 2005)

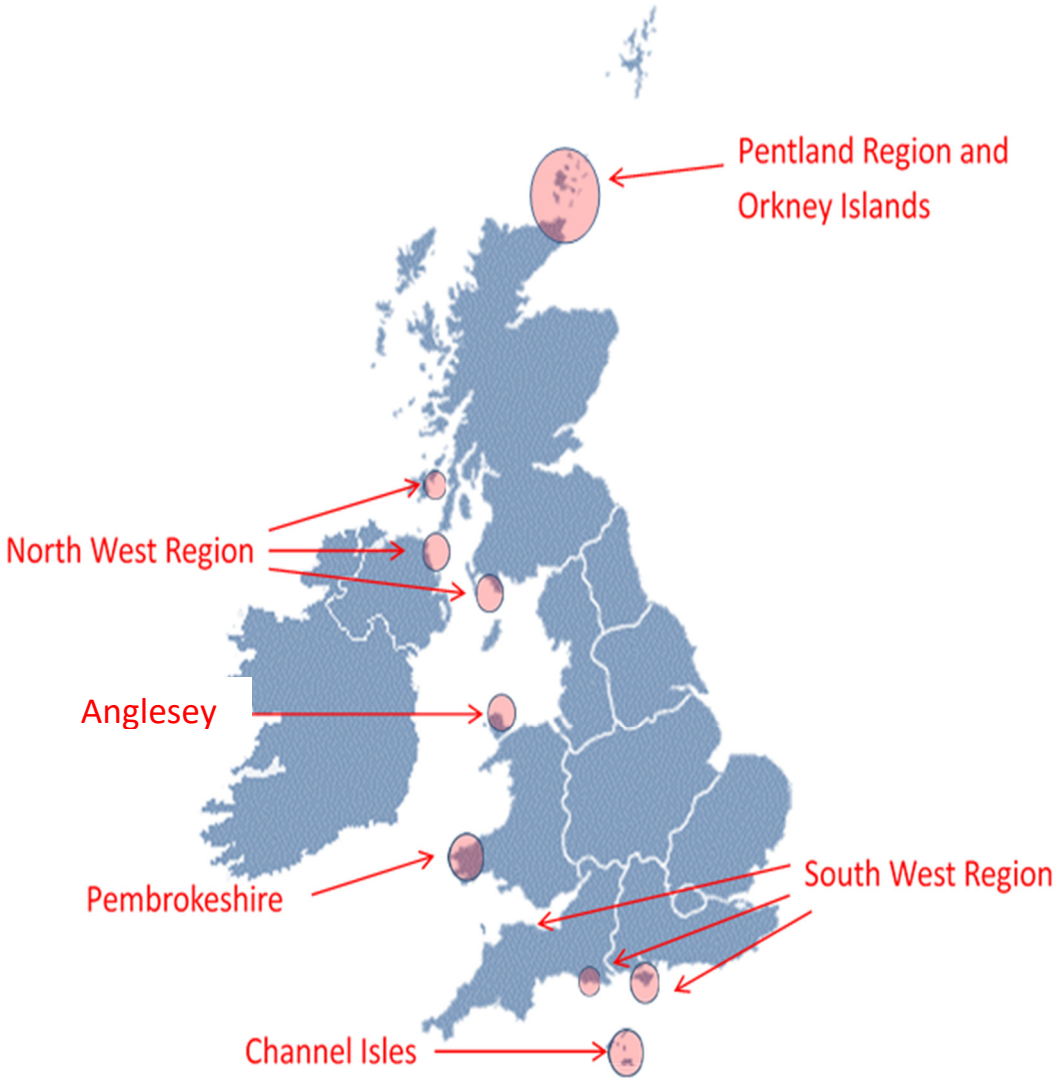

Figure 2-2. Areas with significant tidal resources around the UK (Source of underlying map: http://www.lsamoforumuk.scot.nhs.uk/)

- **Pentland Region and Orkney Islands:**

In this region it is believed that the 61% of the total tidal energy resource of the UK is available. There are five areas featuring high velocity streams, where tidal development could arise, but there are concerns due to high variability of the electricity (variation in tidal current velocities) output throughout the day (Carbon Trust, 2005, Variability of UK Marine Resources). The European Marine Energy Center (EMEC) is a research and test facility focused on marine energy development and is based at Orkney Islands (Fall of Warness). In addition, an energy company named MeyGen was given permission in 2010

to develop a 398 MW commercial array project in the Pentald Firth. The offshore installation of the turbines commenced in 2016. The information regarding the tidal energy potential presented in the following bullet points was recovered from a document commissioned by the Carbon Trust in 2005 referred to as “Variability of UK Marine Resources”

- **Channel Isles Region:**

Up to 13.6% of the energy resource is believed to come from this area. Five sites are identified for potential development and three of them feature medium to high velocity currents (3.5 – 5.5 m/s). The energy aggregate output of the site is constant throughout the day, without significant variations, making it a very good resource, but there are severe practical constraints that limit the potential exploitation (special areas of conservation, commercial shipping, and military activities).

- **South West Region:**

This area represents 9% of UK’s tidal resource. There are nine potential locations across South West Region, but Foreland Point and Portland Bill (Dorset, U.K.) have 80% of area’s resource. The energy aggregate output is smooth.

- **North West Region:**

There are eleven sites around the region, but seven of them concentrate 95% of area’s total capacity. Up to 8% of the total energy resource around the UK is found in North West Region, but the energy output varies during the day. Atlantis has purchased the Islay Sound site from Scottish Power Renewables in 2016 and a commercial array was planned to be deployed in 2018.

- **Northern Isles Region:**

This area represents 8% of the total energy resource, but there is high variability of energy production at different times throughout the day. Only in Bluemull Sound in Shetland is there a smooth energy output.

2.3 Geology at sites with significant tidal resources

Figure 2-2 shows the areas around the UK which demonstrate significant potential for tidal stream energy exploitation according to the literature. Each area is divided into smaller subareas and the offshore bedrock geology for each subarea is discussed in the following bullet points. The geology information was retrieved using BGS DiGMapGB - 250 Offshore. That is a mid-scale (1:250.000) digital map that requires GIS software to be viewed (Quantum GIS was used).

Taking into account the energy resource of each area and the various mechanical properties of the existing rock types, the following broad rock types were initially identified for potential investigation in the future.

- **Sandstone**: Old red Sandstone is found at Pentland Region, Scotland, U.K. which represents 61% of the total UK tidal resource (Carbon Trust, 2005, Variability of UK Marine Resources).

- **Caithness Flagstone:** This rock typically consists of laminated carbonate siltstones and mudstones and is found in the Caithness region, Scotland, U.K. (south mainland part of Pentland Firth).

- **Chalk:** Found at Race of Aldernay (near the Bailiwick of Guernsey, England, U.K.) and Casquets (northwest of Aldernay), which represent together around 6% of the total UK tidal resource (Carbon Trust, 2005, Variability of UK Marine Resources). It is also a material being encountered as a challenging foundation in wider areas of Europe and in other foundation types for renewable energy (Buckley et al., 2018).

- **Slate**: Found at the whole Pembrokeshire region, which represents a significant percentage of the total UK tidal resource (Fairley et al., 2011).

- **Granite**: Found at Guersey North West and Guersey Big Russel, which represent together around 6,5% of the total UK tidal resource (Carbon Trust, 2005, Variability of UK Marine Resources).

- **Schist**: Found around Anglesey which is already chosen for commercial use and its planned capacity is 80 MW. (https://www.dailypost.co.uk/business/business-news/holyhead-underwater-kite-power-stations-12579409).

2.4 Tidal energy generators

In this section, a review of the current technology in tidal generators is provided. Different types of generators are described and more detail is given for those with gravity based foundations.

2.4.1 Foundation types for tidal stream energy generators

A foundation's aim is to secure the whole generator assembly to the seabed. The foundation should withstand axial and shear forces, torsion, overturning moments and the hydrodynamic loading generated by the turbine and imposed by the environment. The foundation also has to be protected from scour and should be installed and removed in a manner that makes the generator's deployment cost effective.

Some examples of different foundation types are briefly mentioned in the following paragraphs and shown in Figure 2-3. It is noted that a predominant foundation geometry and installation technique has not been clearly established (The Crown Estate, 2011, Small et al., 2014).

- **Pile Mounted:** The generator is mounted either on a monopile or on a multiple pin pile jacket. Depending on the competency of the seabed, the piles can be either driven or installed using the drill – drive or the

drill and grouted technique. In some cases the turbine's nacelle can raise above the sea level for maintenance, moving on rails that are placed on the pile.

- **Floating**: The turbine is floating while being connected to the seabed through cables or chains and anchored using gravity or drag embedded anchors. Significant freedom of movement is allowed, such that the device swings as the tidal direction changes.

- **Suction buckets:** Suction buckets represent a possible alternative foundation solution. Monopod or tripod/tetrapod (depending on which is the most economical solution) configurations can be used in order to host the turbine.

- **Gravity Based Structures (GBS)**: The device maintains stability based upon the foundations mass and the interface friction between foundation surface and the foundation. The GBS can be constructed onshore and be in theory deployed in the seabed within a small time window. The availability and the cost of the crane barges required for the installation, depend on the size/mass of the GBS (Fraenkel, 2010). There is no permanent fixture with the seabed, therefore, the recovery of the generator is relatively easy and the environmental impact after decommissioning is minimised. In the next section some types of gravity foundations that are used in prototypes will be mentioned, as this type of foundation seems to be the preferred current solution and potentially the most economical solution for both installation and maintenance.

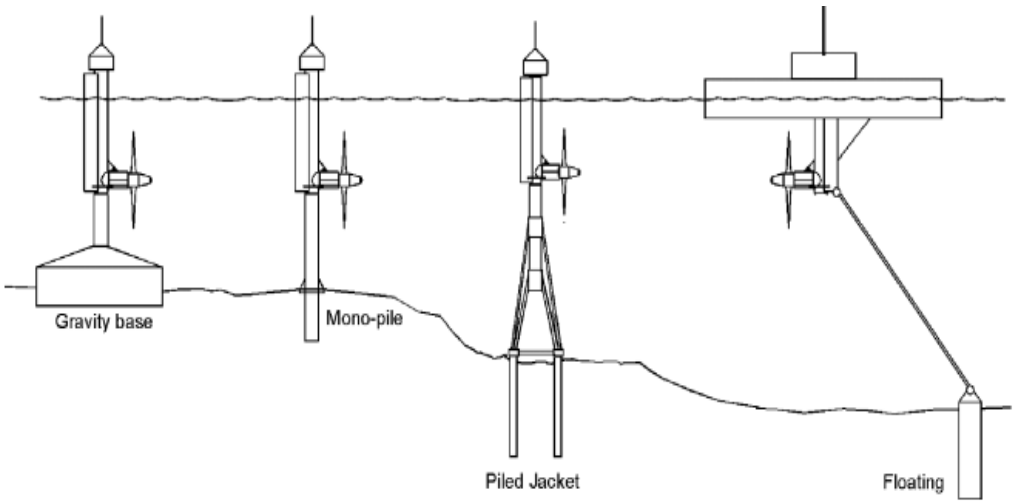

Figure 2-3. Different configurations of foundations for tidal energy generators (Fraenkel, 2002)

2.4.2 Tidal stream generators with GBS

In August 2011 the AR-1000 tidal turbine, from Atlantis resources corporation was the first grid-connected, commercial-scale tidal turbine at the EMEC site in Orkney, Scotland. The maximum power output was 1 MW at a water velocity of 2.6 m/s. It had a 18 m diameter rotor, weighed 1500 tonnes and stood at a height of 22.5 m. AR-1000 is a single rotor turbine, but its design is based on the two-rotor AK-1000 turbine which was manufactured in 2009. In August 2010 the AK-1000 turbine was successfully deployed on its subsea berth at the Fall of Wareness (EMEC: http://www.emec.org.uk/news-this-week-54/), (www.atlantisresourcescorporation.com).

The turbine consists of:

-The turbine nacelle which hosts all the electromechanical systems and the system that connects the nacelle with the supporting pylon.

- The GBS (gravity base structure) with ballast blocks keeps the whole structure in place.

- Support pylon that connects the nacelle to the GBS.

The GBS, made from steel, measures approximately 22m x 22m x 2.5m and weighs 1500 tonnes in air fully assembled (EMEC decommissioning programme). The GBS is designed in a way that the load is distributed over a large area so localised pressure is reduced thus diminishing the possibility of failure under the foundation (30 kPa average foundation stress can be estimated taking into account the generator's mass and the foundation's plan area). No mooring or anchoring is needed. This makes the commissioning and decommissioning of the turbine easier. The ballast needed to keep the structure stable is 1200 tonnes and consists of 6 ballast blocks (200 tonnes each), due to vessel carriage constraints. The ballast blocks are placed on the steel foundation which is in contact with the seabed, resulting in a steel - rock interface.

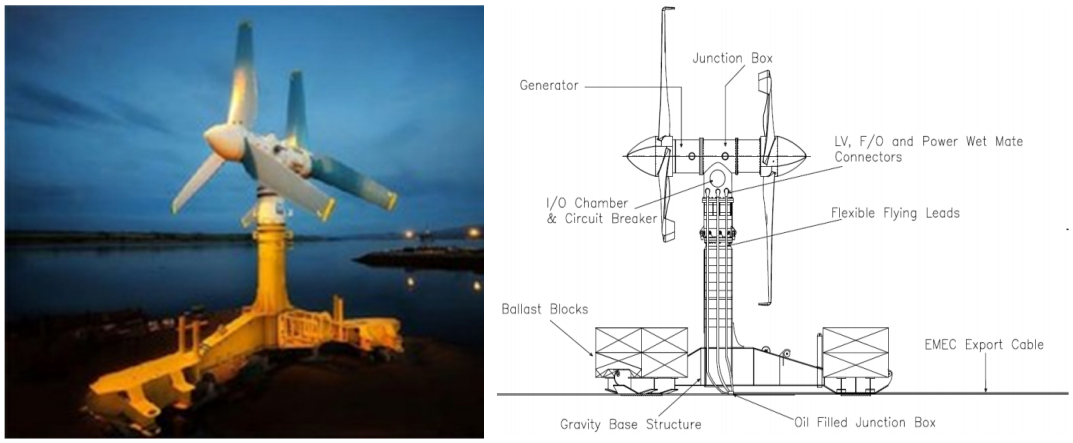

a b

Figure 2-4. (a) Atlantis AK-1000 (Source: news.cnet.com), (b) Atlantis AK-1000 (Source: EMEC Decommissioning Programme)

Tidal Energy Limited has deployed its device Deltastream, in Pembrokeshire's Ramsey Sound in 2015, around four years later than the initial planed deployment (www.globalmaritimealliance.com). The device was decommissioned a few months later due to a fault at its sonar system and the company went to administration in 2016. (https://www.walesonline.co.uk/business/business-news/deltastream-tidal-energy-device-only-12306961).

According to the design, Deltastream's maximum power output was 1.2 MW. Deltastream essentially consists of three individual turbines connected on the tips of an equilateral triangular frame (Figure 2-5). Each lateral length was approximately 36 m. The rotor's diameter was 12 m and the hub height was 14 m. The whole device weighed approximately 250 tonnes (Deltasteam scoping report, 2008).

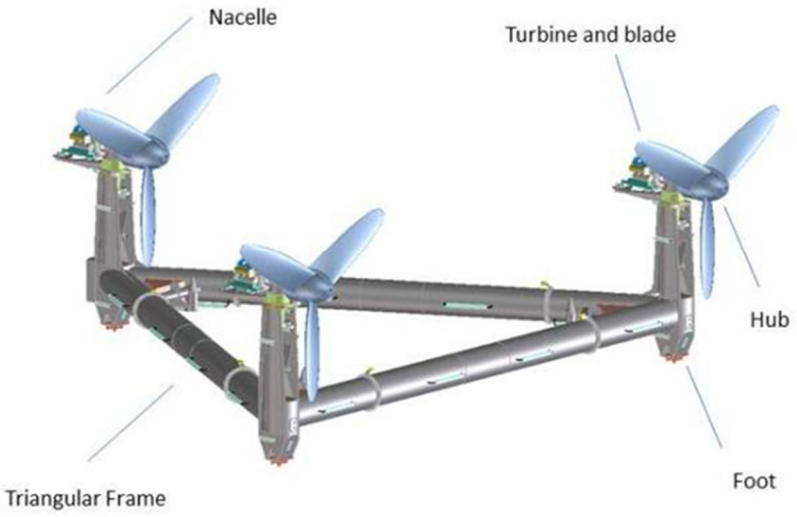

Figure 2-5. Tidal Energy Ltd. Deltastream source: http://www.tidalenergyltd.com/?page_id=640)

The triangular frame was made from tubular steel (around 1.5 m diameter) and was free-flooding, so it used sea water as ballast. The frame was designed in a way that provided a low centre of gravity and drag force making it stable. The whole structure sat on three "rock feet" which are patented by Tidal Energy Limited. Self-levelling devices (e.g. hydraulic feet), can be incorporated, in order to level the device on an inclined seabed. The total contact area between the foundation frame and the seabed was ~ 9.5 m^2 and the average estimated foundation stresses were high (around 260 kPa). A detailed diagram of the "rock feet" is shown in Figure 2-6.

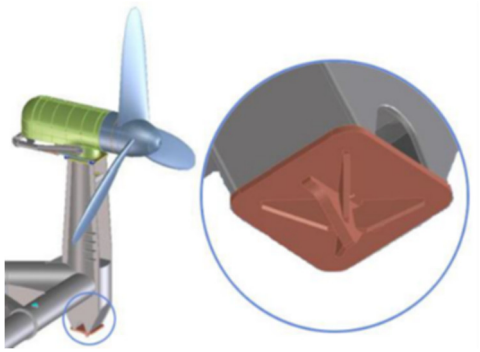

Figure 2-6. Tidal Energy Ltd Deltastream Rock Foot Detail (Source: Deltastream White Paper 2012)

In 2011 Voith set in operation a 110 kW turbine near the island of Jindo (South Korea). The rotor's diameter was 5.3m and the maximum power was produced at current speed of 2.9 m/s. The turbine was a 1:3 scale model demonstrator device (www.voith.com). The generator stood on a concrete gravity foundation and its total weight was approximately 1000 tonnes (Figure 2-7).

The foundation consisted of a concrete plinth (18 m by 9.5 m) and a pre-stressed concrete tower (5 m tall, 2.5 m diameter) which was placed in the middle of the plinth. The tower was large diameter in order to give the required natural frequency to the whole structure rather than to withstand the bending moments (that could be achieved by using a thinner tower). The foundation was constructed onshore and moved to the deployment site by a floating crane where it was placed with the foundations' long direction parallel to the turbine's axis to provide stability against overturning moments acting at the base of the turbine. The total cost of the gravity foundation, including the design and management cost was half a million euros (STRABAG Offshore Wind GmbH).

A larger (1 MW) version of the turbine was deployed at EMEC but it was founded on a monopile instead of gravity foundation. No information was found regarding the seabed geology.

Figure 2-7. Voith Hydro Tidal Turbine's Concrete Gravity Foundation (Source: STRABAG Offshore Wind GmbH)

2.4.3 Considerations for tidal stream generator design

In this section, general information on the loading regime on tidal generators is given and considerations for foundation design are provided.

For example, the seabed geomorphology at potential sites of deployment is complex and challenging. Exposed and weathered bebrock is usually the foundation surface and in some locations it is possibly covered by thin layers of sediments (clay or coarse granular material). The sediments can be moved by the strong wave currents, so the bathymetry changes with time. The seabed is generally undulating and consists of features like boulders, sand dunes, steep slopes and gullies amongst others. Typical foundation design procedures are not available for such formations, so general guidelines for onshore design are usually adopted (Small et al., 2014).

Tidal generators are devices that are hosted in the sea environment, so they have to withstand different loads that stem from various sources leading to a loading regime that is potentially much more complex than structures that are land based.

Tidal generators are subjected to the following types of loads:

- Permanent or Dead Loads

- Live Loads
- Accidental Loads
- Loads induced by the temperature change (contraction or expansion)
- Loads induced by the added mass and inertia of entrained water
- Loads induced by different stages of the construction procedure (EMEC, 2009)

Permanent loads are induced by the structure itself and do not change during its life time. Examples are: the weight of the construction frame, the weight of the generator that converts the kinetic energy into electric and the ballast or any other mass that is used to keep the structure in place. Also all the hydrostatic forces acting on the submerged device are contained in that category.

Live loads are not consistent in magnitude and direction during the device's lifetime. Live loads can be induced for example by someone who accesses the generator in order to maintain it or by the torque and thrust loads induced by turbine's function. Also live loads can be induced by the environment e.g. wind, wave, current, however for tidal generators that are submerged the wind effect can be ignored.

Accidental loads are the loads that can be induced by an accidental incident, such as breakage of a turbine's blade, vessel impact on the generator, fishing nets snagging, anchor dragging etc. These are loads that cannot be predicted but can be considered as a specific load that is induced as part of the design process.

2.5 Shear strength of the rock mass discontinuities

2.5.1 Introduction

As mentioned before, in most of the cases, tidal generators will be submerged at sites where bedrock is exposed, so it is useful to appreciate the fundamentals of rock mechanics applicable for this end use (Small et al., 2014). In the field, rock mass consists of intact rock blocks which are separated by different kinds of discontinuities such as joints, faults, folds, bedding planes and sheared zones. The behavior of the rock mass under loading (stress) is mostly dependent on the interaction between the intact rock blocks and the discontinuities, as these are the weakest points in the rock mass.

2.5.2 Failure criteria for rock mass discontinuities

A linear failure criterion that can be used for stability analysis is Mohr-Coulomb as expressed in Equation 2-2.

$$\tau_f = c + \sigma_n \tan \varphi_b \qquad \text{Equation 2-2}$$

where
τ_f = the peak shear strength at failure, σ_n = normal stress to the discontinuity, c = the peak cohesion, φ_b = the basic friction angle

The basic friction angle corresponds to sliding of smooth horizontal surface and can be determined using the tilting table test method (USBR 6258) as described in detail in 3.2.2.

It should be noted that failure envelopes derived by rock shear testing are usually curved because of the surface roughness, so the following bilinear criterion (Patton 1966 and Goodman 1980) can provide a more realistic description for the shear stress generated along clean discontinuities.

$$\tau_f = \sigma_n \tan(\varphi_b + i) \qquad \text{Equation 2-3}$$

and

$$\tau_f = c_a + \sigma_n \tan \varphi_r \qquad \text{Equation 2-4}$$

Where

τ_f = the peak shear strength at failure, σ_n = normal stress on the discontinuity φ_b = the basic friction angle on sliding smooth horizontal surface, i = angle of inclination of first order asperities, φ_r = the residual friction angle of the material comprising the asperities, c_a = the apparent cohesion derived from the asperities (shear strength intercept)

For unweathered discontinuities the φ_b and φ_r values are the same.

The bilinear failure envelope resulting from the criteria mentioned before is displayed in Figure 2-8.

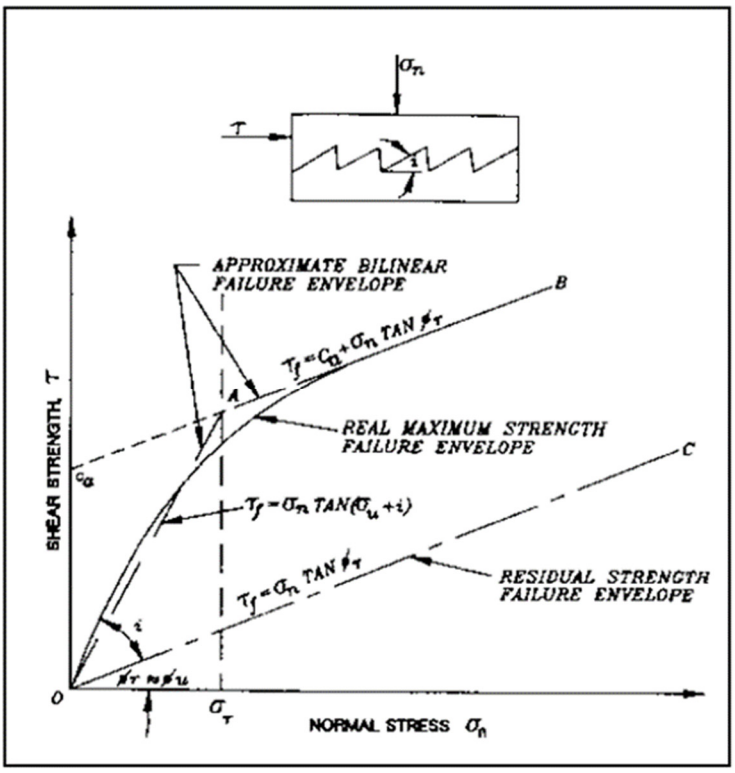

Figure 2-8. Typical approximate bilinear and real curvi-linear failure envelopes for modelled discontinuous rock (Source: Engineering and Design Rock Foundations, U.S. Army Corps of Engineers, 1994)

Barton (1973) proposed a criterion which takes into account the effect of the roughness (JRC) and the compressive strength (JCS) of the walls of the discontinuities.

$$\tau = \sigma'_n tan\left[JRClog10\left(\frac{JCS}{\sigma n}\right) + \varphi_b\right] \quad \text{Equation 2-5}$$

Barton and Choubey (1977) modified that criterion by replacing the basic friction angle φ_b with the residual friction angle φ_r, so that it could be used with more accuracy for weathered discontinuities.

$$\tau = \sigma'_n tan\left[JRClog10\left(\frac{JCS}{\sigma n}\right) + \varphi_r\right] \quad \text{Equation 2-6}$$

The residual friction angle φ_r can be calculated using Equation 2-7 (Barton and Choubey, 1977).

$$\varphi_r = (\varphi_b - 20^o) + 20\left(\frac{j}{J}\right) \quad \text{Equation 2-7}$$

Where:

j = the Schmidt rebound number on a wet and weathered surface , J= the Schmidt rebound number on a dry, sawn and fresh surface.

If the rock joint is not weathered, then the JCS value is the same as the unconfined compression strength (UCS) of the intact rock. If the joint walls are weathered then the JCS may take a value roughly $0.25\sigma_c$ (Barton, 1973).

The JRC can be estimated by comparing a rock joint profile to a table of existing profiles produced by Barton and Choubey (1977). Every profile has its own JRC value ranging from 0-20 from smooth to rough joints.

2.5.3 Effect of roughness on shear strength of rock mass discontinuities

Under field conditions rock joints do not consist of smooth surfaces. Asperities and undulations exist on rock joints and have a significant effect on their shear behaviour. The asperities can be divided in two categories, the first and the second order asperities as shown in Figure 2-9. The first order asperities (waviness) correspond to large surface undulations and the second order asperities (unevenness) are small bumps and folds with higher values of angle i.

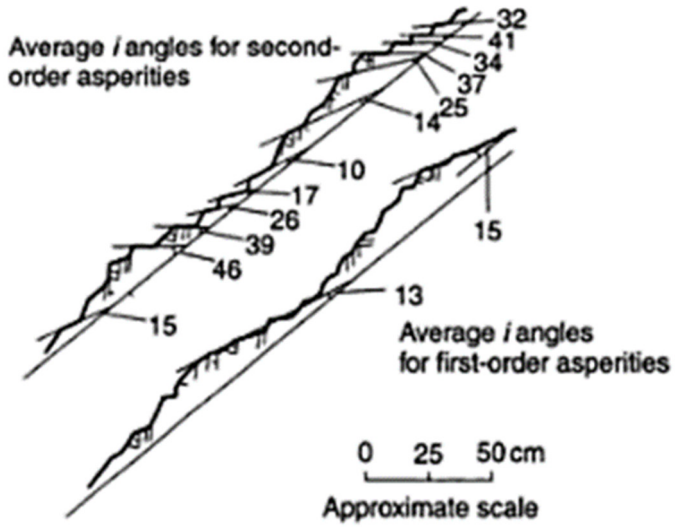

Figure 2-9. Measurement of roughness angles i for first and second order asperities on rough rock surfaces (after Patton, 1966)

The waviness is primarily associated with the dilation during the shearing, while the unevenness (depending on the normal stress) mainly affects the friction angle at low normal stress (Puntel et al., 2005).

When large displacements occur, the first order asperities determine the rock joint's behaviour. During small displacements behaviour is primarily controlled by the second order asperities (Patton, 1966).

A rock joint can be sheared in three different ways depending on the applied normal stress. When the normal stresses on the joint are low then shearing occurs by overriding of the asperities which leads to dilation. At high normal stresses no overriding of the asperities happens and the asperities are sheared by the shearing motion. With normal stresses that are somewhere in the middle a combination of the two pre mentioned different types occurs (Goodman et al., 1968).

When the shearing is occurring under low normal stresses, then behaviour is controlled by the second order asperities (higher *i*). When the normal stresses increase then the first order asperities become predominant (Barton, 1973 and Hoek and Bray, 1981).

2.6 Shearing behaviour of interfaces

Applications in geotechnical engineering are often affected by the interaction of interfaces, as construction materials are in direct contact with soil and rock. For some types of construction this effect is very significant (retaining walls, tunnels, piles etc.), so it is crucial to determine the parameters that dictate or affect the interface behaviour of different materials. That knowledge could lead to more cost effective and safe constructions.

Currently tidal generator GBS are made from steel or concrete and are deployed in areas with high tidal current velocities (above 2 m/s). The tidal currents wash out the seafloor sediments and the rocky seabed is exposed. As a result, the interface behaviour of concrete or steel on rock should be defined. Literature review revealed that relatively little information is available on rock – steel and rock – concrete interfaces, thus other information that could be useful from shearing between other materials was reviewed.

2.6.1 Soil sheared against manufactured material interfaces

Many systematic efforts to investigate the interface behaviour between soil - structure interfaces have been made with Potyondy (1961) and Peterson et al. (1976) being among the first. Potyondy (1961) conducted tests between soil and concrete, steel and wood, while Peterson et al. (1976) tested sand - steel interfaces. Both studies were carried out using the direct shear box. In the 1980's significant research was accomplished on sand - steel interfaces by Usegi and Kishida (1986 a, b) and Kishida and Usegi (1987) by utilising a simple shear apparatus. Research in this field is continuously undertaken by many researchers and various devices have been utilised (e.g. ring shear, curved shearbox etc.). The basic findings are summarised in the following references.

- Interface roughness, particle angularity, soil density, D_{50} and normal stress are amongst the most important factors that govern the interface behaviour

(Peterson et al., 1976, Uesugi and Kishida 1986a, Kishida and Uesugi 1987, Paikowski et al., 1995).

- Interface friction increases as the surface roughness increases but this happens up to a specific limit (critical roughness). That limit is approximately the internal friction of the soil, because if the interface friction is higher, failure is occurring in the soil mass and not through the interface (Peterson et al., 1976, Uesugi and Kishida 1986a, Kishida and Uesugi 1987, Jardine et al., 1993). For example, Figure 2-10 shows that the interface friction angle increases with increasing steel roughness (and consequently with increasing relative roughness ratio) until a plateau is reached. This plateau is practically the internal friction angle of the soil. Similar behaviour was reported by Barmpopoulos et al. (2010) for sand - concrete interfaces (Figure 2-11).

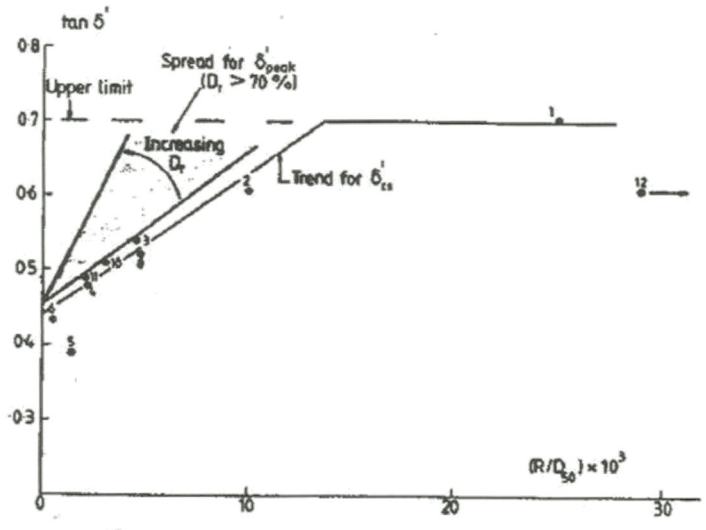

Figure 2-10. Summary of δ' values from parametric study, σ'_n~100kPa, after Jardine et. al 1993

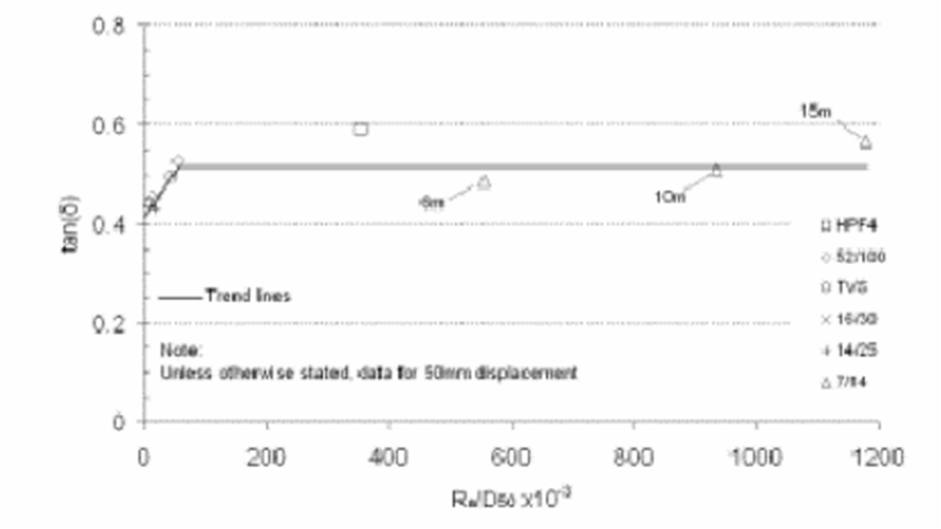

Figure 2-11. Variation of δ vs Relative roughness for concrete sand interfaces (from Barmpopoulos et al., 2010)

Iscimen and Frost (2010), tested Ottawa sand against concrete interfaces and concluded that influence of roughness was very significant. Apart from the peak interface strength, the roughness also influenced the mode of shearing. For increasing concrete roughness, the shearing changed from sliding to a more complex mechanism that involved particle re arrangement within the whole sand specimen. The rougher surfaces also exhibited more “brittle” behaviour where a distinct peak was observed. Iscimen and Frost (2010) also found that as the roughness increased, more displacement was required for the peak friction value to be mobilised).

Danyildiz and Baykal (2010) sheared lightweight aggregates against concrete blocks. They concluded that at low normal stress (50 kPa) the interface behaviour correlates to the grain geometry and roughness. More specifically, shear resistance increases with grain angularity (Figure 2-12). At high normal stresses the interfacial shear strength is significantly affected by the crushing strength of the individual particles. Interface friction angle increases with increasing crushing strength, but that occurs up to a specific value, beyond which the friction angle is not affected by crushing strength. Angularity of the particles decreases from (a) to (c) and so does the interface stress at normal

stress of 50 kPa. FA refers to fly ash only pellets, FA10 refers to 10% cement – 90% fly ash pellets, and FAC20 refers to 20% cement – 80% fly ash pellets.

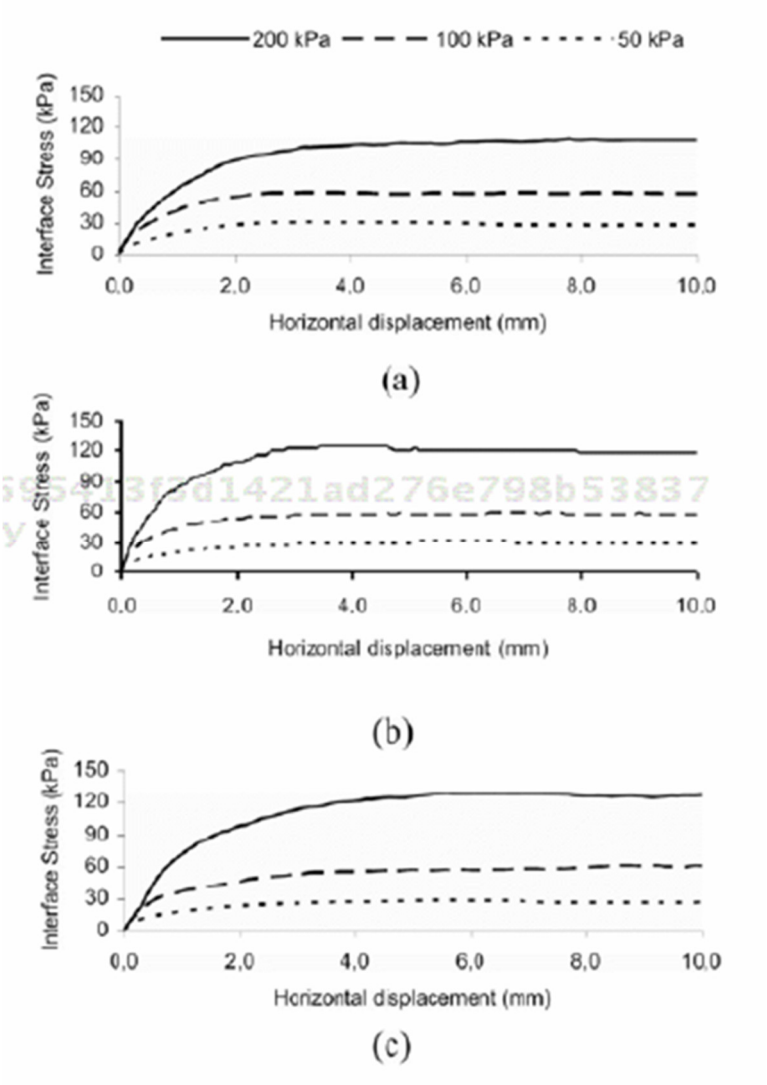

Figure 2-12. Horizontal Displacement – Interface stress curves of concrete against (a) FA: (b) FAC10: (C) FAC20 group pellets (Source: Danyildiz and Baykal 2008)

Table 2-1. Summarises the devices utilised and findings of various published interface studies.

Table 2-1. Selective summary of interface friction tests found in the literature

Author	Type of utilised Apparatus	Results
Potyondy (1961)	Direct shear apparatus, sand on the top of test material (concrete, steel)	δ increases with density, $\delta_{lim} = \varphi_{peak}$
Yoshimi and Kishida (1981)	Ring shear, test material (steel) on top of sand	δ is mainly affected by roughness, irrespective of density
Uesugi et. al (1990)	Simple shear, the sand on top of concrete	δ is affected by roughness and D_{50},
Jardine et. al. (1993)	Direct shear apparatus, sand steel interface	δ_{cv} independent of density, δ_{cv} sharply decreases as D_{50} increases
Iscimen and Frost (2008)	Curved Shear Box, sand on top of various pipes (concrete, frp, steel)	$\delta_{lim} = \varphi_{peak}$
Barmpopoulos et. al. (2009)	Ring Shear Tests, sand on concrete	δ_{cv} increases with decreasing D_{50}
Ho et. al. (2011)	Ring Shear Tests, sand on steel	δ_{cv} varies with the shear displacement magnitude, large scale particle crushing occurs for very large shear displacement (meters)

where:

δ_{lim} = the limiting maximum value of interface friction angle, δ_{cv} = the critical state interface friction angle, φ_{peak} = peak value of internal friction, φ_{cv} = the critical state friction angle, D_{50} = particle size characteristic.

2.6.2 Roughness and waviness

In this section, information about the quantification and measurement of surface roughness is provided. The effect the roughness has on the shearing behaviour of interfaces has been investigated by many researchers and they concluded that it is the most significant factor and determines interface shear strength (Potyondy, 1961, Uesugi & Kishida, 1986, Paikowski et. al, 1995). So it is very significant for our project to examine the alternatives for roughness quantification and measurement.

Interface roughness can be quantified by many parameters, but one of the most frequently used worldwide is R_a which is the computed average of all deviations of the roughness profile from the median(centre) line over the defined length (Figure 2-13) and is defined as seen in Equation 2-5.

$$R_a = \int_0^L |y(x)| dx \frac{1}{L}$$

Equation 2-5

where:
L = surface length, y(x) = the roughness curve

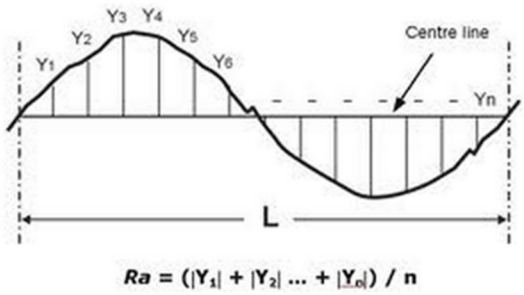

Figure 2-13. Calculation of the average roughness value R_a

Waviness represents the longer spatial wavelength features of a surface and in real scale problems affects the shear behaviour of interfaces in a way similar to that of first order asperities in rock joints (described in 2.5.3). In other words, roughness defines the interface friction between two nominally planar materials, but waviness affects interface shear resistance by causing undulation or interlocking between large asperities. The difference between

roughness and waviness is highlighted in Figure 2-14. All the samples examined in this study has nominally planar surfaces, therefore only the effect of roughness on the shear behaviour of the interfaces has been examined.

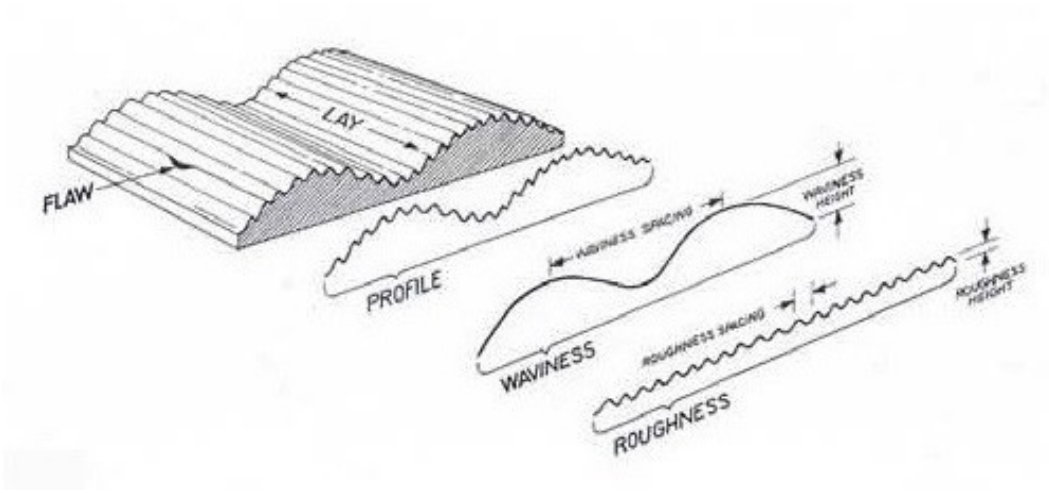

Figure 2-14. Description of roughness and waviness,(source: http://www.mahr.com/index.php?print=1&NodeID=14676&ContentID=15099&Overview=1&ActionID=0&view=1&nl=-1&nld=-1&year=-1)

2.6.3 Rock – concrete interfaces

Concrete dams founded on rock

Dams founded on rock is a research area which investigates rock – concrete interfaces as the sliding resistance of dams is a crucial parameter in the design procedure. Interface angle of friction and cohesion are the two predominant parameters that define the sliding resistance of a rock – concrete interface (Wei et al., 2007).

When concrete is standing on rock without any mechanism that provides cohesion to the surface (i.e. no grout, unbonded contact), then the interfacial friction angle can be measured using the direct shear test (Lo et al., 1991). An important component of this friction angle is the basic friction angle φ_b (see paragraph 2.5.2). Lo et al., 1990, analyzed the strength data of 13 dams operate by Ontario Hydro and concluded that the interface friction among different rock types ranged between 32^o and 39^o.

In some cases there could be bonded contact between the rock and concrete, for example for grouted concrete dams on rock. For this case the interface shear strength can be represented according to Lo and Grass (1994) by Equation 2-6.

$$\tau = (1 - n)c_i + \sigma_n \tan \varphi \qquad \text{Equation 2-6}$$

Where:
n = unbonded fraction of the dam – foundation interface, c_i = cohesion of the intact contact, σ_n = normal stress, φ = angle of friction = φ_b (basic friction angle) + i (roughness angle measured in the field)

Ghosh (2010) conducted field shear tests in order to determine the friction angle and cohesion between cement blocks and outcrops of Hornblend Schist rock. He cast six cement blocks (700 x 600 x 600 mm) in-situ against a fresh hard outcrop and applied shear loading using the configuration shown in Figure 2-15 after three weeks of curing. The normal stress was applied via a 100 ton hydraulic jack, however further details about the applied normal stress during the test were not given.

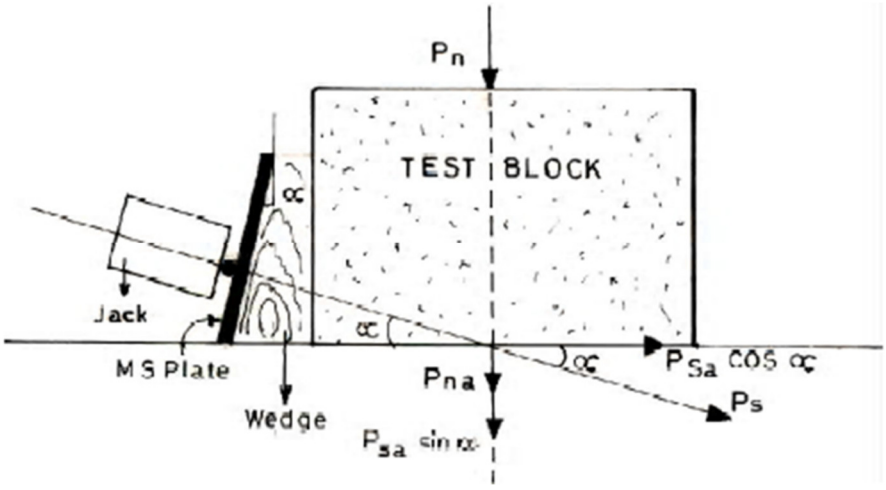

Figure 2-15. Application of forces during the test (Source: Ghosh 2010)

The tests revealed a friction angle of 59^0 and cohesion of 1000 kPa. For most of the tests, initiation of yielding occurred, followed by relatively small increase of shear stress with increasing shear displacement. A sudden drop in shear

stress was noticed after a peak value was reached (Figure 2-16). This behaviour is expected for a cement - good quality rock joint (IS 7746:1991). These values were considered high (Ghosh, 2010) and were attributed to the high surface roughness (saw tooth type) of the test surface.

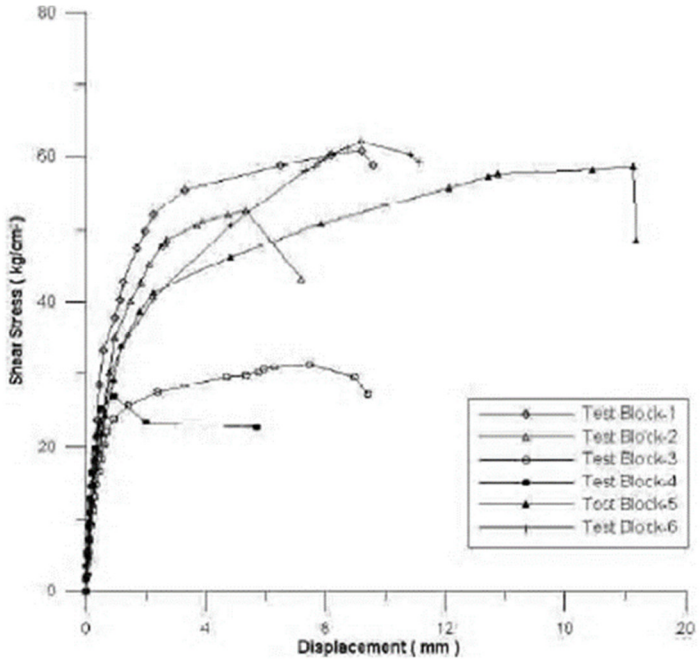

Figure 2-16. Shear stress vs shear displacement of concrete - outcrop interfaces from Ghosh 2010

Rock – concrete interfaces can also be found in rock socketed piles. Clayton et al. (1990), conducted a number of constant normal stiffness direct shear tests between Chalk and concrete in order to investigate the shaft resistance of bored piles in Chalk. When concrete is cast on Chalk, a bond is developed which strength is related to the intact rock's strength.

Analysis of pile load tests socketed piles in various rock types revealed that an important factor that affects piles' behaviour is the roughness of the socket walls (Horvath et al., 1983, Seidel and Collingwood 2001). If the walls are smooth and clean, then brittle behaviour is observed as the shear resistance drops rapidly after the peak shear stress is reached (Figure 2-17). As the roughness increases, the behavior becomes "plastic". Increase in socket walls

roughness also results in higher peak shear stress. It should be noted though, that while a small degree of roughness (2-3 mm deep furrows) is sufficient to change the behaviour from brittle to plastic, a much higher degree of spacing is needed (~ 100mm) to cause a significant increase in shear strength (Pells et al., 1980).

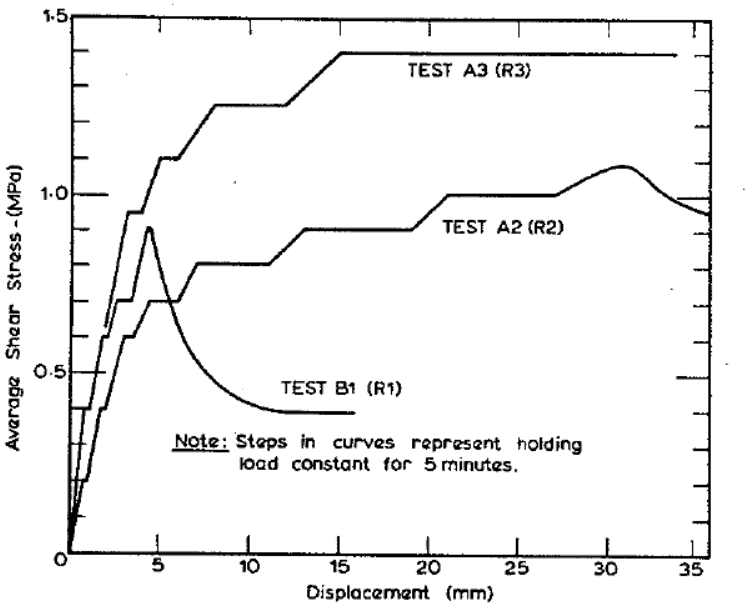

Figure 2-17. Test Results for Clean Sockets with different degrees of sidewall roughness (Source: Pells et al., 1980)

Xue et. al. (2003) also investigated the behaviour of rock socketed concrete piles by conducting direct shear interface testing on un bonded Hawkesbury Sandstone - concrete interfaces. In order to simulate real conditions, a constant normal stiffness configuration was used (Figure 2-18).

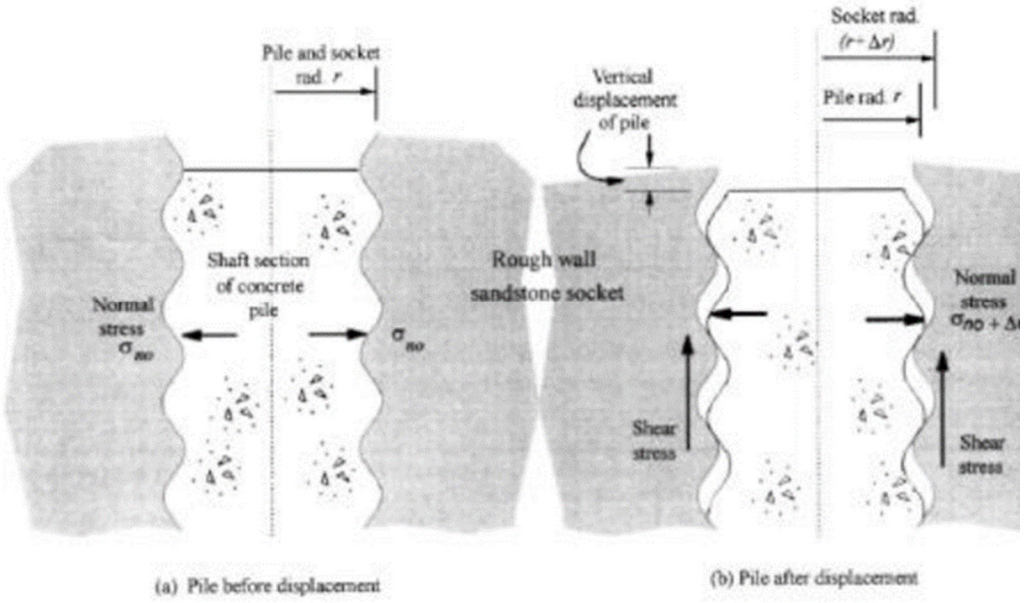

Figure 2-18. Constant normal stiffness conditions (Source: Xue et. al. 2003)

The unconfined compressive strength of the rock and the concrete was ~ 17 and ~ 40 MPa respectively. A large number of tests (around a hundred) using surface profiles of varying geometry (regular or fractal) were conducted. Regular profiles consisted of regular triangles whereas the fractal profiles were less “uniform” as shown in Figure 2-19

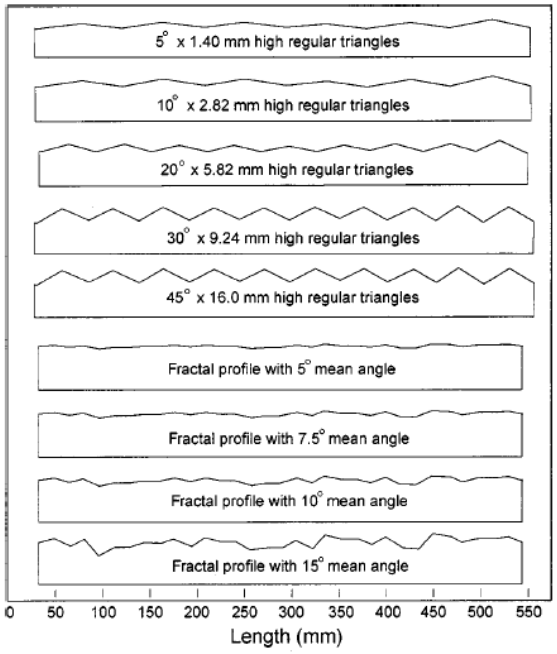

Figure 2-19. Roughness profiles used in tests (from Xue et al., 2003)

Discussion of the test results concluded that the interface shear strength increased with increasing asperities angle and also the behaviour became more brittle as the asperities angle increased. Peak shear stress also increases if any of the normal stiffness or the normal stress increased and the behaviour became more brittle. Fractal surfaces exhibited a less brittle behaviour. The reason being that, when the asperities are identical, they fail simultaneously when the peak shear stress is reached, which isn't the case when the asperities angles differ (fractal surfaces). Wear of the asperities occurred during sliding and increased as the geometry became steeper.

It should be noted here that the stress regime at the interface of a GBS is constant normal stress (rather than constant normal stiffness), since dilation is not constrained, however it was felt that the findings could be potentially applicable to this project (i.e. effect of roughness on shear stress) therefore it was included in the literature review.

2.6.4 Rock – steel interfaces

American Defence Nuclear Agency, DNA (1976) conducted research on the dynamic friction of rock - steel interfaces under high sliding velocities. The dynamic friction between steel and rock under high sliding velocities can be described by the following equation.

$$\tau = \mu\sigma_n \, e^{\,-c*\sigma/\xi} \qquad \text{Equation 2-7}$$

where:

τ = shear stress, σ_n = normal stress, c = sliding velocity,

μ = material property, 0.39 – 0.50 for dry, anhydrous rocks

ξ = material property, 2 GPa x m/s for rocks

This equation describes the findings of a number of dynamic friction tests between various rocks (Tuff, Sandstone and Limestone) and low carbon steel (1020) The coefficient of friction for Dakota Sandstone – steel interfaces was

0.39 (δ ~ 21º) whereas for Solenhofen Limestone it was significantly lower (μ = 0.14, δ ~ 8º) . It should be noted that those tests were conducted under very high sliding velocities (10-30 m/s) and the use of the equation for the shearing rates anticipated for this study (many orders of magnitude less) is questionable.

A field that is not directly related to rock sliding on steel concept, but be useful is the pull out capacity of rock bolts. Pull out tests of swellex bolts were conducted in hard and soft (depending on strength and Young's modulus) rocks (Li and Hakansson, 1999). Swellex bolts are hollow steel bolts that expand as they are filled with high pressure water, as the bolt expands, it compresses against the rock and adapts its shape to fit the irregularities of the borehole. The results revealed that the net friction between the bolts and the rock was higher for softer rocks. On the other hand, bolts in hard rocks, gained capacity due to the mechanical interlocking between the borehole asperities (roughness) and the deformed bolt's sidewall.

2.7 Hardness

The effect of hardness on the shearing behaviour of interfaces has been investigated by a number of researchers.

Tabor (1954) has investigated the effect of hardness, by dragging a metal tip against a flat metal sheet of varying roughness and concluded that the coefficient of friction μ, was higher when the metal sheet was softer than the tip. He also noticed that the hardness of the metal tip should be at least 1.1 – 1.2 times higher than the metal sheet in order for damage (scratching) to occur on its surface. When the metal sheet is harder, then scratching is minimised and only sliding takes place as shown by Bowden and Tabor 1964 (Figure 2-20).

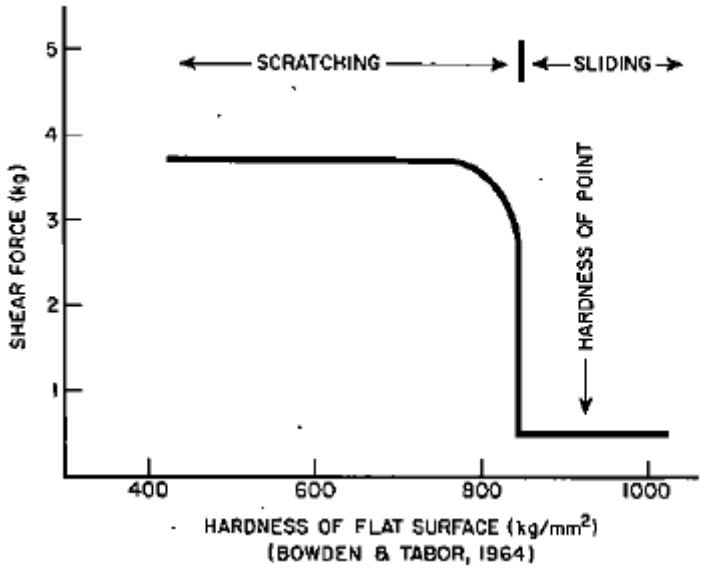

Figure 2-20. Friction between a metal point and a metal sheet of varying hardness after Bowden & Tabor, 1964. (image take from Engelder and Scholz 1976)

Engelder and Scholz 1976, concluded that the deformation of two shearing surfaces depends on the relative scratch hardness. Surface hardness has also been initially identified in tribology as a parameter affecting mechanical performance of interfaces (Williams, 1996).

Dove and Frost (1999) investigated the effect of surface hardness of relatively soft continuum materials (geomembranes) by conducting geomebrane - sand interface tests. They concluded that hardness had a significant effect on the interface shear resistance by defining the mode of shearing. In more detail, when the continuum material is relatively soft, the sand grains are both sliding and ploughing on the continuum surface and the interface resistance increases due to contribution of ploughing. When the hardness of the continuum material increases, the shearing is constrained only to sliding, as the sand grains cannot penetrate the continuum surface and consequently lower values of shear resistance are exhibited. Ploughing is also affected by the shape of the grains, as angular grains exhibit ploughing irrespective to the normal stress level, whereas rounded glass beads exhibit mostly sliding as shown in Figure 2-21.

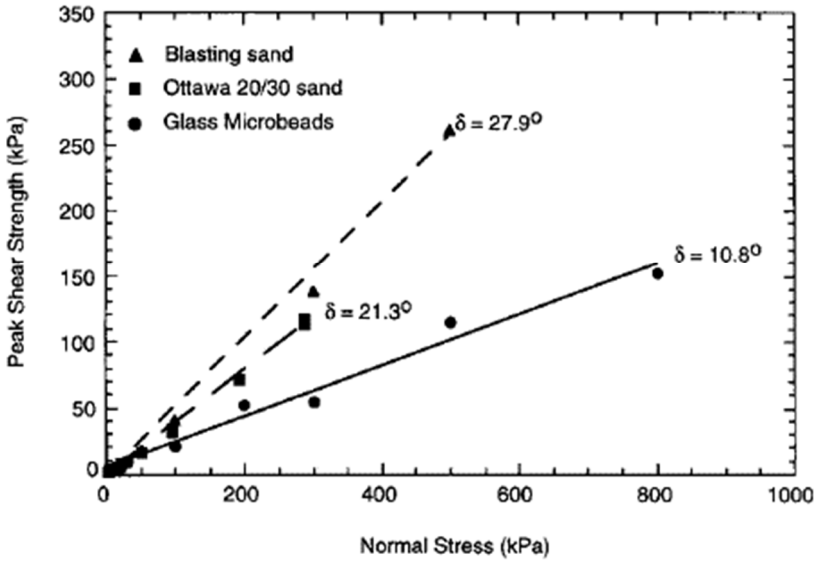

Figure 2-21. Strength Envelopes from Interface Shear Tests on Smooth Geomembrane (from Dove and Frost, 1999)

Abuel Naga et. al., 2018, conducted direct shear box tests between sands and continuum material counterfaces (e.g. steel and glass fiber reinforced polymer) of varying hardness and stated that the shear resistance of a granular – continuum material interface consists of sliding, rolling and ploughing . During shear, the particles of the granular material slide and roll in order to override the asperities of the continuum material (counterface) and the shearing resistance during this process is mainly affected by the surface roughness of the continuum material. When the localised stress at the points of contact is high enough to cause plastic deformation on the counterface, ploughing occurs (i.e. the grains cause deformation or material removal on the counterface). The ploughing component during shear, is mainly affected by the hardness of the counterface material and as a result, the coefficient of friction increases for decreasing hardness of the counterface (Abuel Naga et. al., 2018, Figure 2-22).

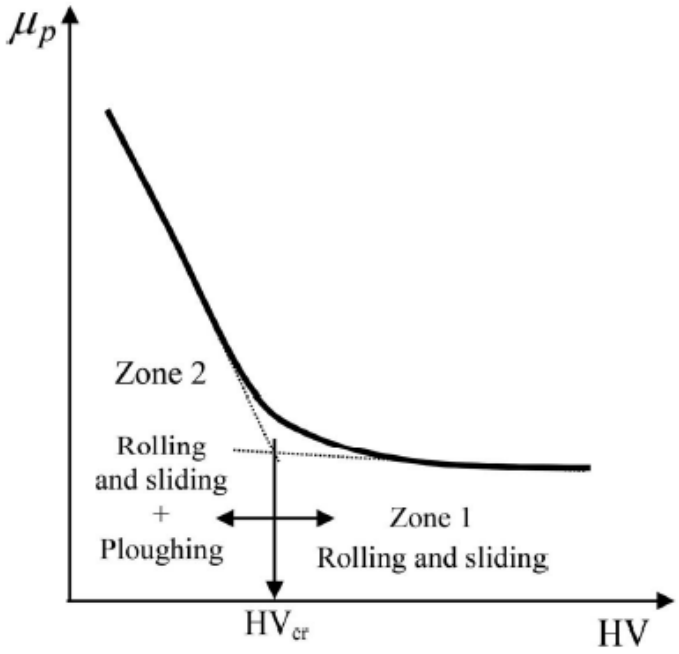

Figure 2-22. Relation between surface hardness and coefficient of friction (from Abuel Naga et. al., 2018)

Indentation Surface hardness of solid materials is quantified by measuring the plastic deformation that is induced by a standard indentation source. The most common hardness scales are Brinell, Vickers, Shore and Rockwell. Minerals and rocks can be characterised based on the Mohs' scale of mineral hardness. This is a qualitative method which refers to the potential of harder materials to scratch softer materials (i.e. it is a relative scale).

2.8 Important findings from literature review

The review of gravity based foundation design for tidal stream energy applications is summarised below. As no predominant foundation geometry or interface has been identified a more fundamental study will be undertaken, to investigate the rock - foundation interface behaviour

1. To date mostly steel and potentially concrete has been used as construction material for GBS. Therefore, this study intends to focus on rock - steel and rock - concrete interface testing.

2. Very limited literature is available on rock – steel interface testing, therefore information from soil – manufactured materials interface testing has been reviewed to identify parameters affecting the interface behaviour.

3. Normal stress and relative roughness of the interface have been identified as factors affecting the shear strength of granular – continuum material interfaces, however further investigation is required for continuum material – continuum material interfaces (i.e. rock – steel and rock – concrete interfaces, where the latter is unboned).

4. The strength of rock (UCS) seems to affect the skin friction of bored piles under constant normal stiffness conditions (CNS), however more research is required for constant normal load conditions (CNL) that apply to GBS for tidal stream generators.

5. Surface hardness of the counterface material dictates the mode of shearing (i.e. if ploughing occurs during shear) for sand – continuum material interfaces, however the effect of relative hardness on continuum – continuum material interfaces needs further investigation.

6. Continuum – continuum material interfaces behave differently to granular - continuum material interfaces, therefore the effect of sediment on the foundation – seabed interface should be investigated as this may occur with the presence of thin veneers of sediment on rock seabeds.

7. Seabed geology varies significantly amongst the deployment sites around the U.K. and this shall be considered for the selection of the most appropriate materials for testing, in order to allow a wide range of parameters to be investigated.

Chapter 3

3 Methodology

3.1 Introduction

This chapter describes the rationale followed to conduct the research along with the experimental equipment and the procedures used. The interface materials investigated and their preparation techniques are also described.

The information gathered as part of the literature review (for similar applications) revealed that the UCS of the foundation surface (seabed) and the roughness of the foundation footing are potentially two parameters that dictate the shearing behaviour of the foundation-seabed interface. The normal stress level is another parameter that affects the shearing behaviour of soil - solid interfaces (e.g. Daniyildiz and Baykal 2010) along with the hardness of the counterface materials, so it was decided that its effect should be examined throughout the different stages of the interface testing programme. The first stage consisted of interface testing using samples with varying UCS (seabed) against steel (foundation footing analogue). In order to achieve controllable properties and repeatable samples, cement mortar was used to simulate a rock seabed material (rock analogues). This is quite a common in the literature, for instance, De Toledo & De Freitas (1993), have used concrete to investigate the shearing behaviour of rock joints. In the second stage, real rock samples were used in order to verify the findings of the tests using the rock analogues. The rock samples were retrieved from various locations around the UK, in order to cover as wide range as possible of the different rock types that are found at locations with significant tidal stream resources, as identified in Chapter 2. Further details about the rock types collected, will be presented later in this chapter.

Foundation footings for tidal generators may be constructed using either steel or concrete, therefore steel and concrete samples were prepared in the laboratory in order to conduct interface testing and represent the foundation (foundation analogue).

The presence of sediment on the seabed was also simulated in a series of experiments by using a thin layer of sand between the foundation and the seabed analogues.

The equipment used to conduct interface testing during the different stages of the project consisted of a conventional 60 x 60 mm direct shear box, a tilt table and a torsional interface shear tester (GDSIST) as described later in this chapter.

Surface roughness characterisation and compressive strength determination of tested materials was also undertaken..

3.2 Testing equipment and procedures

3.2.1 Direct shear box testing

The conventional direct shear box has been widely used for the determination of interface properties of typically soil-solid interfaces, (e.g. Potyondy 1961, Peterson et al., 1976) therefore a square 60 x 60 mm direct shear box from Wykeham Farrance was utilised for the first stages of the interface testing. A shearing rate of 1.2 mm/min and a constant normal stress configuration were adopted. The latter reflects the real field conditions, since the gravity based foundation is free to dilate under the constant normal load applied by the self - weight of the foundation and generator structure. Two LVDT's were used to measure horizontal and vertical displacement (± 25 mm and ± 2.5 mm range respectively) and the shear force was measured by a load cell (± 2.5 kN range). A short travel LVDT (± 2.5 mm) was used for the vertical displacement, as very small vertical displacements were anticipated due to the nature of the

interface to be tested in this project (e.g. rock - steel). All the devices were connected to a PC based logging system for data acquisition purposes.

Initial tests were conducted by placing a steel block (foundation analogue) in the bottom half of the split box and a cement block (rock seabed analogue) on the top half of the split box. This arrangement compromised the accuracy of the measured shear force and was found to be inappropriate at an early stage of the project. This was because the steel block could not be stabilised in the bottom half of the shear box resulting in slight inclination of the steel block which resulted in the cement block placed above catching or snagging on the steel block below (Figure 3-1). It was found to be very difficult to level the steel block in the shear box, so even a very small step between the steel block and the bottom half affected the measured shear stress and generated “spikes” of high shear force (Figure 3-2). Similar problems in the use of the direct shear box, for interface testing have been mentioned in the literature (Fioravante et. al, 1999).

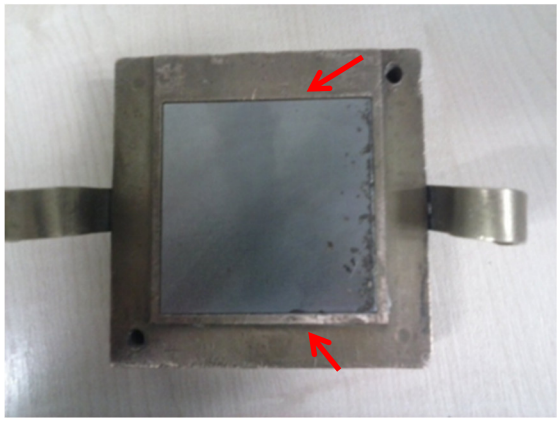

Figure 3-1. Steel block in the bottom half of the shear box, arrows indicating the edges where the cement block can be snagged

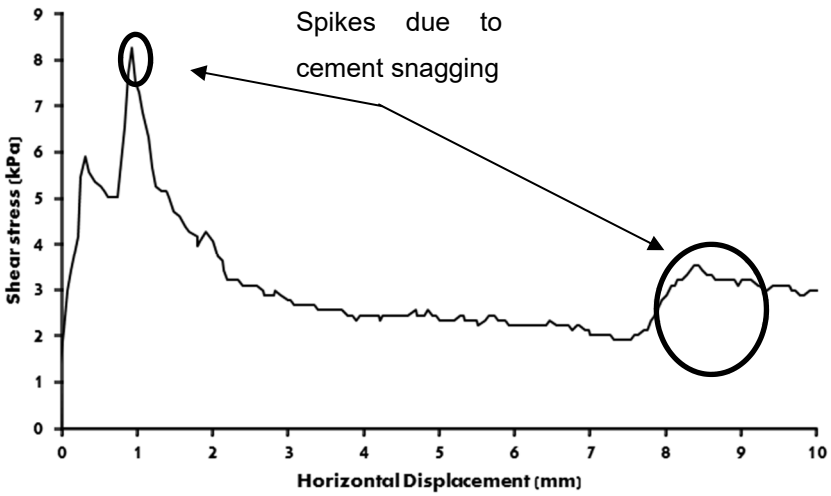

Figure 3-2. Shear stress vs horizontal displacement data for a cement – steel interface.. Spikes due to cement snagging are apparent

In order to resolve this problem, the shear box was modified such that the bottom half of the shear box was replaced by a steel block with the same width and thickness as the outer edges of the upper half of the shear box (Figure 3-3). The steel block had an interchangeable surface in order to use surfaces (foundation analogues) of different roughness. The length of the block was also increased to 95 mm, so that the cement sample placed on the top half was in contact with the steel surface throughout the test removing the need for area correction in the data analysis.

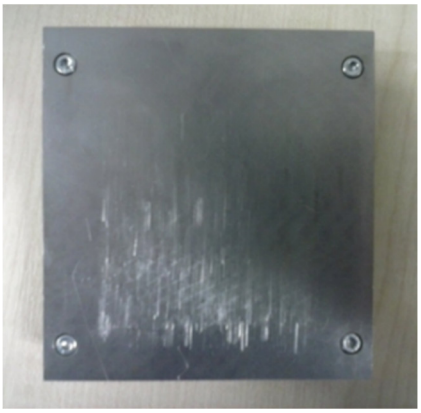

Figure 3-3. Steel block, used instead of bottom half of the shear box

Cement-steel interface tests were conducted at four normal stress levels (σ_v= 10, 50, 100 and 200 kPa) in order to investigate the change of the shearing behaviour with increasing normal stress. This range was selected as it covers

the anticipated average normal stress values applied to the foundation - seabed interface as mentioned in Chapter 2. It was also found that when the applied normal stress was over 200 kPa, the top half of the shear box was tilted during shear, thus affecting the results and limiting the normal stress capacity of the apparatus. The next stage of the direct shear box development was to modify the apparatus to accept small rock cores (rather than square cement rock analogues) or cylinder shaped samples (54 mm diameter and 27 mm high) and conduct real rock - steel interface testing in order to verify the initial findings using the cement rock analogues. Cutting perfect rectangular rock samples that could fit in the shear box (60 x 60 mm) was deemed impractical with the available equipment, therefore the alternative of using cylindrical samples obtained after coring was selected. A custom made fitting was fabricated and placed in the top half of the split box to allow the accommodation of disc shaped samples (Figure 3-4). The fitting consisted of a rectangular brass piece (60 x 60 mm) with a cylindrical (54 mm diameter plus tolerance to allow the sample to move up and down) hole in the center and was attached to the upper part of the split box using screws. Exactly the same procedure, as described before was used to carry out these interface tests apart from the normal stress levels that were changed to 16, 79, 159 and 316 kPa in order to investigate a wider stress level range.

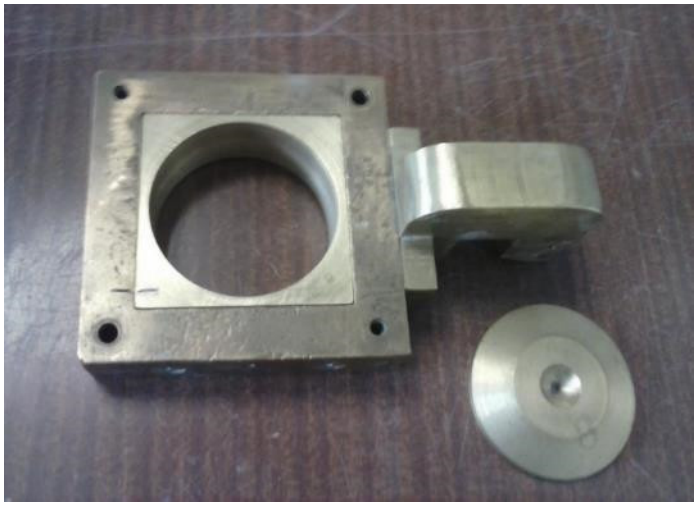

Figure 3-4. Fitting assembly used to accommodate cylindrical samples for shear box testing

However, the following potential source of error was still present and not possible to eliminate due to the solid – solid nature of the test. The rock disc sample is free to move in the upper half of the split box (~0.5 mm clearance between the side walls and the sample), in order to allow vertical displacement, however during testing the rock sample is inevitably in contact with one side of the split box. When this happens, a proportion of the normal stress applied to the sample is transferred to the split box through sidewall friction (rock – brass interface), therefore the actual normal stress at the interface may be lower with the potential to interfere with vertical displacement. This problem may be mitigated by lubricating the interface between the rock side and the split box but the lubricant might transfer to the rock – steel interface during testing, influencing the accuracy of the results. The same principles apply to the shear box tests using soil samples, however in that case only a very thin layer of sand is in contact with the side walls of the split box, whereas the rest of the soil mass is free to deform under the effect of the applied normal and the shear deformation. Therefore, the effect of the side wall friction is much smaller for tests using soil samples compared to solid-solid tests.

3.2.2 Tilt table

The tilt table test is commonly used to determine the basic friction angle φ_b of rocks, therefore a tilt table from Controls Group with overall dimensions (265 x 170 x 260 mm) was utilised to define the basic friction angle of the various rock types tested. The apparatus consists of a tilting plane, a gauge for angular measurement and a locking arrangement to fix the final table position (Figure 3-5). This test offers a quick and inexpensive way for primary assessment of the interface shear strength without the need of specialist equipment.

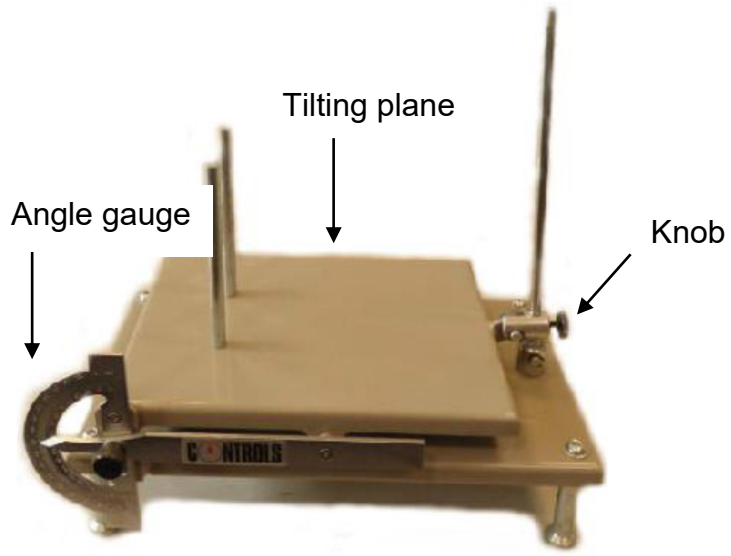

Figure 3-5. Tilt table apparatus

The basic friction angle φ_b of rock is a parameter used to assess the shearing resistance of discontinuities and refers to planar dry and fresh surfaces. The basic principal of the test is to place two saw cut rock samples, one on top of the other on a horizontal plane. The bottom sample is fixed against sliding and then the plane is tilted slowly within a 0-50^o range, until the top sample slides over the lower sample. As soon as this occurs, the inclined plane is locked (via the locking screw) and angle of the plane to the horizontal is calculated by subtracting the reading of the angle gauge from 90^o. There are various techniques for the execution of the test, depending on the type of the samples (number, shape, size etc.), (Alejano et. al, 2012). For the tests undertaken in this project (taking into account the shape and size of the available rock samples) disc shaped samples were normally used of 54 mm diameter and 27 mm height.

Irrespective of the effort put into saw cutting perfectly flat sample surfaces, there is still a chance that minor irregularities will be present on the surface. This means that the actual contact area of the two samples is smaller than the optimum and may result in rotation of the top sample relative to the lower one (Alejano et al., 2012, Figure 3-6). When this happens, the test is repeated and the reading of the φ_b is not taken into account, as failure does not occur due to uniform shearing. A human errors during the test (e.g. misreading of angle

gauge) or variation in inclination rate might affect the accuracy of the results, each test was repeated three times and the average value was selected as φ_b (according to USBR 6258).

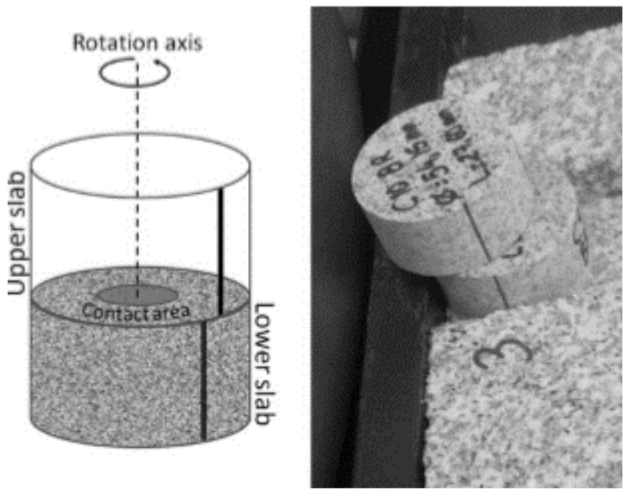

Figure 3-6. Rotational failure during a tilt test (after Alejano et al., 2012)

Apart from the conventional basic friction angle determination test (Figure 3-7a), the tilt table can also be used to quickly asses the interface properties testing of various interfaces at low normal stress levels. For instance, Najjar et al. (2003), have tested shear resistance between pipeline materials and the supporting soils. Therefore, tilt table tests between rocks - steel interfaces were carried out by placing a steel plate on the moving plane with a rock sample placed on top (Figure 3-7b); and the results were compared to those found through the IST tests (introduced later) in order to evaluate the applicability of the tilt table test.

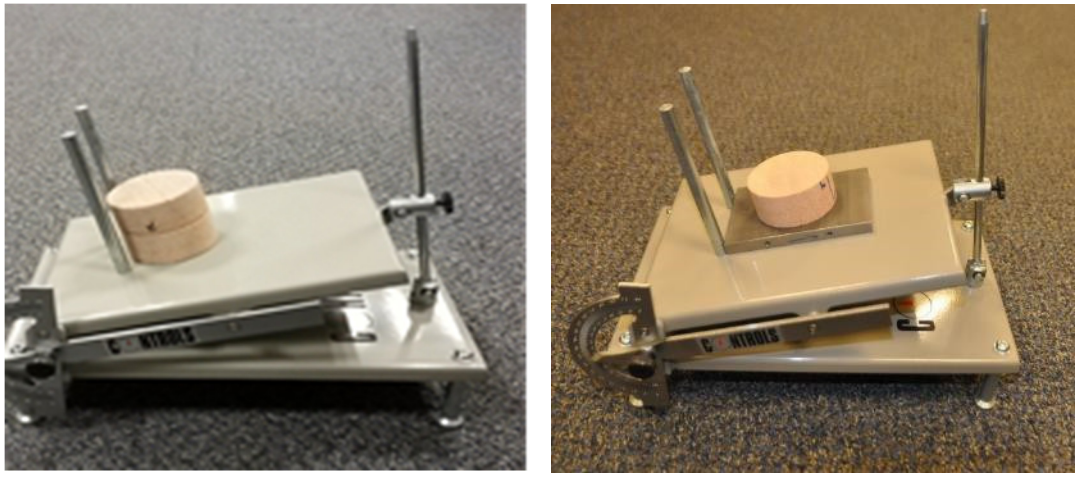

a B

Figure 3-7. (a) Basic friction angle test configuration (sandstone samples), (b) sandstone-steel interface test configuration

3.2.3 Interface Shear Tester (IST)

As mentioned previously, a series of modifications were applied to the conventional direct shear box which were designed to increase the accuracy and the reliability of the results from interface testing of rigid blocks, however some sources of error were still present. In order to mitigate the aforementioned weakness of the direct shear box, a bespoke computer controlled GDS interface shear tester device (IST) was purchased and utilised for the final stage of the laboratory testing plan (Figure 3-8a). The apparatus is designed to apply constant normal stress and continuous rotation to the interface under test and consists of an axial actuator at the top of the rig which can apply up to 5 kN of vertical load. Below the actuator is a combined load/torque cell arrangement with a capacity of 5 kN and 200 Nm respectively. At the base of the rig is a rotational actuation system capable of applying torque up to 200 Nm and rotating at rates up to 0.5 degrees/s. The upper axial actuator applies the normal load to the samples under test and is fixed against rotation, whereas the rotational actuator applies the torque from below. A special clamping system was developed in-house to allow rectangular interchangeable foundation interface elements (the same used for shear box testing) of 65 x 90 mm with a thickness of 8 mm to be clamped at the base of

the rig above the rotational actuator as well as cylindrical (54 mm diameter and 27 mm high) foundation elements to allow the performance of rock - steel and rock - concrete interface tests (Figure 3-8b). Similarly, below the upper load/torque cell a clamping device was developed to clamp short round rock samples (54mm diameter and 27 mm high). During the test, the rock sample was fixed in position whilst the foundation interface sample rotated at a predetermined rate. The GDSIST used here is an evolution of that previously used by Kuo et al. (2015) for the low stress interface testing of pipelines (referred to as the CAMTOR device). This previous device incorporated an outer pressure cell and allowed the testing of soil samples up to 70 mm in diameter and 20 mm thickness against steel elements and was used to simulate low effective stress pipeline interfaces.

The GDSIST has the capability to undertake computer controlled load and strain controlled tests, based either on axial or torsional actuator readings. The device can apply effectively infinite rotation deformation which can be used to simulate large strain events e.g. foundation sliding or the driving of a pile against rock to determine residual values of interface friction angle δ_{res}. During the tests torque and normal load were measured using a calibrated torque/load cell and vertical and rotational deformation measurements were internally provided by the stepper motor counts.

The tests were conducted under constant normal load (CNL) conditions as per shear box tests. Four different normal stress levels similar to those used in the shear box testing of 16, 79, 159 and 316 kPa were used in all tests and samples were generally tested dry and not submerged. Tests using both dry and saturated samples were carried out (not submerged and submerged respectively) exclusively for Chalk samples as the moisture content significantly affects Chalk's mechanical properties (Matthews and Clayton, 1993). Two additional stress levels (700 and 1000 kPa) were also used for Chalk testing, to investigate the crushability of Chalk at increasing normal stress.

The steps for a typical IST test are outlined below.

1. Prepare test specimens (rock and steel or concrete)
2. Saturate the cores if required (only for Chalk samples)
3. Place the steel or concrete sample on the rotating clamp at the base of the rig.
4. Place the rock cylinder in the upper holding clamp ensuring good horizontal alignment with the lower interface.
5. The two testing surfaces are then brought into contact and the required normal stress is applied automatically through the GDSLAB software.
6. The target total rotational strain was set at the start of the test with tests undertaken to a typical equivalent horizontal displacement of 10 mm at a constant rotational speed of 0.02 degrees/s, which corresponds to a linear displacement rate of approximately 0.005 mm/s. Automated sampling of normal load, torque, radial deformation, normal deformation, time since start of test was undertaken at 1 second intervals and written to a spreadsheet on an adjacent PC.

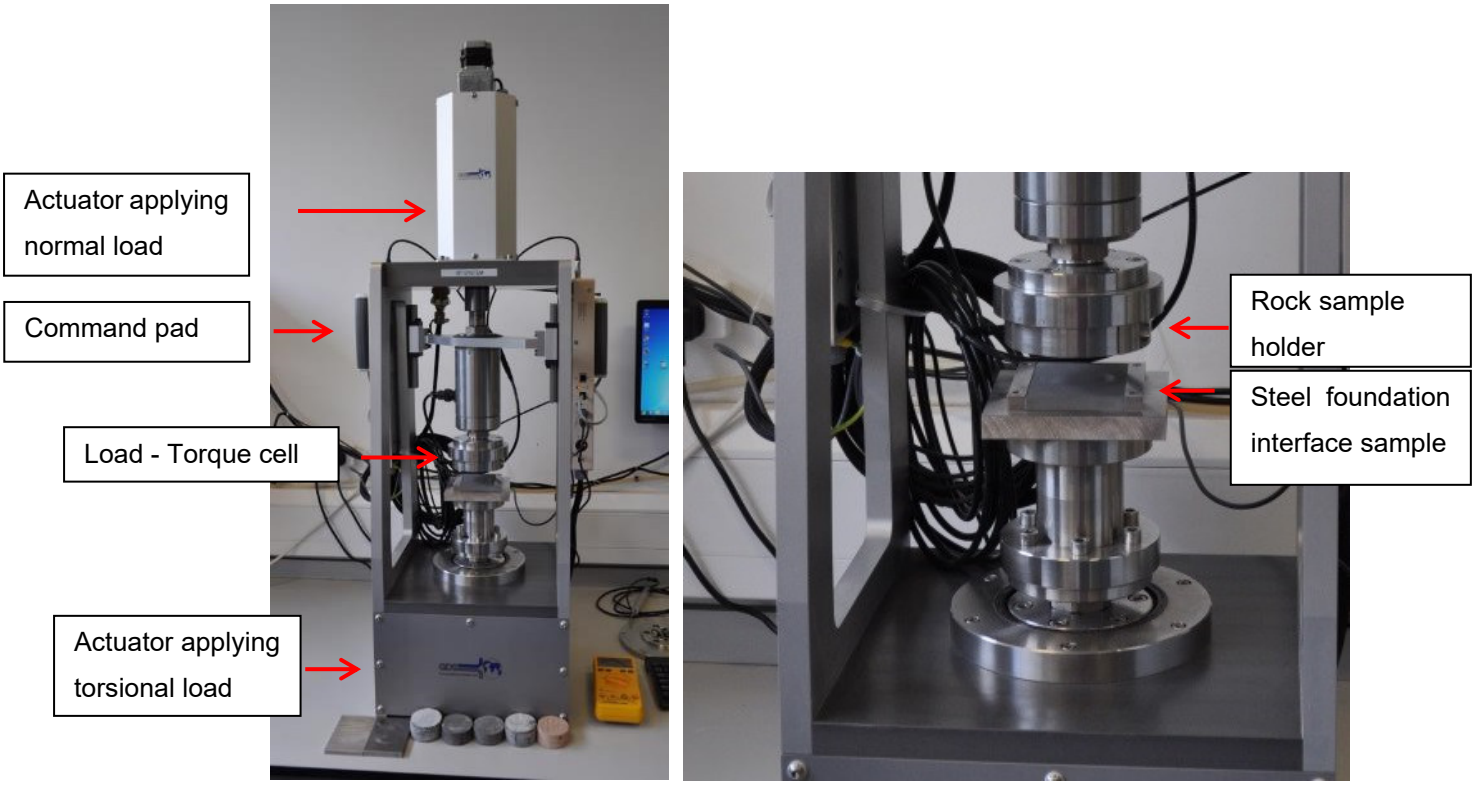

Figure 3-8. (a) Photograph of the Interface Shear Tester, (b) detailed view of the Interface Shear Tester sample mounting arrangement

Determination of shear stress and displacement from IST results

The torque measured during IST testing was converted to average shear stress as per Equation 3-1 as per Saada and Townsend (1981) for ring shear testing assuming uniform distribution of shear stress. Annular samples could have potentially been used, however it was decided to use disc shaped samples (as for the shear box tests) for consistency.

$$\tau = \frac{T}{\int_0^r 2\pi R^2 dR} = \frac{3}{2\pi r^3} T$$ Equation 3-1

Where:

τ = average shear stress

T = applied torque

r = rock sample radius

The radial deformation is converted to a linear displacement at a reference point considered at a distance equal to half of the radius length from the centre of the sample using Equation 3-2.

$$d = \theta \frac{r\pi}{360}$$ Equation 3-2

Where:

d = linear displacement

θ = measured rotational displacement

r = rock sample radius

IST testing simulating the presence of seabed sediment between interfaces

As mentioned earlier, the seabed sediment over the underlying rock may be washed out due to local conditions (e.g. high velocity water currents) at the areas of interest (Small et al., 2014), leaving exposed seabed as a foundation surface. However, a small amount of sediment might still be present on the seabed, in between the foundation surface and the footing. In order to evaluate

its effect on the sliding resistance of the foundation, all the rock - steel interface tests were repeated with the presence of a sediment layer in between the foundation and the seabed analogue. Rock – concrete interface tests with the presence of a sediment layer were not carried out due to time limitations. A layer of HST 95 sand was prepared to simulate the sediment at every test. This is a common test sand used at the University of Dundee and its properties are described in detail by Lauder (2011).The layer was “prepared in an attempt to consist of a single grain thickness” in order to avoid the generation of side friction due to the sample “sinking” into the sand during shearing and evaluate only the interface shearing behaviour of the interacting materials. After a number of trials, it was found that the spreading of 0.5 grams of sand on top of the foundation analogue using a small spatula created a single grain thick sand layer and constituted a time efficient and repeatable procedure. Figure 3-9 shows a steel foundation analogue with the sand layer on top, the area that is not covered in sand is not in contact with the rock sample and consequently does not affect the test results. Further information on the test sand is provided later in this chapter.

Figure 3-9. Foundation analogue with “single grain thick” sand layer, prior to testing

Saturated IST testing

All of the tests were conducted not submerged apart from those that involved Chalk samples and which were carried out both not submerged (using dry samples) and submerged (using saturated samples). In order to conduct testing of submerged and saturated interfaces, a custom made Polymethyl

methacrylate (PMMA, also known by the trade name perspex) box (bath) was manufactured and placed on top of the lower rotational actuator clamping system (Figure 3-10). The saturated rock sample was clamped using the top holder and the bath was filled with de aired and de-ionised water as quickly as possible, in order to prevent drying of the saturated sample.

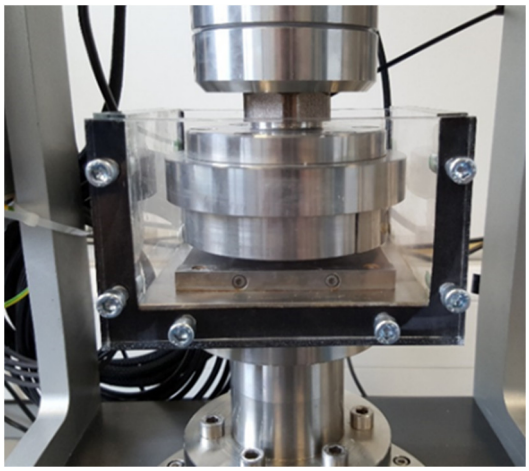

Figure 3-10. Detailed view of Perspex bath used for saturated testing

The interface was kept under constant normal stress before the initiation of shearing in order to allow the excess water pressure dissipation at the interface, for the same reason the shearing rate was kept low at 0.005 mm/s of equivalent horizontal displacement.

Dry density and saturation moisture content determination (BS 1377-2: 1990) of Chalk samples highlighted that the moisture content of the Chalk was below the 90% minimum level of saturation recommended for field identification procedures, therefore tests using both dry and saturated samples were carried out. Sample saturation (for Chalk samples) was achieved by applying 95 kPa vacuum to submerged (in de-aired/de-ionised water) samples for 24 hours. In order to ascertain the level of saturation, the moisture content after following the aforementioned process was compared to the saturation moisture content w_s=11.49 % of the Chalk (calculated according to BS 1377-2:1990) for three trial samples and very high levels of saturation were achieved as shown in Table 3-1.

Table 3-1. Level of saturation of Chalk samples

Saturation moisture content of Chalk, w_s=11.49%		
	Moisture content w (%)	Level of saturation (%)
Test sample 1	11.45	99.7
Test sample 2	11.47	99.8
Test sample 3	11.44	99.6

3.3 Rock samples

As it has been discussed in the literature review, tidal stream generators should be deployed at geographic locations that comply with specific conditions (i.e. strong water currents, no interference with ship routes, archelogy, sea life etc.). These areas around the UK have been identified in Chapter 2 and the predominant seabed geology has been identified.

Several different rock types have been identified, making it difficult to retrieve and test all these individual types during the project duration. Therefore, it was decided that the study should be limited to five rock types which were subjected to extensive laboratory investigation. Therefore, after taking into account the energy resource of each U.K. region, the mechanical properties of the various rocks and the ability to retrieve a significant amount of samples (enough to cover the needs of the testing); Sandstone, Flagstone, Andesite, Limestone and Chalk were selected.

Field trips to beach locations with exposed wave cut platforms and quarries in close proximity to the sea were carried out to retrieve the samples. Wave cut platforms may also offer an opportunity to identify any issues complicating the deployment of gravity based foundations but the recovery of representative samples for laboratory testing is generally difficult in-situ (many locations are considered sites of special scientific interest (SSSI) or outstanding natural beauty where sample recovery is prohibited). In addition, larger samples could be recovered from quarries for laboratory testing and they also allow comparison between UCS in fresh rock samples and those exposed to repeated wetting and drying in a beach environment. Quarries were visited to collect samples of rock types related to or from the same sequences as those

found at the coastline. These quarries were selected to be as close as possible to the wave cut platforms.

3.3.1 Sandstone

Sandstone is one of the predominant rock types found at Pentland Firth Region U.K., which represents 61% of the total UK tidal resource (Carbon Trust, 2005, Variability of UK Marine Resources). Therefore, it was decided to visit John O' Groats and Caithness, in order to collect rock samples for lab testing and to become more familiar with the environmental and geological conditions (onshore only) occurring at places with high tidal energy resource potential.

Sandstone blocks were retrieved from a disused quarry (Figure 3-11) approximately 3.5 km south of John O' Groats (ND37150 70138, off A99). Blocks with rough dimensions of 250 x 150 x 100 mm (although not perfectly rectangular) were selected, as they were relatively easy to carry and most importantly, competent enough to obtain cores appropriate for testing.

Figure 3-11. Disused sandstone quarry (ND37150 70138), near John O' Groats

A sandstone wave cut platform at a beach located 200m north east of John O' Groats (ND38299 73382) and 3.4 km north north east of the quarry was also visited during the field trip. The obvious dip of the rock has led to fronts of stratigraphy in the wave cut platform that give rise to a saw-blade type structure with a leading edge and an inclined shielded zone (Figure 3-12). The leading edges were repeated at an approximately cyclic separation of 5.5m.

a b

Figure 3-12. Wave cut platform at John O' Groats, repeating stratigraphy leading edges in the sandstone strata can be seen (ND38299 73382). The Island of Stroma is visible on the horizon (subfigure a)

The sandstone found in the region is characterised as Old Red Sandstone and is generally medium grained (British Geological Survey, 1989). The colour ranges between yellow (first disused quarry) and bright brick-red (John O' Groats beach) depending on the level of the rock sequence (Geological Survey of Scotland, 1914). In the field it was slightly weathered (grade 1) characterised as medium strong (after BS 5930:2015). Figure 3-13 shows a Sandstone block after coring (a) and a typical Sandstone sample appropriate for interface testing (b).

a b

Figure 3-13. (a) Sandstone block after coring, (b) typical Old Red Sandstone sample.

It should be noted here that the descriptions and strength characterisations of the rocks presented in this thesis were made according to BS 5930:2015.

3.3.2 Flagstone

During the same field trip, a second wave cut platform was visited. It was just North of Castletown, ND19305 68858 (Figure 3-14a), where Caithness Flagstone is present. In contrast to the previous beach, the distance between the consequent saw tooth leading edges varied between 3m and 7m and the dip ranged between 5° and 7°. To collect samples similar to the Caithness Flagstones identified in the wave cut platform at Castletown, Achscrabster (ND07829 63333) an active Caithness Flagstone quarry was used (Figure 3-14b) which is situated 12.7km to the south west of Castletown. Other inland quarries are present closer to Castletown but these have been inactive for many years resulting in significant weathering making them unsuitable for sampling. Slabs with typical dimensions of 350 x 200 x 50 mm were collected. The Flagstones are generally laminated and are not easy to obtain at greater thickness, making the extraction of cores for UCS testing in the laboratory impossible.

a b

Figure 3-14. (a) Caithness Flagstone wave cut platform at Castletown (ND19305 68858), UK. Line displays saw-blade type structure, (b) Achscrabster Caithness flagstone quarry (ND07829 63333)

Caithness Flagstones are laminated siltstones and mudstones and their colour ranges from dark blue-grey to very pale greenish (Geological Survey of

Scotland, 1914). The rock samples collected from the quarry were fine grained; dark-grey in colour and fresh since the rock exposure is renewed regularly (active quarry). In-situ strength assessment classified the rock as strong (BS 5930:2015). On the other hand, the rocks at Castletown (wave cut platform and beach deposits) had a lighter blue-grey colour possibly due to weathering. A typical Caithness flagstone used for various stages of interface testing is shown in the following figure.

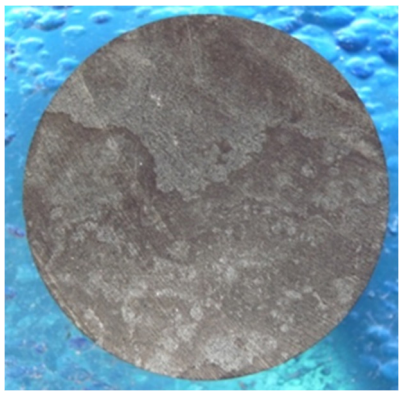

Figure 3-15. Typical Caithness Flagstone sample

3.3.3 Limestone

The broader region of Dunbar was visited in order to collect Limestone samples. This area does not represent a site for potential tidal stream generation but was visited as it was felt that the exposed Llimestone and nearby quarry represented a rock type that may be encountered at a tidal stream locations in the future. A wave cut platform at Barn Ness (close to Dunbar, south east Scotland, NT71693 77366) was visited. The geology comprised sedimentary rocks, with sequences of Sandstones, Mudstones and Carboniferous Limestones exposed in the wave cut platform. These consisted of Middle Skateraw and Lower Skateraw Limestone (Figure 3-16a) which were grey and grey-brown in colour and fossiliferous in places with brachiopods and crinoids (British Regional Geology 1971).

Just 2km south east of Barn Ness wave cut platform lies a large active Limestone quarry. This was used to collect Middle Skateraw Limestone samples. A fine grained, grey coloured Carboniferous Limestone from the Lower Limestone Group is quarried there (British Regional Geology 1971).

The exposures were fresh and the in-situ UCS estimation fell in very strong class (BS 5930:2015). The research team was only allowed in under escort for a short period of time due to blasting schedule which allowed only limited inspection of the in-situ setting. Figure 3-16b shows a typical sample after coring.

a b

Figure 3-16. (a) Lower Skateraw Limestone formations at Dunbar wave cut platform, (b) Middle Skateraw Limestone sample

3.3.4 Andesite

As with Limestone, an additional quarry (not associated with wave cut platforms) was also visited to collect samples of an igneous rock type to make the study more generally applicable. Therefore, Ardownie quarry located 8 km north east of Dundee (NO48752 33934) was used to retrieve Andesite blocks. The quarry lies in the igneous Ochil volcanic formation, formed approximately 398 to 416 million years ago in the Devonian Period (BGS website). This is a fine grained, fresh, very strong dark grey coloured igneous rock as can be seen in Figure 3-17.

Figure 3-17. Andesite sample

3.3.5 Chalk

Chalk is the last type of rock that was retrieved. In areas in the south of the U.K. that have been identified as of significant tidal stream potential (e.g. Race of Aldernay and Casquets, which represent around 6% of the total UK tidal resource, Carbon Trust, 2005), the seabed may consist of Chalk. Chalk is a rock with extraordinary characteristics (Lord et al., 2002) and may also be encountered at areas where driven pile solutions for offshore wind applications could be considered.

The samples were collected from the active Imerys Mineral Limited's Quarry, Westwood, Beverley, HU17 8RQ, UK (501740, 438256). Blocks of Chalk typically 350 by 300 by 280 mm were obtained directly after quarrying and prior to crushing for use in the chemical industry. Unfortunately due the working status of the quarry and the required health and safety regulations, the research team were not directly involved with the sampling of the Chalk thus making it difficult to comment on the structural setting of the Chalk in-situ. The Chalk is White Chalk from the Flamborough Chalk Formation (Upper Chalk unit, Northern province English Chalk) referred to informally as the Flamborough Sponge Bed (Lord et al., 2002, Whitham, 1991 & 1993). This source of material was selected due to the fresh nature of the Chalk (i.e. recently quarried, immediately placed under cover) and the fact that the Chalk was free from flints that may interfere with characterisation and interface testing.

The Chalk was characterised using both field and laboratory techniques prior to interface shear testing and the results are summarised in Table 3-2. These results classify the Chalk as of very high density according to CIRIA 574 (Lord et al., 2002). The Chalk on return to the laboratory had a very low moisture content of 0.3%. Dry density and saturation moisture content determination (BS 1377-2: 1990) highlighted that the moisture content of the Chalk was below the 90% minimum level of saturation recommended for field identification procedures so the Chalk was saturated prior to these tests by applying 95 kPa vacuum to submerged samples. Samples were also dried in order to investigate the effect of moisture content on the unconfined compressive strength (UCS), tensile strength and interface shear resistance behaviour.

Table 3-2. Summary of key Index properties for the Chalk samples

Property	Chalk
Dry density, ρ_d (Mg/m^3)	2.06
Porosity, n (%)	23
Voids ratio, e	0.3
Saturated moisture content, m_{sat} (%)	11.4
Specific gravity, G_s	2.7
UCS, dry samples (MPa)	30.00
UCS, saturated samples (MPa)	9.30
Tensile strength, T_0, dry samples (MPa)	1.10
Tensile strength, T_0, saturated samples (MPa)	0.96
Young's Modulus, dry samples (GPa)	8.60
Young's Modulus, saturated samples (GPa)	2.85

The stress strain curve from a UCS test on a dry Chalk sample is shown in Figure 3-18.

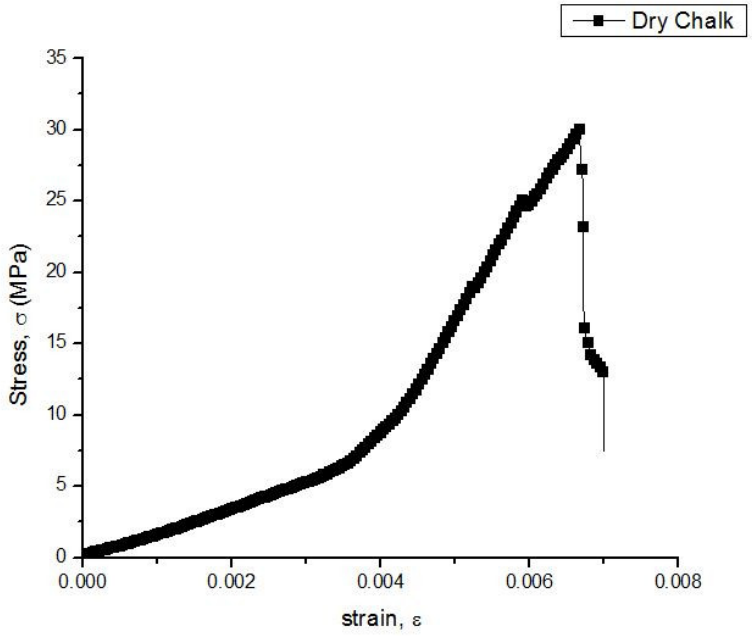

Figure 3-18. Stress vs strain curve from a UCS test on a dry Chalk sample

3.3.6 In-situ determination of UCS for rock samples

The Schmidt hammer rebound number (N), using an L-type Schmidt hammer, was recorded during the field visits, in order to estimate the Uniaxial Compressive Strength (UCS) of the rock exposures in-situ. It should be noted that due to operational restraints (e.g. ongoing blasting at quarries), the rebound number was not recorded in-situ for some of the rocks (e.g. Andesite and Chalk). The L-type hammer contains a spring with 0.735 Nm impact energy and the measurements were taken following the procedure described in the following.

At each test location, the surface was cleaned and any loose rock fragments were scaled off. An approximately square grid of 20 points with separation of 40 mm was created and a rebound number was recorded at every point (Figure 3-19). Every reading was corrected for the inclination of the hammer relatively to the horizontal after Basu and Aydin (2004). According to the International Society of Rock Mechanics (ISRM) revised version 2009, the rebound number N is obtained by averaging the 20 recorded values in total

(Aydin 2009) and not limiting readings to the 10 higher values, as suggested by Brown (1981).

a b

Figure 3-19. In-situ recording of the rebound hardness number (N) using an L-type Schmidt Hammer. (a) Caithness Flagstone (ND07829 63333), (b) John O'Groats Sandstone (ND37150 70138)

In the literature many correlations between N and UCS are available, but taking into account the rock types used for the creation of these correlations as well as the coefficient of determination R^2 for every relationship, the relationship proposed by Kilic and Teymen (2008) was selected in order to estimate the UCS. Equation 3-3 was established based upon the comprehensive testing of 19 different rock types ($R^2 = 0.94$).

$$UCS = 0.0137*N^{2.2721}$$

Equation 3-3

The following table summarises the in-situ determined UCS values for Sandstone, Flagstone and Limestone samples at the different locations visited (i.e. wavecut platforms and quarries).

Table 3-3. UCS determined in-situ at visited locations.

Rock type	Location	UCS (MPa) after Kilic and Teymen (2008)
Old Red Sandstone	John O' Groats Quarry (Disused)	82.2
Old Red Sandstone	John O' Groats wave cut platform	86.3
Catithness Flagstone	Achscrabster Quarry (Active)	157.2
Caithness Flagstone	Castletown wave cut platform	110.0
Middle Skateraw Limestone	Dunbar Quarry (Active)	115.8
Middle Skateraw Limestone	Barn Ness wave cut platform	45.0

3.3.7 Determination of UCS in the laboratory

The rebound hardness number is a useful non-destructive method to estimate the UCS in the field, however, destructive tests should also be carried out to get more accurate results for research purposes.

Unconfined compression (direct method) UCS can be directly and accurately determined by the unconfined compression test, which consists of the crushing of rock cylinders under constant strain rate without any lateral confinement. According to ISRM, the cylinder should have height to diameter ratio equal to 2. For this research, 54 mm diameter samples were used, therefore 108 mm high samples were needed. Due to the inconvenient dimensions of the rock blocks of some of the rock types that were retrieved (not thick enough), cores appropriate for crushing were only obtained from Sandstone and Chalk samples. Three tests were carried out for both rock types using dry samples, whereas saturated Chalk samples were also crushed, since the mechanical properties of Chalk can vary significantly with moisture content. The arithmetic average of the three tests was specified as UCS and the results are listed in the next table.

Table 3-4. UCS values obtained from unconfined compression test (direct method).

Rock type	UCS (MPa)	
	Dry sample	Saturated sample
Old Red Sandstone	31.5	-
Chalk	30.0	9.3

It is quite common in rock mechanics, to correlate the tensile strength to UCS. Tensile strength is the maximum tensile stress the rock material can withstand. The most common tensile strength determination in the lab is by conducting the Brazilian test. The Brazilian test is an indirect method of tensile strength measurement, but is widely used because is much easier than conducting a direct pull uniaxial test.

In the Brazilian test, disc shaped specimens, are loaded in compression across their diameter. This loading generates tensile stresses perpendicular to the loading, in the plane of the disc face (Figure 3-20a).

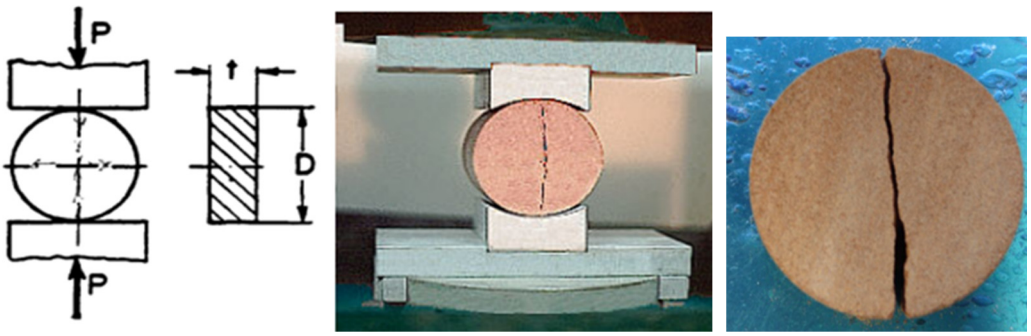

a b

Figure 3-20. (a) Principles of Brazilian test, (b) sandstone disc after failure where tensile cracking is apparent

Apparent tensile strength is calculated by Equation 3-4.

$$T = \frac{2P}{\pi t D}$$ Equation 3-4

Where:

T is tensile strength, *P* is maximum compressive load, *D* is diameter and *t* is the thickness of test specimen.

Equation 3-5 was used to correlate tensile strength to UCS and was proposed by Altindag and Guney (2010), after analysing raw experimental data from various rock types, found in the literature.

$$UCS = 12.308TS^{1.0725} \quad \text{Equation 3-5}$$

Three tests per rock type were carried out and the mean value was used to calculate UCS after Equation 3-5. The results are summarised in Table 3-5. Where available, compressive strength values obtained from the direct unconfined compressive (UCS) test were used in the analysis. Otherwise, compressive strength values obtained from the Brazilian test were considered.

Table 3-5. UCS values obtained from Brazilian test.

Rock type	Tensile strength (MPa)	UCS (MPa) after Altindag and Guney (2010)	Classification after BS 5930:2015
Sandstone	2.60	34.30	Medium strong
Flagstone	10.00	145.15	Very strong
Limestone	10.80	157.95	Very strong
Andesite	13.00	192.75	Very strong
Chalk (dry)	1.10	13.65	Weak
Chalk (sat)	0.96	11.80	Weak

3.4 Materials and preparation techniques

3.4.1 Cement mortar

Portland cement (PC) CEM I 52.5N conforming to BS EN 197-1:2011, was used to produce cement mortar samples with controlled UCS that were used as rock analogues. Potable water and PC were mixed in a Hobart mixer for 90 seconds and then cast in 60 x 60 mm moulds in order to fit in the direct shear

box (Figure 3-21). Each mould can accommodate four samples and two moulds we manufactured in order to increase the sample production. The mould was filled up to a height of 20 mm, vibration was applied for 10 seconds and the samples were then covered by a damp cloth for 24 hours. Demoulding took place after 24 hours and the samples that needed further curing (depending on the desired strength, Figure 3-22) were then put into a water bath at 20 ± 2 ^{o}C for two days. The mortar surface that was in contact with the bottom steel plate of the mould was used for testing, since it was more controllable. In addition, menisci were formed at the opposite side of the mortar samples (top surface in contact with air), due to surface tension. The menisci had to be removed and a surface parallel to the one tested had to be created in order to assure vertical application of the normal load on the sample. Therefore, each sample was lapped on a lapping (or grinding) table for approximately 90 seconds to remove the menisci.

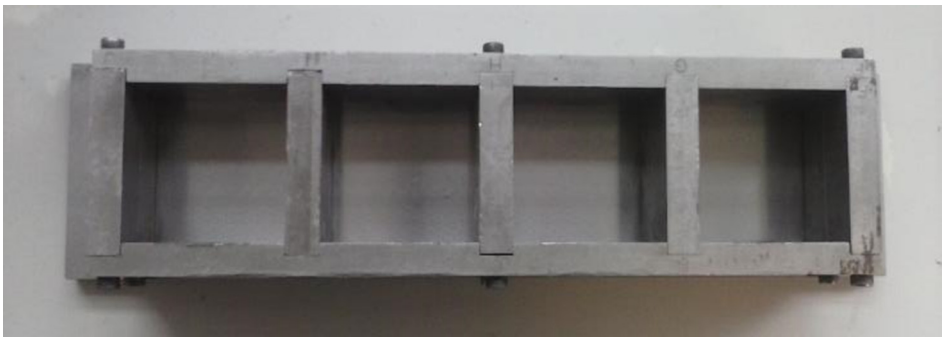

Figure 3-21. Mould used for preparation of rock analogues

By changing the water – cement ratio and the curing time as shown in Figure 3-22, compressive strengths of 15 MPa (weak rock equivalent), 35 MPa (medium strong rock equivalent) and 65 MPa (strong rock equivalent) were achieved. The strength characterisation of the samples (weak, medium strong and strong) is made according to BS 5930:2015.

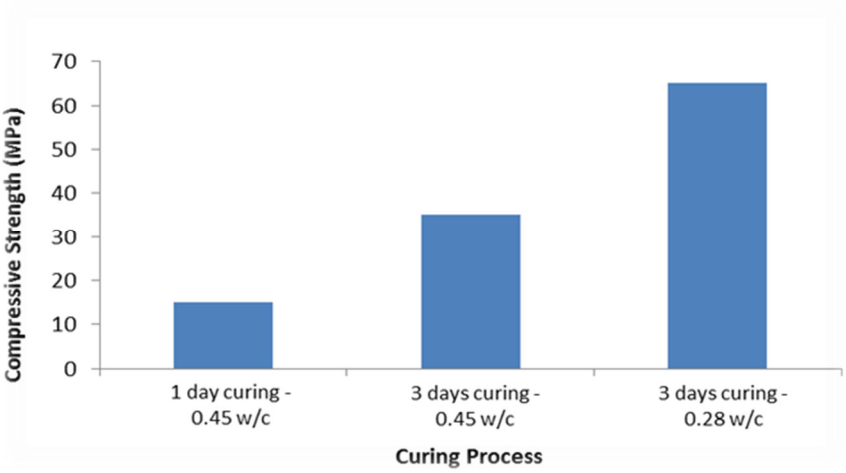

Figure 3-22. Variation of unconfined compressive strength of cement mortar samples with respect to preparation and curing process

The surface roughness of each sample was determined prior to testing (further details later in the chapter). The controlled conditions of the preparation process resulted in very similar and repeatable surfaces and no noticeable variation was recorded between the samples. Therefore a representative R_a value of 2.4 μm was used for the analysis. A typical sample is shown in Figure 3-23.

Figure 3-23. Mortar sample used as rock analogue

3.4.2 Steel

Mild steel was used to prepare rectangular (65 x 95 mm) plates that represented foundation analogues for the three stages of interface testing. As discussed in Chapter 2, roughness has a major effect on the interface

behaviour, therefore different preparation techniques (polishing, machining) were applied and resulted in a wide range of surface roughness, whereas an average centreline roughness of R_a = 2.4 μm was obtained for untreated mild steel.

Polishing with a surface grinder using a BAA60 – K7V wheel resulted in an average surface roughness R_a= 0.4 μm. This was used as the lowest benchmark of roughness since it was the smoothest surface tested. In practice is quite unlikely that a steel footing will be polished before placing on the seabed (i.e. R_a will not be lower than 2.4 microns). However, using such a low value in testing allowed greater understanding and evaluation of roughness' effect on shear behaviour over a wider range.

The aforementioned preparation techniques could reproduce only a single roughness value, therefore the "shaping" technique capable of creating a wider range was utilised. A shaper is a type of machine tool that uses linear relative motion between the workpiece and a single-point cutting tool to machine a linear toolpath. Its cut is analogous to that of a lathe, except that it is linear instead of rotational. The machine allows the shaper tool to travel forward at a constant predetermined length each time (step), while it is grooving the steel surface in a direction perpendicular to the direction of travel. By changing the position of the shaping tool relevant to the plane of the steel plate (i.e. vertical distance) and the step of forward travel, uniform surfaces with different R_a values of 7.2 and 34 μm were created. These surfaces are referred to as machined in the following.

All the different types of foundation analogues used for testing are shown in Figure 3-24.

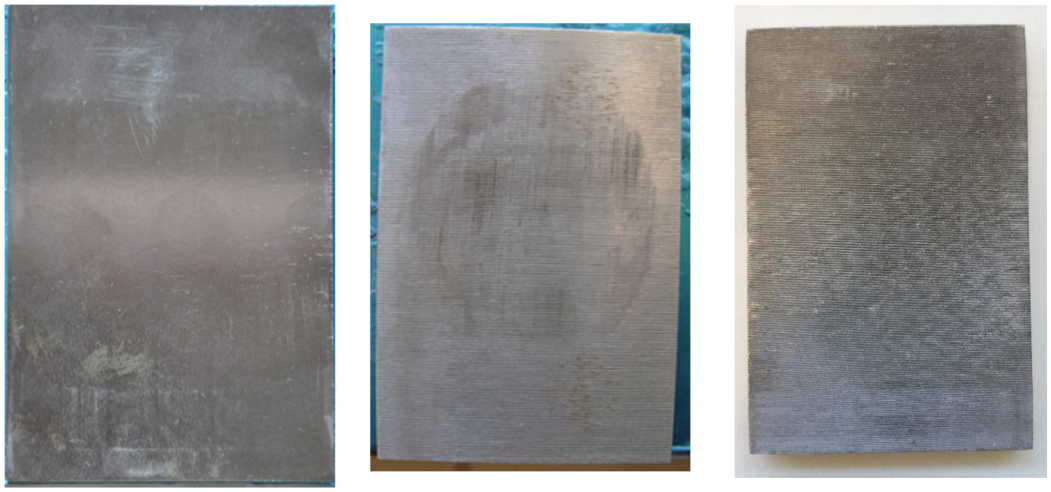

a b c

Figure 3-24. (a) polished R_a=0.4 μm, (b) machined R_a=7.2 μm, (c) machined R_a=34.0 μm

The surface roughness of each plate was characterised before testing and R_a and R_t were recorded, following the process that is described later in this chapter. All the recorded values are listed in Table 3-6.

Table 3-6. Surface properties of steel plates

Type of steel plate	Roughness average R_a (μm)		Maximum profile height R_t (μm)	
	Parallel to shearing direction	Perpendicular to shearing direction	Parallel to shearing direction	Parallel to shearing direction
Polished	0.4	0.4	2.9	3.5
Machined	7.2	1.4	34.2	13.8
Machined	34.0	5.2	131.5	32.9

3.4.3 Concrete

Concrete cylinders were cast into moulds of 300 mm height and 150 mm diameter (Figure 3-25a). The cylinders were then sub-cored and saw cut (details later in the chapter) in order to obtain disc shaped samples (54 mm diameter, Figure 3-25b) appropriate for IST testing. The aim was to prepare a C60 mix in order to comply with the recommendations for offshore concrete

structures found in the literature (Sandvik et al., 2004). The mix proportions are listed in Table 3-7.

a b

Figure 3-25. (a) mould used to cast concrete cylinders, (b) concrete disc used for interface testing

Table 3-7. Concrete mix proportions

	Cement	Water	Coarse Aggregates			
			Sand	10 mm	20 mm	Total
	w/c = 0.50					
kg per m^3	370	185	925	890	-	2370

Slump = 130mm

Considering the plan dimensions of the disc samples it was decided to use a maximum of 10 mm aggregates in order to avoid any possible interference on the interface properties in case an aggregate was exposed during saw cutting. UCS was determined by crushing 100 x 100 mm cubes using a hydraulic crusher, three specimens were tested each time and the average was calculated; all the values are concentrated in Table 3-8.

Table 3-8. UCS of concrete samples

Days of curing	Cement UCS (MPa)
7	46.45
28	61.50

3.4.4 Sand

As mentioned earlier, the sediment is expected to be washed out at areas where the tidal stream generators will be placed (Small et al., 2014), however a thin layer of HST 95 sand was placed on top of the foundation analogue in series of interface tests in order to simulate the case of remaining seabed sediment. This is a fine silica sand with rounded particles and has been extensively used by researchers at the University of Dundee (Lauder 2011, Jeffrey 2012), detailed properties determined by Lauder (2010) are listed in Table 3-9.

Table 3-9. Physical properties of HST 95 sand

Soil Property	HST 95
d_{10} (mm)	0.1
d_{30} (mm)	0.12
d_{60} (mm)	0.14
G_s	2.63
γ_{max} (kN/m^3)	1760
γ_{min} (kN/m^3)	1461
e_{max}	0.769
e_{min}	0.467
φ_{crit}	32°
δ_{crit}	24°
Shape	Rounded

3.4.5 Coring and saw cutting of rock and concrete samples

Rock and concrete samples had to undergo a specific process in order to be suitable for interface testing. This process involved coring and saw cutting. The rock blocks (retrieved from field trips) were initially cored using a HILTI rock coring drill. A diamond core drill bit with internal diameter of 54 mm was used and since H/D ratio of 1:2 had to be achieved for testing, the cores were then cut to a 27 mm thickness, using a tile masonry saw.

a b

Figure 3-26. (a) rock coring drill, (b) tile masonry saw

3.5 Surface roughness characterisation

3.5.1 Methods of surface roughness measurement

Roughness parameters are typically measured by utilising profilometers. This is the most common surface measurement technique mentioned in the literature by various researchers (e.g. Deitz and Lings 2010, Iscimen and Frost 2010). Profilometers are separated into contact and non-contact, depending on their measuring mechanism. There is also a wide range of such devices, depending on their accuracy and the range of measurement.

For contact profilometers, the vertical movement of a diamond stylus recorded while it is pulled at a constant rate across the measured surface. An analogue signal is generated by the vertical position of the stylus, which is the converted into a digital format which can be further analysed and displayed. An example of using a profilometer in order to assess the influence of roughness in interface friction is as follows.

A stylus profilometer Taylor-Hobson Talysurf series 2 was used by, Staheli et al. (2006), Iscimen and Frost (2010), in order to determine the micro level surface roughness of various pipe materials.

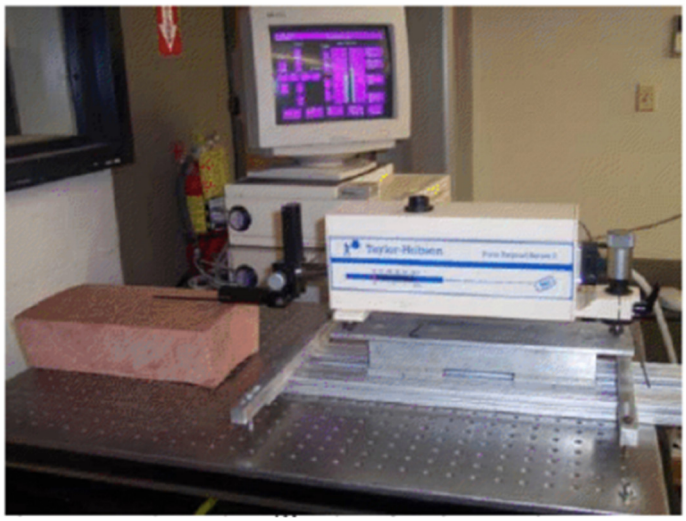

Figure 3-27. Taylor-Hobson Talysurf series 2 stylus profilometer (Source: Iscimen and Frost 2008)

In the example of Staheli et al., a sapphire ball (2 μm diameter) was placed at the tip of the stylus. During every test the stylus crossed 50 mm on the pipe and created a representing 2D surface profile. Stylus vertical position was recorded at specified length increments. A Profilometer's accuracy is affected by parameters such as the size of the stylus tip, the load on the stylus and any accidental perpendicular movement of the stylus.

In order to define the accuracy of the results, profile measurements occurred in six locations of each material and five times (very close proximity) for each location. In addition, one measurement at each location was repeated five times. Following this routine 54 tests were generated for each material.

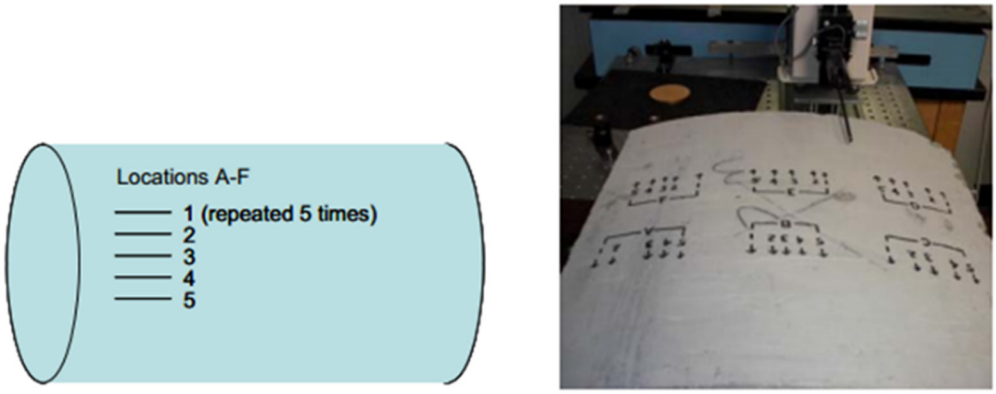

a b

Figure 3-28. (a) typical arrangement for pipe surface profile testing, (b) material during surface characterization, (Source: Staheli et al., 2006)

A non-contact method (Roland LPX-60, Figure 3-29) of laboratory determination of the various parameters that define a rock joint's roughness (peak frictional angle, JRC, dilation angle, asperity angle) has been used by Tam et al. in 2008. That is an automated 3D laser scanner that uses a spot-beam triangulation method and can be utilised to produce digital surface profiles for rock core surfaces.

Figure 3-29. Roland 3D Laser scanner at the University of Hong Kong (Source: Tam et. al, 2008)

Contact profilometers are cheaper than non-contact and do not require modelling. On the other hand, non-contact devices are faster, require less maintenance and are more reliable. In this project all of the tested surfaces are relatively uniform, therefore a contact stylus profilometer was selected and purchased.

A hand held Taylor Hobson Surtronic Duo stylus contact profilometer (Figure 3-30) was used to determine the average centreline roughness and the maximum profile height, R_a and R_t respectively. The range of measurement is 40 µm for R_a and 199 µm for R_t. The traverse length of each measurement is 5 mm with a rate 2 mm/s, allowing the repeat of many measurements (to increase the accuracy of the results) quickly. The accuracy of the device is 5% of the reading ± 0.1 µm and is considered acceptable for the scope of the project. Calibration of the device was carried out periodically against a standard roughness profile with R_a = 5.81 µm (supplied with the device).

Figure 3-30. Taylor Hobson Surtronic Duo stylus contact profilometer

3.5.2 Determination of roughness parameters

In order to determine representative surface parameters, five different positions on the square/rectangular (cement mortar and steel) samples were measured and the measurement was repeated three times at each position, resulting in 15 measurements per sample (Figure 3-31a). The round samples (rock and concrete) were measured at four different positions, three times at each position resulting in 12 measurements per sample (Figure 3-31b). For each sample the arithmetic average of all the measurements was considered as the representative value.

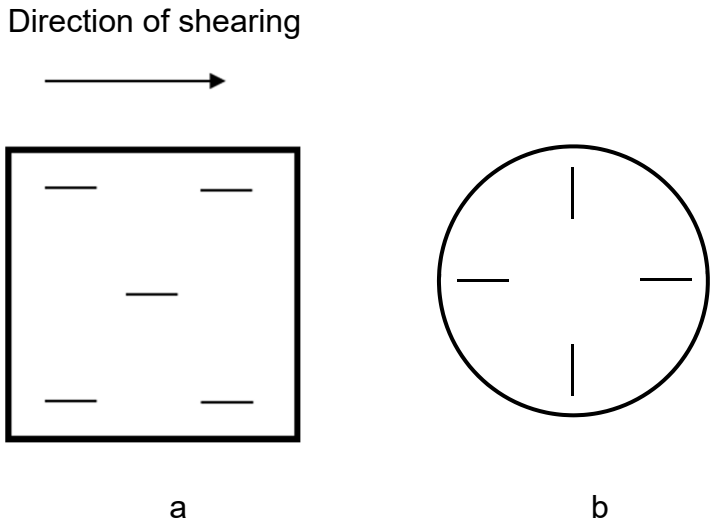

Figure 3-31. Measurement pattern used for (a) rock analogue and steel samples, (b) rock and concrete samples. The straight lines indicate the position of measurement.

3.6 Mohs hardness measurement

The scratch resistance of the test samples was determined by the Mohs hardness test. The test compares the scratch resistance of a sample compared to another reference sample of a known scratch resistance (Mohs value). For example if reference sample A scratches sample B, then specimen has higher Mohs value than sample B. If sample A cannot scratch sample B, then sample B has higher Mohs value than sample A. If two samples are of the same hardness, then it is difficult for a scratch to occur.

The test is performed on a smooth and free of scratches surface of the test sample B. The sample B is firmly held against the test table with one hand, and the other sample of known hardness (sample A) is held on the other hand. A pointy edge of sample A is firmly pressed and dragged along sample B. The surface of sample B is then examined to determine whether a scratch has been developed or not and the test is repeated to confirm the outcome. A steel file (Mohs = 7), a piece of glass (Mohs = 6), a copper penny (Mohs = 3) and a finger nail (Mohs = 2.5) were used as reference materials. The Mohs hardness values of the tested samples are listed in Table 3-10.

Table 3-10. Mohs hardness values of samples used for interface testing.

Material	Mohs Hardness
Sandstone	7
Flagstone	3
Andesite	6
Limestone	4.5
Chalk	2.5
Steel	4
Concrete	5

3.7 High level summary of testing undertaken

The procedures followed in order to obtain the data for the project were described thoroughly in this chapter. An overview of the test stages followed through the research is shown in Table 3-11.

Table 3-11. Summary of interface testing to be carried out

	Interface	Equipment	Varying parameters
Stage 1	cement mortar (rock analogue) vs steel (foundation analogue)	-Direct shear box	-UCS of cement mortar -normal stress -steel roughness
Stage 2	rock vs steel	-Direct shear box	-rock types –normal stress -steel roughness
Stage 3	-rock vs steel -rock vs steel with sand layer -concrete vs rock	-IST -Tilt table	-rock types -normal stress -steel roughness

Stage 1 consists of the interface testing of cement mortar samples against (rock analogue) steel samples (foundation analogues). These tests were carried out utilising the modified shear box described previously. The tests were carried out at normal stress levels of 10, 50, 100 and 200 kPa.

For Stage 2, the rock analogues were replaced by real rock samples. The rock samples were round instead of square (for the reasons described earlier in this chapter), the applied normal stress levels for the same applied normal load were increased to 16, 79, 159 and 316 kPa. These tests were also carried out using the modified shear box. The results from stages 1 and 2 are presented and discussed in Chapter 4 and were mainly used as indicators of the factors that affect the shearing behaviour of the interfaces and were further examined in Stage 3.

Stage 3 was carried out on the IST and constitutes the main part of the testing programme. Rock – steel (with and without the presence of sediment) and rock – concrete interface testing was carried out. Sandstone, Flagstone, Andesite and Limestone samples were tested dry against steel with three levels of roughness (with and without the presence of sand on the interface) and one type of concrete. Chalk samples were tested both dry and saturated against three types of steel and one type of concrete. The results of these tests are analysed in Chapters 5, 6 and 7. Tilt table tests were also carried on these interfaces to evaluate its applicability on the characterisation of interfaces at the early stage of design.

Chapter 4

4 Direct shear box interface testing

4.1 Introduction

An extensive three stage programme of interface testing was carried out throughout the project.

The first stage of the project aimed to identify the controlling parameters of solid - solid interface testing using the direct shear box to conduct rock analogue testing. The literature review revealed some potential controlling parameters (e.g. surface roughness and material strength), however this information did not refer to rock - steel interfaces, therefore further investigation was needed before focusing the laboratory programme on specific parameters and means of testing. In the second stage various rock types were used in order to generate values useful for the foundation design process and to confirm where possible the initial findings from rock analogue testing.

The interface shear tester (IST) was utilised in the third stage in order to tackle the issues and limitations of the shear box that were identified at the previous stages and to generate data useful for detailed analysis. This is described later in Chapters 5, 6 and 7.

Data derived from laboratory testing of various interface combinations were used to describe the shearing behaviour of rock - steel and rock - concrete interfaces. The effect of surface roughness, normal stress level, UCS/rock type was examined and their influence on shear strength (peak and ultimate interface friction angle) and shear behaviour was evaluated.

4.2 Direct shear box interface testing of rock analogues

Interface tests between rock analogues (cement mortar) and steel were carried out to investigate the effect of rock UCS, steel surface roughness and normal stress level. Rock analogues (as described in section 3.4.1) with UCS of 15, 35 and 65 MPa were tested under normal stress, σ_n = 10, 50, 100 and 200 kPa against steel plates with roughness, R_a = 0.4 μm. This R_a value was selected in order to diminish as much as possible the effect of the surface roughness on the behaviour of the interface and investigate only the effect of UCS. The strongest rock analogues (65 MPa) were also tested against steel plates with R_a = 8.5 and 34 μm allowing the investigation of the effect of steel roughness. The rock analogues with UCS = 65 MPa were selected for these tests, because this value was considered (by the author) to be more representative of the rock strength range of the rock types that were examined in this project. The surface roughness average of the cement mortar analogues was 2.4 μm.

4.2.1 Determination of data points comparison

Before presenting test results it is necessary to define which values of shear stress (obtained from the tests) were considered for the analysis. Some interface tests (usually those conducted using a smooth steel plate with R_a = 0.4 μm against the strongest cement mortar samples with UCS = 65 MPa) displayed “brittle” behaviour (Figure 4-1). In this case, a peak in shear stress observed at low displacement levels which then drops rapidly and tends towards a stable value as the shear deformation increases. Thus, a peak (highest value at shear displacement between 0 and 4 mm) and an ultimate value (lowest value at shear displacement between 7 and 8 mm) were defined as δ_{peak} and δ_{ult} respectively. It should be noted here, that although the total shear displacement of the shear box during a test is 10 mm, data only up to a total deformation of 8 mm was considered in order to avoid any instrument effects close to the termination of the test.

In contrast, other tests (usually when rough steel plates were used, i.e. R_a = 8.5 and 34 μm) indicated a response which is similar to elastic perfectly plastic behaviour (Figure 4-2) where a peak is not observed. In this case, a yield point was selected which was the point of intersection between the trend lines of the "elastic" and the "plastic" regions. An ultimate value at shear displacement 7-8 mm was also reported.

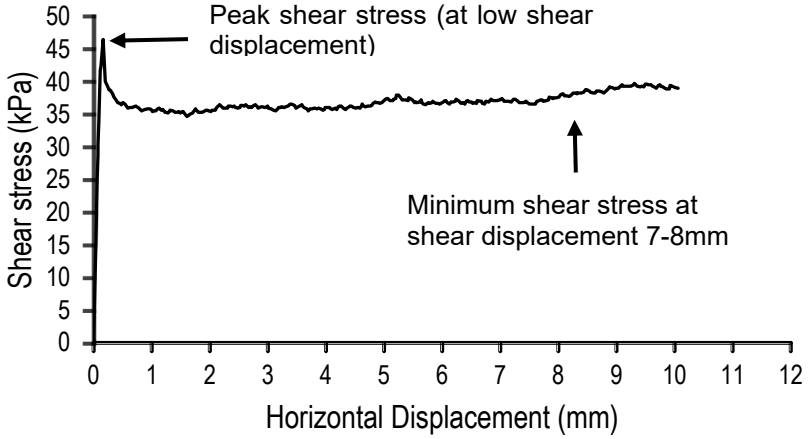

Figure 4-1. Typical shear stress vs horizontal displacement from smooth steel - cement mortar interface testing at a normal stress of 200 kPa and cement mortar with UCS = 65 MPa. (Steel R_a = 0.4 μm, Cement mortar R_a = 2.4 μm)

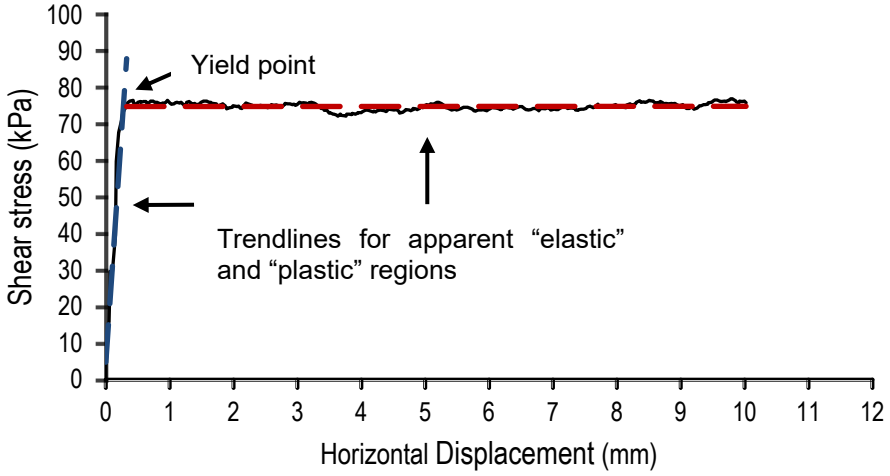

Figure 4-2. Typical shear stress vs horizontal displacement graph from steel - smooth cement interface testing at normal stress of 100 kPa and cement mortar with UCS = 35 MPa (Medium Strong) (Cement R_a = 2.4 μm)

4.2.2 Effect of rock analogue UCS

Only data from tests between rock analogues (R_a = 2.4 μm) and smooth steel (R_a = 0.4 μm) were used to investigate the effect of UCS on the strength of the interface. The smoothest available surfaces for both materials were used in an attempt to reduce the effect of surface roughness and isolate the effects of analogue strength (UCS) on shear resistance.

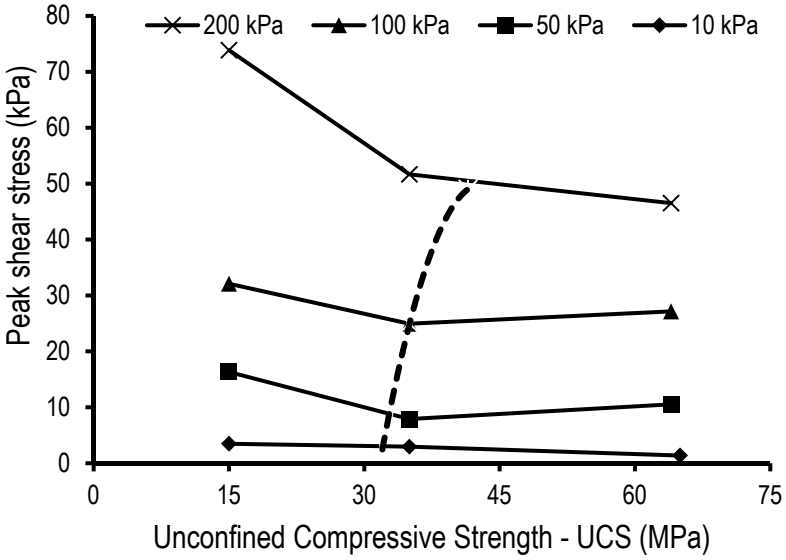

Figure 4-3. Relationship between peak shear stress and UCS for rock analogues against smooth steel with R_a=0.4μm. Dashed line indicates the transition points contour

Shear stress was normalised by the applied normal stress, resulting into the coefficient of friction μ which is plotted in Figure 4-4.

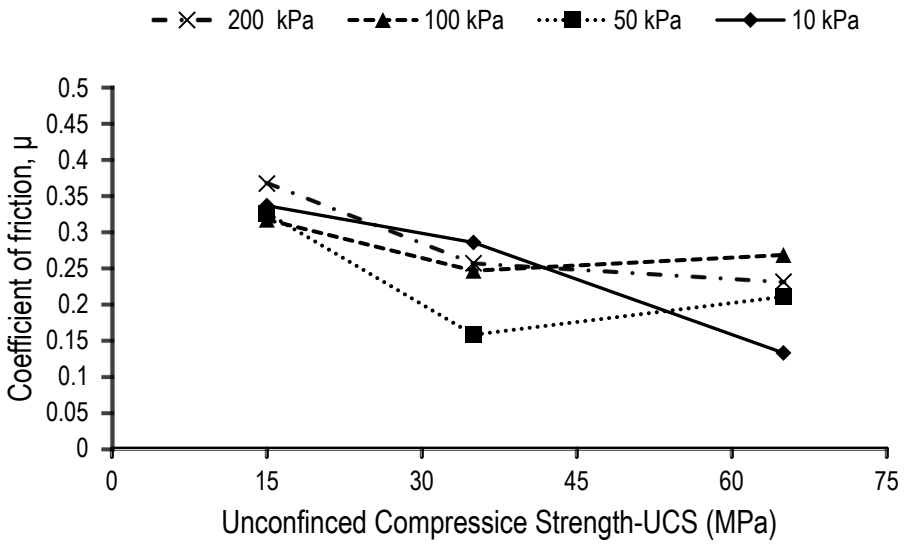

Figure 4-4. Coefficient of friction μ considering peak values vs UCS for rock analogues against smooth steel with R_a=0.4μm at four normal stress levels

From Figure 4-3 it can be seen that the samples with the lowest compressive strength (15 MPa) exhibit the higher values of shear stress even at low stress levels. More specifically, at a normal stress of 50 kPa, the developed shear stress for the weakest samples is 55 % higher than the samples with the highest compressive strength (65 MPa). At a normal stress level of 200 kPa there is a difference of 59 %.

In Figure 4-3 it is shown that at normal stresses between 10 kPa and 100 kPa, the shear resistance is quite similar for the cement samples with UCS values of 35 MPa and 65 MPa (medium strong to strong rock equivalent). As the normal stress is increased to 200 kPa the sample with UCS of 35 MPa seems to display enhanced shear resistance possibly as a result of surface damage.

It can be seen (Figure 4-4) that the influence of UCS becomes more pronounced as the stress level increases. For example, for normal stress of 100 kPa there is practically no difference between the generated shear stress for cement samples with UCS = 35 MPa and UCS = 65 MPa.

This behaviour indicates that the strength of the sample appears to affect the mode of shearing. The strongest samples interact to a lesser degree with the

steel surface, but as the UCS decreases, this “sliding” is accompanied by damage on cement’s surface (absorption of energy) which increases the interface strength significantly. This apparent transition in shearing mode appears to occur at higher values of compressive strength as the level of normal stress increases. The dashed line in Figure 4-3, is a proposed contour which connects the apparent transition points at each stress level; to the left of this contour is the region where significant increase in shear strength is noticed (with reducing UCS). This behaviour appears to indicate a critical UCS/σ_n ratio that denotes the transition of the shearing mode from pure sliding to sliding with damaging or localised crushing, and thus enhancing the performance of the interface. This ratio equals to 670, 350 and 207.5 for normal stresses of 50 kPa, 100 kPa and 200 kPa respectively. It seems that in this case, a tactic of designing foundations that induce high normal stresses at the interface (i.e. small plane area) will potentially lead to higher interface resistance and be more effective in weak to medium strong rocks.

The effect of the compressive strength (UCS) on the ultimate shearing behaviour (horizontal displacement 7 - 8mm) is shown in Figure 4-5 and Figure 4-6.

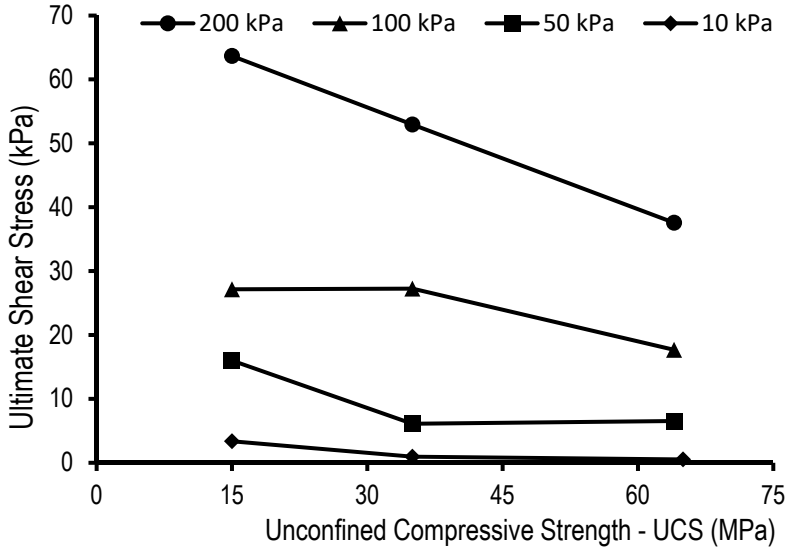

Figure 4-5. Relationship between ultimate shear stress and UCS for rock analogues against smooth steel with R_a=0.4μm.

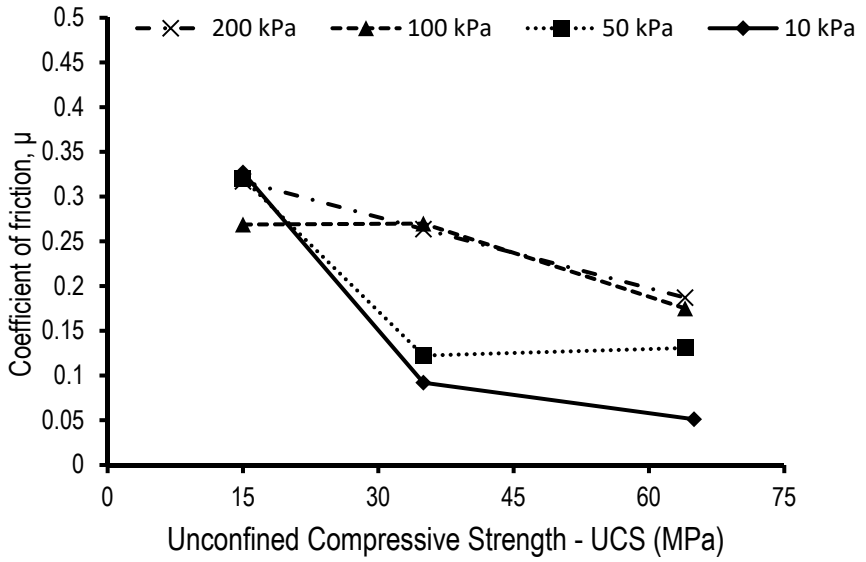

Figure 4-6. Coefficient of friction μ considering ultimate values vs UCS for rock analogues against smooth steel with R_a=0.4μm

The strongest samples exhibit the lowest shear stress values at all the normal stress levels. At normal stresses of 10 kPa and 50 kPa, the ultimate shear stress is relatively similar for UCS values of 35 MPa and 65 MPa, but the effect of the compressive strength is more pronounced as the normal stress level increases (i.e. 100 kPa and 200 kPa).

The peak (τ_{peak}) and ultimate (τ_{ult}) shear stress for the previously discussed tests are also summarized in Table 4-1 and the failure envelopes are shown in Figure 4-7.

Table 4-1. Rock analogue with varying strength (UCS = 15, 35 and 65 MPa) – smooth steel (R_a = 0.4 μm).

	UCS (MPa)					
Normal stress (kPa)	15		35		65	
	τ_{peak} (kPa)	τ_{ult} (kPa)	τ_{peak} (kPa)	τ_{ult} (kPa)	τ_{peak} (kPa)	τ_{ult} (kPa)
10	3.5	3.4	3.0	1.0	1.4	0.5
50	16.3	16.0	7.9	6.1	10.5	6.5
100	32.1	27.2	24.9	27.3	27.2	18.7
200	73.9	63.7	51.7	52.3	46.5	38.8

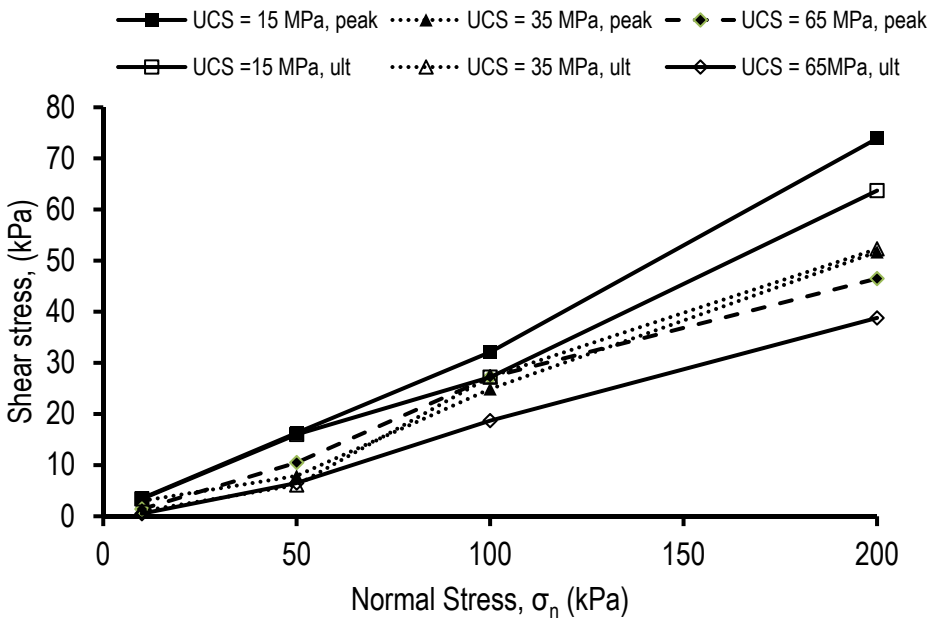

Figure 4-7. Failure envelopes for rock analogue (of varying UCS) – steel (R_a = 0.4 μm) interfaces

In summary, interface shear strength seems to be increasing for decreasing compressing strength (UCS), both at low and large horizontal displacements. It should be mentioned, that low values of interface friction angles δ were exhibited (especially for analogues with UCS = 65 MPa). This was because very smooth (polished) steel (R_a = 0.4 μm) was used in the experiments, in

order to minimise the effect of roughness and allow the effect of the strength of rock to be investigated.

In the experiments presented next, rougher steel plates are used and significantly higher interface friction angles (δ_{peak} and δ_{ult} for peak and ultimate values respectively) are observed as shown in Table 4-2.

Table 4-2. Summary table of interface friction angles recorded for all the rock analogue – steel interface combinations

	Interface				
Rock UCS (MPa)	15	35	65	65	65
Steel R_a (μm)	0.4	0.4	0.4	8.5	34
σ_n (kPa)	Measured peak interface friction angle, δ_{peak} (°)				
10	18.6	16.0	7.6	27.4	23.6
50	18.1	9.0	11.9	34.8	34.4
100	17.6	14.2	15.9	33.4	33.2
200	20.2	14.4	13.0	31.4	34.9
σ_n (kPa)	Measured ultimate interface friction angle, δ_{ult} (°)				
10	18.1	5.3	2.9	18.5	12.0
50	17.8	7.0	7.5	25.3	33.2
100	15.0	15.4	10.5	26.9	32.4
200	17.6	14.6	10.9	26.7	36.4

4.2.3 The effect of steel roughness on shearing behaviour

Flat smooth (R_a = 2.4 μm) rock analogues were used in these tests, with compressive strength of 65 MPa (strong rock analogue). This value of UCS was selected because it was assumed as more representative for the UCS range of rock types encountered in the wider project (30.0 – 192.7 MPa).

The effect of steel roughness on the shearing behaviour of interfaces has been investigated previously and a relative roughness ratio (R_{max}/D_{50}) was introduced by Uesugi and Kishida (1986) and described by Jardine et al. (1993) for sand - steel interface testing for piles. Figure 4-8 suggests that interface shear strength increases with increase relative roughness ratio up to an upper limit beyond which the interface friction angle becomes higher than the internal friction angle of the sand and failure occurs within the sand mass.

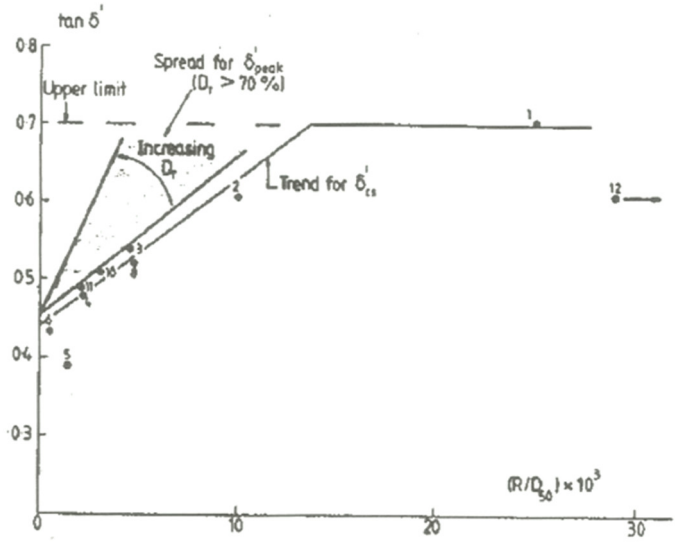

Figure 4-8. Summary of δ' values from parametric study, σ'_n~100kPa, after Jardine et. al 1993

A similar relative roughness ratio of steel to cement in this case ($R_{a,steel}/R_{a,cem}$) has been adopted for this study to aid discussion of the results. It can be seen in Figure 4-9 and Figure 4-10 that an increase in steel roughness increases the developed shear stress, but this does not occur for all the stress levels and for all the roughness ranges.

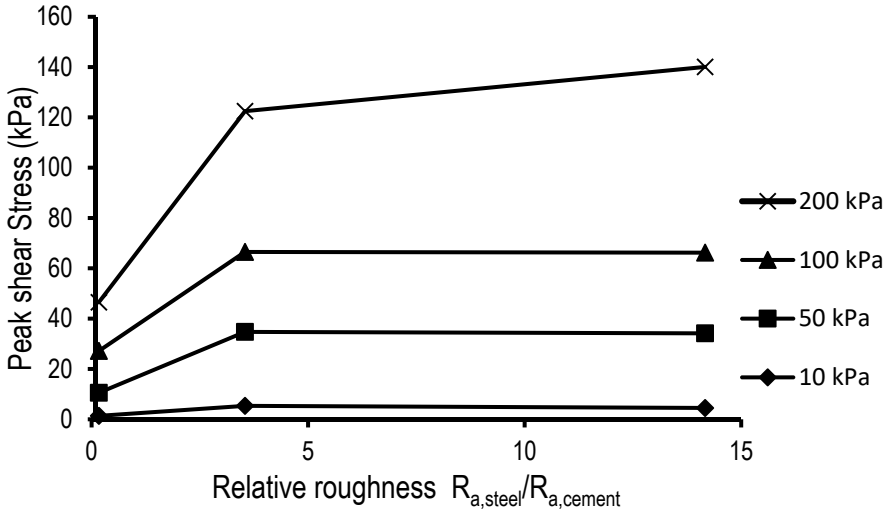

Figure 4-9. Relationship between peak shear stress and relative roughness for strong rock analogues (UCS = 65 MPa), rock analogue R_a = 2.4 μm

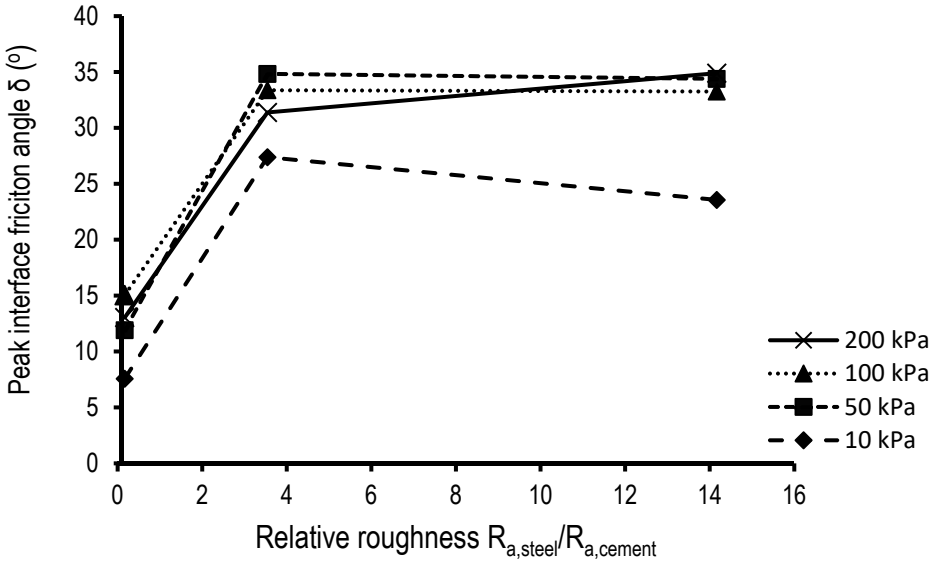

Figure 4-10. Interface friction angle δ considering peak values vs steel R_a for strong rock analogues (UCS = 65 MPa), rock analogue R_a = 2.4 μm

An increase in roughness from 0.4 microns to 8.5 microns is sufficient to increase significantly (more than 100%) the developed shear stress independently of the stress level (δ increases from 13.5° up to 31.3°. It can be seen that a further increase in roughness (from 8.5 to 34 microns) has little effect on the developed shear stress (increase occurred at a significantly lower rate, δ = 35.2° at 34 μm) for normal stresses between 10 and 100 kPa. The

variation of coefficient of friction μ with increasing roughness is shown in Figure 4-10.

This suggests that for a given roughness of a rock analogue ($R_{a,cem}$ = 2.4 μm in this case), there is an upper limit in steel roughness (i.e. critical relative roughness ratio), above which, further increase does not significantly enhance the interface behaviour. This is the value which establishes the maximum interlocking of the interface. This "upper limit" value is expected to increase as the cement roughness increases. In other words, there is a critical cement to steel R_a ratio (i.e. relative roughness between steel and cement) at which significant increase in the interface resistance occurs. This critical value lies between 0.17 (ratio for steel with R_a = 0.4 μm) and 3.54 (ratio for steel with R_a = 8.5 μm).

The curves for normal stresses of 50 and 100 kPa are almost identical (Figure 4-10) and that reveals that in this stress range, the shear behaviour is independent of the applied normal stress.

At normal stress of 200 kPa, the increase in the value of the developed shear stress is higher between the steel plates with R_a = 0.4 μm and R_a = 8.5 μm, than it was for normal stresses below 100 kPa. Also at this stress level, an increase in roughness from 8.5 to 34 microns results in a noticeable (18 %) increase in the generated shear stress.

Results considering the ultimate values are plotted in the following graphs.

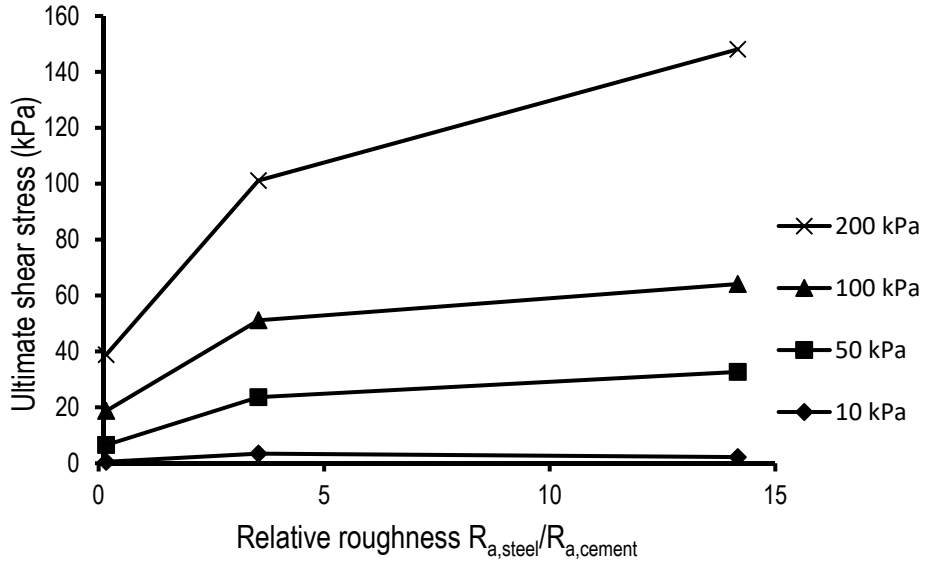

Figure 4-11. Relationship between ultimate shear stress and relative roughness for strong rock analogues (UCS = 65 MPa), rock analogue R_a = 2.4 µm

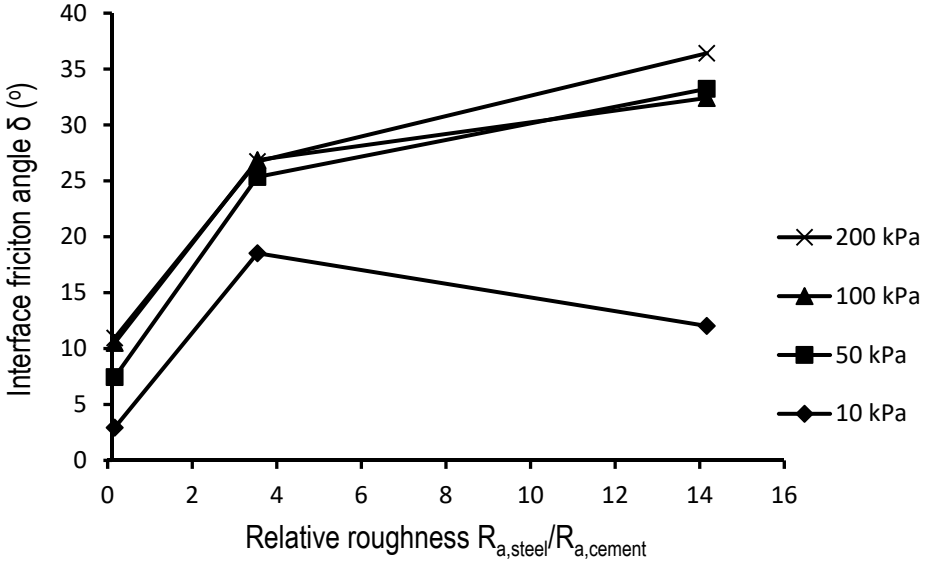

Figure 4-12. Coefficient of friction μ considering ultimate values vs steel R_a for strong rock analogues (UCS = 65 MPa), dashed line indicates rock analogue R_a = 2.4 µm

As shown in Figure 4-11 and Figure 4-12, an increase in steel roughness increases the large displacement (8 mm) shear strength of the interface. This increase is more significant between 0.4 and 8.5 microns than between 8.5 and 34 microns. The curves for 50 kPa and 100 kPa are identical, revealing that the shear behaviour is independent of the stress level in that range. At

normal stress of 200 kPa the rate of increase in shear strength with roughness, becomes slightly higher for both cases (0.4 μm -8.5 μm, 8.5 μm – 34 μm) and this might indicate a normal stress effect.

An interesting observation is that the strength at large displacement for the rougher plates (R_a = 8.5 μm and R_a = 3 4 μm) is quite similar to the peak shear strength (roughly 0.5 mm), so an increase in roughness generates a non-brittle interfacial behaviour. For R_a = 34 μm and normal stress of 200 kPa, the large displacement shear strength is higher than the strength at a low horizontal displacement. When a rough steel plate is used (either R_a = 8.5 μm or R_a = 34 μm), the actual area of contact between the two bodies (cement block and steel plate) is smaller than the nominal plane area of contact. During shearing, the asperities of the rough steel plate are scratching the surface of the cement sample which leads to an increase in the generated shear stress. An increase in the normal stress intensifies that phenomenon, as shown in Figure 4-13. The polished (white) areas on the samples denote the damage caused during shearing and it is clear that the damaged area increases as the normal stress increases. The generation of this damage absorbs energy, resulting in generation of significantly higher values of shear strength compared to the polished steel plate.

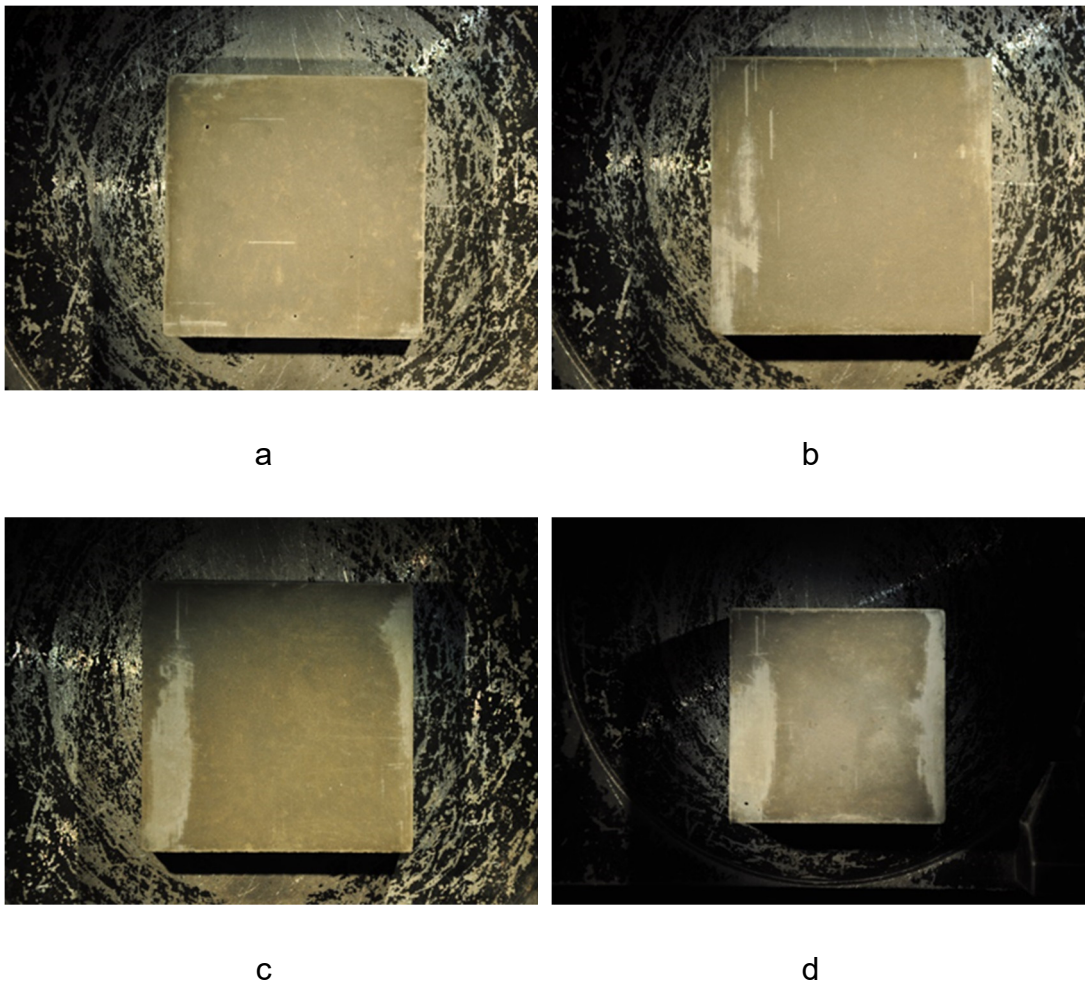

Figure 4-13. Rock analogues after shearing against steel plate with R_a = 34 μm at normal stress of (a) 10 kPa, (b) 50 kPa, (c) 100 kPa and (d) 200 kPa

Summarising at this point, we notice that an increase in steel roughness is beneficial for the shear strength of the interfaces, but this benefit is only significant up to the transition from a very smooth (steel with R_a = 0.4 μm, relative roughness ratio equals 0.17) surface to a rough surface (steel with R_a = 8.5 μm, relative roughness ratio equals 3.54) when sheared against a cement sample of R_a =2.4 μm. Further roughening of the steel (R_a = 8.5 μm to R_a = 34 μm) has a greater effect on the large displacement shear strength. Also there is a normal stress effect, as an increase in normal stress enhances the effect of the roughness on the interface behaviour.

4.2.4 Alpha (α) factor approach

As discussed previously, the shear strength of the interface seems to be affected by the factors such as the UCS and the applied normal stress. Therefore a framework should be developed to allow the "calculation" of the interface shear strength based on these parameters. It was felt, that this framework could be based on the adhesion factor approach that is commonly used to calculate the ultimate skin friction of rock socket piles by utilising the following empirical equation.

$$q_s = \alpha\beta q_{uc} \qquad \text{Equation 4-1}$$

Where:
α is adhesion factor
β is a correlation factor related to the discontinuity spacing in the rock mass
q_{uc} is rock unconfined compressive strength (UCS)

Figure 4-14 displays adhesion factor alpha (α) vs q_{uc} graphs proposed by Rosenberg and Journeaux (1976), Horvath (1978) and Williams and Pells (1981), where it can be seen that α has values between 0.05 and 0.8.

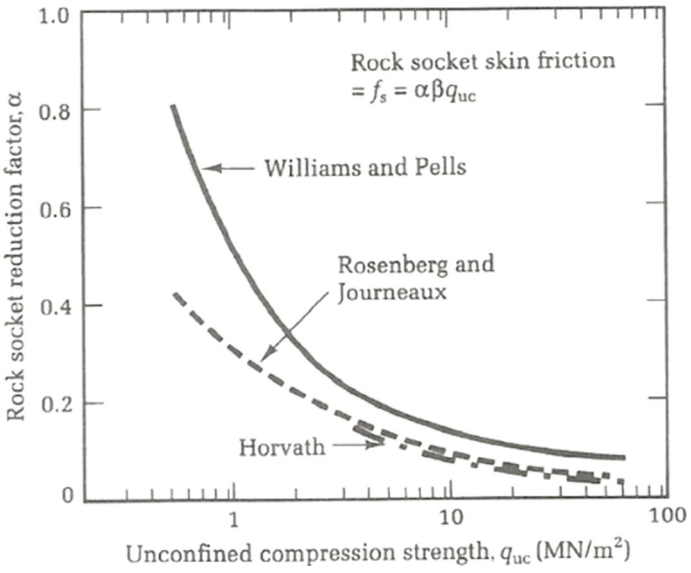

Figure 4-14. Rock socket skin friction related to the uniaxial compression strength of intact rock (Source: Tomlinson 2001)

Adhesion factor vs UCS graphs were plotted (Figure 4-15 and Figure 4-16) using the data gathered from the shearbox tests between steel with R_a = 0.4 μm and rock analogue with R_a = 2.4 μm (Table 4-1); to verify if the behaviour of the tested interfaces can be described by an adhesion factor type approach. Both, peak and ultimate values of shear stress were considered and UCS was normalised over normal stress as it appeared that the behaviour is affected by normal stress. Correlation factor β was not taken into account (considered equal to 1) since artificial rock analogues are considered and the samples do not correspond to a real rock exposure.

The test data seem to be well described by a power law trend that looks similar to that found in the literature for rock socket piles (Figure 4-14) and is described by the following equation.

$$a = b\left(\frac{UCS}{\sigma_n}\right)^c \qquad \text{Equation 4-2}$$

Where *UCS* = unconfined compressive strength of rock (or analogue in this case), σ_n= normal stress and b, c arithmetic are fitting constants.

In this case α is several orders smaller in magnitude due to the significantly lower normal stress (and generated shear stress), compared to socketed piles. For socketed piles, the surrounding rock mass confines the shaft, so normal stress is not constant during shearing and increases significantly at specific points as dilation occurs. This is different in the case of the shear box tests results presented here, were the normal stress is kept constant and the sample is free to dilate. The other significant differences apart from constraint conditions are the significantly lower normal stresses tested (likely to be found for tidal stream generators compared to rock socket piles, Ziogos et al., 2015b) and the inherent difference in the contact/bonding between say a cast in-situ rock socket pile and a gravity base foundation placed on rock where no bond occurs (between rock and concrete or steel and concrete). For this reason, it was felt that it was more appropriate to adopt the term alpha factor (α) instead of adhesion factor. UCS was also normalised by the vertical stress during

interface testing as this was seen to have a significant effect over the relatively low stresses likely to be encountered at the rock - steel interface (as also observed in section 4.2.3 above). It is assumed such a normalisation is not applied for rock socket piles due to the high confining stresses and difficulty in determining the actual in-situ stress at the bonded interface.

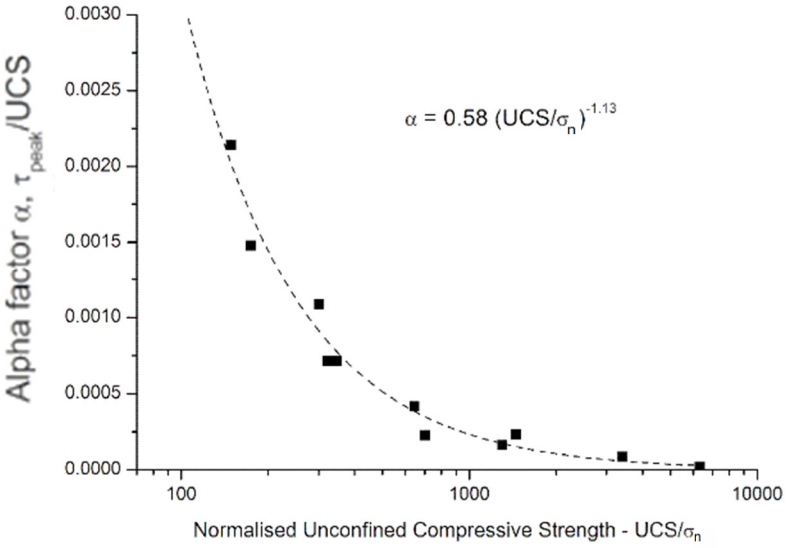

Figure 4-15. Alpha factor α vs normalised UCS of rock analogue (R_a = 2.4 µm), considering peak values

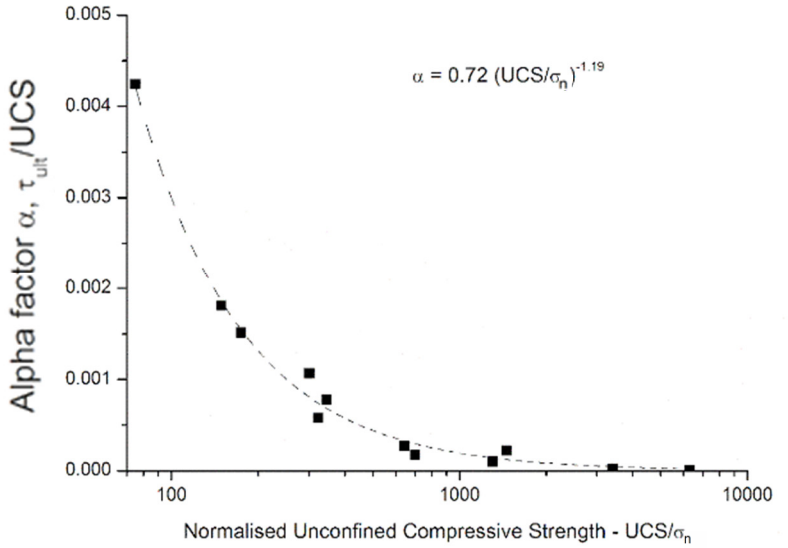

Figure 4-16. Alpha factor α vs normalised UCS of rock analogue (R_a = 2.4 µm), considering ultimate values

The following graphs (Figure 4-17, Figure 4-18) display the alpha factor α taking into account the variation in the steel roughness plotted on log-log axes to allow easier comparison of the results.

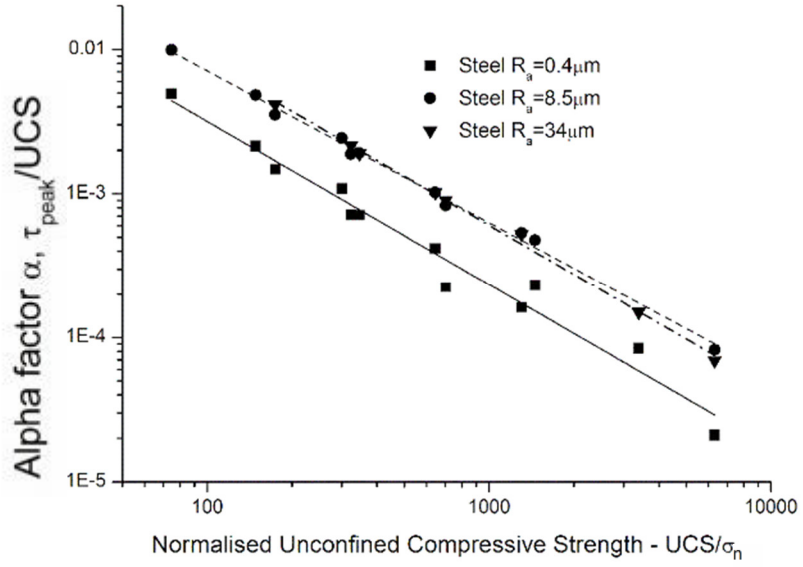

Figure 4-17. Alpha factor vs normalised UCS of rock analogue (R_a = 2.4 μm) for varying steel roughness, considering peak values

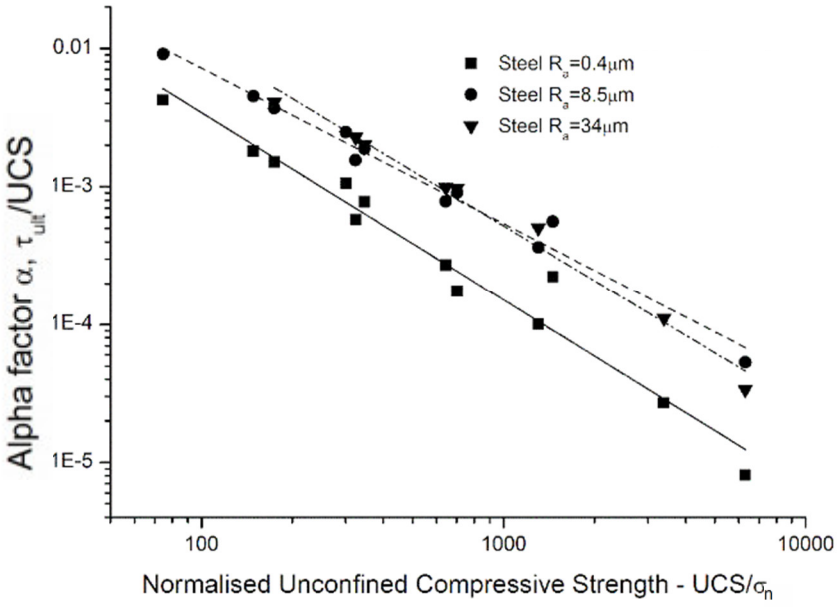

Figure 4-18. Alpha factor vs normalised UCS of rock analogue (R_a = 2.4 μm) for varying steel roughness, considering ultimate values

The shape of the curve is now linear (since the axes are log-log), but again the alpha factor attains higher values as the UCS/σ_n ratio decreases for increasing steel roughness as explained before. It is also apparent, that for a given UCS/σ_n ratio, the alpha factor increases significantly when the relative roughness ratio obtains values over 3.54 (corresponding to steel R_a = 8.5 μm).

4.3 Shear box interface testing with rock samples

The rock analogues offered controllable properties and allowed the identification of controlling parameters on the interface shear behaviour. The next step though, was to use real rock samples in order to obtain interface properties needed for the design of foundations. At this point the results from Sandstone, Flagstone, Limestone and Andesite testing will be presented. Chalk is a rock with extraordinary mechanical behaviour (Lord et al., 2002), therefore its shear characteristics will be discussed and assessed separately in Chapter 7. The same rationale as per the rock analogue tests was followed (i.e. tests at four different normal stress levels against steel plates with different roughness values). As described in Chapter 3, disc shaped rock samples were used and due to the smaller plan area (compared to the square rock analogues) higher normal stresses were achieved in this testing series (the maximum load capacity of the direct shear box has already been reached/used for the rock analogues testing). Normal stress levels of 16, 79, 159 and 316 kPa were used and the rock samples were tested against steel with R_a = 0.4 and 7.2 μm. The steel with R_a = 34 μm was not used, because in the meantime the IST apparatus had been received and it was decided that it would be more time efficient to move on to using this device instead of carrying out more testing with the direct shear box.

4.3.1 Results and discussion

Shear stress vs horizontal displacement graphs, have the same form, irrespective of the rock type and the steel roughness. Shear stress peaks on initiation of displacement and then attains a stable value (ultimate) as the

shear displacement increases. Figure 4-19 shows the shear stress vs displacement graphs of Sandstone - steel (R_a = 7.2 µm) tests which are very similar to the graphs for the other rock types (Figure 4-20).

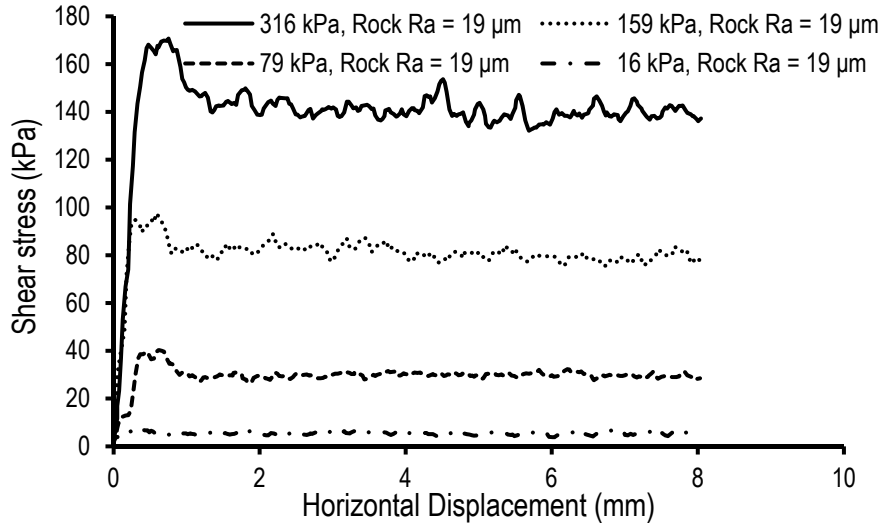

Figure 4-19. Shear stress vs horizontal displacement graph from machined steel (R_a = 7.2 µm) - Sandstone (R_a = 19 µm) interface testing at four normal stress levels

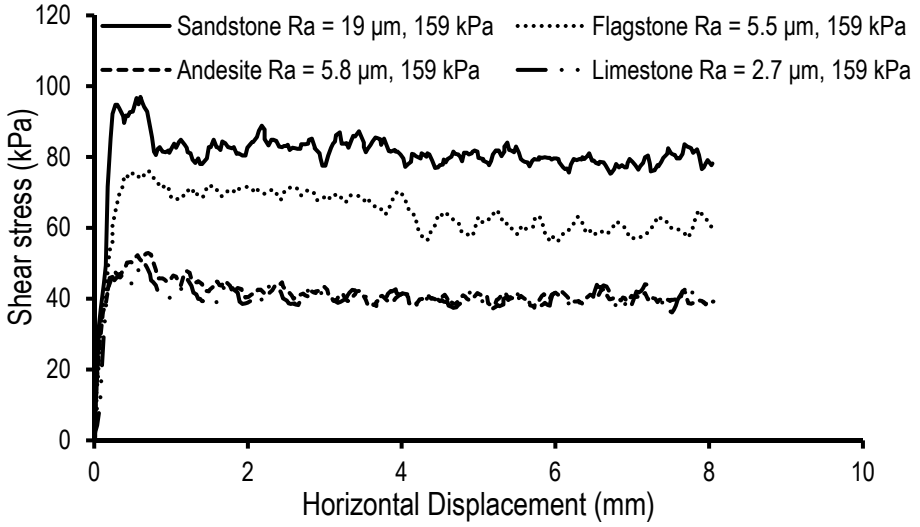

Figure 4-20. Typical shear stress vs horizontal displacement graph for four different rock types against machined steel (R_a = 7.2 µm)

The surface roughness and the UCS differs between the rock types used in the study, therefore the isolation and evaluation of the effect of the UCS on its own is not as straightforward as in the case of the rock analogues. The

following graphs show the change on the interface friction angle for the different rock types (and UCS values). Values of 31.5, 145, 158 and 192 MPa refer to Sandstone, Flagstone, Limestone and Andesite respectively. Due to the fact that only two types of steel roughness were used, it wasn't possible to determine a critical relative roughness ratio. In addition, each rock type has different R_a value, resulting to four relative roughness ratio values for a given R_a value of steel. The effect of relative roughness ratio (considering rock samples) is discussed in section 5.6.1.

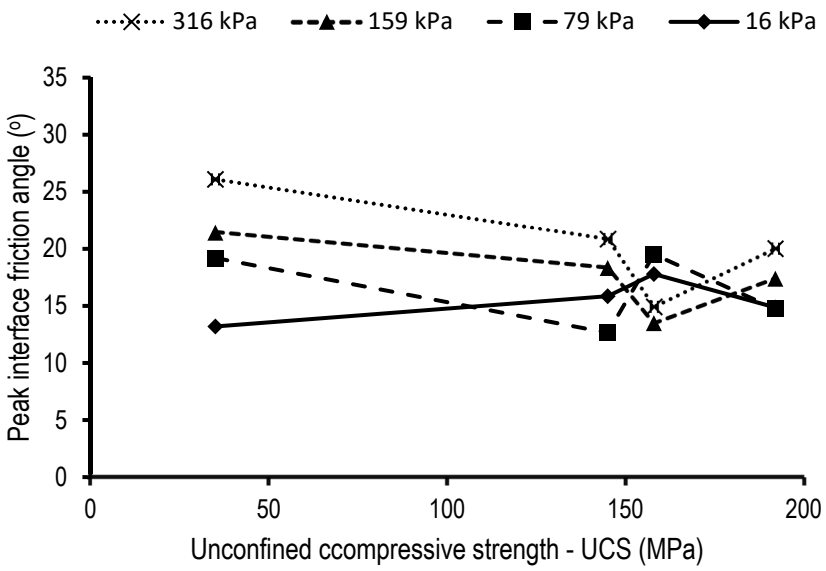

Figure 4-21. Interface friction angle δ considering peak values vs UCS for rock samples against smooth steel with R_a = 0.4 μm

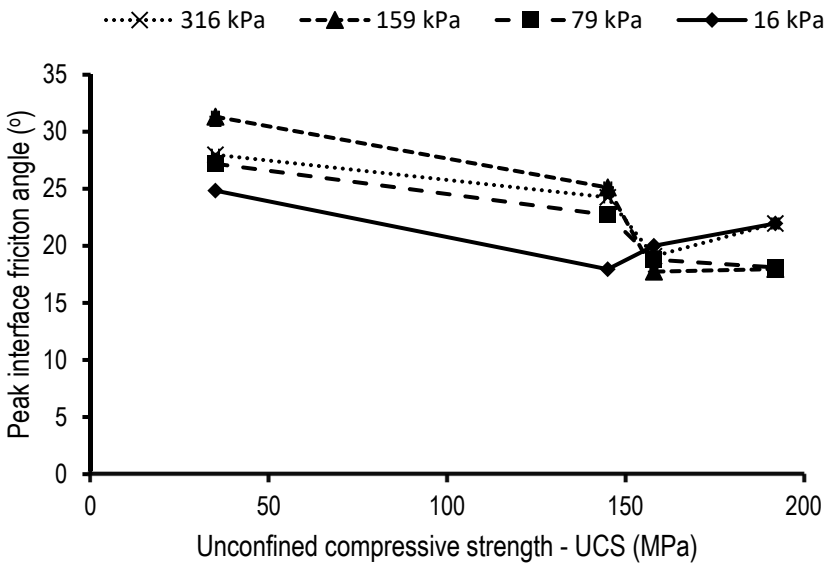

Figure 4-22. Interface friction angle δ considering peak values vs UCS for rock samples against machined steel with R_a = 7.2 μm

In Figure 4-21 and Figure 4-22 it is shown that peak interface friction angle tends to increase as UCS decreases. This behaviour is more apparent for Sandstone samples, whereas a clear trend cannot be distinguished between the Flagstone, Limestone and Andesite samples. Sandstone samples exhibit higher friction angles than the other three rock types irrespective of the steel roughness. This could potentially happen because Sandstone UCS is much lower compared to the other three rock types (~550 and ~450 % lower than Andesite and Limestone respectively) and this difference is enough to enhance the performance of the interface even against the polished steel. In section 4.2 it was shown that the relative roughness ratio affects the interface behaviour and it was also revealed through the literature review that the relative hardness of the interface materials might also be a controlling factor. When rock samples are used (instead of rock analogues), the relative roughness and relative hardness ratios vary amongst the rock – steel interfaces, therefore it is preferable to try and analyse the effect of these factors as presented later in sections 5.3.3 and 5.5.1.

On the other hand, rather similar values are obtained for Flagstone, Limestone and Andesite, especially against polished steel (R_a = 0.4 μm). It seems, that

this level of steel roughness is not adequate to “activate” the apparent effect of UCS as limited interaction appears to be occurring between the steel and the rock. As the steel roughness increases, better interlocking occurs at the interface between the rock asperities and steel texture, making the apparent influence of rock strength (UCS) more crucial. For steel R_a = 7.2 μm, Flagstone exhibits higher friction angle values compared to Andesite (and Limestone) despite having very similar surface roughness (R_a = 5.5 and 5.8 μm for Flagstone and Andesite respectively), possibly due to the lower UCS. As explained before for the rock analogues, it appears that in weaker samples, the steel causes surface damage during shearing which causes energy absorption and consequently increase to the shear strength.

Despite having lower UCS, the Limestone samples do not exhibit higher shear strength than the Andesite. This is probably, due to the lower (> 50 %) surface roughness of the Limestone samples. Lower UCS favours the increase of the shear strength, whereas the lower R_a has the opposite effect.

To summarise, the interface strength seems to increase as the compressive strength decreases and that happens for both types of steel used. This agrees with the findings from the tests using the rock analogues. It should be noted here that from these results only a general trend can be noted which may be influenced by the relative roughness ratio which varies amongst the rock – steel interfaces. The surface roughness of saw cut Andesite and Flagstone is similar (around 5.5 μm), but the surface of the Sandstone samples is much higher (19 μm). Thus the effect off UCS variation is easier to compare for the Andesite and Flagstone as they have similar surface roughness (and relative roughness ratio). Sandstone yields the highest values due to the combined effect of both greater roughness and lower compressive strength. The test data from the rock – steel shear box tests are summarised below. .The relative roughness ratio $R = R_{a,steel}/R_{a,rock}$ is also listed for each rock – steel combination.

Table 4-3. Sandstone (R_a = 19 μm) – steel interface testing summary results

Normal stress (kPa)	Steel R_a (μm)			
	0.4 (R = 0.021)		7.2 (R = 0.379)	
	τ_{peak} (kPa)	τ_{ult} (kPa)	τ_{peak} (kPa)	τ_{ult} (kPa)
16	3.8	2.4	7.5	5.5
79	27.3	17.3	40.3	40.3
159	62.3	45.4	96.6	81.2
316	141.7	90.5	167.6	142.5

Table 4-4. Flagstone (R_a = 5.5 μm) – steel interface testing summary results

Normal stress (kPa)	Steel R_a (μm)			
	0.4 (R = 0.073)		7.2 (R = 1.310)	
	τ_{peak} (kPa)	τ_{ult} (kPa)	τ_{peak} (kPa)	τ_{ult} (kPa)
16	4.6	2.5	5.3	3.0
79	17.6	12.4	32.9	32.8
159	52.6	28.1	74.4	59.6
316	120.0	83.4	142.1	115.6

Table 4-5. Andesite (R_a = 5.8 μm) – steel interface testing summary results

Normal stress (kPa)	Steel R_a (μm)			
	0.4 (R = 0.069)		7.2 (R = 1.241)	
	τ_{peak} (kPa)	τ_{ult} (kPa)	τ_{peak} (kPa)	τ_{ult} (kPa)
16	4.3	2.2	4.6	3.3
79	20.7	12.7	25.7	20.
159	49.7	29.6	51.5	40.6
316	115	65.3	127.2	91.8

Table 4-6. Limestone (R_a = 2.7 μm) – steel interface testing summary results

Normal stress (kPa)	Steel R_a (μm)			
	0.4 (R = 0.148)		7.2 (R = 2.667)	
	τ_{peak} (kPa)	τ_{ult} (kPa)	τ_{peak} (kPa)	τ_{ult} (kPa)
16	5.2	2.5	5.9	5.5
79	27.8	15.5	26.7	201.4
159	38.1	26.1	50.8	40.7
316	84.2	59.7	109.2	82.3

4.3.2 Alpha factor considering results from rock samples

The data from the interface testing presented in 4.3.1, are plotted in Figure 4-23 and Figure 4-24 in terms of alpha factor (α) considering peak and ultimate values respectively. The data points are annotated for the rock type and steel roughness and alpha factor contours (as per Equation 4-2) have been plotted for each R_a value. It should be noted here that both axes are using a logarithmic scale for clarity, therefore the contours appear to be linear, whereas they are curved if they are plotted on linear axis. The fitting constants b, c of the contours are listed in the figures. The contour corresponding to the

rougher steel (R_a = 7.2 μm) is higher for both peak and ultimate values and indicates an apparent effect of steel roughness and relative roughness ratio on the interface strength.

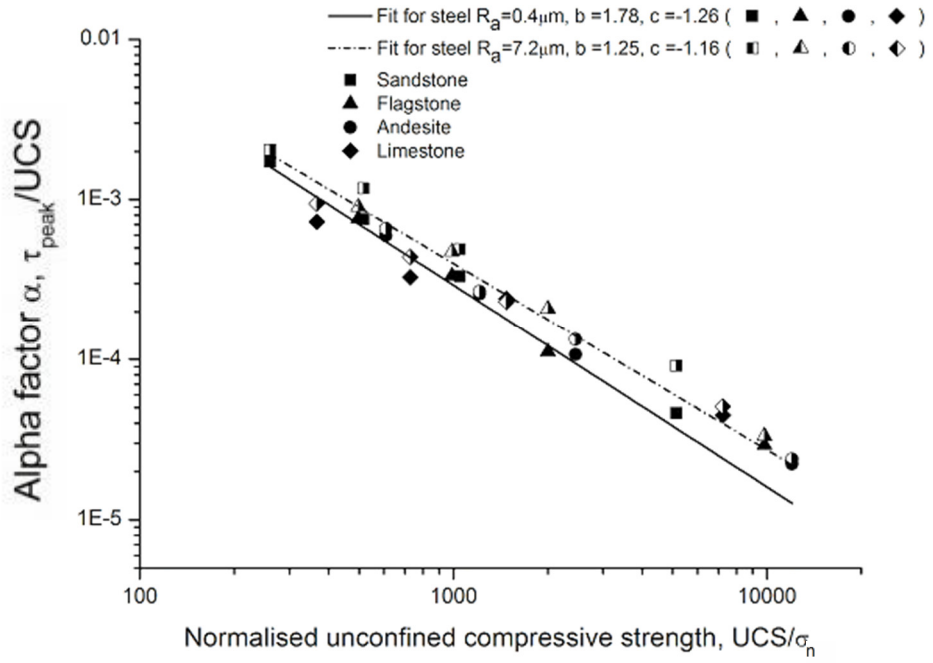

Figure 4-23. Alpha factors for rock – steel interfaces (shearbox), considering peak values

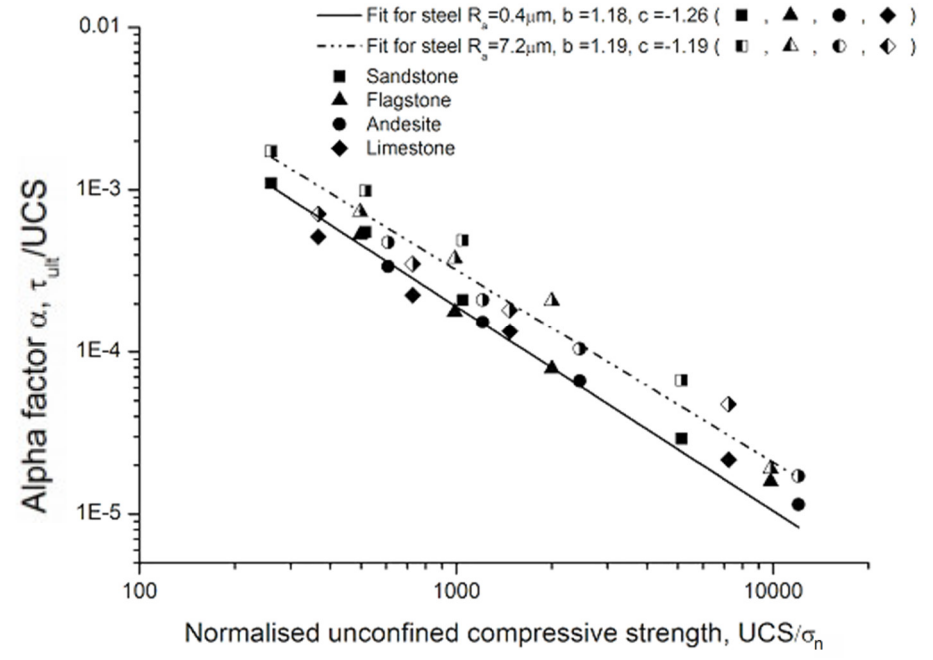

Figure 4-24. Alpha factors for rock – steel interfaces (shear box), considering ultimate values

For steel R_a = 0.4 μm, R ranges from 0.021 (Sandstone) to 0.148 (Limestone), whereas for steel R_a = 7.2 μm, R takes values between 0.379 (Sandstone) and 2.667 (Limestone). The apparent distance between the contour lines for steel R_a = 0.4 and 7.2 μm, indicates that the increase of relative roughness ratio is beneficial for the shear strength of the interface. However, since only two types of steel were examined in this case, we cannot determine if the critical R value lies between 0.021 and 2.667 (this would be the case if further increase in steel R_a wouldn't have significant effect) or if critical R is greater than 2.667 (this would be the case if increase in steel roughness would lead to significant increase in shear strength). Although, results from analogue testing suggest the prior.

4.4 Summary

In this chapter, data from interface testing from rock analogue – steel and rock – steel interfaces using a modified shear box has been presented. The rock analogue offered controlled material properties and discussion of the results, revealed potential effects of UCS and surface roughness on the interface shear strength. A relative roughness ratio $R_{a,steel}/R_{a,cement}$ has been adopted as it was shown that the relative roughness ratio of the surface roughness of the counterfaces affects the interface shear behaviour. The adhesion factor approach, used for the calculation of the skin friction of piles, has also been modified and an alpha factor (α) framework has been suggested to calculate the interface shear stress based on the UCS of the rock analogue and the applied normal stress on the interface. The data from the tests using the rock analogues in direct shear are limited, however the same framework seems able to capture the data for the rock – steel interface tests. The data from the rock – steel interfaces are rather limited since only steel with R_a = 0.4 and 7.2 μm was used, because during the testing programme a new test apparatus (IST) was acquired and it was used to perform a more extensive test programme (i.e. more rock types, wider steel R_a range etc.) which is presented in Chapters 5, 6 and 7. The data of the IST tests was also used to enhance the alpha factor approach framework that was introduced in this chapter.

Chapter 5

5 Advanced rock – steel interface testing using the IST

5.1 Introduction

In the previous chapter, the process followed, in order to develop the alpha factor framework was presented. The shear box interface testing of rock analogues, offered controlled parameters for UCS and roughness and lead to the development of a simple empirical equation that allows the estimation of shear strength using UCS and applied normal stress as variables (section 4.2.4). This was useful to identify the parameters affecting the shearing behaviour of interfaces, however data using real rock samples (instead of analogues) is needed for industrial practice and real application. Analysis of the results also revealed a potential effect of surface hardness on the shearing behaviour.

Some primary data from shear box interface testing using rock samples has already been presented in Chapter 4. However, the Interface Shear Tester (IST) was acquired after this initial work, and after evaluating its capabilities and quality of results, it was decided to stop the shear box testing and carry out a more extended plan utilising the IST only. The mode of shearing in the IST is torsional (in contrast to the shear box which is direct shear); therefore to allow comparison most of the shear box parameter investigations were repeated in the IST. This allowed better comparison of the results since they were all obtained from the same apparatus. Tests were carried out to an equivalent shear displacement of 10 mm. The peak interface friciton angle (δ_{peak}) is defined as the maximum value at a shear displacement up to 4 mm and the ultimate interface friction angle (δ_{ult}) is defined as the minimum value in the region of 8 - 10 mm

Chapter 5 is focused on Rock – steel interface testing where Sandstone, Flagstone, Limestone, Andesite and Chalk were tested against steel with

surface roughness R_a = 0.4, 7,2 and 34 μm (resulting in relative roughness ratios between 0.021 and 12.592), using the IST.

Chapter 6 consists of rock – concrete and rock – sand – steel interface testing. In rock – concrete interface testing, Sandstone, Flagstone, Limestone and Andesite samples have been tested against concrete samples that represented a GBS made of concrete. The concrete samples were saw cut, exhibiting an omnidirectional roughness (R_a = 6.8 μm and relative roughness ratio between 0.357 and 2.518) and had a UCS of 61.5 MPa. In rock – sand - steel testing, the tests of the previous rock – steel tests were repeated in order to investigate the effect of a thin sand layer (i.e. coarse grained seabed sediment) on the overall behaviour of the interface.

Chalk samples were also testing utilising the IST. However, Chalk is a rock type with unusual characteristics whose mechanical properties are significantly affected by the moisture content (Lord et al., 2002). Consequently, guidelines exclusively for characterisation and engineering in Chalk have been developed through the years (e.g. Lord et al., 2002). Therefore, it was felt more appropriate to present the results of Chalk interface testing in a separate chapter of this thesis (Chapter 7).

In Chapter 5 results from all the other rock types considered in this study (Sandstone, Flagstone, Andesite and Limestone) are presented and discussed.

5.2 General results from rock-steel testing

Figure 5-1 to Figure 5-4 show the normalised shear stress over the normal stress (i.e. coefficient of friction μ) vs horizontal displacement curves from various rock type and steel roughness combinations. The large number of normal stress and rock - steel interfaces made it impractical to present all the μ – displacement curves, therefore each rock type was plotted against one type of steel roughness at four different normal stress levels.

The various interface combinations indicate relatively similar response, a typical result shows a slightly elevated initial shear stress followed by a slight reduction in shear stress post peak (or yield as defined in Figure 4-1 and Figure 4-2) and then remaining relatively constant until the end of the test. It is apparent that peak shear stress is observed at increasing displacement levels as normal stress increases (Figure 5-2).

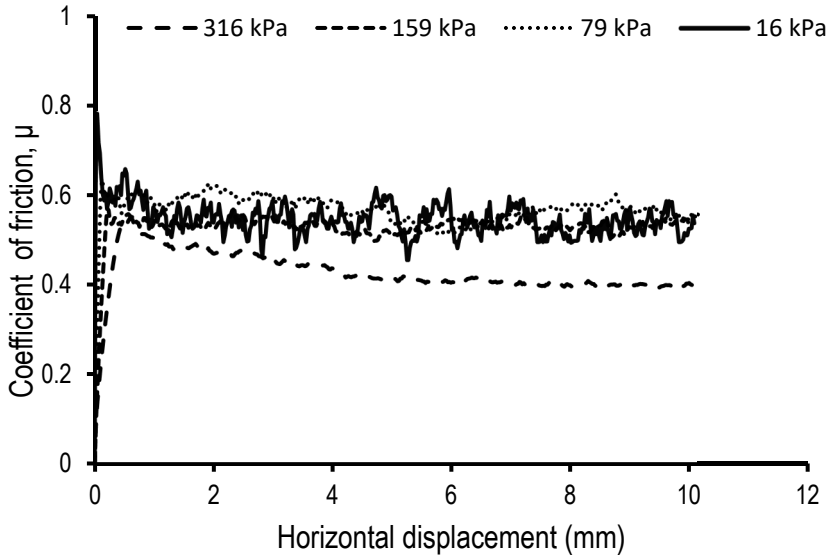

Figure 5-1. Coefficient of friction μ vs horizontal displacement for Sandstone samples against steel R_a = 0.4 μm

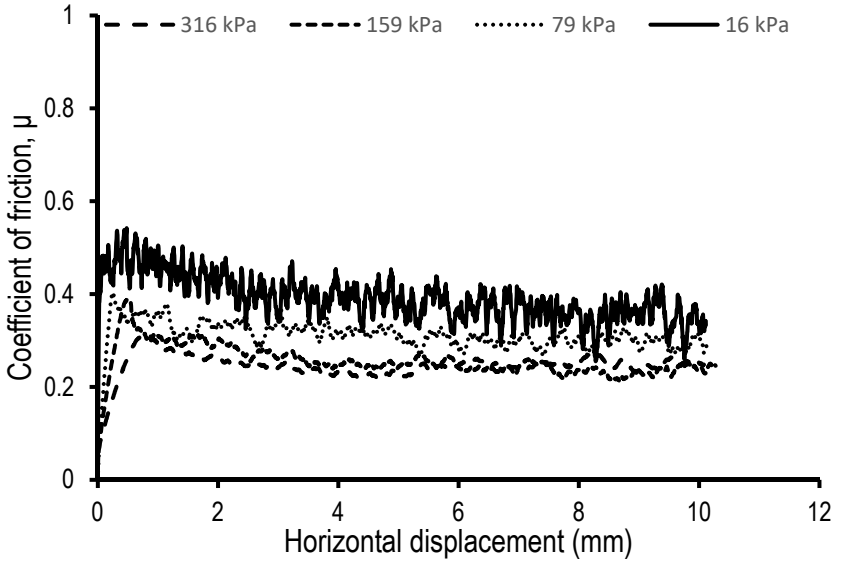

Figure 5-2. Coefficient of friction μ vs horizontal displacement for Flagstone samples against steel R_a = 7.2 μm

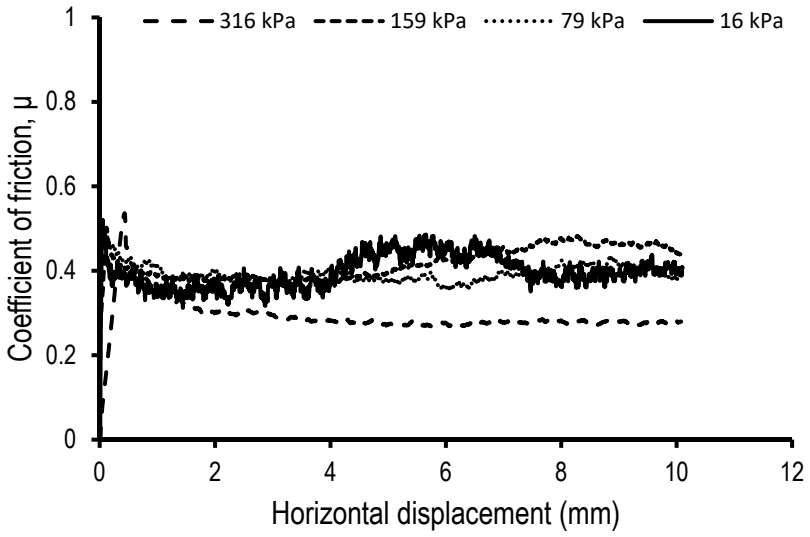

Figure 5-3. Coefficient of friction μ vs horizontal displacement for Andesite samples against steel R_a = 0.4 μm

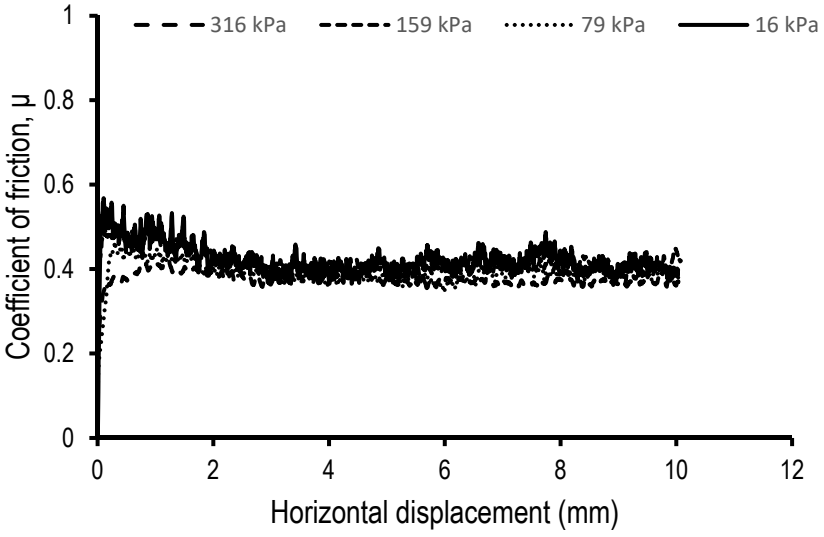

Figure 5-4. Coefficient of friction μ vs horizontal displacement for Limestone samples against steel R_a = 34.0 μm

The curves are rather “noisy” compared to those of conventional interface testing of say sand – steel interfaces due to the solid nature of the rock samples. The asperities on the steel surface apply force to the grains of the sand during shearing (conventional soil testing), therefore the grains are displaced and the sand sample is deformed (compliant interface). When two solid samples are sheared (i.e. steel and rock), the asperities of both elements

of the interface are interacting, however the shear stress generated is not adequate to cause significant deformation of the samples (i.e. none compliant interface, especially under low normal stress levels). As a result, the shear stress generated fluctuates “following” the surface topography (micro roughness).

In previous soil – steel interface studies (Uesugi and Kishida 1986, Jardine et al., 1993) it was found that the behaviour of the interface is affected by the surface characteristics of both elements that make up the interface (i.e. shape and size of sand grains, roughness of steel etc.), therefore taking account of only the steel surface roughness is not appropriate and a relative roughness ratio was proposed ($R_n = R_{max}/D_{50,}$ where R_{max} is the vertical distance between the highest peak and lowest valley of the surface profile measured) to investigate the overall effect of the roughness characteristics. A similar approach was adopted by Ziogos et al. (2015b), Ziogos et al. (2017), from rock analogue (cement) – steel and rock – steel interface testing. Roughness average R_a is the most widely recognised value for surface characterisation (Dietz and Lings 2010) and has been used widely in literature (e.g. Barmpopoulos et al., 2010, Fuggle and Frost 2010), therefore a relative roughness ratio R = $R_{a,steel}/R_{a.rock}$ is adopted for the various rock – steel interface combinations. Steel plates with R_a = 0.4, 7.2 and 34.0 μm were used, leading to values of roughness ratio (R) between 0.021 (rock significantly rougher than steel) and 12.592 (steel significantly rougher than rock). The test results for the various rock – steel interface combinations are summarised in Table 5-1 and the R values for the different rock – steel combinations are listed in Table 5-2 .

Table 5-1. Summary of results from rock – steel interface testing

Rock type	Normal stress (kPa)	R_a (μm)					
		0.4		7.2		34.0	
		Peak friction angle (°)	Ultimate friction angle (°)	Peak friction angle (°)	Ultimate friction angle (°)	Peak friction angle (°)	Ultimate friction angle (°)
Sandstone	16	37.7	29.4	40.4	28.0	41.2	28.0
	79	32.3	29.1	35.8	30.0	35.1	28.6
	159	29.7	27.9	33.8	27.8	31.5	26.4
	316	29.2	26.1	30.9	27.4	30.9	26.0
Flagstone	16	33.3	25.4	28.5	17.7	37.7	22.1
	79	23.6	14.6	21.6	15.3	36.3	25.3
	159	20.2	11.2	21.2	12.5	33.2	22.8
	316	18.00	12.5	17.5	14.1	32.4	22.8
Andesite	16	27.3	20.2	35.5	23.9	38.3	24.5
	79	29.7	22.2	29.7	20.2	33.4	23.4
	159	26.7	21.6	26.7	18.8	29.3	20.0
	316	25.4	20.8	26.6	20.6	25.2	22.3
Limestone	16	16.9	12.8	33.1	27.3	30.0	20.8
	79	13.5	9.6	28.8	19.1	24.9	19.9
	159	13.1	8.9	17.5	11.4	26.4	21.2
	316	9.9	6.8	14.6	9.3	23.1	19.7

Table 5-2. Relative roughness ratio R for various rock – steel interfaces

	Relative roughness ratio R = R_a,steel/R_a,rock			
Steel R_a (μm)	Sandstone	Flagstone	Andesite	Limestone
0.4	0.021	0.073	0.069	0.148
7.2	0.379	1.310	1.241	2.667
34.0	1.789	6.181	5.862	12.592

5.2.1 Results for fixed steel roughness

Figure 5-5 to Figure 5-7 show how the behaviour of the interface varies for the four different rock types when the value of steel roughness is fixed.

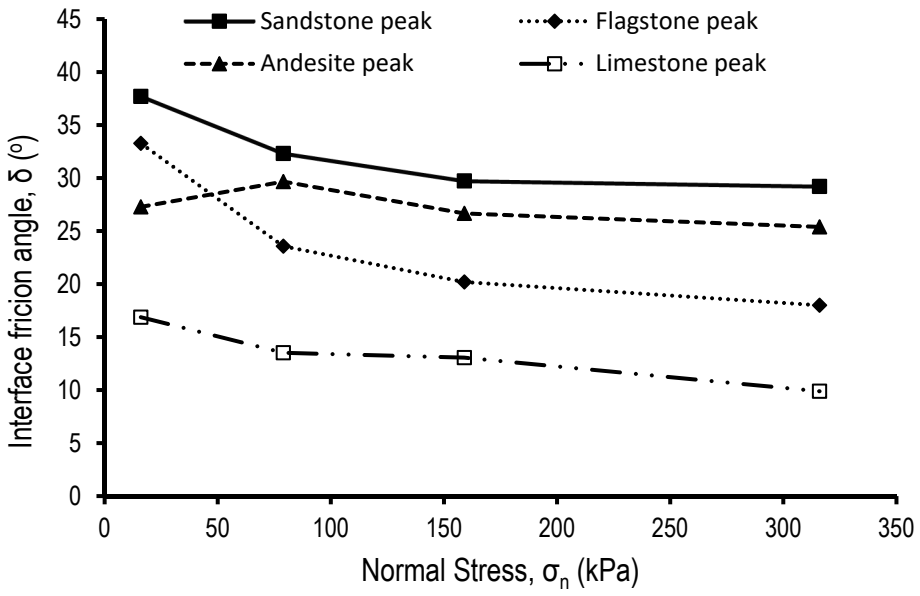

Figure 5-5. Comparison of δ_{peak} from interface testing of four rock types against steel with R_a = 0.4 μm

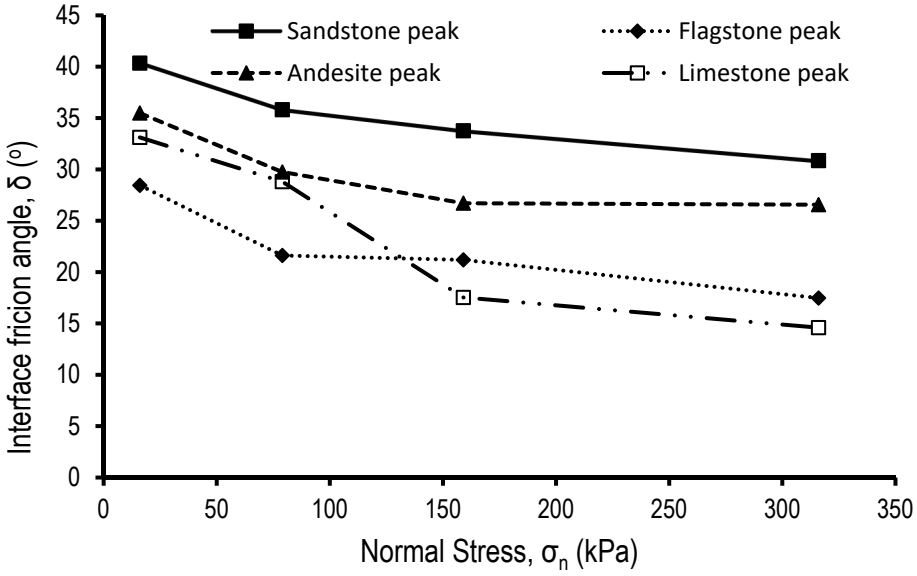

Figure 5-6. Comparison of δ_{peak} from interface testing of four rock types against steel with R_a = 7.2 μm

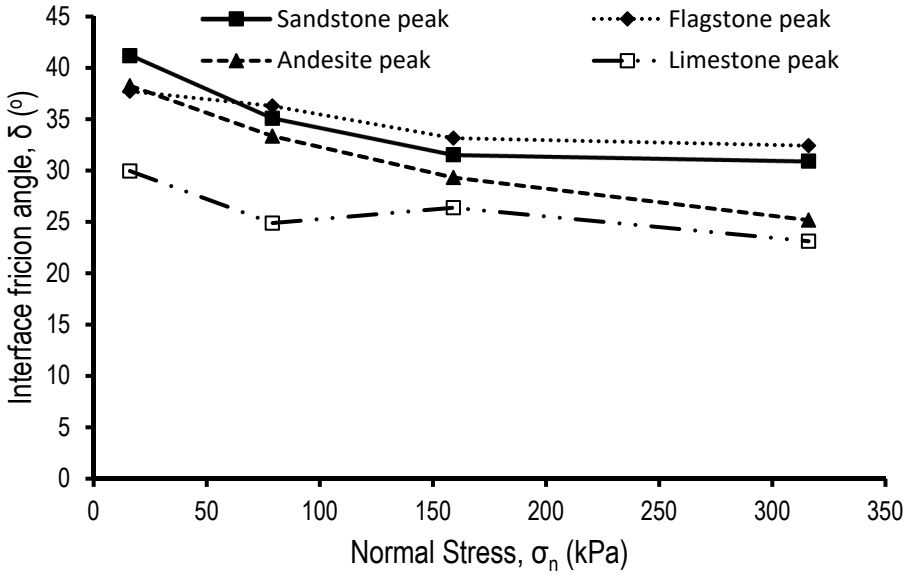

Figure 5-7. Comparison of δ_{peak} from interface testing of four rock types against steel with R_a = 34 μm

The interface exhibits the highest interface friction angle (δ) values (considering both peak and ultimate, though only peak values are shown here to avoid repetition) when Sandstone (the roughest of the rock types tested) is used. Flagstone and Andesite have very similar R_a values (0.3 μm difference)

and resulted in comparable interface friction angles. Limestone is significantly smoother resulting in the weakest interface (especially for steel R_a = 0.4 μm).

The effect of surface roughness, in terms of relative roughness ratio R = $R_{a,steel}/R_{a,rock}$ will be discussed more, later in this thesis, in section 5.5.1 where equations for the estimation of shear strength during the design process are presented.

5.3 Effect of normal stress on the shear behaviour

Interface tests were carried out under four different normal stress levels (16, 79, 159 and 316 kPa) in order to investigate its effect on the shear strength and the overall behaviour of the interface. Figure 5-8 to Figure 5-15 show how the peak and ultimate interface friction angles of the various rock types against the various steel interfaces change in terms of the applied normal stresses. These figures show the basic friction angle (φ_b) and the results from tilt table testing of each interface because it was felt that in some cases, it could be an indicator of the overall behaviour of the interface independent of normal stress. The results are also annotated with the roughness ratio, R. The tilt table value for all the rock – steel R_a = 7.2 μm interfaces lies between the values for steel R_a = 0.4 and 34 μm, therefore it was omitted from the figures for the sake of clarity.

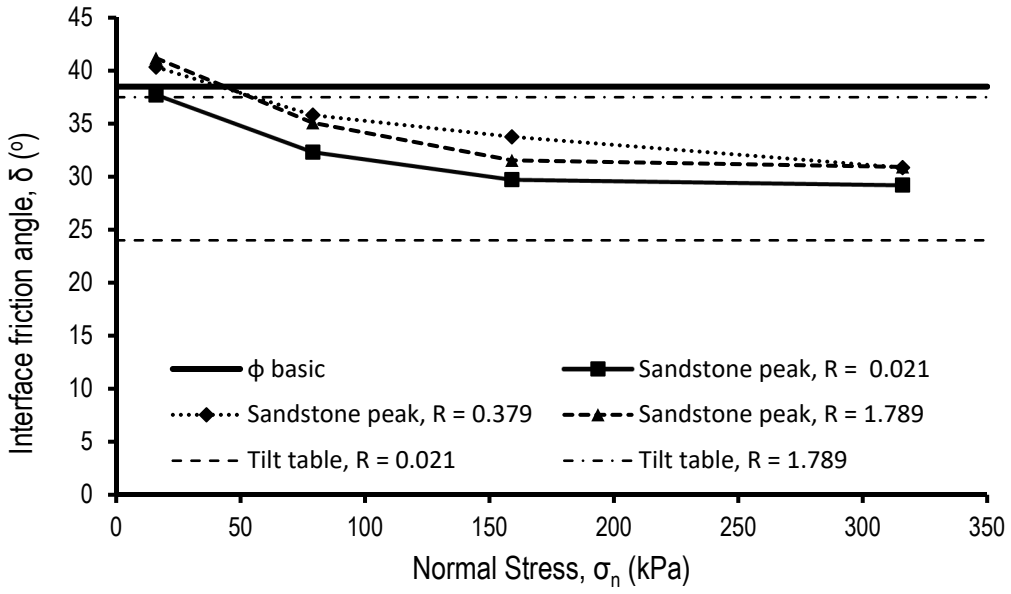

Figure 5-8. Variation of peak interface friction angle for Sandstone-steel interfaces of varying roughness, Sandstone R_a = 19 μm

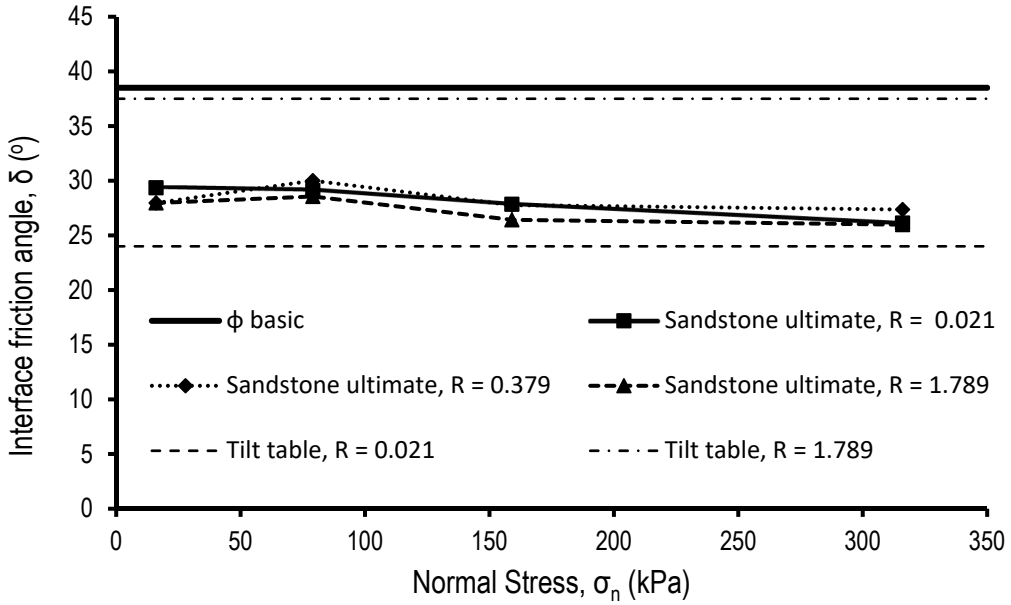

Figure 5-9. Variation of ultimate interface friction angle for Sandstone-steel interfaces of varying roughness, Sandstone R_a = 19 μm

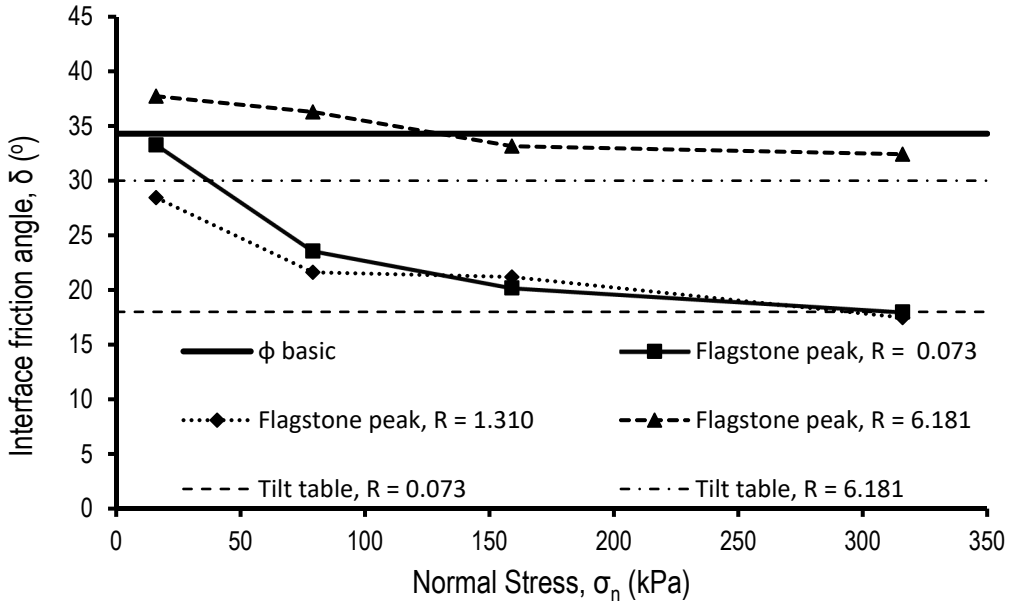

Figure 5-10. Variation of peak interface friction angle for Flagstone-steel interfaces of varying roughness, Flagstone R_a = 5.5 µm

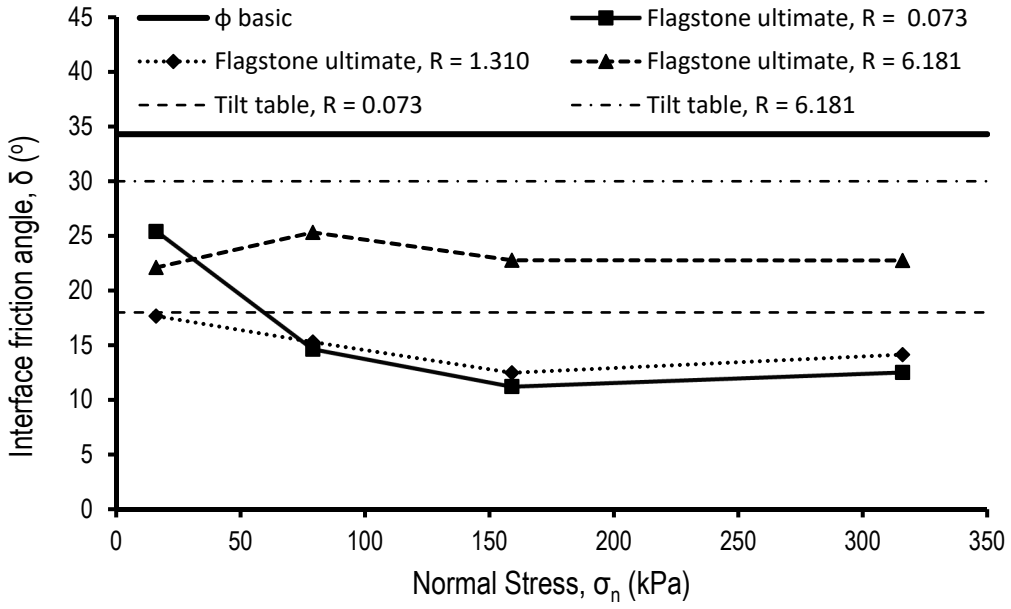

Figure 5-11. Variation of ultimate interface friction angle for Flagstone-steel interfaces of varying roughness, Flagstone R_a = 5.5 µm

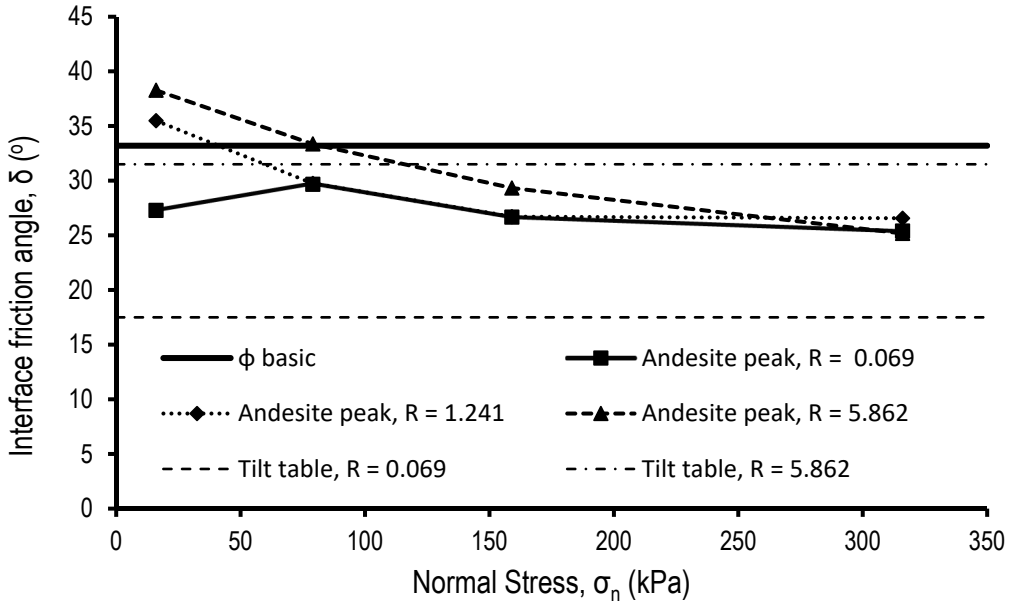

Figure 5-12. Variation of peak interface friction angle for Andesite-steel interfaces of varying roughness, Andesite R_a = 5.8 µm

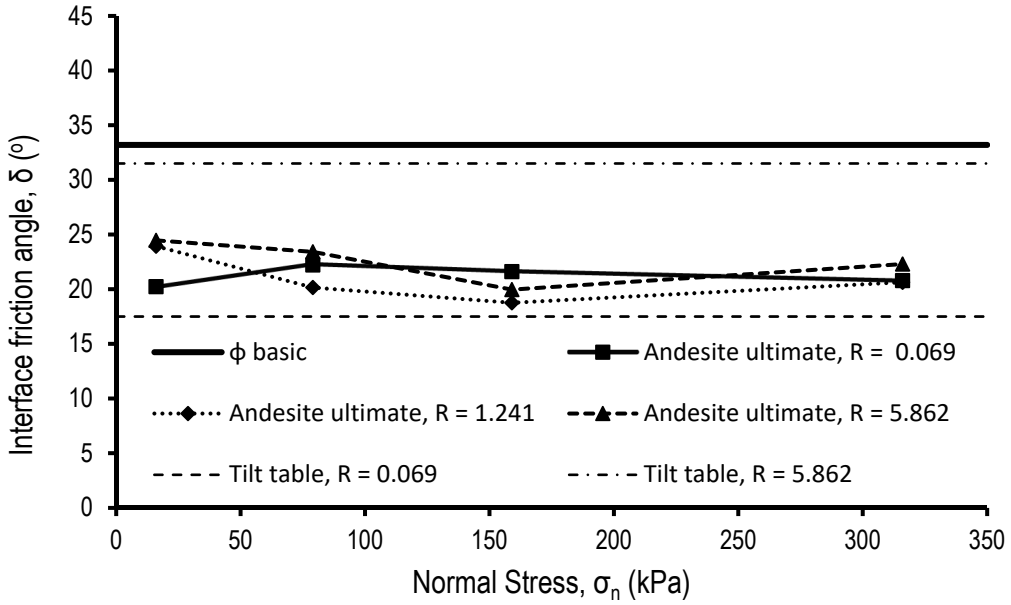

Figure 5-13. Variation of ultimate interface friction angle for Andesite-steel interfaces of varying roughness, Andesite R_a = 5.8 µm

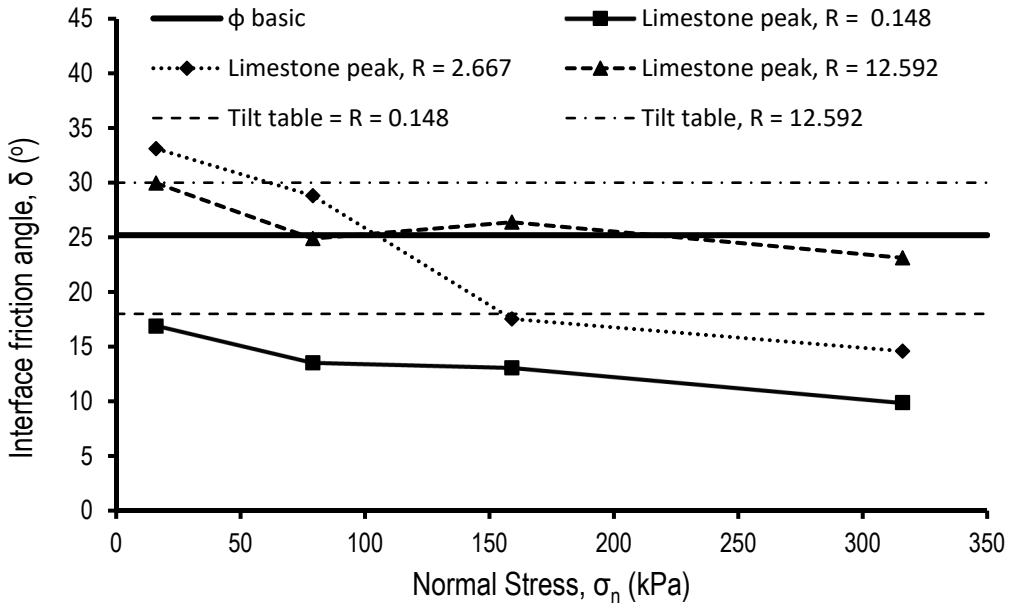

Figure 5-14. Variation of peak interface friction angle for Limestone-steel interfaces of varying roughness, Limestone R_a = 2.7 μm

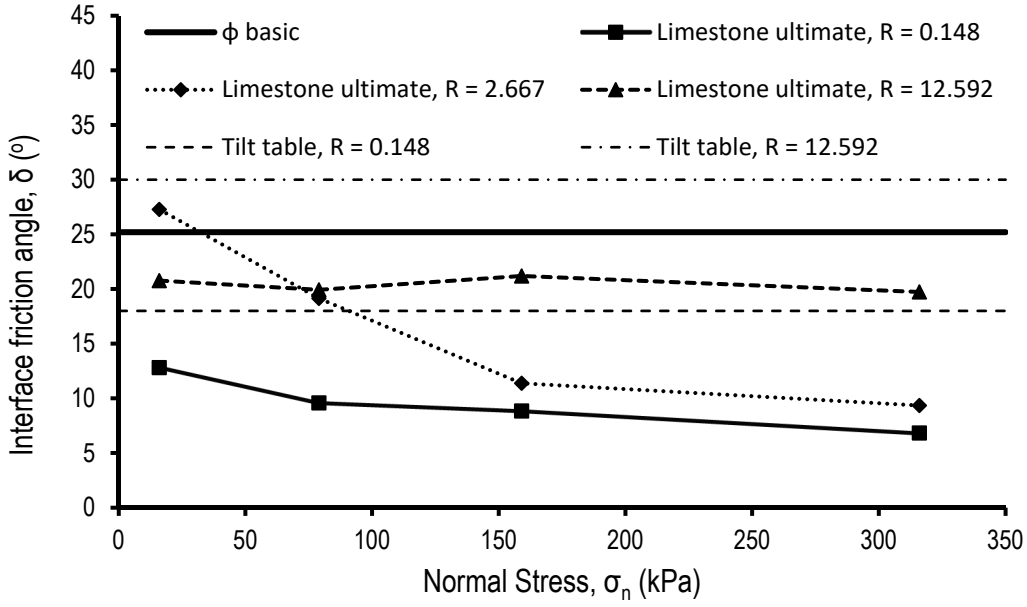

Figure 5-15. Variation of ultimate interface friction angle for Limestone-steel interfaces of varying roughness, Limestone R_a = 2.7 μm

In Figure 5-8 to Figure 5-15 it is shown that irrespective from the rock type, the interfaces typically exhibit the highest friction angle at normal stress of 16 kPa. The interface friction angle decreases with increasing normal stress up to 159 kPa and tends to a lower value between 159 and 316 kPa where little variation

is noticed and a plateau is reached. This decrease of interface friction angle with increasing normal stress is in accordance with the findings of Abuel Naga et al. (2018). They investigated the effect of the continuum surface properties (roughness and hardness) on the shear behaviour of continuum – granular material interfaces and found that the interface friction angle (in terms of coefficient of friction in this case) is reduced with increasing normal stress. They conducted interface shear box tests at normal stress of 55.5, 97.3 and 183.5 kPa and a drop of up to ~ 25% was noticed when normal stressed increased from 55.5 to 183.5 kPa (Figure 5-16), however the mechanism was not discussed further.

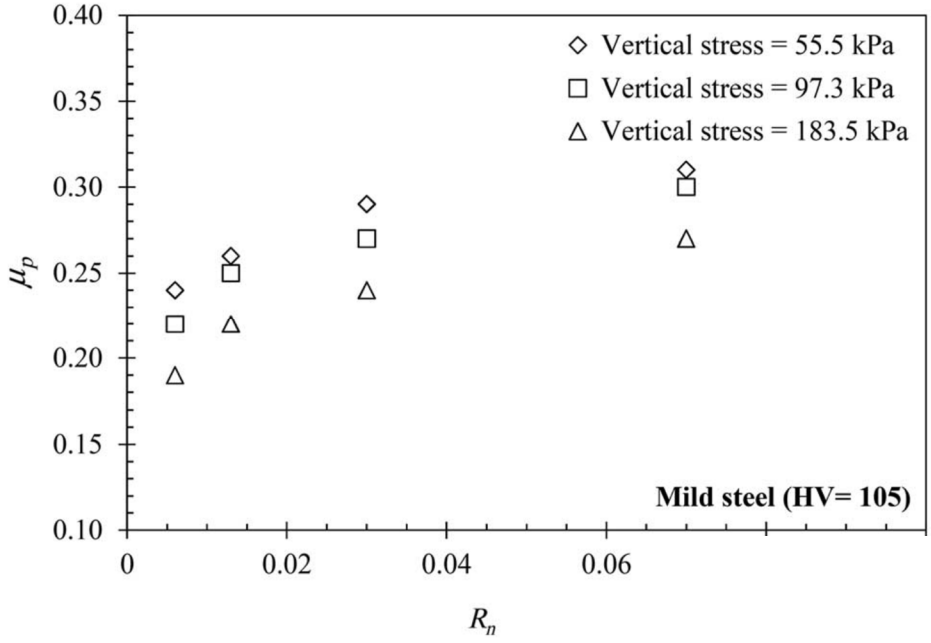

Figure 5-16. Effect of normal stress on interface friction angle of continuum material – sand interfaces. Modified from Abu Haga et al. (2018)

Based on figures Figure 5-1 to Figure 5-4 and also by comparing the peak and ultimate values for each individual rock – steel combination (Figure 5-8 - Figure 5-15) it can be seen that all the interfaces exhibit a rather “brittle” behaviour. The ultimate friction angles are typically significantly lower than the peak values (over 50% in some cases). At low normal stress level (16 kPa), peak interface friction angle values tend to the φ_b which is usually (apart from Limestone) higher than tilt table results for the rock – steel R_a = 34 μm interfaces.

When polished steel (R_a = 0.4 μm) is used as foundation analogue, the roughness ratio (R) values vary between 0.021 (Sandstone) and 0.148 (Limestone). The Sandstone which has the roughest surface (R_a = 19 μm) – polished steel interface is the strongest, exhibiting δ_{peak} between 38° and 29° and δ_{ult} between 29° and 24° depending on the applied normal stress. In the case of Flagstone (R_a = 5.5 μm), the interface yields lower peak (δ_{peak} = 33°-18°) and ultimate values (δ_{ult}= 25° - 13°) depending on normal stress. Whereas, for Andesite (R_a = 5.8 μm) – polished steel interface, δ_{peak} ranges between 27° and 25° and δ_{ult} is remarkably consistent around 21 irrespective of normal stress. When Limestone (R_a = 2.7 μm) which is the smoothest rock tested here is used as foundation surface, the interface becomes significantly weaker, exhibiting δ_{peak} between 17° and 10° and δ_{ult} between 13° and 7°. The friction angle values for the Limestone – polished steel interface seem significantly low and it is believed that they are dictated by the very low surface roughness of both interacting materials (i.e. Limestone and steel).

Figure 5-17 and Figure 5-18 present how the interface friction angle (peak and ultimate respectively), changes with increasing relative roughness ratio R for each rock type. For ease of comparison and representation, the average interface friction angle of the tests at 159 and 316 kPa (where the interface seems to be more “predictable” as described above) has been considered for each individual rock – steel combination. The relative roughness ratio (R) ranges between 0.021 (Sandstone) and 0.148 (Limestone) for steel R_a = 0.4 μm, between 0.379 and 2.667 for steel R_a = 7.2 μm and between 1.789 and 12.592 for steel R_a = 34 μm. Sandstone and Limestone are the rock types with the highest and lowest surface roughness respectively and consequently they determine the upper and lower bound of the ratio for a specific steel surface roughness.

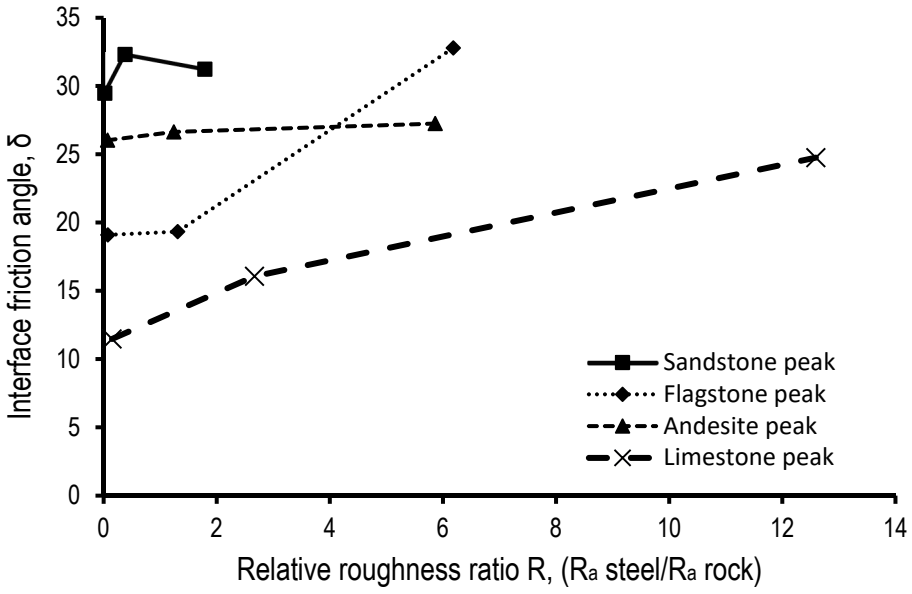

Figure 5-17. Interface friction angle vs relative roughness ratio R, considering average peak values of rock – steel interfaces at 159 and 316 kPa

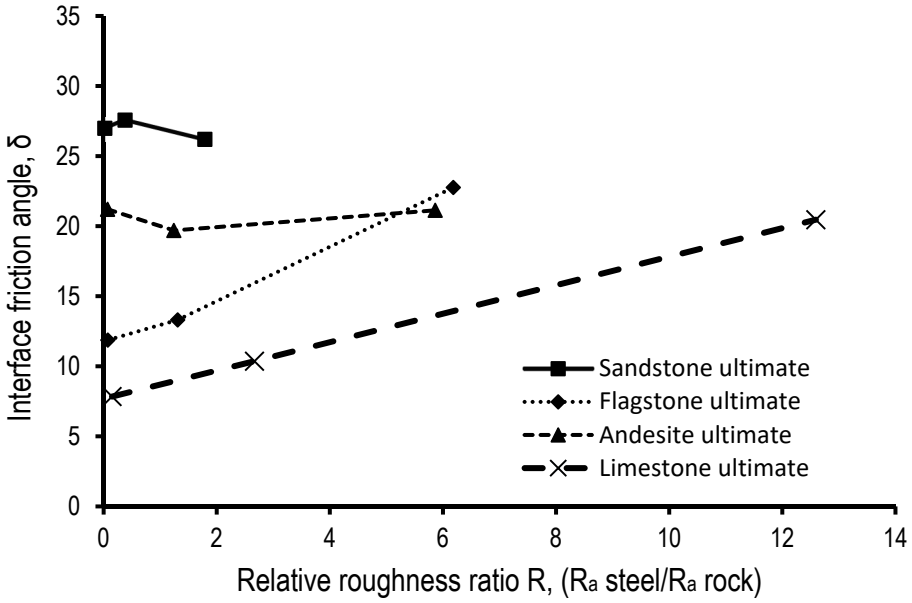

Figure 5-18. Interface friction angle vs relative roughness ratio R, considering average ultimate values of rock – steel interfaces at 159 and 316 kPa

It is apparent that the variation of relative roughness ratio R doesn't have the same effect on all the rock – steel interfaces. Sandstone and Andesite interfaces aren't significantly affected by the value of R whereas the interface friction angle for Flagstone and Limestone interfaces increases significantly

for increasing R throughout its whole range. This behaviour is different to that exhibited for continuum material – sand interfaces (Jardine et al. 1993, Abuel-Naga et al., 2018), where the upper limit of the interface shear strength is defined by the internal friction angle of the granular material. Increasing R leads to an increase of interface friction angle until the interface shear strength is higher than the internal friction of the granular material; at this point the shear band "moves" away from the interface and into the soil mass, due to the "compliance" of the granular material.

5.3.1 Behaviour of Sandstone and Andesite interfaces

Despite the fact that Sandstone-steel interface exhibits higher δ values compared to Andesite-steel interface (irrespective of the steel roughness), the overall behaviour of the two interface types is very similar as far as the effect of normal stress and relative roughness ratio R is concerned (e.g. Figure 5-8, Figure 5-12, Figure 5-17). For that reason, it was felt that they should be considered together.

The relative scratch hardness has been identified in the literature as a factor that affects the shear deformation of continuum – continuum (Engelder and Scholz 1976) and continuum – granular material interfaces (Abuel-Naga et al., 2018). When one of the two counterfaces is harder, then ploughing occurs during shear (Engelder and Scholz 1976). In this study, a relative hardness ratio M equal to Mohs,steel/Mohs,rock has been considered to determine whether ploughing will occur. The Mohs hardness value for the Sandstone is 7, for the Andesite is 6 and for the mild steel is 4, resulting in M values of 0.57 and 0.67 for Sandstone and Andesite interfaces respectively (i.e. the rock is harder than the steel). This means that no ploughing of the steel into the rock surface takes place during shearing, although rock asperities could plough into the steel surface. The effect of relative hardness on the interface behaviour is discussed in more detail in 5.3.3.

In Figure 5-8 and Figure 5-12 it can be seen that peak interface friction angle values are higher for low normal stresses (up to 79 kPa) and increase with

increasing steel roughness. As normal stress increases (159 and 316 kPa), peak interface friction angle reduces and the effect of steel roughness becomes less apparent (i.e. the data become closer together on moving to the right).

It is assumed that for lower normal stress values (16 and 79 kPa) the interface is free to dilate and the asperities of the rock override the asperities of steel during shearing, therefore δ_{peak} increases as R_a increases (higher steel asperities). For higher normal stress levels (159 and 316 kPa) dilation is partially suppressed and part of the rock asperities plough into the steel surface during shearing. This is in accordance with the normal (or vertical) displacement as shown in Figure 5-19 measured during shearing. The displacement is positive (dilatant) for normal stress of 16 kPa and negative (contractive) for normal stress of 316 kPa. In addition, dilation seems to be greater for increasing steel R_a and roughness ratio R (at normal stress of 16kPa), whereas at normal stress of 316 kPa the contraction is similar irrespective of steel roughness. The contraction at normal stress of 316 kPa indicates that damage/ploughing occurs during shearing.

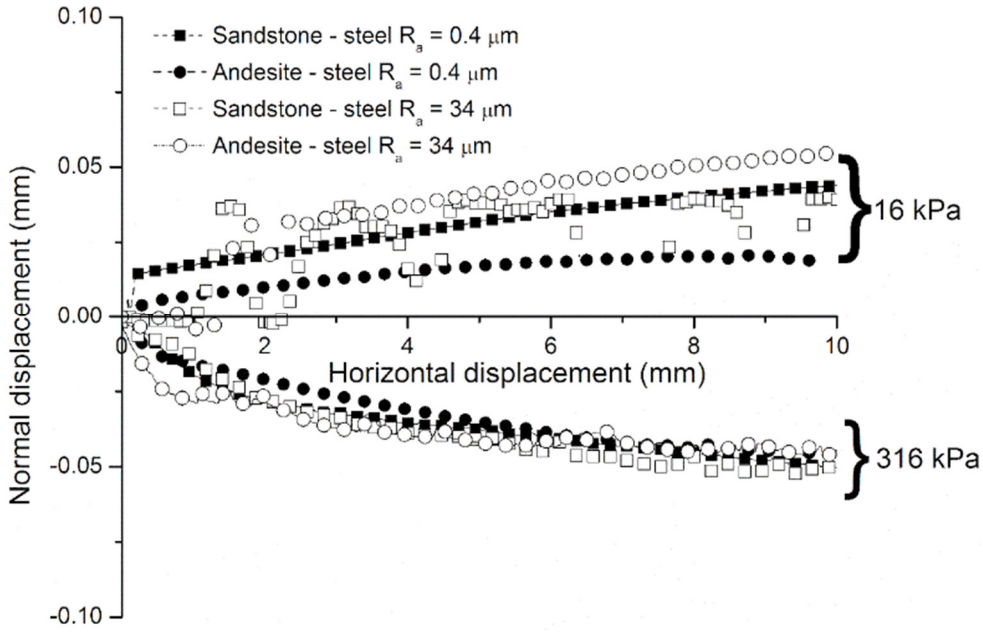

Figure 5-19. Normal displacement vs shear displacement for Sandstone and Andesite against steel of R_a = 0.4 and 34 μm

As far as δ_{ult} is concerned, the effect of both normal stress and steel R_a is rather minimal at larger strains or displacements as can be seen in Figure 5-9 and Figure 5-13. Therefore, once the initial low stress dilation has occurred or the surface has been damaged the shearing behaviour on the interface for the harder Sandstone and Andesite becomes independent of the initial surface steel roughness or normal stress.

The tilt table tests using steel R_a = 0.4 μm lie below the lower values observed from IST testing (typically for steel R_a = 0.4 μm) as far as peak and ultimate values are concerned. Thus, tilt table test seems to be able to provide a lower bound value for Sandstone – steel and Andesite – steel interfaces.

5.3.2 Behaviour of Flagstone and Limestone interfaces

Flagstone – steel and Limestone – steel interfaces exhibit similar behaviour to each other, albeit Flagstone interfaces tend to yield higher interface friction angle values. Both rock types have a Mohs hardness value similar to that of mild steel (4 on the Mohs scale). Limestone has a value of 4.5 and Flagstone has a value of 3 on the Mohs scale.

The interfaces exhibit the highest δ_{peak} values for σ_n = 16 kPa because dilation is taking place and consequently δ_{peak} increases with increasing steel R_a (Figure 5-10, Figure 5-14 and Figure 5-20). As σ_n increases (159 and 316 kPa), dilation is suppressed (Figure 5-20) however the effect of steel R_a is still apparent (i.e. δ_{peak} is higher for steel R_a = 34 μm) in contrast to what was shown before for Sandstone and Andesite interfaces. This happens because Flagstone and Limestone exhibit hardness values very close to that of the steel element. Therefore it is believed that higher localised normal stress at the point of contact is required for ploughing to occur. As the normal stress increases, ploughing of the steel asperities into the rock surface (or vise versa depending on which material is harder) takes place during shearing. It is also apparent, that contraction (i.e. indicating ploughing) for Sandstone and Andesite interfaces (contraction values in Figure 5-19) is almost double the values noticed for Flagstone and Limestone interfaces (Figure 5-20) This behaviour is in accordance with Engelder 1978, who showed that the mode of shearing

depends on the applied normal stress and the hardness of the counterface materials. This phenomenon is more pronounced as steel R_a increases (for a given σ_n), because actual applied normal stress at the contact points is potentially much higher compared to the nominal σ_n which is calculated as an average value ($\frac{applied\ normal\ force}{plan\ area\ of\ rock\ sample}$). This seems to affect both the peak and ultimate interface friction angle. The effect of both steel and rock hardness is discussed further in the next section (5.3.3) utilising the relative hardness ratio M (as defined earlier) for the investigated rock – steel interfaces.

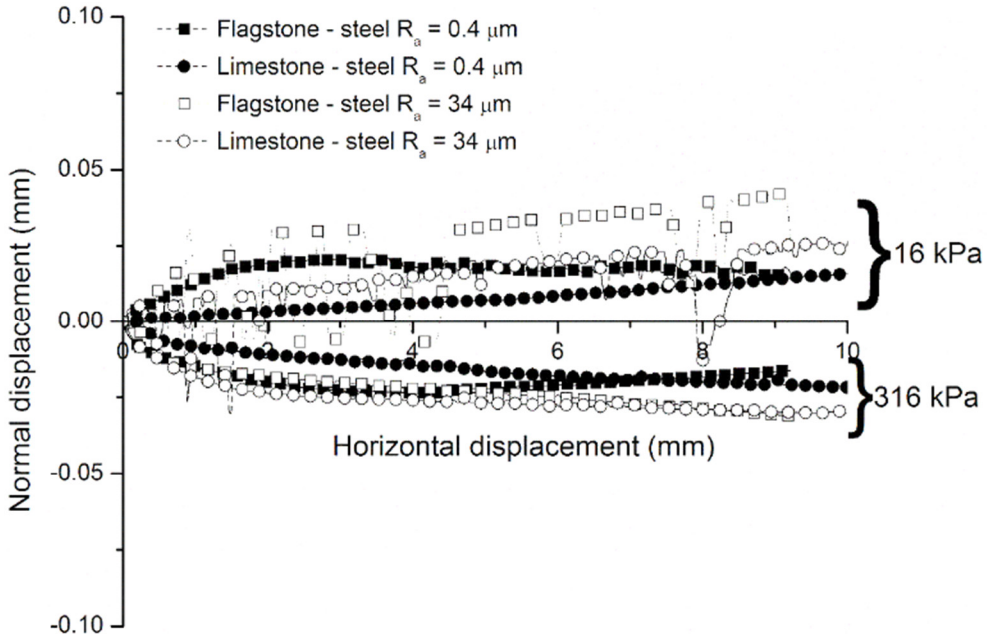

Figure 5-20. Normal displacement vs shear displacement for Flagstone and Limestone against steel R_a = 0.4 and 34 μm

As far as the peak values of interface friction angle are concerned, the tilt table test provides a lower bound value for the Flagstone – steel interfaces, irrespective of steel R_a. The tilt table tests seem to overestimate the ultimate values of shear resistance for steel R_a = 0.4 and 7.4 μm, thus a lower bound value can only be provided for steel R_a = 34 μm when the ultimate values are considered. The tilt table seems to overestimate the interface friction angle (compared to the IST) for Limestone – steel interfaces irrespective of the steel roughness, apart from the case of σ_n = 16 kPa. Therefore, it could be used to characterise Limestone – steel interfaces when the applied normal stress does not exceed 16 kPa.

5.3.3 Effect of relative hardness

Hardness has been previously identified as a factor that influences the behaviour of rock interfaces (Engelder 1976) and taking into account that the Mohs hardness values of the investigated rocks are quite different, relative hardness ratio M = $M_{,steel}/M_{,rock}$ has been adopted and its effect on interface friction angle δ are shown in Figure 5-21 and Figure 5-22. Each figure contains three δ values per rock type (one per steel R_a) and a contour line that groups the data points for each steel R_a value. As shown previously (Figure 5-8 to Figure 5-15), δ varies significantly between 16 and 159 kPa, whereas it seems to settle between 159 and 316 kPa. Therefore, the average value of δ taking into account only the values at 159 and 316 kPa has been considered.

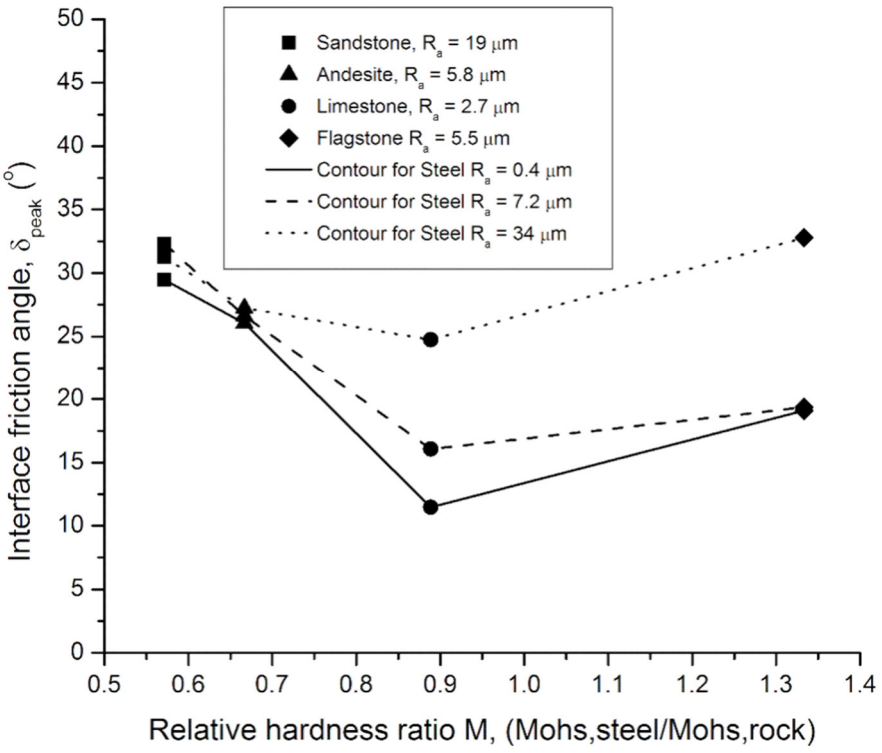

Figure 5-21. Interface friction angle δ vs relative hardness ratio M, considering average peak values of tests at 159 and 316 kPa

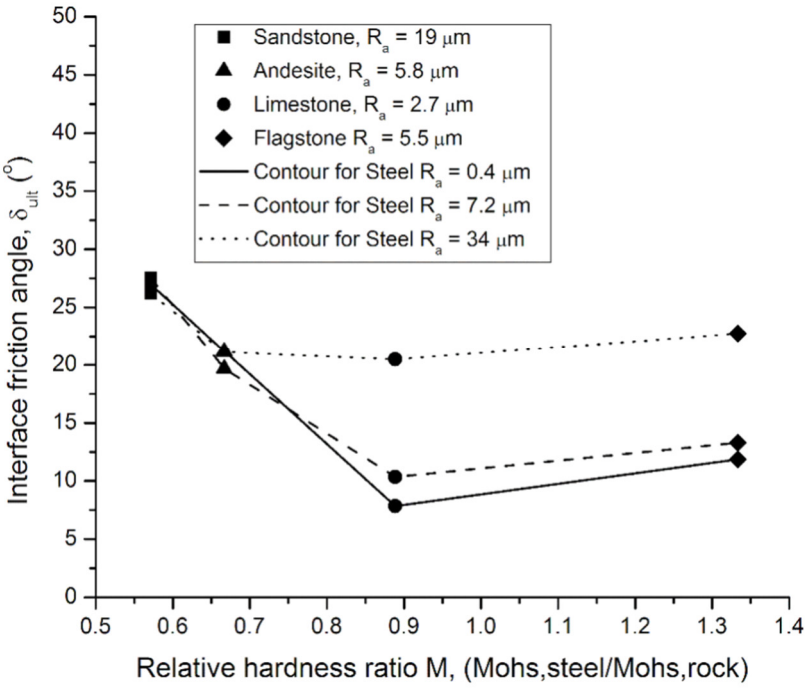

Figure 5-22. Interface friction angle δ vs relative hardness ratio M, considering average ultimate values of tests at 159 and 316 kPa

In Figure 5-21 and Figure 5-22 it can be seen that the contour lines for peak and ultimate values exhibit very similar trends although ultimate values are lower (as previously shown). Sandstone – steel interfaces (M = 0.57) exhibit the highest values and Limestone – steel interfaces (M = 0.89) exhibit the lowest values. For steel R_a = 0.4 and 7.2 μm, interface friction angle values drop significantly between M = 0.57 and M = 0.89 and then δ increases again for M = 1.33 (Flagstone – steel). For steel R_a = 34 μm a similar pattern is followed, where Limestone – steel interface again exhibits the lower values of δ, although the difference to the δ values of Andesite – steel and Flagstone – steel interfaces is not as apparent as for steel R_a = 0.4 and 7.2 μm. In other words, it seems that the interface shear strength exhibits the lowest value when M is close to 1, whereas it increases as M displays values significantly different to 1. The Mohs hardness value for the steel used in this study is 4 and as Mohs scale ranges between 1 and 10, the potential lower and upper limit values for M are in theory 0.4 and 4 respectively.

Mohs hardness ratio M gives values close to 1, when the hardness of the steel and the rock are similar (e.g. 0.89 for Limestone – steel). In this case, it is

believed that ploughing (of the harder material into the softer) is reduced during shearing, thus leading to lower δ values. As the steel roughness increases, the localised stress at the points of contact is higher (fewer contact points) and ploughing becomes more apparent. If the rock is significantly harder than the steel (i.e. M tends to 0.4), then sliding and ploughing of the rock into the steel takes place even under low normal stress levels, leading to an increase in the interface shear strength. In a similar manner, when then steel is significantly harder than the rock (i.e. tends to 4 which is the maximum value for steel with M = 4), ploughing (scratching) of the steel into the rock takes place. However, taking into account the data points in Figure 5-29 and Figure 5-30, it is believed that δ is higher when M tends to 0.4 (i.e. rock harder than the steel), because steel is more ductile than rock. Therefore, it is felt that more energy is dissipated when rock ploughs (causing scratches) into the steel compared to when the steel ploughs into the rock surface.

It should be noted here that the surface roughness varies across the different rock types, therefore although in this section the data has been discussed considering the effect of the relative hardness ratio M, however there is also an effect of relative roughness ratio R on the obtained values of δ (as has been discussed in previous sections of this thesis). In order to evaluate R's influence, it was decided to re plot interface friction angle δ vs M (Figure 5-23), considering only δ values obtained from tests with comparable values of relative roughness ratio R. As shown in Table 5-3, data from tests with R of 1.789 (Sandstone), 1.309 (Flagstone), 1.241 (Andesite) and 2.667 (Limestone) have been considered.

Table 5-3. Values of relative roughness ratio R, considered for data shown in Figure 5-31

Rock type	Range of relative roughness ratio R for steel R_a = 0.4 – 34 µm	R chosen as a reference for comparison
Sandstone	0.021 - 1.789	1.789 (steel R_a = 34 µm)
Flagstone	0.073 - 6.181	1.309 (steel R_a = 7.2 µm)
Andesite	0.069 – 5.86	1.241 (steel R_a = 7.2 µm)
Limestone	0.148 – 12.593	2.667 (steel R_a = 7.2 µm)

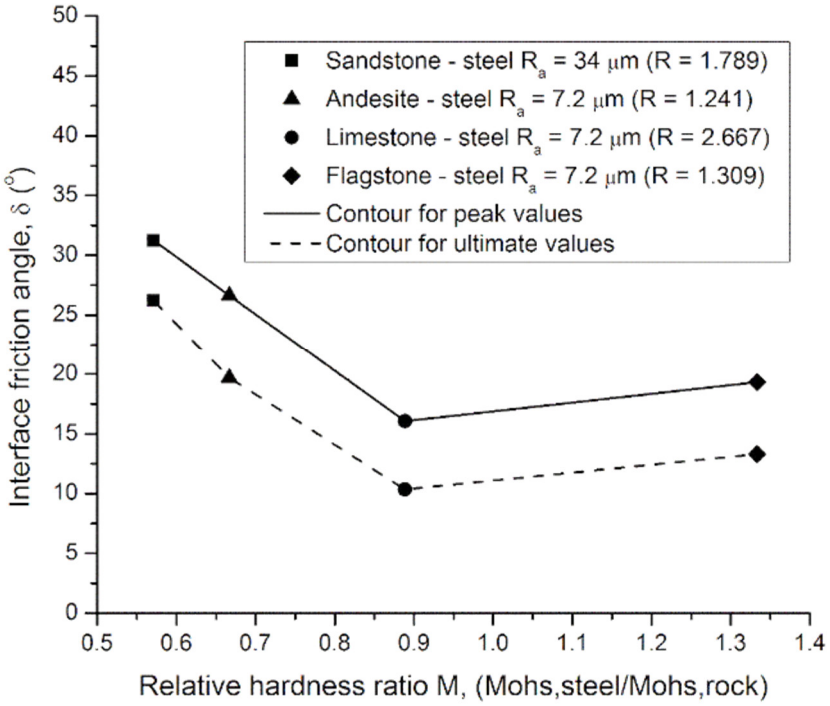

Figure 5-23. Interface friction angle δ vs relative hardness ratio M, considering average ultimate values of tests at 159 and 316 kPa, considering data from selected tests with comparable roughness ratio R

The contours in Figure 5-23 look very similar to those displayed in Figure 5-21 and Figure 5-22, suggesting that the discussion presented above about the effect of relative hardness ratio M on the interface friction angle δ is valid, even if inevitably the surface roughness of the different rock types is different.

5.4 Failure envelopes

The following graphs present the failure envelopes of the interface for the different rock types. The envelopes appear to be curved especially for lower normal stresses.

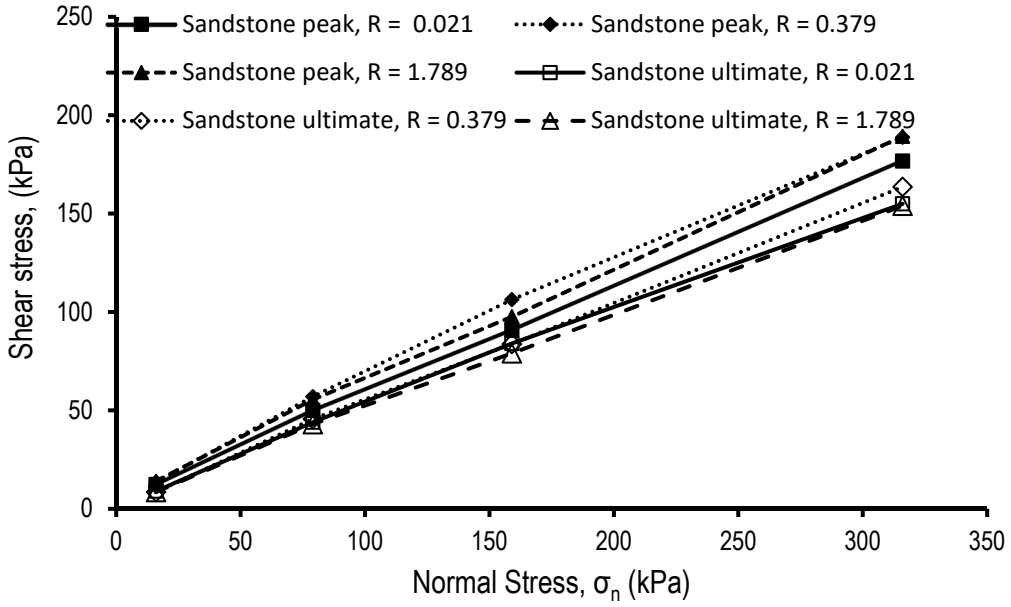

Figure 5-24. Failure envelopes for Sandstone –steel interfaces

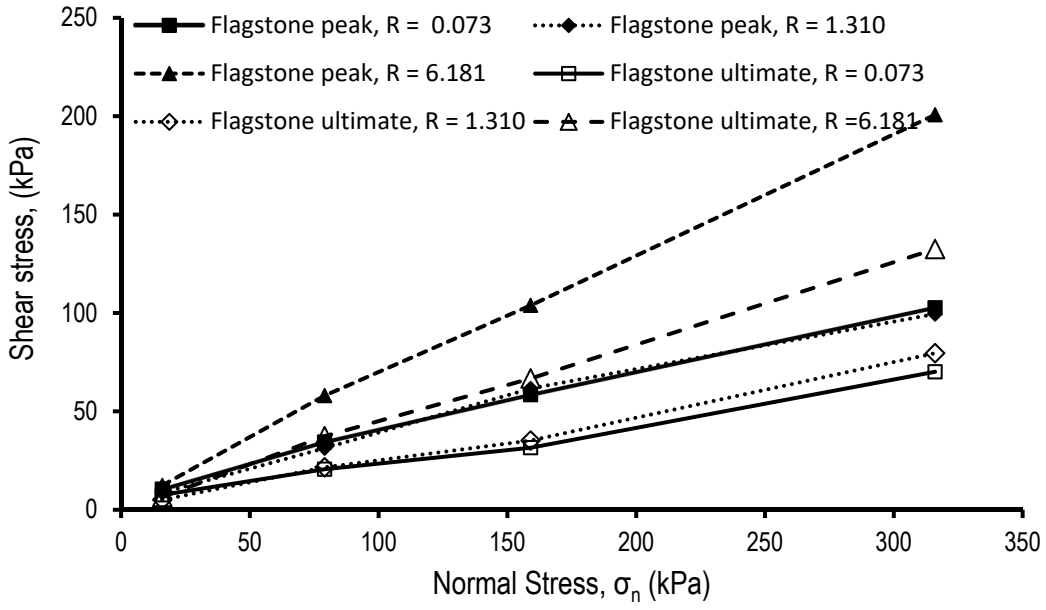

Figure 5-25. Failure envelopes for Flagstone – steel interfaces

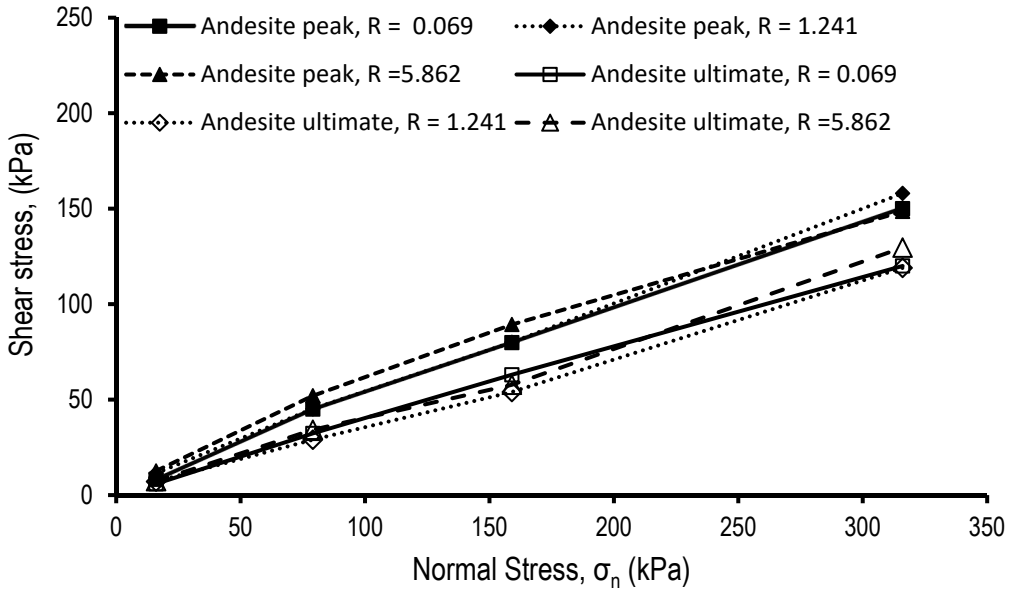

Figure 5-26. Failure envelopes for Andesite –steel interfaces

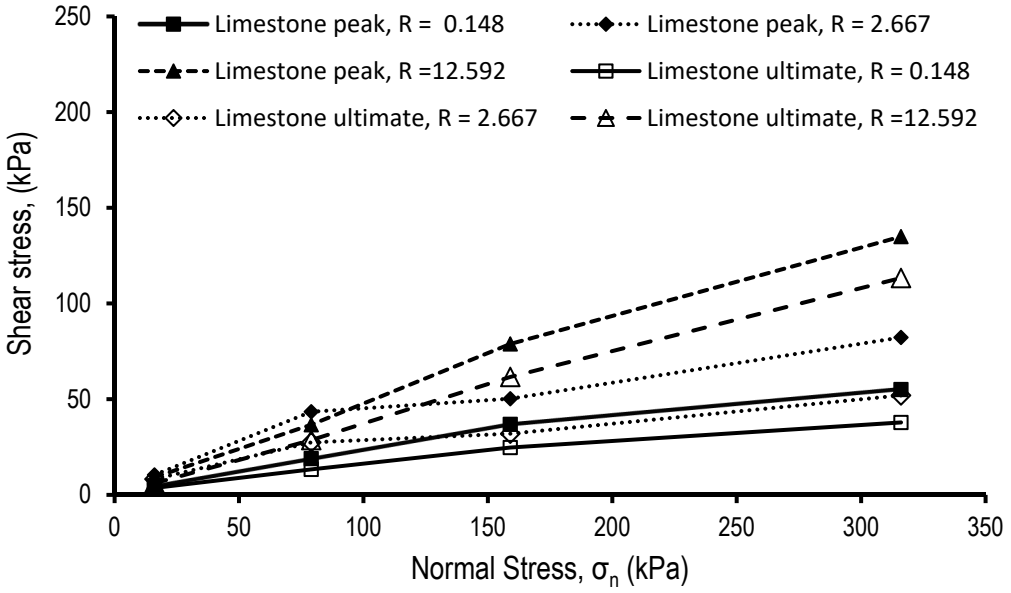

Figure 5-27. Failure envelopes for Limestone – steel interfaces

Peak and ultimate shear stresses display curved (bilinear) behaviour. Higher friction angles are observed for low normal stresses (16 - 79kPa) whereas lower values are observed when the applied normal stress increases (79 - 316 kPa). This suggests that a linear failure envelope should be avoided when determining interface friction angles for the design of foundations and the anticipated normal stresses should be taken into account. If the anticipated

normal stress is between 79 and 316 kPa then a linear envelope could be considered for all the rock types apart from the Limestone. At lower effective stress (up to 79 kPa), the interface is free to dilate leading to higher interface friction angles, whereas for higher σ_n, dilation is suppressed and consequently lower friction angles are observed. This behaviour though seems to be influenced by steel roughness and rock surface hardness as descried previously in this chapter and adopting purely a friction envelope approach to design would be overly simplistic.

5.5 Final stage of alpha factor analysis

The Alpha factor approach was been introduced in Chapter 4 to present the data from rock analogue – steel interfaces testing. This approach can also be applied on the results from rock – steel interfaces. Figure 5-28 and Figure 5-29 display peak and ultimate apha (α) factors (i.e. τ/UCS) for the different rock – steel interfaces from IST testing, presented earlier in this chapter.

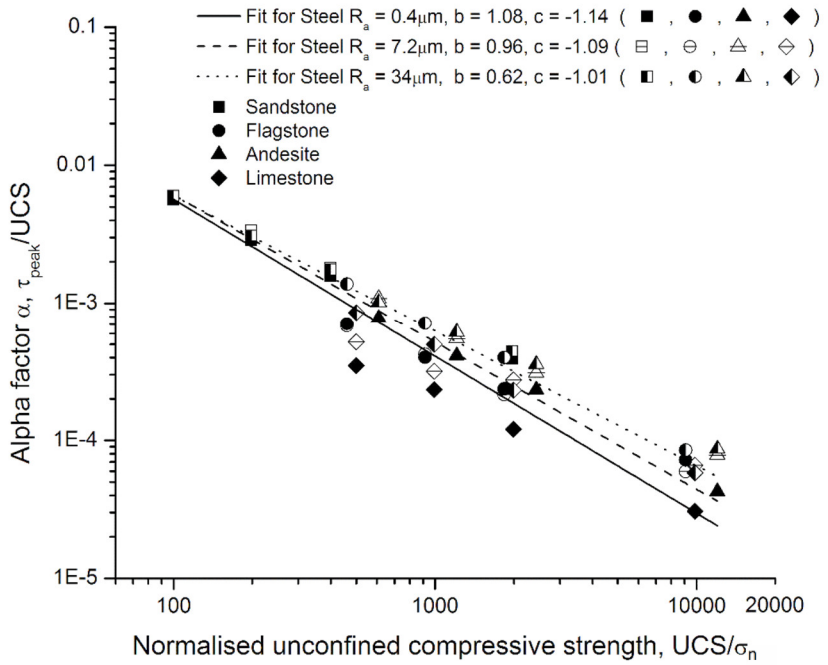

Figure 5-28. Alpha factors for rock – steel interfaces (IST), considering peak values

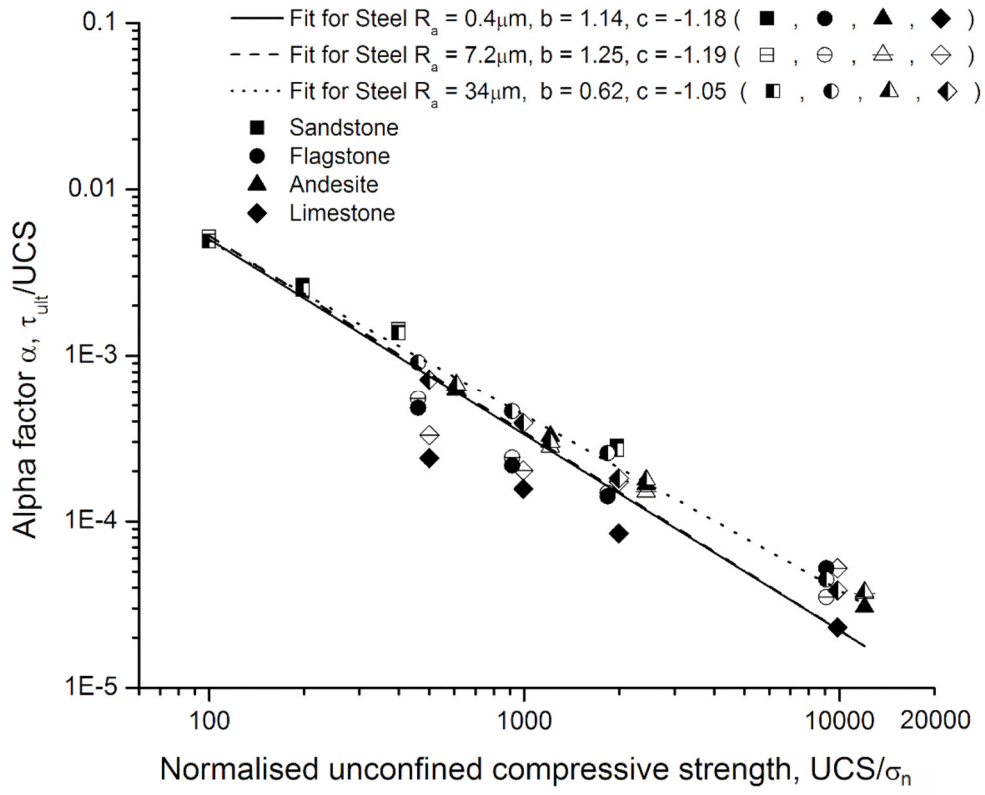

Figure 5-29. Alpha factors for rock – steel interfaces (IST), considering ultimate values

Contours have been plotted for the α values of all the rock types for each value of steel R_a (i.e. 3 contours per graph) and the fitting constants b, c for each contour are listed in Table 5-4.

Table 5-4. Summary table of arithmetic fitting constats b and c.

Steel R_a	Peak		Ultimate	
	b	c	b	c
0.4	1.08	-1.14	1.14	-1.18
7.2	0.96	-1.09	1.25	-1.19
34.0	0.62	-1.01	0.62	-1.05

Equation 4-2 can be solved for shear stress (τ) leading to:

$$\tau = b\frac{UCS^{(c+1)}}{\sigma_n^c} \qquad \text{Equation 5-1}$$

Where: τ = shear stress, *UCS* = unconfined compressive strength, σ_n = normal stress and b, c arithmetic fitting constants.

Equation 5-1 can be used to estimate the anticipated shear strength of a steel GBS placed on exposed seabed. If UCS cannot be determined in the lab (i.e. lack of in-situ samples), values found in the literature (e.g. memoirs of local geology) can be used. It should be noted that samples might be weathered and this needs to be taken into consideration as this might affect the UCS as described further in Chapter 8. Arithmetic constants b and c shall be selected according to the roughness (i.e. preparation) of the GBS footing. It is suggested that this equation is used for UCS of 31.5 – 192.7 MPa, normal stress of 16 – 316 kPa and steel R_a of 0.4 – 34 μm, i.e. within the range of the values used to derive it. Using values outside of this range requires extrapolation and the validity of the results might be questionable without further testing.

5.5.1 Simplified equations

Equation 5-1 contains two fitting parameters (b and c) which makes its use relatively complicated. Therefore, it was deemed appropriate to "fix" one of the two parameters and develop an equation that could be more easily used during the design process. In the previous section, it became apparent that b varies significantly with steel roughness (and consequently the relative roughness of the interface), whereas c is less sensitive to roughness changes. In addition, c being an exponent in Equation 5-1 affects primarily the shape (curvature) of the alpha factor vs normalised unconfined strength graph. On the other hand, b is a multiplier in the same equation and significantly affects the magnitude of alpha factor. Therefore, it was decided to use a constant value of c irrespective to steel roughness. For peak values, c was "fixed" to -1.08 (arithmetic average of -1.14, -1.09 and -1.01), whereas for ultimate values it was fixed to -1.14 (average of -1.18, -1.19 and -1.05). Least squares regression analysis was then used to calculate the b values that correspond to the "fixed" values of c. Figure 5-30 and Figure 5-31 display the variation of

b with the relative roughness ratio of the interface (R = $R_{a,steel}/R_{a,rock}$), considering peak and ultimate values respectively.

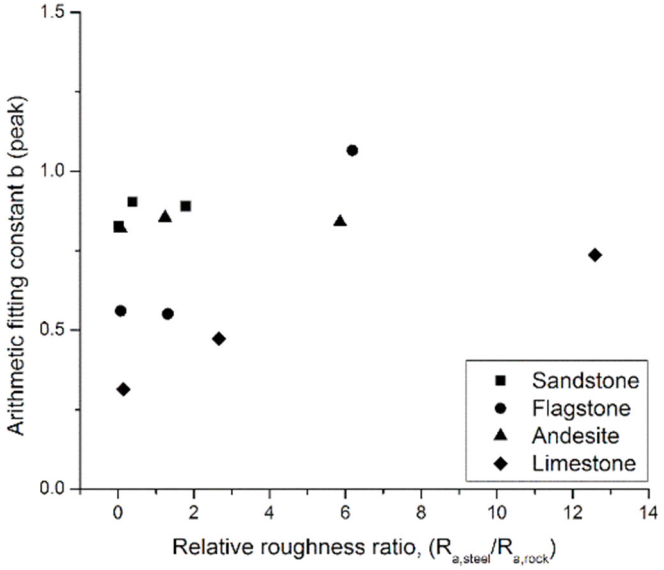

Figure 5-30. Variation of fitting parameter b with relative roughness of the interface (considering peak values of all the rock types combined)

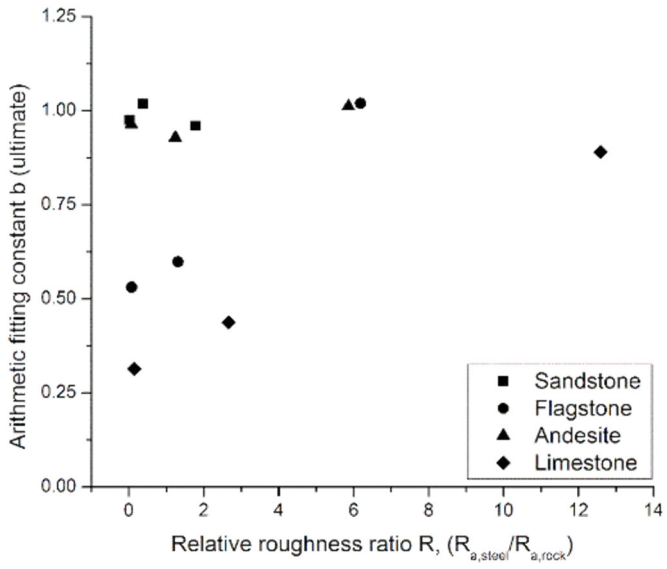

Figure 5-31. Variation of fitting parameter b with relative roughness of the interface (considering ultimate values of all the rock types combined)

Looking at the graphs, it can be seen that for relative roughness values of up to ~ 3, the data seems to have a parabolic shape whereas for values between 6 and 13 a linear pattern is followed. As a result, various attempts to describe

the whole dataset (for peak and ultimate values individually) using a single equation were unsuccessful since the match was not satisfactory.

As described earlier, Sandstone - steel and Andesite - steel interfaces seem to exhibit similar behaviour, possibly due to the similar Mohs hardness value (and consequently similar relative hardness ratio M,steel/M,rock). For the same reason, Flagstone - steel and Limestone - steel interfaces also exhibit similar behaviour. Therefore, it was decided to investigate the variation of b with relative roughness, for these two groups of rocks, individually.

Figure 5-32 and Figure 5-33 show the effect of the relative roughness ratio R on the arithmetic fitting constant b, for both peak and ultimate values from Sandstone – steel and Andesite – steel interfaces.

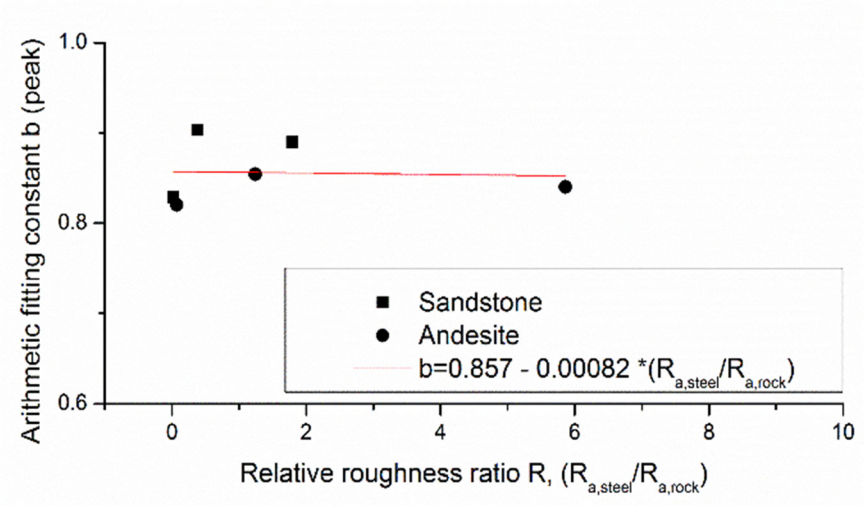

Figure 5-32. Variation of fitting parameter b with relative roughness of the interface (considering peak values of Sandstone and Andesite interfaces)

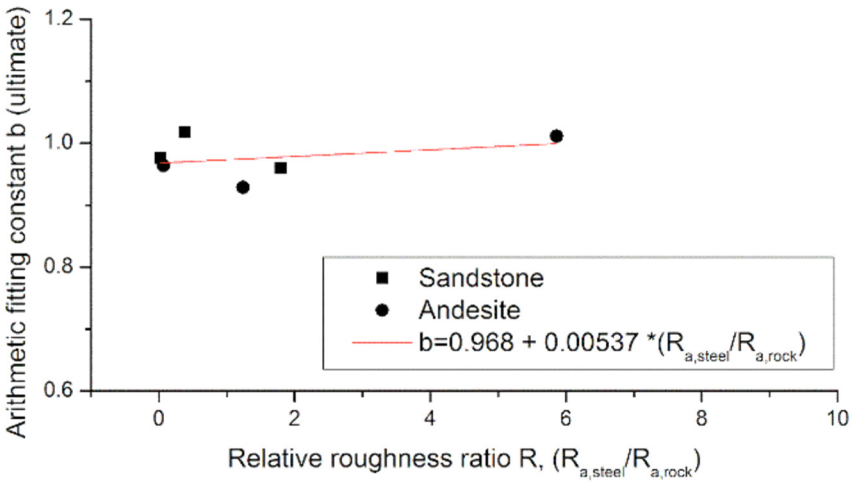

Figure 5-33. Variation of fitting parameter b with relative roughness of the interface (considering ultimate values of Sandstone and Andesite interfaces)

For Sandstone and Andesite interfaces the relative roughness ratio ranges between 0.021 and 5.862. The variation of arithmetic fitting constant b can be described by Equation 5-2 and Equation 5-3 for peak and ultimate values respectively.

$$b = 0.857 - (0.00082\ R) \qquad \text{Equation 5-2}$$

$$b = 0.968 + (0.00537\ R) \qquad \text{Equation 5-3}$$

Where b is arithmetic fitting constant and R is the relative roughness ratio ($R_{a,steel}/R_{a,rock}$).

Between R = 0.021 and R = 5.862, b peak and b ultimate values vary by 0.5 % and 3.2 % respectively. This trend, denotes a relatively minimal effect of R on arithmetic fitting constant b. Especially for peak values, the value of b seems to be unaffected by R and R could potentially be ignored in this case.

Flagstone – steel and Limestone – steel interfaces were examined as a group and the variation of b relevant to the relative roughness ratio R of these interfaces is presented in Figure 5-34 and Figure 5-35 for peak and ultimate values respectively.

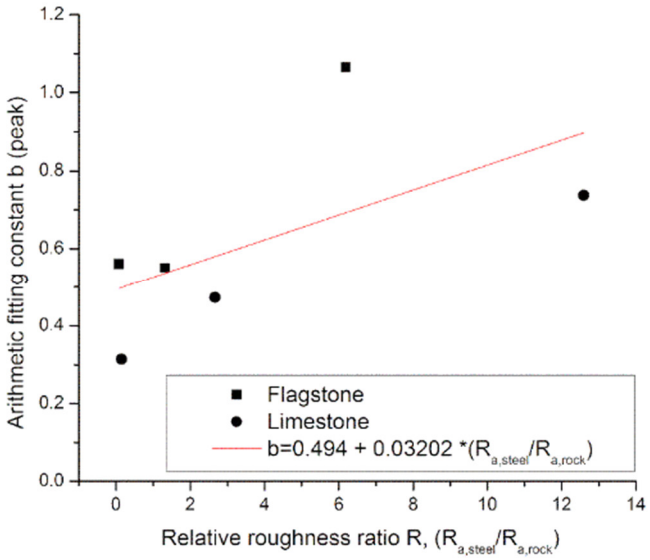

Figure 5-34. Variation of fitting parameter b with relative roughness of the interface (considering peak values of Flagstone and Limestone interfaces)

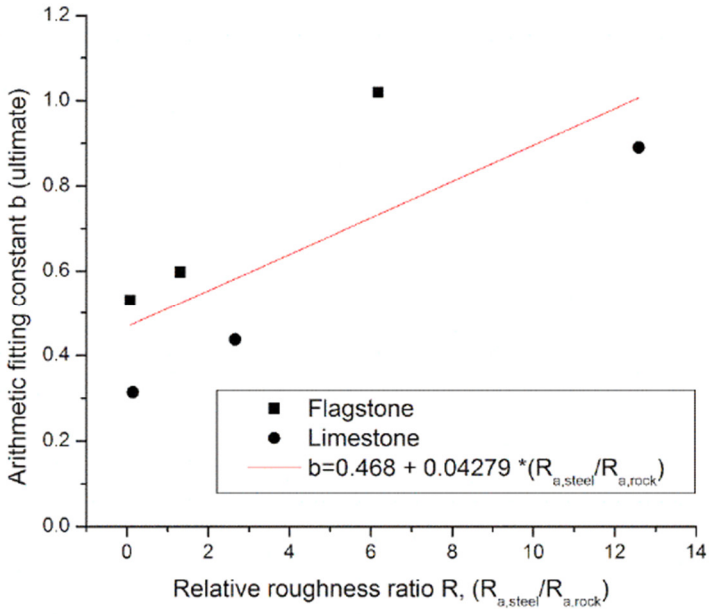

Figure 5-35. Variation of fitting parameter b with relative roughness of the interface (considering ultimate values of Flagstone and Limestone interfaces).

For Flagstone and Limestone interfaces the relative roughness ratio ranges between 0.073 and 12.593. The variation of b within this range is expressed by Equation 5-4 and Equation 5-5.

$$b = 0.494 + (0.03202\ R) \qquad \text{Equation 5-4}$$

$$b = 0.468 + (0.04279\ R)$$ Equation 5-5

Where b is arithmetic fitting constant and R is the relative roughness ratio ($R_{a,steel}/R_{a,rock}$).

It is apparent that the data points for Flagstone lie relatively parallel to those of Limestone, albeit quite higher. Therefore, the suggested linear equations can be used to get an "average" value of b that lies within the two data sets. More specifically, the "average" b peak and b ultimate values vary by 80 % and 113 % respectively, exhibiting a significant effect of relative roughness ratio R, on the value of b and consequently the shear strength of the interface. This finding is in contrast to the findings of Sandstone and Andesite interfaces which are not affected by the value of R. It is believed that this difference can be explained by taking into account the relative hardness ratio of the interfaces, as has been described in more detail in section 5.3.3.

Fixed values for arithmetic fitting constant have been selected as described in the previous paragraphs, therefore Equation 5-1 can be replaced by Equation 5-6 and Equation 5-7 for peak and ultimate values respectively.

$$\tau_{peak} = \mathrm{b}\frac{\mathrm{UCS}^{(-0.08)}}{\sigma_n^{-1.08}}$$ Equation 5-6

$$\tau_{ult} = \mathrm{b}\frac{\mathrm{UCS}^{(-0.14)}}{\sigma_n^{-1.14}}$$ Equation 5-7

Where τ = shear stress, *UCS* = unconfined compressive strength, σ_n = normal stress and b arithmetic fitting constant.

Two different sets of equations (for peak and ultimate values) have been suggested for the calculation of b, therefore guidance on which equation to choose depending on the characteristics of the rock – steel combination is provided next.

If the rock type of the seabed where the GBS is going to be placed, is the same as one of the aforementioned rock types (e.g. Old Red Sandstone, Flagstone etc), then the equations that were developed using data from this rock type can be used (i.e. Equation 5-2 and Equation 5-3 or Sandstone or Andesite and Equation 5-4 and Equation 5-5 for Flagstone or Andesite). In the case where a different rock type is examined, the selection of the appropriate equation can be based on the relative hardness ratio M of the foundation seabed interface. Equation 5-2 and Equation 5-3 shall be used for $0.57 \leq M \leq 0.67$. Equation 5-4 and Equation 5-5 shall be used for $0.89 \leq M \leq 1.33$ (which is the range of the M values from the samples used to derive the equations). However it is believed that Equation 5-4 and Equation 5-5 could also be used (cosnervatively since these equations will typically lead to lower values of b compared to Equation 5-2 and Equation 5-3) for M values between 0.67 and 0.89. As mentioned earlier, M in theory can take values between 0.4 and 4.0 (considering steel Mohs hardness = 4), however the aforementioned equations shall not be used for relative hardness M values out of the range used in this study.

5.5.2 Comparison of test data and alpha factor approach data

Figure 5-36 show how the interface shear strength calculated from Equation 5-2 and Equation 5-4 (depending on the rock type) compared with the test data. The calculated shear stress values were converted to friction angles to aid ease of comparison and representation.

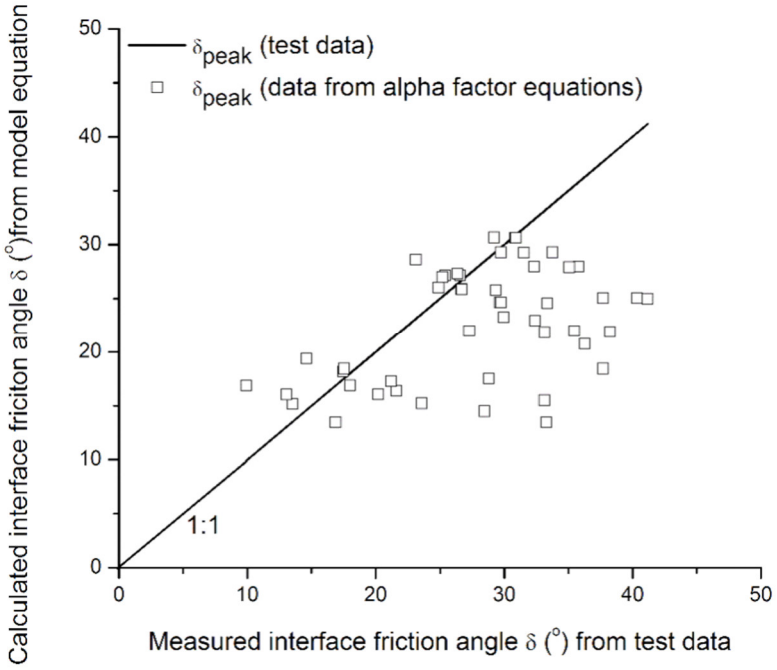

Figure 5-36. Comparison of calculated data and test data from all the normal stress levels used (i.e. 16 – 316kPa), considering peak values

In Figure 5-36 it can be seen that around 50% of the calculated data (peak values) lie close to the measured values (i.e. around the line) whereas the rest lie quite a lot lower. The data that lie lower correspond to normal stress of 16 and 79 kPa where the interfaces exhibit an “erratic” behaviour with higher interface friction angles than for normal stress of 159 and 316 kPa (as shown discussed earlier). This “erratic” behaviour cannot be captured very well by the model equations and the values are under estimated (which is on the “safe” side) as one b value is calculated for the whole range of normal stress,(i.e. 16 – 316 kPa). However, it is felt that it would be preferable to design the GBS in a way that at least 159 kPa of normal stress is applied on the interface, as beyond this point, the effect of the normal stress on the shear behaviour is minimised leading to a more “predictable” interface resistance.

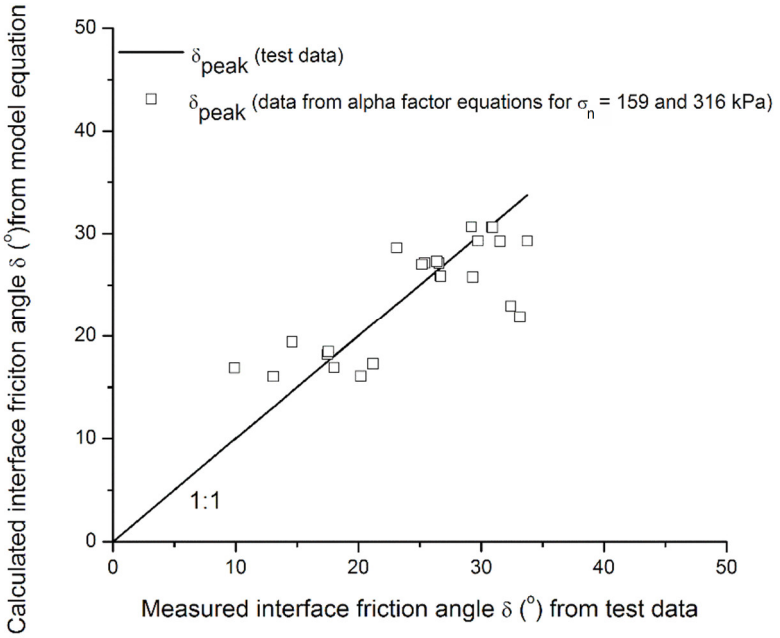

Figure 5-37. Comparison of calculated data and test data from the normal stress levels of 159 and 316 kPa, considering peak values

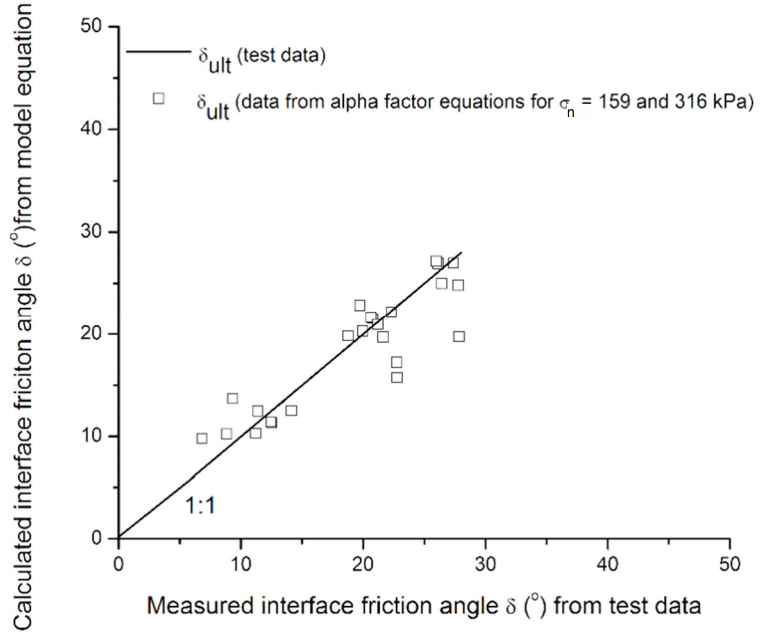

Figure 5-38. Comparison of calculated data and test data from the normal stress levels of 159 and 316 kPa, considering ultimate values

Figure 5-37 and Figure 5-38 present only data corresponding to normal stress of 159 and 316 kPa. where a good agreement between the calculated and measured data is shown, indicating that Equation 5-2 to Equation 5-5 can be used (depedning on the Mohs harndess ratio M) to calculate the peak and

ultimate anticiapted shear strength for normal stress over 159 kPa. It is also suggested to carry out the design based on the ultimate values when displacement > 4mm are expected during the lifespan of the tidal stream energy generator. It has been shown earlier that these values are always lower than the peak values, therefore it is deemed “safer” to estimate the shear strength of the interface based on Equation 5-3 and Equation 5-5.

In order to develop the alpha method approach, the data set was split into two parts (Sandstone - Andesite and Flagstone – Limestone) and two sets of equations were created based on the value of the relative hardness ratio M. As it has already been discussed, it seems that the interface shear strength is affected by various factor such as UCS, normal stress, relative roughness ratio R and relative hardness ratio M. It should be noted here that a harder rock doesn’t necessarily have higher UCS. For example Sandstone is consisted of hard silica grains but the matrix is weak leading to a lower UCS value compared to “softer” rocks (e.g. Flagstone)

5.6 Summary

Data obtained through IST testing of rock – steel interfaces have been presented in this chapter. Analysis of the results allowed the investigation of the factors that influence the interface shear behaviour. A summary of the findings presented in this chapter is given below.

1. Normal stress affects the behaviour of rock – steel interfaces, thus linear failure envelopes should not be considered. Dilation occurs for normal stress of 16 – 79 kPa leading to higher peak values, whereas for normal stress of 159 – 316 kPa, the behaviour is more linear and dilation is suppressed, thus lower peak values are observed.

2. Normal stress level of at least 159 kPa seems to be more appropriate for design, since the behaviour is more predictable in contrast to the “erratic” behaviour observed between 16 and 79 kPa.

3. Ultimate values of interface friction angle are quite lower than the peak values are reached within small shear displacement (8 - 10 mm). Therefore, it is felt that ultimate values should be preferably used for design.

4. The behaviour of two shearing surfaces could potentially be correlated with the relative scratch hardness of the counterface materials (Engelder and Scholz 1976, Abuel-Naga 2018). It seems that when the hardness of the two counterfaces (rock and steel) differs by more than 50% (e.g. Sandstone and Andesite), the shearing consists of sliding and ploughing (irrespective of steel R_a) and the interfaces exhibit similar behaviour, albeit Andesite exhibits lower interface friction angles. In contrast, Flagstone and Limestone interfaces have relative hardness ratio M close to 1 as Mohs hardness of the two counterface materials (rock and steel) differs by less than 50% (1.33 for Flagstone and 0.89 for Limestone interfaces). As a result, it is felt that higher localised stress is required for ploughing to occur, hence the interfaces seem to be affected by the roughness of the steel (higher R_a leads to higher localised stress due to fewer points of contact).

5. Increasing steel roughness, tends to increase the interface shear strength, however this seems to be more apparent for the cases where M is closer to 1 (i.e. Flagstone and Limestone). When M is significantly different to 1 (i.e. Sandstone and Andesite), the effect of steel roughness is minimised as the normal stress level increases and ploughing occurs.

6. The alpha factor approach seems to capture the behaviour of rock – steel interfaces and a power function can be used to estimate the shear strength of interfaces within the UCS and normal stress range used in this study. Relative hardness ratio M is believed to have significant effect on the shear behaviour, therefore two different sets of equations have been proposed depending on the value of M (Equation 5-2 - Equation 5-3 and Equation 5-4 - Equation 5-5).

Chapter 6

6 Special cases of interface testing

The greatest part of the testing programme focused on rock - steel interfaces and has been presented and discussed in Chapter 5. However, rock – sand – steel (i.e. with a sand layer between the rock and the steel) and rock – concrete interface tests were also carried out, as it was felt that they could represent foundation – seabed interfaces that could be potentially encountered in real life applications. Due to time limitations, one type of sand layer (i.e. type of sand and thickness) was used for the rock – sand – steel testing and one type of concrete was used for the rock – concrete tests. As, a result the dataset used for analysis and discussion were smaller compared to those used in Chapter 5 for the rock – steel interfaces.

6.1 Rock – concrete interface tests

To date, the majority of the GBS that have been used to support prototypes or commercially deployed (e.g. MeyGen project) tidal stream generators are made of steel or steel below concrete ballast which is not in contact with the rock surface. Hence the interface testing so far, has been focused on steel – rock interfaces. However, concrete has also been used in some cases such as the Sea Turtle Tidal Test Project, where a concrete plinth has been used to support the Voith Hydro tidal turbine (Strabag Offshore Wind GMBH). For this reason, interface tests on rock – concrete interfaces have also been carried out as part of this research.

Sandstone, Flagstone, Andesite and Limestone were tested against concrete samples using the IST. Tests at normal stress of 16, 79, 159 and 316 kPa were carried out and the total shear displacement was 10 mm for each test (the same as per the rock – steel tests). The concrete samples had a R_a value of 6.8 μm, Mohs hardness value of 5 and UCS value of 61.5 MPa, whereas for the steel samples presented earlier, R_a ranged between 0.4 and 34 μm and

Mohs hardness value was 4. More details about the preparation of the concrete samples can be found in section 3.4.3.

6.1.1 Results

Figure 6-1 and Figure 6-2 present the effect of the applied normal stress on the peak and ultimate interface friction angles respectively of rock – concrete interfaces.

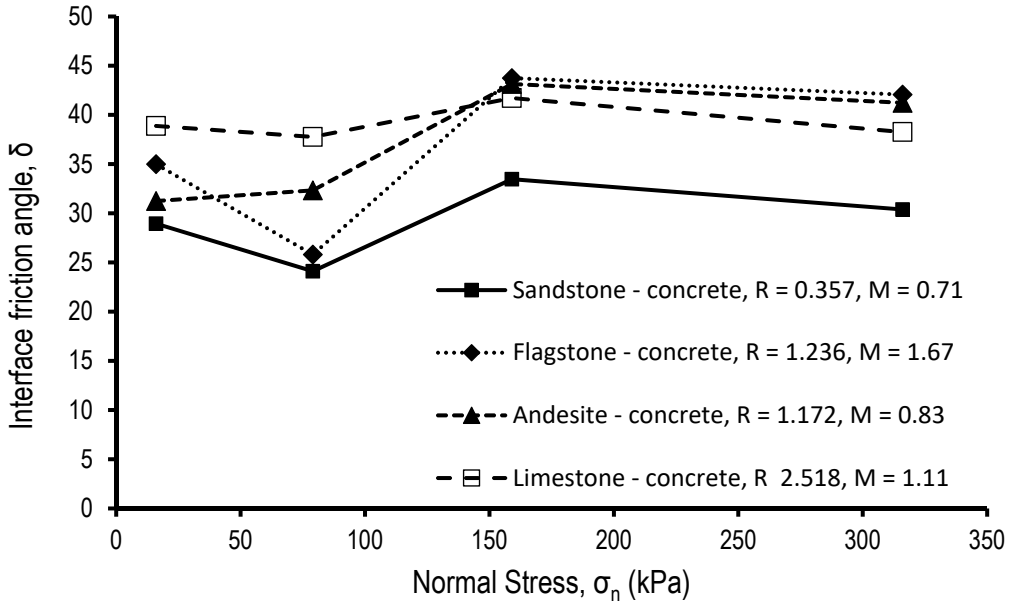

Figure 6-1. Comparison of δ_{peak} from interface testing of four rock types against concrete

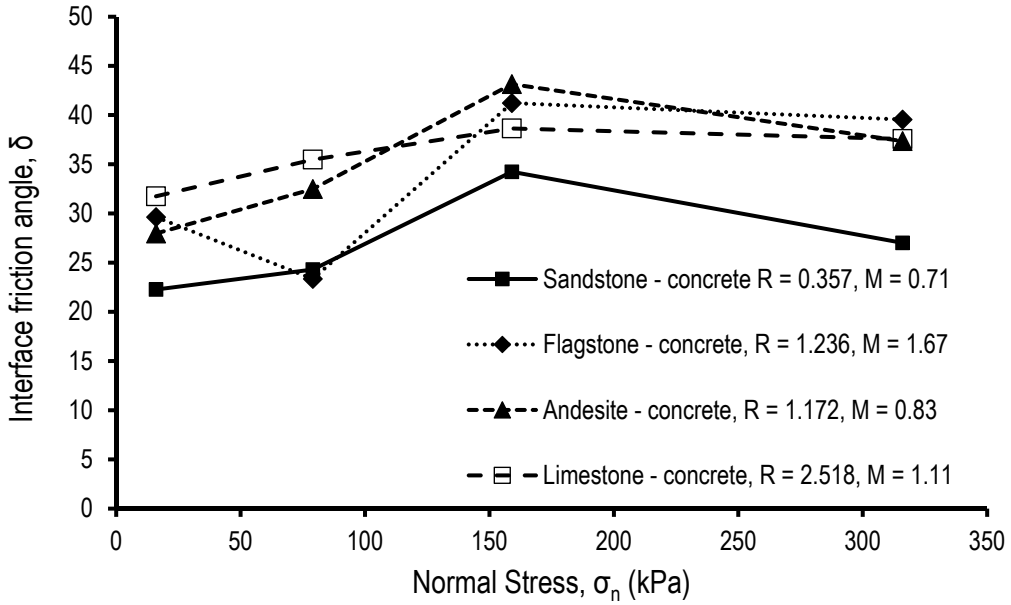

Figure 6-2. Comparison of δ_{ult} from interface testing of four rock types against concrete

The interfaces seem to exhibit lower shear strength for normal stress up to 79 kPa, whereas higher values are noted for normal stress between 159 and 316 kPa, irrespective of the rock type. It is believed that low normal stress (up to 79 kPa) is not adequate to establish intimate contact between the rock and concrete however when the normal stress increases, better mating occurs along with ploughing (damage) on the interface, leading to an increase in the shear strength for both peak and ultimate values.

Flagstone, Andesite and Limestone interfaces, exhibit similar values especially when the applied normal stress is between 159 and 316 kPa. In this range, the peak interface friction angle is around 41° and the ultimate is between 38° and 43°. Sandstone interfaces exhibit lower shear strength, however the shape of the relationship (i.e. variation of δ with σ_n) is similar to those of the other three rock types. An obvious reason for this difference is not apparent, however it is believed that it could be related to the relative roughness and relative hardness of the interface as described next.

6.1.2 Effect of relative roughness and hardness ratios

It has already been discussed in the steel – rock interface testing section, that the relative roughness of the interface is a factor that affects the shearing behaviour of the interface. The R_a of the concrete samples was 6.8 μm, whereas it was 19, 5.5, 5.8 and 2.7 μm for Sandstone, Flagstone, Andesite and Limestone respectively. As a result, the relative roughness ratio R ($R_{a,concrete}/R_{a,rock}$) ranges between 0.36 and 2.52. This range is significantly lower than the one noted for the rock – steel interfaces (R between 0.02 and 12.59). Figure 6-3 shows the variation of the interface friction angle δ of the rock concrete interfaces with R. As shown, in Figure 6-1 and Figure 6-2, δ varies for normal stress up to 79 kPa, whereas it is almost constant between 159 and 316 kPa. To allow comparison, average peak and ultimate friction angles for normal stress range between 159 and 316 kPa have been considered. It should be noted that the average values were calculated considering the coefficient of friction and not the friction angles, as the tangent function is nonlinear.

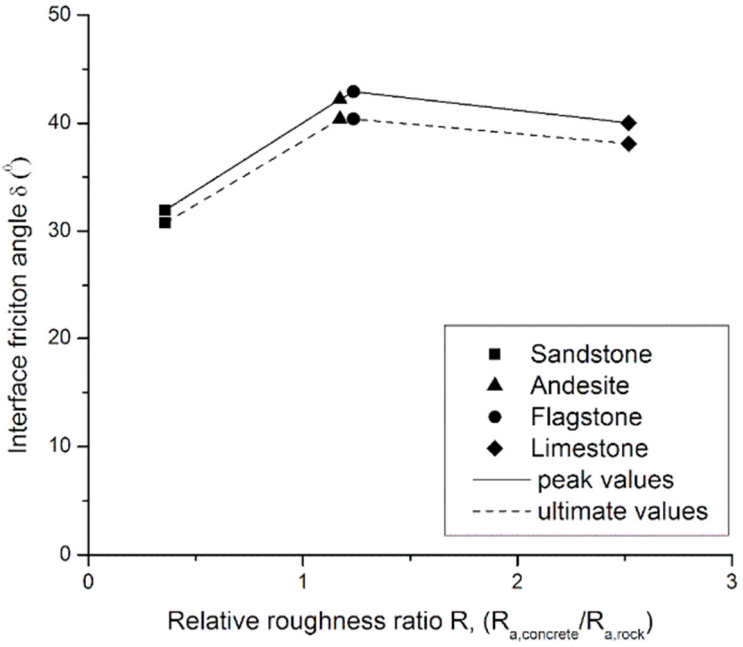

Figure 6-3. Average interface friction angle vs relative roughness ratio R, for rock – concrete interfaces

The observed friction angle seems to increase significantly with increasing R values up to ~ 1. For R values between ~ 1 (Andesite and Flagstone) and 2.5 (Limestone) δ values exhibit a slight drop, potentially indicating an optimum relative roughness ratio of ~ 1. Sandstone is much rougher than concrete and this could mean that during shear, concrete is sliding on the top of the Sandstone asperities, thus preventing good interlocking of the interface. This leads to significantly lower shear strength compared to the other rock – concrete interfaces that are of similar and apparently more "compatible" relative roughness.

The Mohs hardness of the concrete samples is 5 resulting in relative hardness ratio M (Mohs,concrete/Mohs,rock) of 0.71, 1.67, 0.83 and 1.11 for Sandstone, Flagstone, Andesite and Limestone – concrete interfaces respectively.

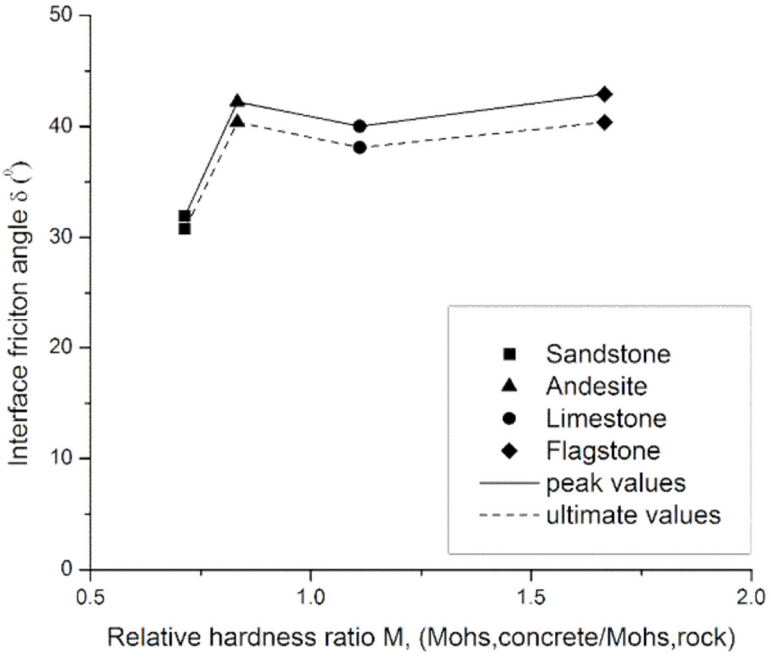

Figure 6-4. Average interface friction angle vs relative hardness ratio M, for rock – concrete interfaces

As shown in Figure 6-4, average interface friction angle increases significantly (from ~ 32^o to ~ 42.5^o) as M increases from 0.71 to 0.83, however further increase of M up to 1.67 appears to have a rather minimal effect. It seems that δ reaches a plateau for M = 0.83 and further increase doesn't influence the

strength of the interface. This behaviour is quite different to that shown for rock – steel interfaces (Figure 5-21, Figure 5-22 and Figure 6-14) where δ increases as M moves away from 1. Figure 6-5 shows the variation of average interface friction angle in the relative roughness ratio (R) and relative hardness ratio (M) space, however a distinctive trend is not apparent.

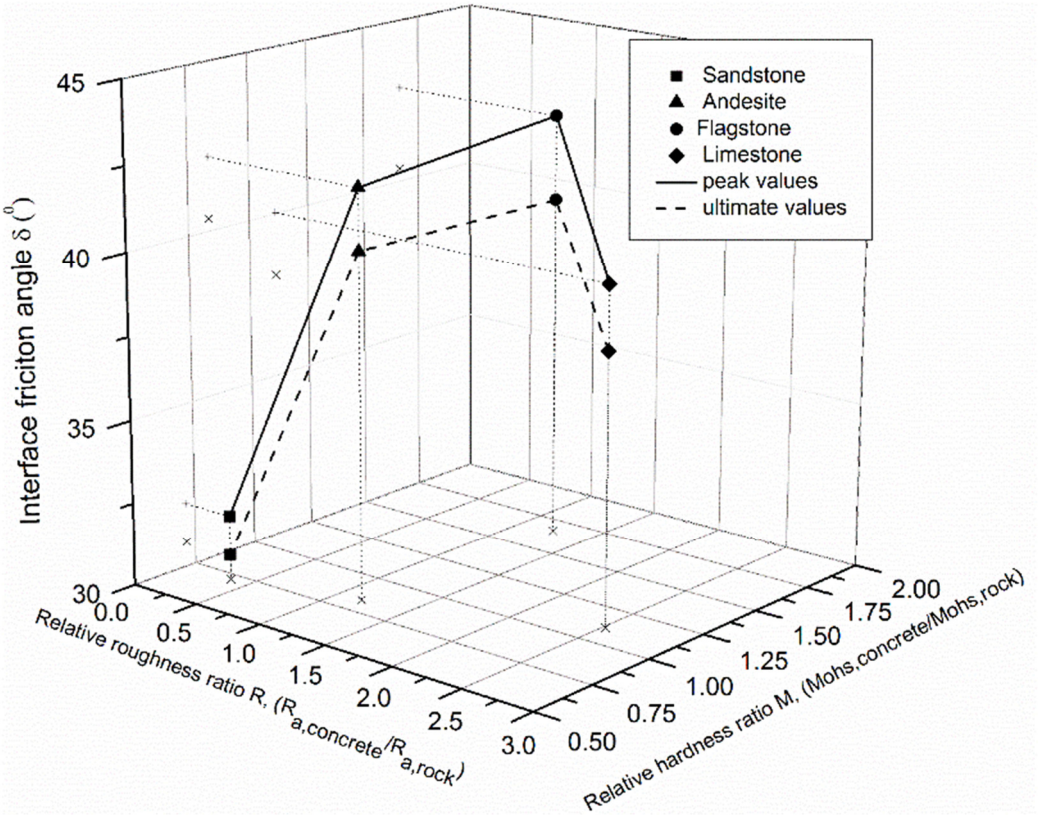

Figure 6-5. Schematic representation of variation of average interface friction angle in the R – M space

The overall shear strength consists of sliding and ploughing. Sliding involves the movement of one counterface over the asperities of the other counterface and is primarily influenced by the relative roughness ratio R. Ploughing takes places when the (shear induced) localised stress is adequate to cause damage on the “softer” counterface material and is mainly controller by hardness (Abuel-Naga et al., 2018) and consequently the relative hardness ratio M (ploughing is pronounced for values different to 1 as discussed earlier and shown in Figure 5-21 and Figure 5-22). However, concrete is a material that is more brittle than steel and its mechanical properties are more similar

and comparable to those of rock. Therefore, it was felt that the relative UCS ratio U (as described in Equation 6-1):

$$U = UCS_{concrete}/UCS_{rock}$$

Equation 6-1

could be employed to investigate the behaviour of the rock – concrete interfaces. The UCS of concrete is 61.5 MPa and it ranges between 31.5 and 192.7 MPa for the different rock types, resulting in a range of U values between 0.32 and 1.95. Figure 6-6 shows the influence of U the on the average interface friction angle of the rock – concrete interfaces.

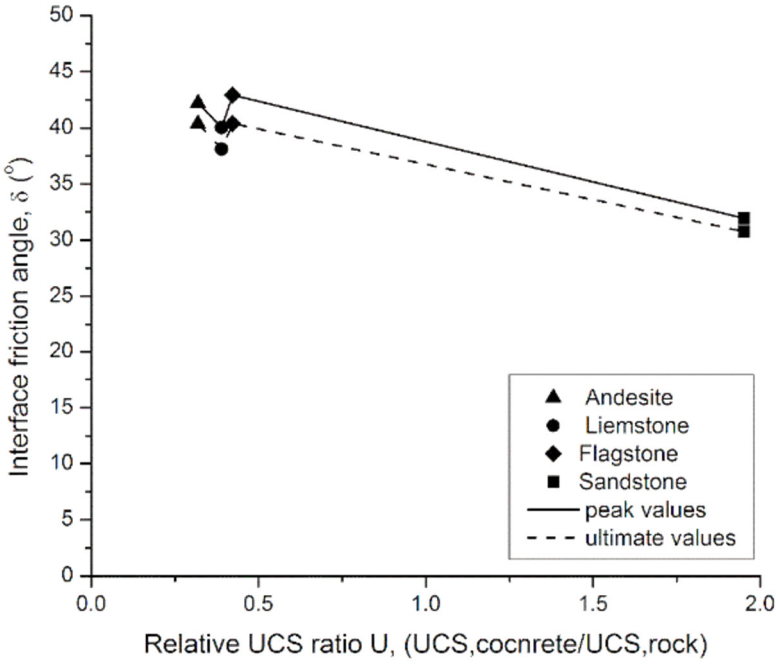

Figure 6-6. Average interface friction angle vs relative UCS ratio U, for rock – concrete interfaces

Flagstone, Andesite and Limestone interfaces have similar values of ratio U (i.e. rock significantly stronger than concrete) and similar values of average interface friction angle (40°- 42° for peak values and 38°- 40.5° for ultimate values) whereas, the U ratio for Sandstone – concrete interfaces is 1.95 (i.e. concrete twice as strong compared to rock) and the average interface friction angles are significantly lower (32° for peak and ~31° for ultimate values).

Flagstone, Andesite and Limestone interfaces seem to have similar behaviour and yield very similar values of average interface friction angle. These rocks have comparable values of relative roughness ratio, R (roughness lower than the concrete) and very similar relative UCS ratio, U (significantly stronger than the concrete). It is believed that sliding and ploughing (surface damage) occurs during the shearing of these interfaces. This is seen in the normal deformation of the interfaces (at normal stress of 316kPa) shown in Figure 6-7 where comparable values of contraction are observed for Flagstone, Andesite and Limestone interfaces.

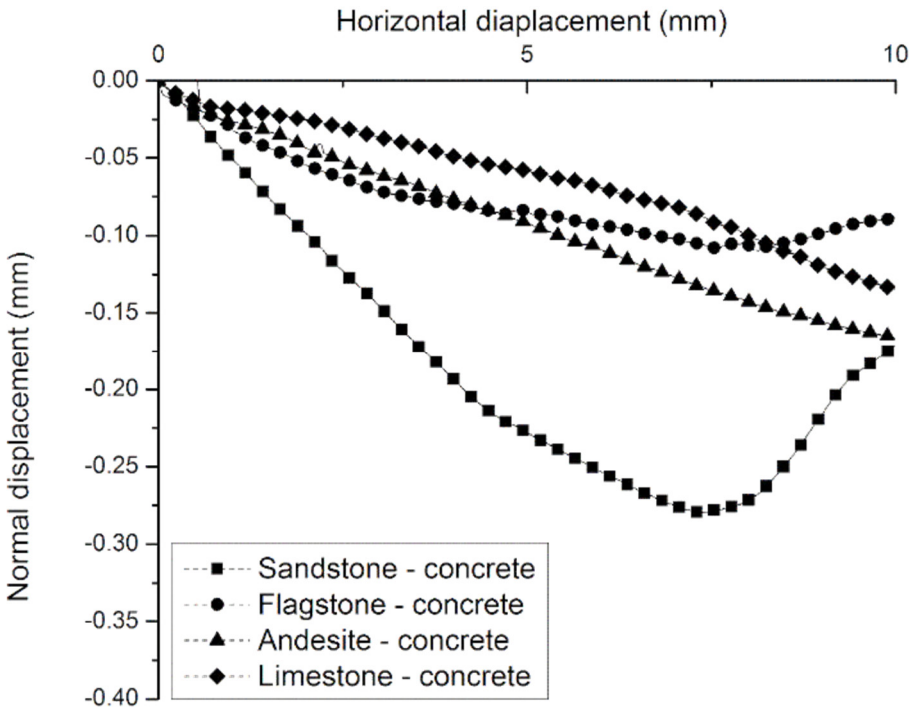

Figure 6-7. Normal displacement vs shear displacement for rock – concrete interfaces at normal stress of 316 kPa

Sandstone – concrete interface is the only one where the concrete is stronger than the rock (U ratio > 1) and yields average interface friction angle values significantly lower than the rest of the interfaces examined. The relative hardness ratio M, of the interface is 0.71, therefore, ploughing is expected to occur during shear. As discussed previously, ploughing is generally contributing to the shearing resistance of the interface, thus increasing the strength of the interface. However, for Sandstone – concrete interfaces, it is

likely that the sand grains are removed during shear, because the concrete is significantly stronger than the rock (U ~ 2, i.e. the Sandstone asperities are harder than the concrete but they are weakly cemented and removed during shear). As a result, the ploughing of the Sandstone asperities into the concrete is supressed, although the contraction of the interface is significantly greater (almost double) compared to the rest of the interfaces, possibly due to the breakage/removal of the Sandstone asperities.

6.1.3 Alpha factor design approach

Alpha factors for the rock – concrete interfaces are plotted in Figure 6-8 and Figure 6-9.

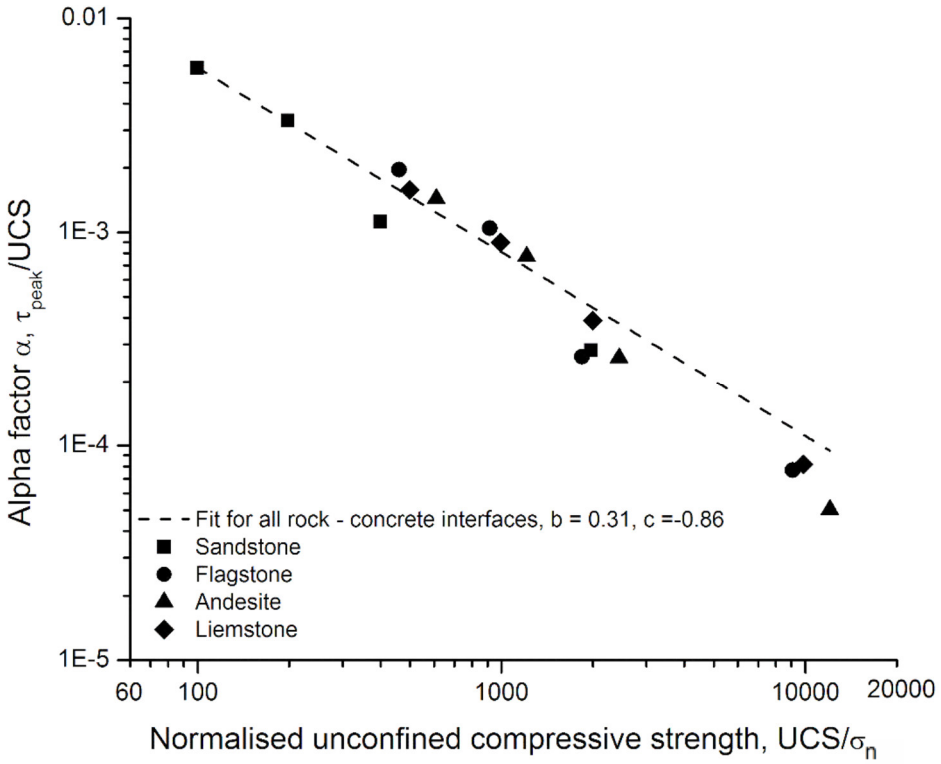

Figure 6-8. Alpha factors for rock – concrete interfaces (IST), considering peak values

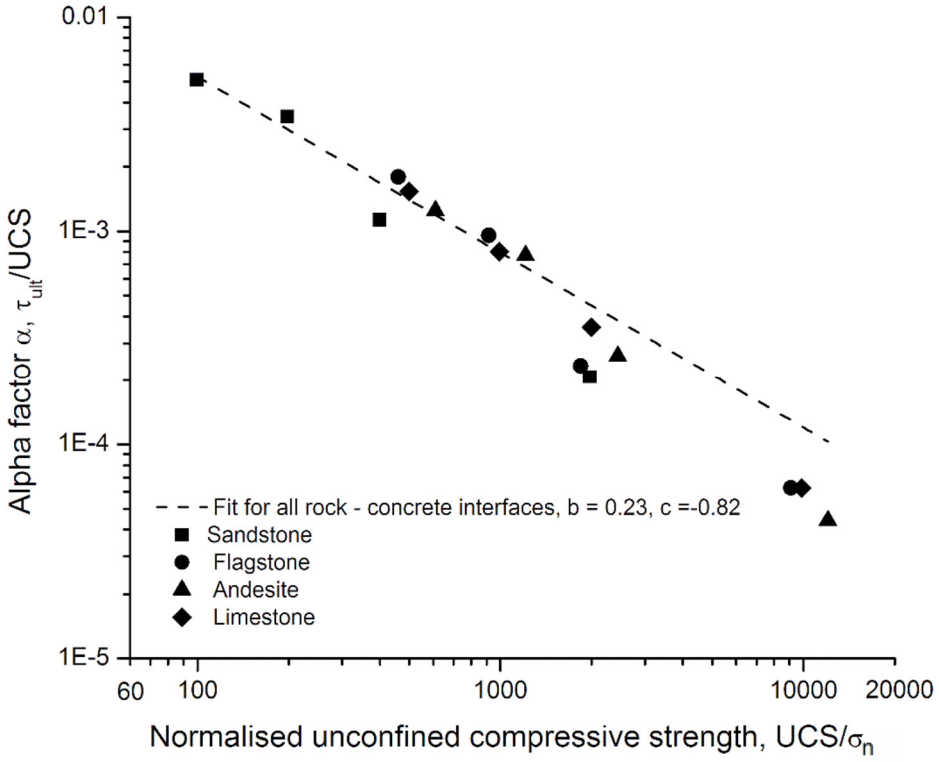

Figure 6-9. Alpha factors for rock – concrete interfaces (IST), considering ultimate values

One type of concrete was used for all the tests therefore one fit curve was determined for peak and one for ultimate values (the UCS value on the graphs refers to the rocks as per. Equation 4-2). Fitting constants b and c for peak and ultimate values are summarised in Table 6-1 and can be used to calculate the available shear stress using Equation 5-1.

Table 6-1. Arithmetic fitting constants considering alpha type approach for peak and ultimate values of rock – concrete interfaces

Arithmetic fitting constant	Peak values	Ultimate values
b	0.31	0.23
c	-0.86	-0.82

As shown in Figure 6-3 the results for peak and ultimate values are rather similar, denoting that the rock – concrete interfaces exhibit a “ductile” behaviour (i.e. no significant decrease in post peak shear strength), especially for normal stress of 159 and 316 kPa.

The curve captures the behaviour for UCS/σ_n of 100 to 2440, whereas the fit is less good for UCS/σ_n of 9090 to 12044. The latter values of UCS/σ_n correspond to normal stress level of 16 and 79 kPa. As has already been discussed (Figure 6-1, Figure 6-2), rock – concrete interfaces behave rather "erratically" within this normal stress range, hence the alpha value approach does not capture this behaviour well. Taking into account this "erratic" behaviour it is felt that when a concrete GBS is going to be placed on exposed seabed, the footing shall be designed in a way that at least 159 kPa (i.e. 0.25% of concrete UCS) normal stress is induced. In this case, the behaviour of the interface is captured as shown in Figure 6-10 and Figure 6-11.

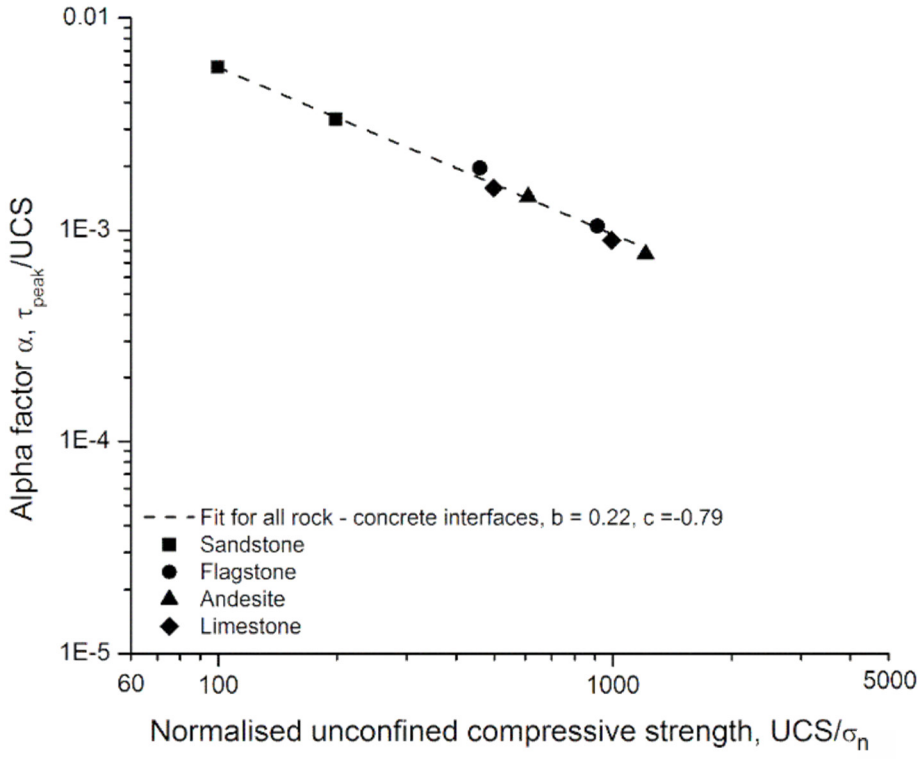

Figure 6-10. Alpha factors for rock – concrete interfaces (IST), considering peak values at normal stress of 159 and 316 kPa

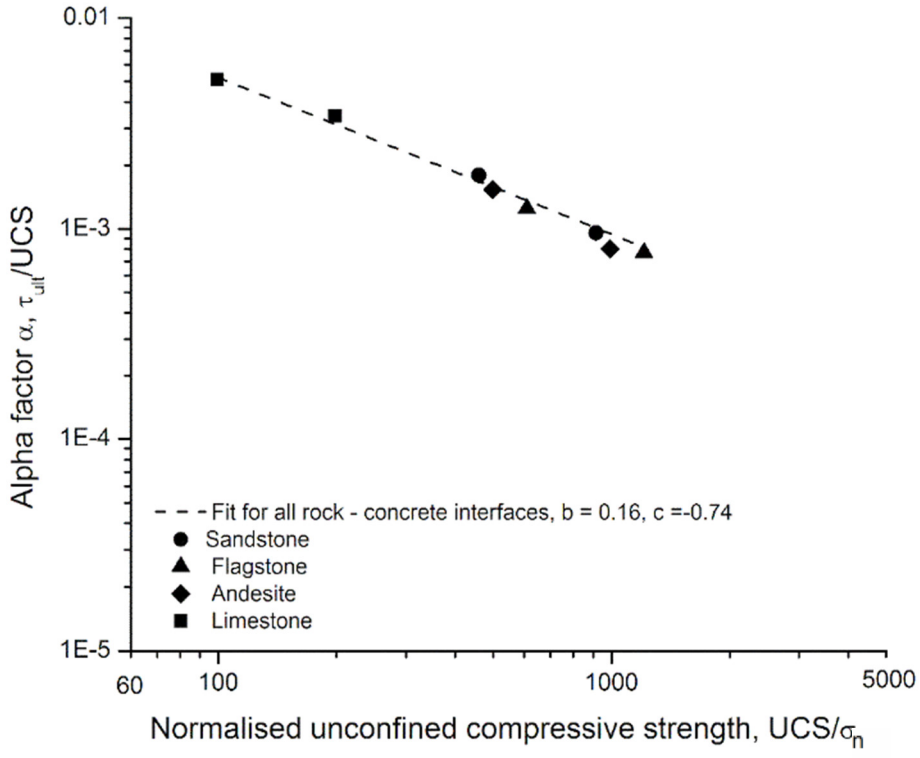

Figure 6-11. Alpha factors for rock – concrete interfaces (IST), considering ultimate values at normal stress of 159 and 316 kPa

Table 6-2 summarises the fitting constants b and c that can be used to calculate the available shear stress using Equation 5-1

Table 6-2. Arithmetic fitting constants considering alpha type approach for peak and ultimate values of rock – concrete interfaces at normal stress of 159 and 316 kPa

Arithmetic fitting constant	Peak values	Ultimate values
b	0.22	0.16
c	-0.79	-0.74

6.1.4 Comparison of rock – concrete and rock - steel interfaces

In general, rock – steel interfaces exhibited higher shear strength when steel R_a = 34 μm (Figure 5-8 - Figure 5-15). In some cases (e.g. Sandstone), the steel roughness (and the relative roughness ratio R) seem to have less

significant effect compared to other rock – steel interfaces (e.g. Limestone), however the values at 34 μm can be considered as upper limit values for the individual rock – steel interface combinations. Therefore, the values of the rock – concrete interfaces were normalised against the values of the respective rock – steel (R_a = 34 μm) interface and an interface friction angle ratio = rock – concrete (δ_c) over δ rock – steel (δ_{st}) has been calculated.

The variation of the average interface friction angle with relative hardness ratio M, is different between rock – steel and rock concrete interfaces, as shown in Figure 6-12. The range of M is wider for rock – concrete interfaces and a distinctive lower value of δ_{peak} when M is close to 1 is not apparent. Therefore, a relative UCS ratio U was also utilised in section 6.1.2, to explain the behaviour of the rock – concrete interfaces.

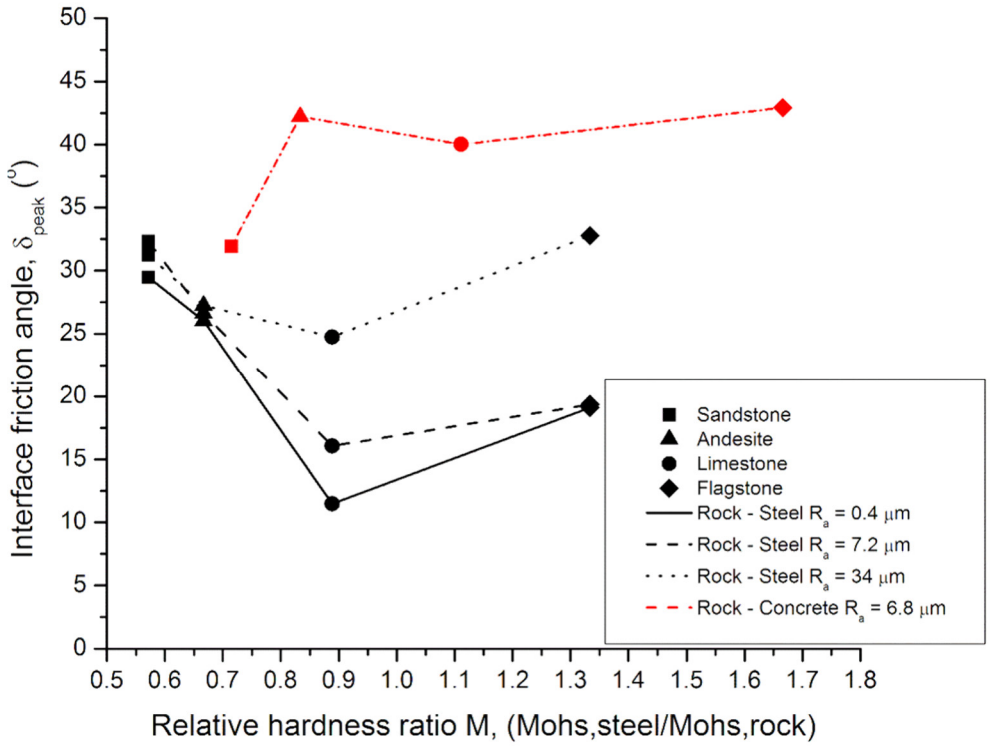

Figure 6-12. Interface friction angle vs relative hardness ratio M, for rock – concrete and rock – steel interfaces, considering peak values

In Figure 6-13 and Figure 6-14 it is shown that in general the rock - concrete interfaces seem to be stronger than the rock - steel at higher stress (i.e. 159 – 316 kPa) and maybe steel is marginally better at low stress (i.e. 16 – 79 kPa).

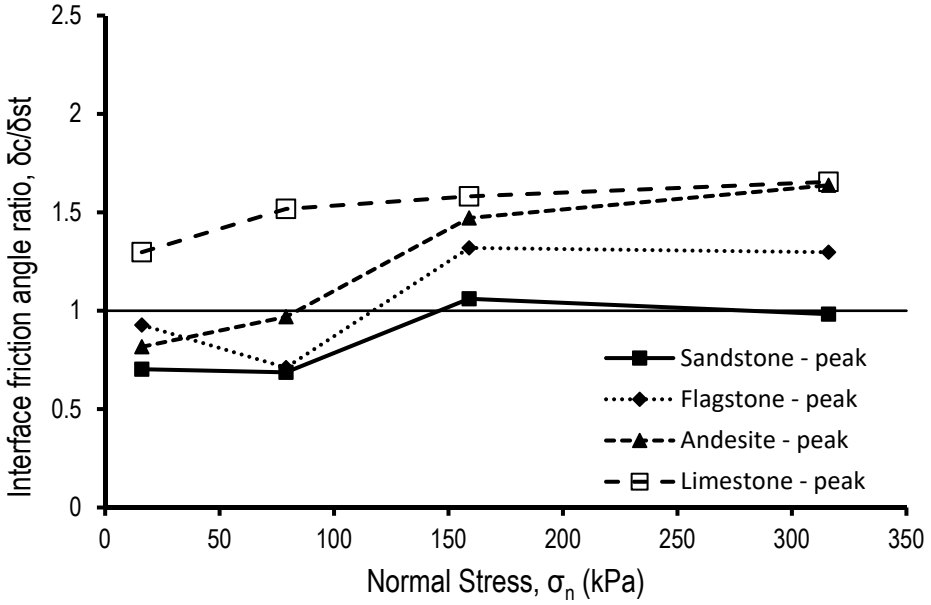

Figure 6-13. Normalised interface friction angles for rock concrete interfaces over rock steel (R_a = 34 μm) interfaces, considering peak values

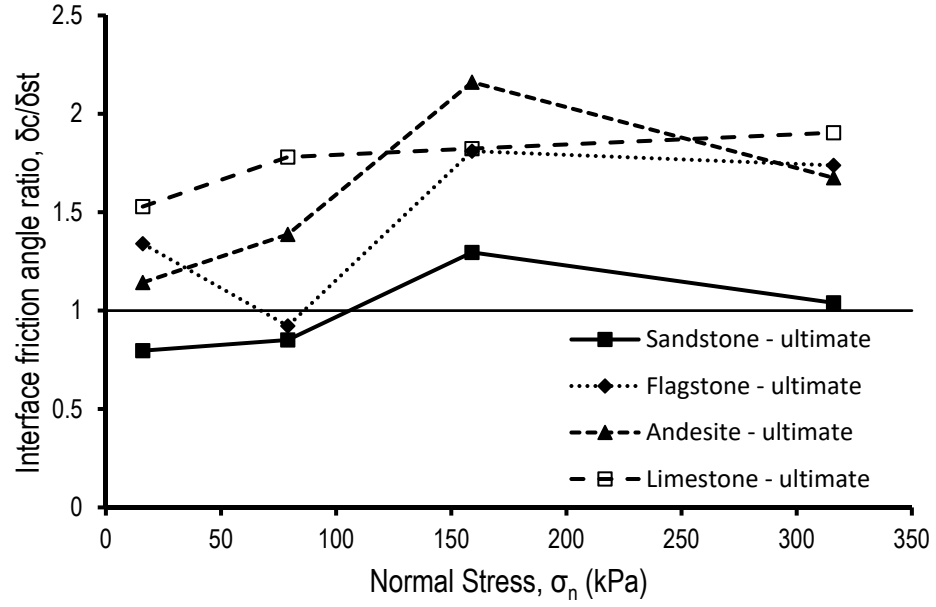

Figure 6-14. Normalised interface friction angles for rock concrete interfaces over rock steel (R_a = 34 μm) interfaces, considering ultimate values

When the applied normal stress is up to 79 kPa, the interface friction angle ratio for the Sandstone interfaces, give values between 0.7 and 0.9 (considering both peak and ultimate values, Figure 6-13 and Figure 6-14). This means that the Sandstone - concrete interface appears to be weaker than the Sandstone – steel interface at this normal stress range. When the normal stress range is between 159 and 316 kPa, the ratio takes values close to 1, denoting similar shear strength for both types of interfaces. Figure 6-7 shows the normal displacement for the rock – concrete interfaces at normal stress of 316 kPa. It can be seen that Sandstone – concrete interface contracts ~ 0.30 mm which is significantly greater than the value noticed for Sandstone – steel interfaces at the same normal stress (~ 0.06 mm as shown in Figure 5-19). As discussed, in 6.1.2, it is believed that the Sandstone asperities are removed during shearing of Sandstone – concrete interfaces (because U = 1.95), explaining the significant difference in the normal deformation. Nevertheless, the average interface shear strength is similar for Sandstone – steel and Sandstone – concrete interfaces, resulting into (δ_c/δ_{st} ~ 1).

As far as Flagstone and Andesite interfaces are concerned, the ratio of interface friction ranges between 0.7 and 0.93 when considering peak values and between 0.9 and 1.4 when considering ultimate values, for normal stress up to 79 kPa. When the applied normal stress is higher (159 and 316 kPa), the concrete interfaces are significantly stronger as the ratio ranges between 1.3 and 2.1. According to Table 6-3, relative hardness ratio M, for Flagstone – concrete interface is 1.67 whereas for Flagstone – steel it is 1.33. This could suggest that the mode of shearing is sliding and ploughing and the ploughing component is magnified for Flagstone – concrete interface, since the difference of M from 1 is increased. In Figure 6-7 it is shown that the Flagstone – concrete interface contracts ~ 0.11 mm, whereas the value for the Flagstone – steel interface is ~ 0.03 mm. This is expected because concrete asperities are more brittle/removable compared to those of steel. For Andesite, the value of M is closer to 1 (from 0.67 to 0.83) when steel is replaced with concrete. It seems though that M = 0.83 is still adequate to allow shear induced ploughing to occur. The contractive normal displacement for the Andesite – concrete interface (~ 0.16 mm, Figure 6-7) is significantly greater than the contraction

observed for the Andesite – steel interface (~ 0.05 mm, Figure 5-19). This suggests, that the overall deformation/damage of the asperities during shear is greater for the rock – concrete interface, leading a significant increase of the interface shear strength when steel is replaced by concrete. It should be noted that for both rock types, R decreases significantly and tends to 1 when steel is replaced with concrete. Therefore, it is felt that for rock – concrete interfaces (brittle counterface materials), R value close to 1 is beneficial for the interface strength as it leads to better mating of the two interfaces, thus enhancing the sliding and ploughing components of the shear strength.

Limestone - concrete interfaces exhibit slightly lower shear strength compared to Flagstone and Andesite – concrete interfaces (Figure 6-1 and Figure 6-2) but are significantly stronger than the Limestone – steel interfaces irrespective of the normal stress level. It is also noticeable that Limestone – steel interfaces are by far the weakest amongst the rock – steel interfaces. The distance of the relative hardness ratio M from 1 is the same no matter if steel or concrete is used as counterface. However, Limestone – concrete interface contracts significantly more than the Limestone – steel interface (0.13 mm and 0.02 mm respectively according to Figure 6-7 and Figure 5-20), suggesting that significantly more damage/ploughing takes place for the Limestone – concrete interfaces. Therefore it is suggested that the significant increase in the shear strength is attributed to the fact that rock and concrete asperities are deformed more (compared to Limestone –steel interfaces), thus enhancing the shear strength.

By comparing rock – steel and rock – concrete interfaces it appears that the interface shear strength increases when ploughing occurs and it is increasing with the potential deformability of the asperities of the counterface materials. I.e. the rock – concrete interfaces contract more than the rock – steel interfaces (at a normal stress of 316kPa) and exhibit higher shear strength. However, it appears that enhancement of the shear strength due to ploughing may be limited when shearing (or removal) of the asperities of one of the counterface materials is taking place (e.g. Sandstone – concrete interfaces, with U ~ 2).

Table 6-3. Summary table of relative roughness and relative hardness ratios for rock – steel and rock – concrete interfaces

Rock type	Steel (R_a = 34 μm)		Concrete (R_a = 6.8 μm)	
	Relative roughness ratio R	Relative hardness ratio M	Relative roughness ratio R	Relative hardness ratio M
Sandstone	1.79	0.57	0.36	0.71
Flagstone	6.18	1.33	1.24	1.67
Andesite	5.86	0.67	1.17	0.83
Limestone	12.59	0.89	2.52	1.11

Figure 6-15 and Figure 6-16 show how the rock – concrete data points compare with the alpha factor approach, determined earlier for rock –steel interfaces.

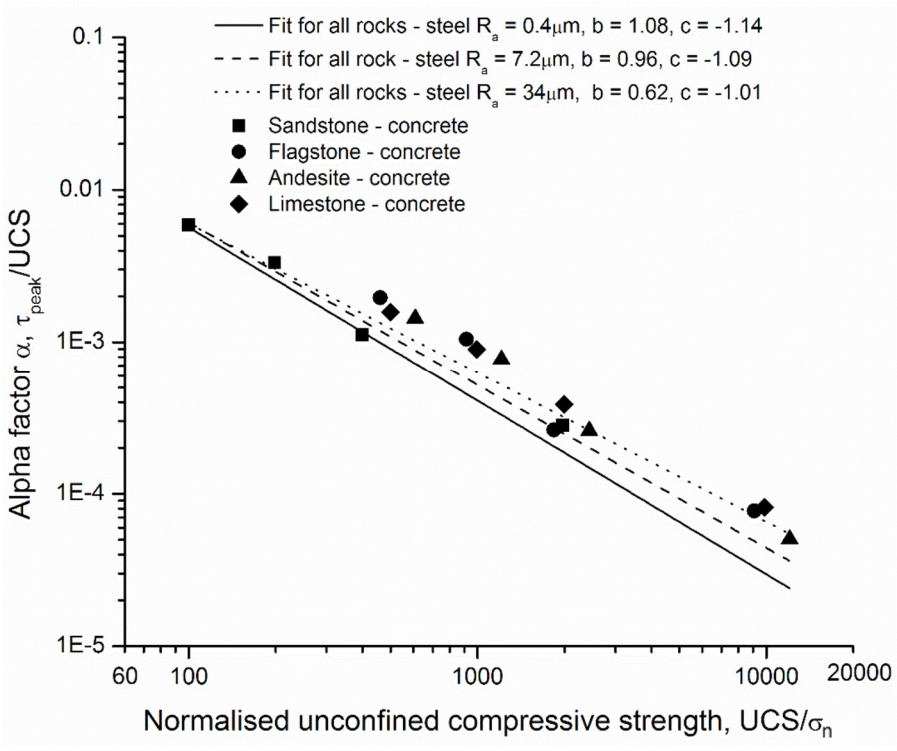

Figure 6-15. Alpha factor of rock – concrete interfaces compared with contours from rock – steel interfaces (IST), considering peak values

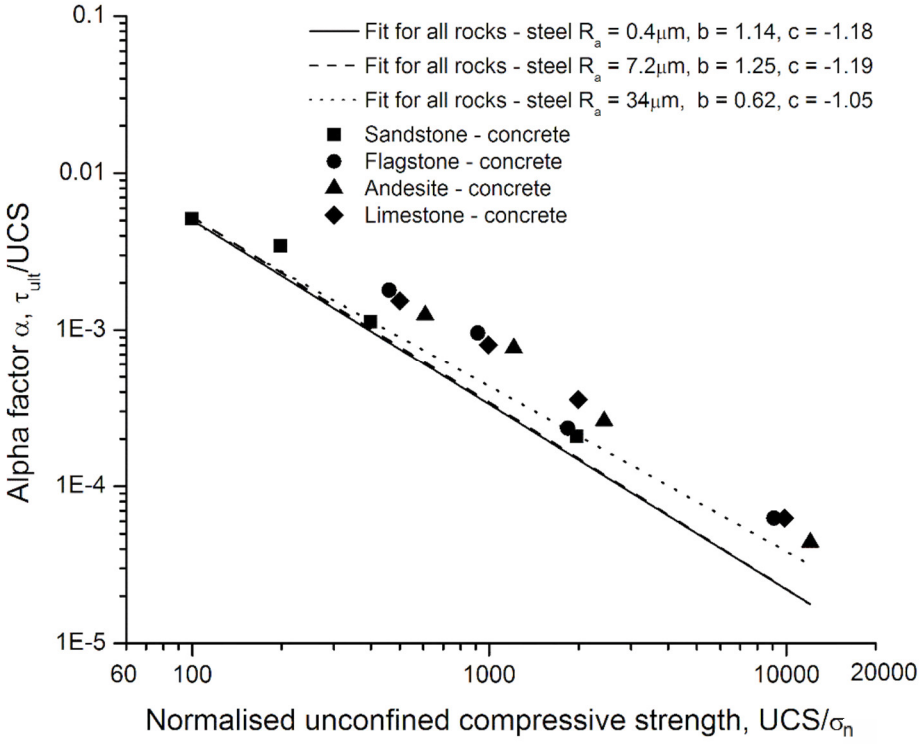

Figure 6-16. Alpha factor of rock – concrete interfaces compared with contours from rock – steel interfaces (IST), considering ultimate values

A discussed earlier, rock – concrete interfaces seem to exhibit higher interface shear strength compared to the rock - steel interfaces, therefore alpha factor values tend to lie above the rock –steel fit curves. (Figure 6-15). The difference is more significant as far as ultimate values are concerned (Figure 6-16). The maximum values of alpha are approximately the same for both types of interfaces but this reflects the similar behaviour of Sandstone – steel and Sandstone – concrete interfaces (i.e. Sandstone – concrete data point lie on top of the rock –steel curves). Sandstone has by far the lowest UCS (31.5 MPa) and consequently (as $\alpha = \tau/\text{UCS}$) the highest alpha factor compared to the rest of the rock types.

In the case of Flagstone, Andesite and Limestone, the data points describing rock – concrete interfaces lie above the rock-steel fit curves, as these rock types exhibit higher shear strength when the counterface is concrete instead of steel.

It is apparent that typically rock – concrete interfaces exhibit higher shear strength than the rock – steel interfaces (especially at normal stress between159 and 316 kPa).This indicates that GBS made of concrete might be more efficient. However, it is noted that only one type of concrete (i.e. concrete mix and surface finish) has been investigated, therefore further testing would be required to optimise this behaviour.

6.2 Testing to simulate the presence of granular sediment at the interface

Seabed sediment may be washed out at locations with high energy potential (Small et al., 2014), due to the high velocity of the water currents. However, in order to consider the cases where this may not occur completely, it was decided to carry out a series of simple tests designed to investigate the effect of granular seabed sediment at the interface on the shear behaviour of the foundation. The same testing programme as presented in section 5.2 was followed (i.e. the same rock types, foundation analogues, normal stress levels, etc), however a thin sand layer was placed on the foundation analogue before each test. More details about the properties of the sand and the preparation of the sand layer are available in Section 3.2.3.

6.2.1 Rock – sand – steel interfaces

Figure 6-17 to Figure 6-20 show the normalised shear stress (coefficient of friction μ) vs horizontal displacement curves for various rock – sand – steel interfaces. It can be seen that the data is quite “noisy” especially at lower normal stress levels. The peak interface strength is mobilised at higher horizontal displacement for increasing normal stress. This observations are similar to those made for the rock – steel interfaces that have been examined in Chapter 5.

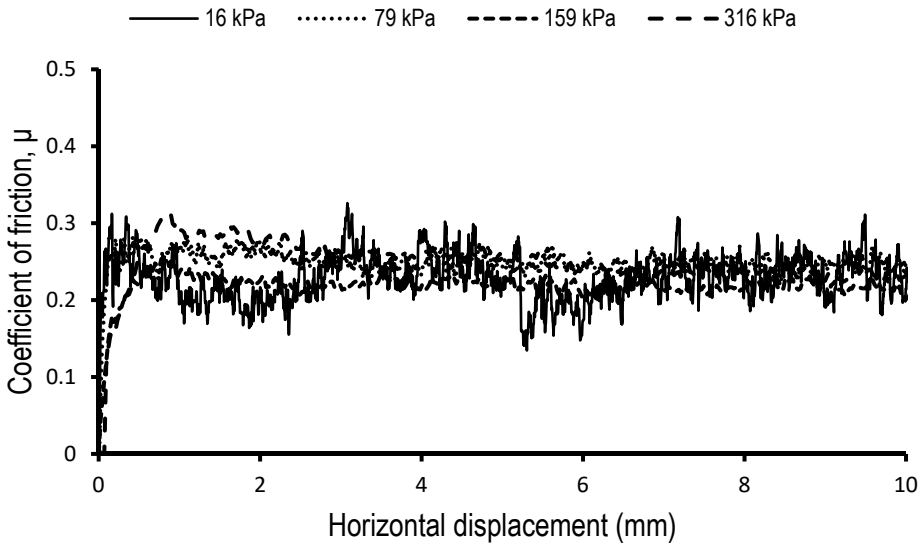

Figure 6-17. Coefficient of friction μ vs horizontal displacement for Sandstone - sand – steel interfaces (steel R_a = 0.4 μm)

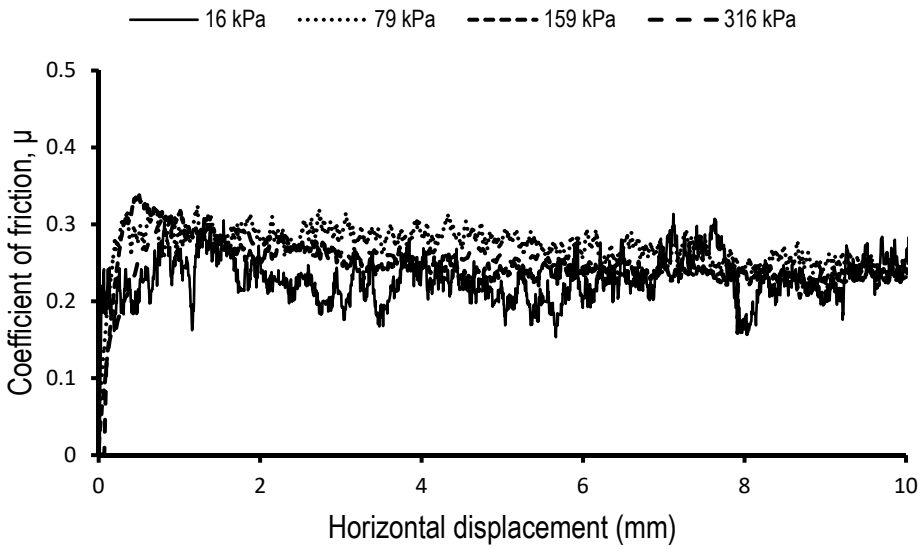

Figure 6-18. Coefficient of friction μ vs horizontal displacement for Flagstone - sand – steel interfaces (steel R_a = 0.4 μm)

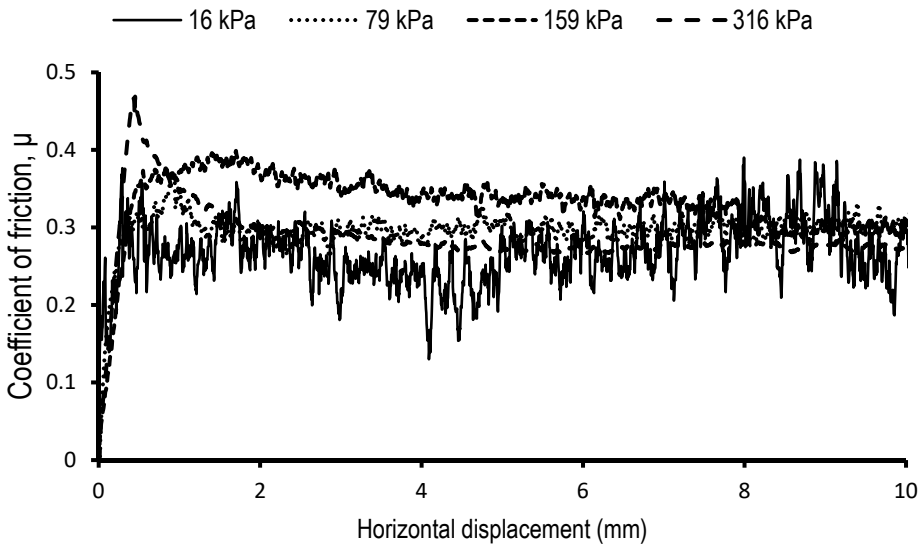

Figure 6-19. Coefficient of friction μ vs horizontal displacement for Andesite - sand – steel interfaces (steel R_a = 0.4 μm)

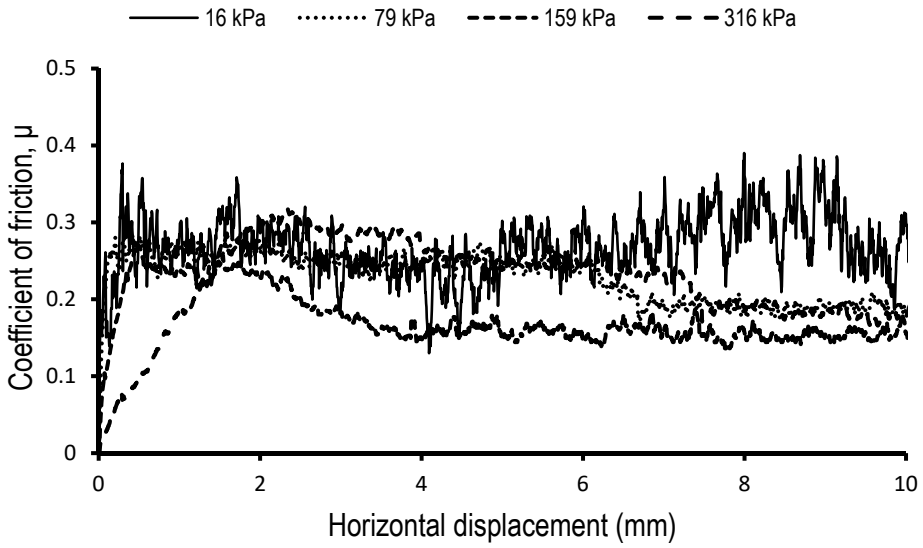

Figure 6-20. Coefficient of friction μ vs horizontal displacement for Limestone - sand – steel interfaces (steel R_a = 0.4 μm)

Table 6-4. Summary of results from rock – sand - steel interface testing

Rock type	Normal stress (kPa)	R_a (μm)					
		0.4		7.2		34.0	
		Peak friction angle (°)	Ultimate friction angle (°)	Peak friction angle (°)	Ultimate friction angle (°)	Peak friction angle (°)	Ultimate friction angle (°)
Sandstone - sand	16	19.2	9.5	20.8	11.2	19.2	7.8
	79	15.8	12.1	14.8	13.1	14.2	12.1
	159	14.2	11.3	14.6	13.5	17.3	13.4
	316	17.3	12.4	17.4	14.4	18.7	17.4
Flagstone - sand	16	17.7	13.6	20.0	14.4	25.9	15.2
	79	18.0	12.6	20.5	10.1	26.2	18.8
	159	18.6	12.2	17.9	10.8	26.2	23.4
	316	15.3	13.0	17.6	12.7	32.4	28.6
Andesite - sand	16	20.7	13.7	24.2	15.7	23.0	17.7
	79	20.5	15.0	22.1	15.7	22.1	16.8
	159	21.7	15.2	23.2	17.4	24.1	20.5
	316	25.0	16.1	23.1	22.3	25.5	25.7
Limestone - sand	16	18.3	10.8	20.6	11.1	25.8	18.1
	79	15.8	9.5	15.3	12.4	22.8	19.3
	159	15.1	8.3	16.9	11.4	24.2	20.3
	316	17.7	9.7	22.3	18.1	30.2	26.7

The apparent effect of the sand layer is reflected on the following figures, however the behaviour of the interface varies depending on the rock type. The interface friction angle values of the tests containing sand (δ_s) were normalised by the interface friction angle values δ for rock steel that were presented earlier in section 5.2 and correspond to interfaces free of sediment. This resulted in an interface friction angle ratio P = δ_s/δ_{st} that was used in the analysis of the results. The figures are annotated with the relative roughness ratio R = $R_{a,steel}/R_{a,rock}$ as defined in Chapter 5.

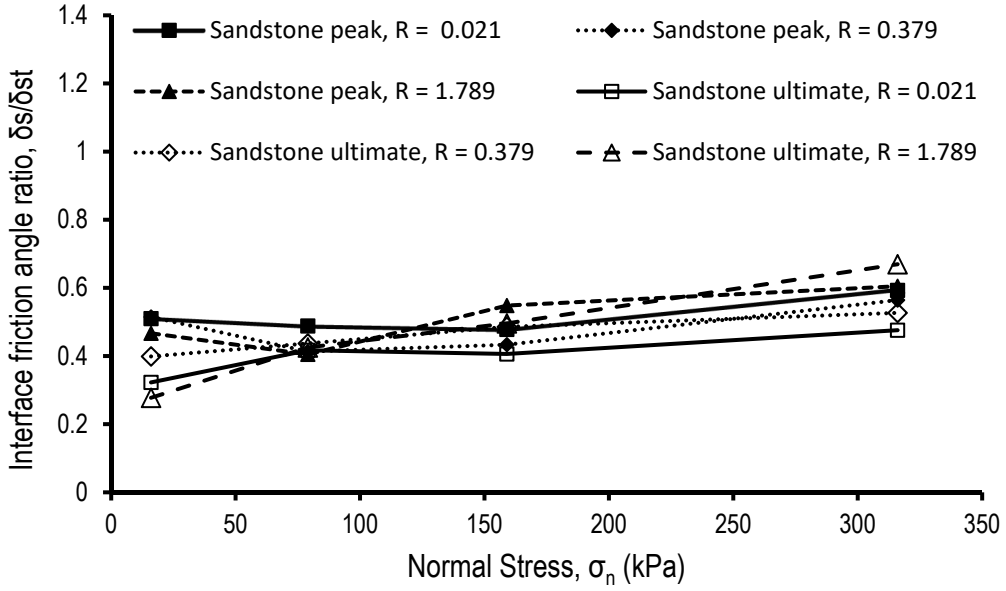

Figure 6-21. Normalised interface friction angles for Sandstone – sand –steel interfaces, considering peak and ultimate values

The presence of the sand layer significantly decreases the strength of the Sandstone – steel interface as denoted by the friction angle ratio which ranges between 0.48 - 0.60 for peak and between 0.28 - 0.67 for ultimate values. The reduction is greater at the lowest normal stress level (16 kPa) which is apparent for ultimate values as shown in Figure 6-21. The mechanisms of the overall shear resistance of granular – continuum interfaces are suggested to be rolling, sliding and ploughing (Abuel-Naga et al., 2018). It could be that in this case the sand grains are rolling during shear and effectively acting as ball bearings (i.e. a rolling component is induced which was not present in the Sandstone – steel interface). As the normal

stress increases, the rolling is progressively suppressed and the shearing mode changes to primarily sliding and ploughing, leading to an increase of the ultimate interface friction angle. The Mohs hardness of the sand grains and the Sandstone is the same (7), therefore it is believed that there is no change in the ploughing potential across the Sandstone – steel and Sandstone- sand – steel interfaces. However, the sand layer being a non-continuum material, constitute a more compliant counterface compared to Sandstone (continuum material), leading to a decrease on the shear strength of the interface.

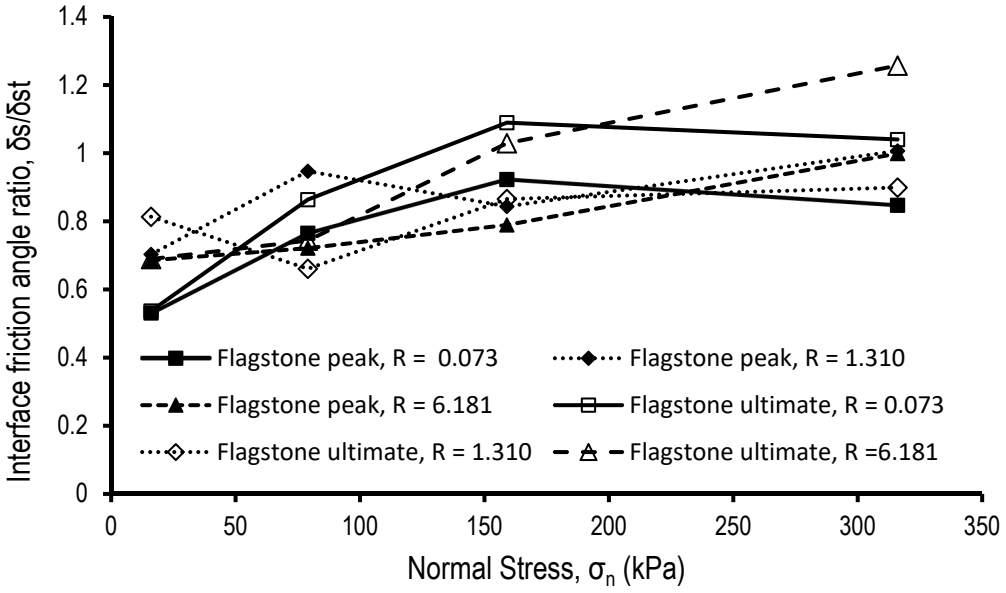

Figure 6-22. Normalised interface friction angles for Flagstone – sand –steel interfaces, considering peak and ultimate values

For Flagstone – sand - steel interfaces, the interface friction angle ratio yields values between 0.53 and 0.80 for σ_n= 16 kPa where the shearing mode would be assumed to be mainly rolling of the sand grains. It is assumed that as the normal stress level increases, the rolling component is suppressed. In addition, the hard sand grains (7 on Mohs scale) plough into both the steel (4 on Mohs scale) and Flagstone (3 on Mohs scale) surfaces, increasing the shear stress generated. For σ_n = 159 and 316 kPa, ploughing is apparently more pronounced and P displays values of 0.93 and 1.2. Sand reduces the interface strength for normal stress up to 79 kPa. For higher values, the effect

of sand on the interface is diminished (P close to 1), however for ultimate values it is even beneficial for the interface strength, since the sliding resistance increases (P = 1.2).

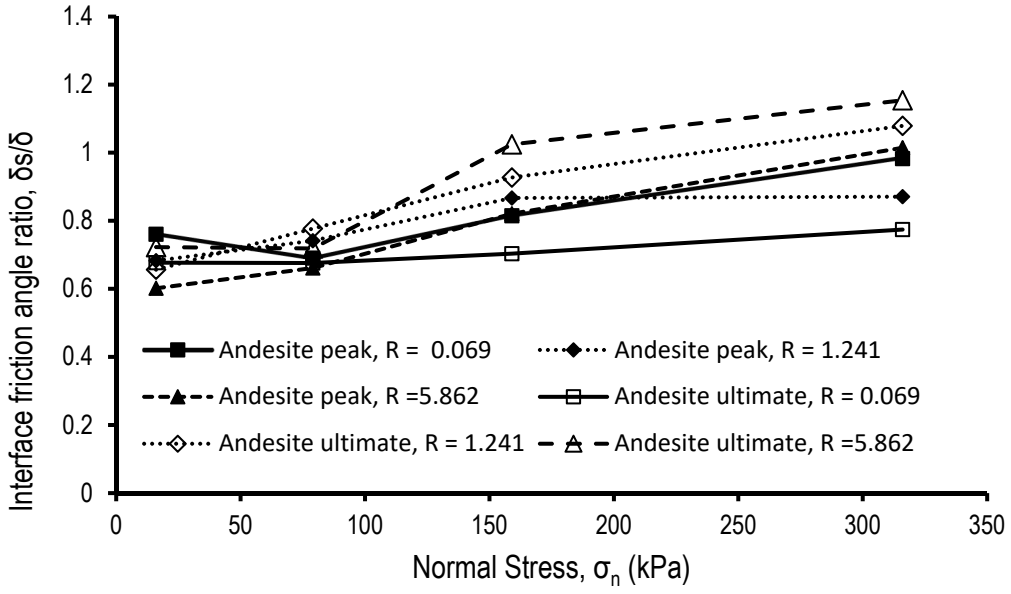

Figure 6-23. Normalised interface friction angles for Andesite – sand –steel interfaces, considering peak and ultimate values

Andesite – sand – steel interfaces exhibit behaviour quite similar to that of Flagstone described above. This could be attributed to the phoughing of the sand grains (7 on Mohs scale) into the Andesite and steel surfaces (6 and 4 on Mohs scale respectively) during shear, in the same way as described above for Flagstone. The relative hardness ratio (Mohs,steel/Mohs,rock) for the Andesite - steel interface is 0.67, whereas for the steel – sand combination it is 0.57 (4/7) and for the rock – sand part is 0.86 (6/7). Therefore, it is believed that the ploughing component of the interface shear strength could be increased especially for normal stress between 159 and 316 kPa.

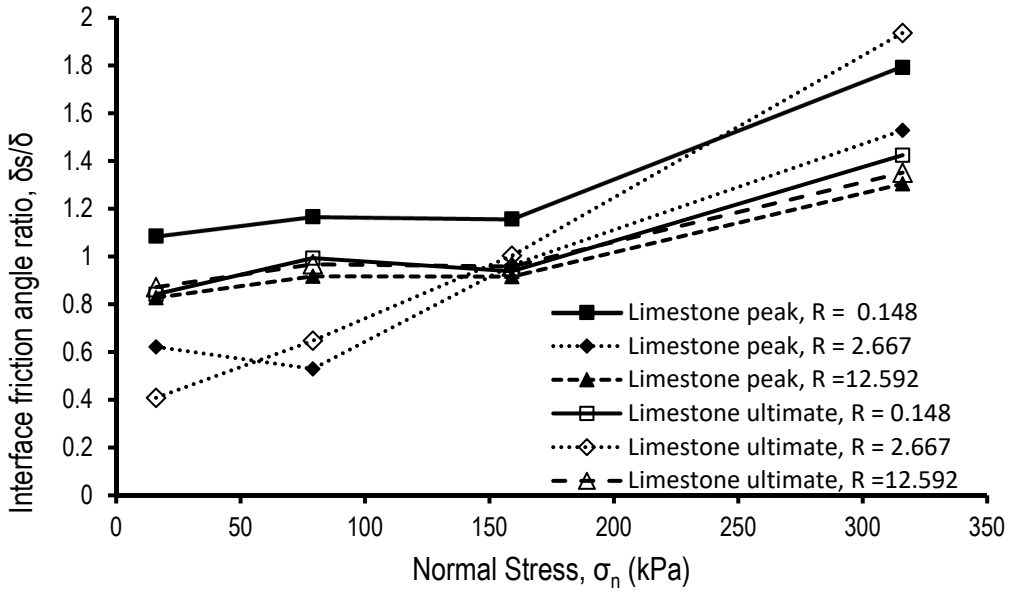

Figure 6-24. Normalised interface friction angles for Limestone – sand –steel interfaces, considering peak and ultimate values

The presence of sediment on Limestone, reduces the ultimate sliding resistance for σ_n up to 79 kPa as denoted by the interface friction angle ratio that ranges between 0.4 and 1.0 (depending on the steel R_a). Relative hardness ratio M for the Limestone – steel interface is 0.89, whereas for the steel – sand combination is 0.57 and for the Limestone – sand combination is 0.64. Therefore, as the normal stress increases, the ploughing component (of the sand grains in both the Limestone and steel surfaces is increased significantly. The rolling component tends to decrease the interface strength however it is believed that it reduces with increasing normal stress leading to an overall increase of the shearing resistance, up to 90 % (compared to the no sediment case).

Summarising, it seems that when the applied normal stress is up to 79 kPa, the presence of seabed sediment reduces the sliding resistance of the interface. This happens because the sand grains roll during shear acting effectively as ball bearings.

For higher normal stress, the rolling is suppressed and the scratch hardness of the interface materials influences the overall behaviour. This is a factor that

has been identified in the literature (Engelder 1976) and it seems that the difference between the Mohs hardness of the rock and the sand grains is crucial to determine whether or not the sand sediment will increase the interface shear strength when higher normal stress is applied. Sandstone and silica sand have the same value on Mohs scale (7), therefore no increase on shear resistance is noticed. Albeit, the interface with the sediment exhibits consistently lower values (up to ~ 50% decrease compared to the free of sediment interface) due to the increased compliance of the sand layer and the remaining effect of sand grain rolling. Andesite is 6 on Mohs scale, therefore the presence of sand grains increases the difference in hardness relative to the steel surface and leads to a slight increase on the shear strength of the interface when normal stress of at least 159 kPa is applied. Following the same rationale, Flagstone (3 on Mohs scale) and Limestone (4.5 on Mohs scale) interfaces exhibit higher sliding resistance (under high normal stress) when sediment is present. It should also be noted that as the difference in hardness relative to the steel increases, lower applied normal stress is adequate to increase the interface strength. This means that for a given rock - steel interface (and consequently a given difference in scratch hardness between the rock the sand and the steel), there is a threshold in applied normal stress (e.g. ~160 kPa for Andesite and Limestone), beyond which, the ploughing of the sand grains during shear becomes significant and the presence of seabed sediment increases the shear strength of the interface.

Relative roughness R_{max}/D_{50} has been identified (Uesugi and Kishida 1986, Jaradine et al., 1993) as a parameter that describes the effect of the surface roughness on the shear strength of continuum material – granular interfaces (e.g. offshore steel piles driven in sand). In a similar manner, ratio R_s (as defined in Equation 6-1) has been considered for the sand - steel part of the interfaces in order to investigate the effect of the steel surface roughness on the shear strength of the rock – sand – steel interfaces.

$$R_s = R_{a,steel}/D_{50}$$

Equation 6-2

After Lauder (2010), D_{50} = 0.13 mm for the HST95 sand used in the tests, therefore R_s exhibits values of 0.0031, 0.0554 and 0.2615 for steel R_a of 0.4, 7.2 and 34 μm respectively. The range of steel roughness (0.4 – 34 μm) is wider than the range of the rock samples roughness (2.7 – 19 μm), therefore is was deemed more appropriate to investigate the effect of steel roughness instead of rock roughness.

Figure 6-25 and Figure 6-26 show how interface friction angle δ of different rock - sand – steel interfaces, changes with varying R_s. As mentioned previously, tests were carried out under four normal stress levels, however to aid comparison and clarity of graphs, a δ value corresponding to the average of the coefficient of friction at normal stress of 159 and 316 kPa was considered for each case.

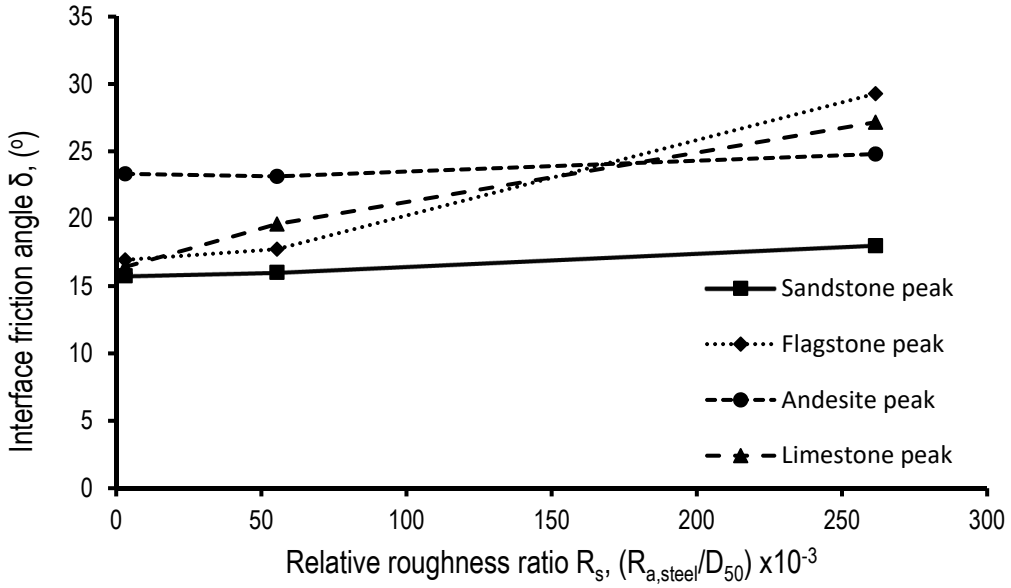

Figure 6-25. Interface friction angle δ vs relative roughness ratio R_s for rock – sand – steel interfaces, considering peak values

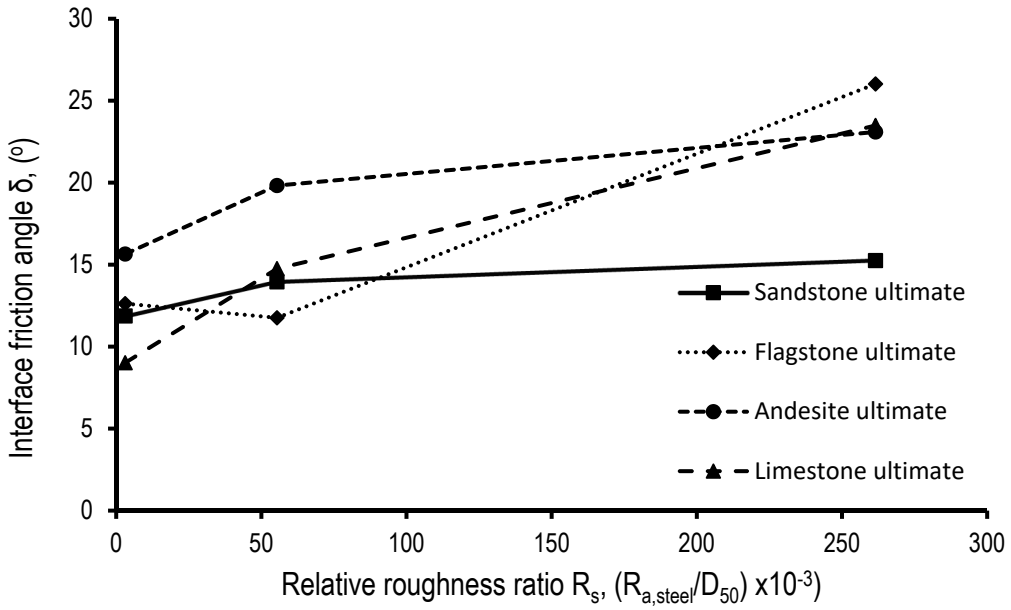

Figure 6-26. Interface friction angle δ vs relative roughness ratio R_s for rock – sand – steel interfaces, considering ultimate values

Relative roughness ratio R_s seems to have minimal effect on the Sandstone and Andesite – sand – steel interfaces. Whereas δ for Flagstone and Limestone – sand – steel interfaces, increases significantly with increasing R_s. It is assumed that as the R_s increases (i.e. steel roughness increases), more sand grains are "captured" by the steel surface and consequently sliding of sand grains on the steel surface is reduced. As a result, the interface shear strength is significantly affected by the rock – sand part of the interface and consequently the rock – sand relative hardness ratio. Sandstone – sand interface has a relative hardness ratio of 1 (7/7), therefore no ploughing of sand into the Sandstone is expected to occur irrespective to the roughness of the steel. Andesite – sand interface has a relative hardness ratio of 0.86 (6/7), indicating a relatively restricted ploughing of sand grains into the Andesite surface, hence the increase in steel roughness doesn't seem to have a noticeable effect. On the other hand, the rock/sand relative hardness ratio is 0.43 (3/7) and 0.64 (4.5/7) for Flagstone and Limestone – sand interfaces respectively. Therefore, the ploughing of sand grains into the rock surface is pronounced as the steel - sand relative roughness ratio (R_s) increases, leading to a continuous increase in the overall interface shear strength. As the steel roughness also increases it will effectively grab the sand grains and give the

steel the same contact hardness as the sand (Sandstone) and cause more interface damage than the steel alone.

This behaviour is slightly different to that observed by Jardine et al. (1993) for sand – steel interfaces, where the interface shear strength increased for increasing steel roughness up to a point where a plateau was reached and further increase in steel roughness had no practical effect. In this case, the upper end of the interface shear strength was limited by the internal friction angle of the sand (i.e. the shear band moved into the sand mass when the sand steel interface strength was higher). However in this case, a granular material (sand) is placed between two continuum materials (rock and steel) and when the sand grains are “trapped” by the asperities of the steel (i.e. high R_s value), the interface shear strength seems to be influenced by the relative hardness ratio of the rock – sand part of the interface, as this ratio indicates whether (and to what extend) ploughing of sand grains into the rock surface will occur.

To summarise, it seems that when the sand grains are significant harder than the steel and of similar hardness to the rock, the shear strength of the interface seems to be practically unaffected by the steel - sand relative roughness ratio R_s. On the other hand, shear strength increases for increasing R_s when sand grains are significantly harder than the steel and the rock. In any case, rock – sand – steel interfaces exhibit the higher values of shear strength for normal stress between 159 and 316 kPa.

6.3 Summary

Data obtained through IST testing of rock – concrete and rock – sand – concrete interfaces have been presented in this chapter. Analysis of the results allowed the investigation of the factors that influence the interface shear behaviour. A summary of the findings presented in this chapter is given below.

1. Rock – concrete interfaces seem to yield higher values of interface friction angle than rock - steel interfaces possibly due to the higher

damage/ploughing during shear (with the exception of interfaces with Sandstone at normal stress of 16 – 79 kPa). This becomes more apparent for normal stress of 159 – 316 kPa.

2. The presence of a sand layer on the interface changes the mode of shearing of the interface. For normal stress up to 79 kPa, the sand grains appear to roll on the interface thus reducing the shear strength (compared to the free of sediment interface). For higher normal stress (up to 316 kPa), rolling is suppressed and the relevant scratch hardness of the interface materials seems to influence the shear behaviour.

3. When the hardness (M) of the sand grains is higher than the steel and similar to the rock, then the interface friction angle is not affected by R_s ($R_s = R_{a,steel}/D_{50}$). In contrast, the friction angle increases with increasing R_s when the sand grains are harder than the steel and the rock of the interface, suggesting enhanced damage and ploughing.

Chapter 7

7 Chalk interface testing

Chalk is a rock with unusual characteristics (Lord et al., 2002) whose behaviour differs to the other rock types. For this reason, guidelines (e.g. Lord et al., 2002, C574) and specialist conferences (e.g. Engineering in Chalk 1989 and 2018) for characterization and engineering exclusively in Chalk have been held. Therefore, it was felt that it was be preferable to examine it independently from the other rock types.

Interface tests between Chalk (saw cut with R_a = 3.1 μm) - steel interfaces at normal stresses relevant to those anticipated for real tidal stream projects (Ziogos et al., 2015b), were carried out in order to obtain friction properties necessary for the determination of the sliding resistance of a GBS. The UCS of Chalk has previously been found to vary significantly (more than 50%) with saturation levels with lower strengths for saturated samples compared to dry ones (Matthews and Clayton, 1993). Therefore, tests using both dry and saturated samples were carried out in order to examine the variation of UCS on the shear resistance and behaviour of the interface. In addition, the effect of steel roughness was also investigated (R_a = 0.4 - 34 μm) along with the effect of normal stress (σ_n= 16 - 1000 kPa) over relatively short displacements of 10 mm during shear. The normal stress extended to higher values (1000 kPa) compared to the other rock types, because it was felt that it could have significant effect on the shear behaviour. The results from Sandstone - steel interface testing that have already been presented in Chapter 5 (σ_n = 16 - 316 kPa) were considered to allow comparison between the interface behaviour of Chalk and a typical sedimentary rock (i.e. Sandstone) that exhibits more “conventional” behaviour. Sandstone and dry Chalk have very similar UCS (~30 MPa) and also have the two more “extreme” values of relative hardness M among the rock – steel interfaces considered in this study. As mentioned previously, M for Sandstone – steel is 0.57 whereas Chalk has a Mohs

hardness value of 2.5, resulting in a relative hardness ratio M (Mohs,steel/Mohs,rock) of 1.6.

In addition to the tests designed to investigate the behaviour of Chalk relevant to tidal stream generator GBS foundations (low normal stress and low displacement) an additional set of tests were undertaken to very large cumulative displacements (7.0 m). These tests were to check the potential of the IST device but also to consider the displacements that may be encountered in driven piling or underneath a sliding foundation or tow head used in the offshore oil and gas industries.

As per the other rock types examined in this study, Chalk was also tested against concrete at normal stress of 16, 79, 159 and 316 kPa, using both dry and saturated Chalk samples.

7.1 Results from Chalk – steel interface testing

Figure 7-1 to Figure 7-3 show the normalised shear stress - displacement curves from saturated Chalk - steel interface tests on steel of increasing roughness.

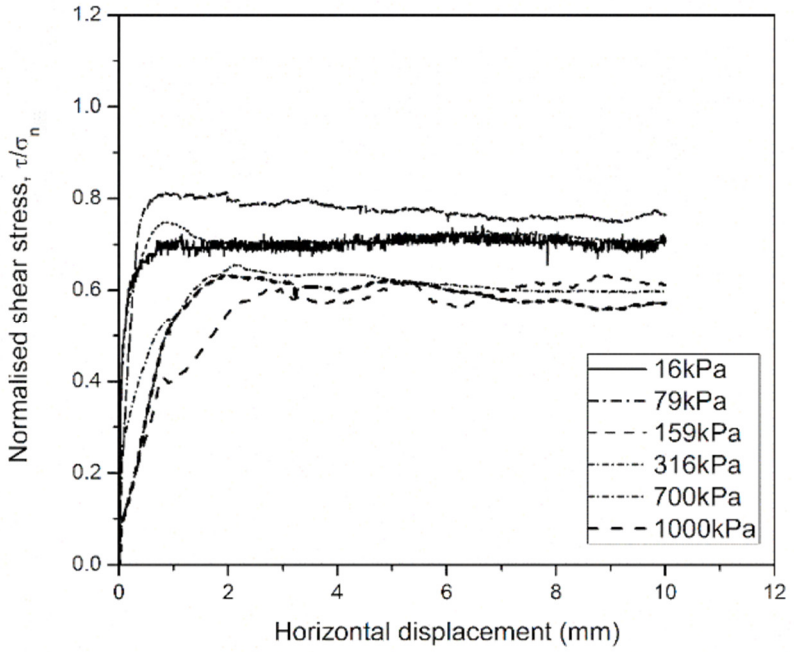

Figure 7-1. Normalised shear stress plotted against horizontal displacement for saturated Chalk samples against steel R_a = 0.4 µm

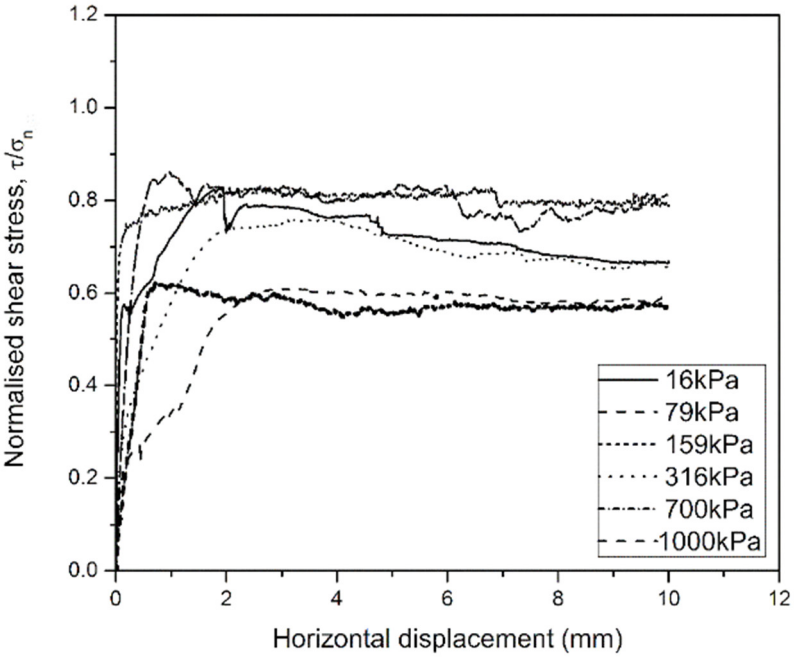

Figure 7-2. Normalised shear stress plotted against horizontal displacement for saturated Chalk samples against steel R_a = 7.2 µm

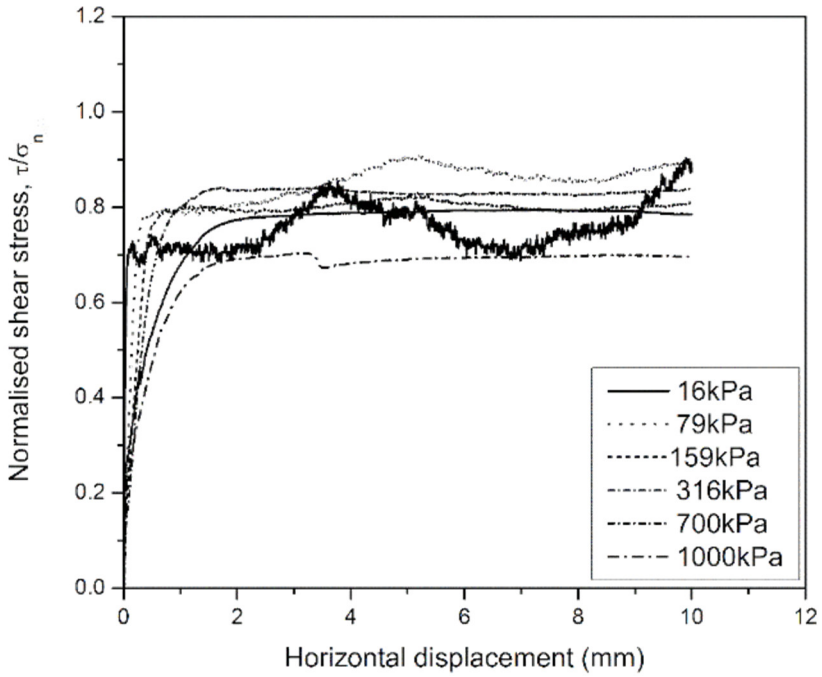

Figure 7-3. Normalised shear stress plotted against horizontal displacement for saturated Chalk samples against steel R_a = 34 µm

A typical result shows a slightly elevated initial shear stress followed by a slight reduction in shear stress post peak (or yield) and then remaining relatively constant until the end of the test. This is similar to the behaviour reported by Chan et al., 2019. It is apparent that yielding or peak shear stress is observed at increasing displacement levels as the normal stress on the Chalk increases, as seen in Figure 7-1 to Figure 7-3 for normal stresses above 159 kPa. It is also noticeable that as the normal stress increases there is an increase in shear resistance up to a normal stress of 79 - 159 kPa and then a reduction in the shear resistance with the lowest shear resistances associated with the highest normal stress of 1000 kPa. Table 7-1 shows the summarised results of testing where δ_{peak} is defined as the maximum value at a shear displacement up to 4 mm and δ_{ult} is defined as the minimum value in the region of 8 - 10 mm.

Table 7-1. Summary of results from interface testing of Chalk-steel interface

Normal stress (kPa)	Initial sample State*	Post test sample condition$	R_a (μm)					
			0.4		7.2		34.0	
			Peak shear stress (kPa)	Ultimate shear stress (kPa)	Peak shear stress (kPa)	Ultimate shear stress (kPa)	Peak shear stress (kPa)	Ultimate shear stress (kPa)
16	D	I	13.9	7.5	13.5	11.0	12.62	11.5
16	S	I	11.5	10.5	13.0	10.5	13.5	12.0
79	D	I	75.5	57.5	76.9	60.5	72.5	70.5
79	S	I	65.0	59.0	70.2	58.0	72.0	69.5
159	D	I	136.0	106.0	147.5	131.0	143.0	141.0
159	S	I	119.0	112.0	132.5	125.5	131.0	127.0
316	D	I	287.0	273.5	235.6	215.5	318.0	316.0
316	S	I	207.5	188.0	237.2	215.0	266.0	263.5
700	D	SD	500.0	433.5	476.3	410.6	614.0	606.5
700	S	SD	450.0	399.0	432.5	400.0	558.0	546.0
1000	D	NI	748.0	739.5	650.3	600.5	803.5	643.0
1000	S	NI	600.0	560.5	608.5	582.0	705.0	694.0

* S = saturated, D = dry samples

$ I =intact, SD = surface damage, NI = non-intact samples

The results in Figure 7-4 show the tests for Sandstone sheared against steel of R_a= 7.2 μm where the curves are “noisy” because sandstone is rougher and

harder (Mohs hardness 7), whereas it is apparent that higher interface shear stresses are mobilised in the softer Chalk (Mohs hardness 2.5).

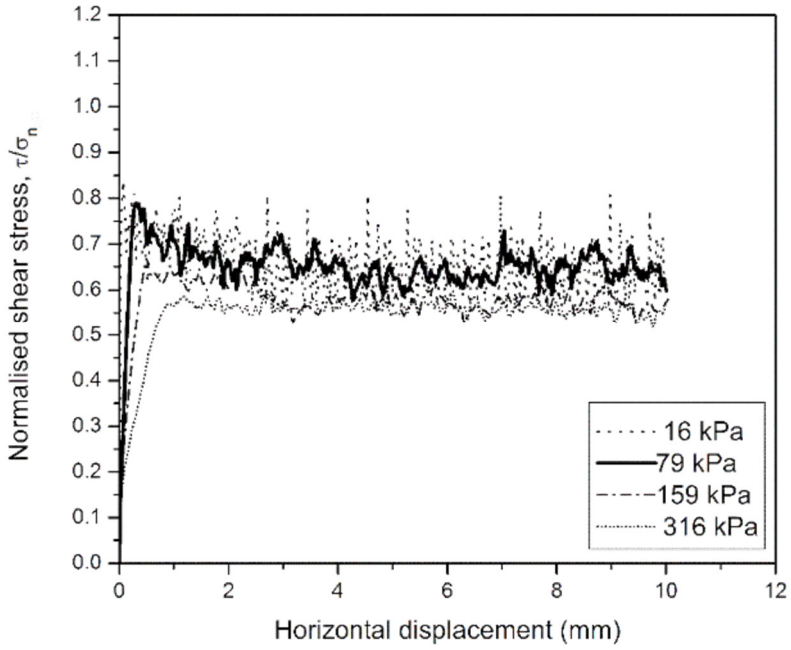

Figure 7-4. Normalised shear stress plotted against horizontal displacement for Sandstone samples against steel R_a = 7.2 µm

Figure 7-5 - Figure 7-7 show the results of IST testing of the saturated and dry Chalk against the various steel interfaces in terms of the different normal stresses. The figures are also annotated for the basic friction angle (φ_b) of the Chalk – Chalk interface and for the Chalk – steel interface testing carried out ustilising the tilt table (more details about this test can be found in Section 3.2.2). The applicability of the tilt table test is discussed further in Section 8.4).

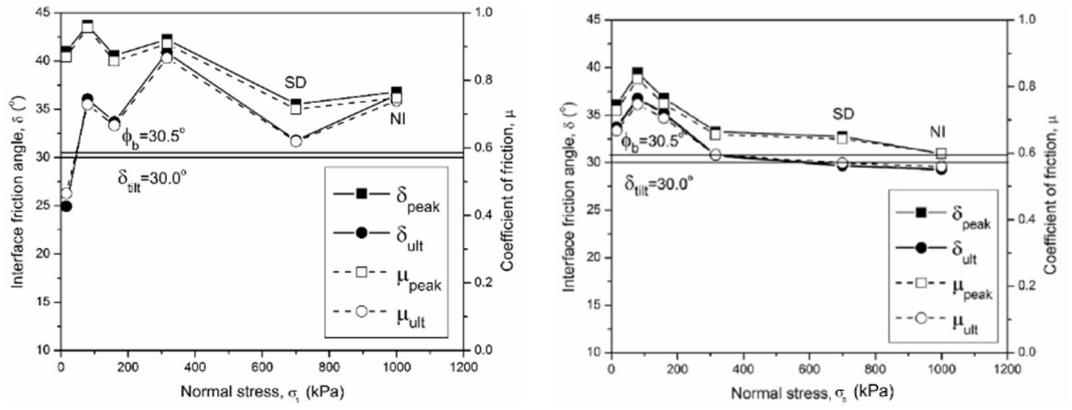

a b

Figure 7-5. Variation of interface friction angle and coefficient of friction for Chalk–steel interface test for steel with R_a= 0·4 μm against (a) dry and (b) saturated Chalk

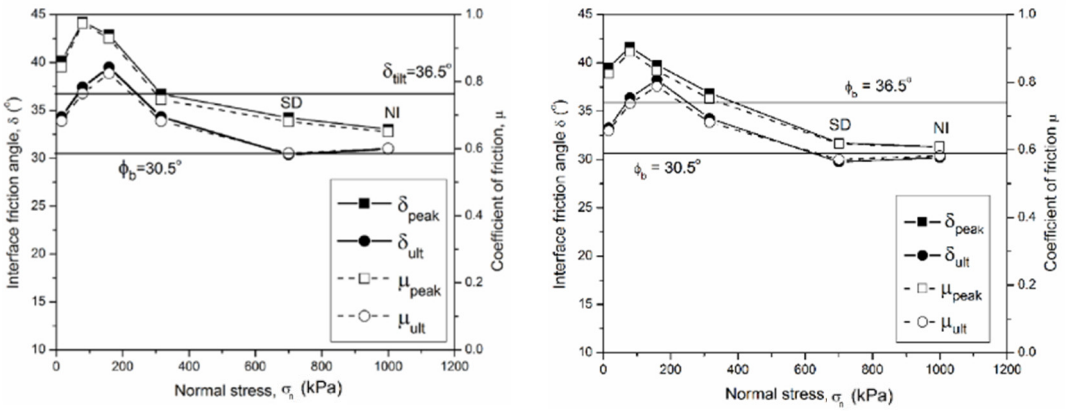

a b

Figure 7-6. Variation of interface friction angle and coefficient of friction for Chalk–steel interface test for steel with R_a= 7·2 μm against (a) dry and (b) saturated Chalk

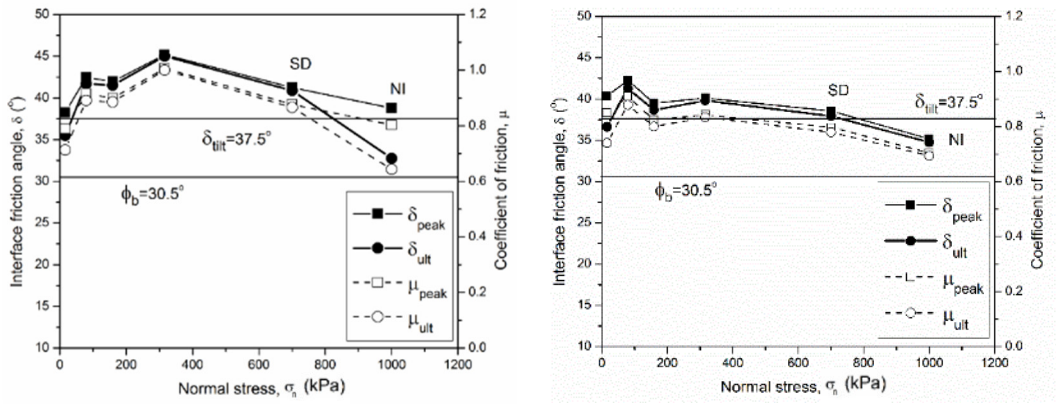

Figure 7-7. Variation of interface friction angle and coefficient of friction for Chalk–steel interface test for steel with R_a=34 μm against (a) dry and (b) saturated Chalk

For the dry tests the peak interface friction angles δ_{peak} range from 33º to 45º and δ_{ult} from 25º to 45º. For saturated tests, δ_{peak} ranges from 31º to 42º and δ_{ult} from 29 º to 41º; similar values are reported by Buckley et al., 2018. The results indicate that the interface behaviour varies with increasing normal stress in a non-linear manner. This suggests that a simple constant friction angle obtained from Mohr-Coulomb approach to represent interface shearing may not be appropriate in the case of Chalk. This is in contrast to the behaviour shown previously for the other rock types, as they seemed to tend to a linear behaviour between 159 and 316 kPa (although a constant friction angle is not recommended in these cases either). The peak interface friction angles are somehow affected by the degree of saturation (the values are ~ 10% higher for the dry tests). However, the significant variation of UCS change noted between dry and saturated Chalk samples (69% reduction in UCS from dry to saturated) is not clearly reflected by the interface shear strength. All of the figures have been annotated with the value of the interface friction angle derived from the low stress tilt table testing (which will be discussed further in the next chapter) and the basic Chalk - Chalk friction angle (again obtained from tilt table testing as described earlier).

Post – test sample examination revealed that significant damaged occurred on the Chalk surface during shear and for higher normal stress (700 and 1000 kPa), parts of the Chalk surface were chipped off or tensile structural failure

occurred. As an aid to investigate this behaviour the tensile strength of Chalk T_0 was considered, along the relative hardness ratio that has been introduced previously.

Irrespective of the steel roughness, the interface resistance exhibits a low value at normal stress of 16 kPa which may indicate poor interlocking between the Chalk and steel interface as the applied stress is not adequate to bring the two solid bodies into intimate contact and shearing is occurring on the top of the asperities (steel and Chalk). This is in contrast to the behaviour described earlier for the other rock – steel interfaces and could potentially indicate that the ploughing component of the shear strength is more important than the sliding component. The relative hardness ratio M for the Chalk – steel interface is 1.6 indicating that ploughing of the steel asperities into the Chalk surface occurs and contributes significantly to the interface shear strength. It is assumed that as the normal stress increases, the interface gains higher shear strength, as better interlocking is established between the normal stresses of 79 and 159 kPa (7.2 to 16.6% of the Chalk tensile strength, T_0) and the ploughing component of the shear strength is pronounced. At these stress levels the shearing is accompanied by observable damage on Chalk surface (result of ploughing), seen as layer of powder (dry samples) or Chalk putty (saturated tests) on the steel interface on post test sample separation. This behaviour is similar to that noted for rock analogues (cement blocks) by Ziogos et al. (2015b). For normal stresses from 316 kPa to 1000 kPa the ultimate interface friction angle reduces to values typically between 30 and 35° and in the majority of cases appears to be approaching the basic Chalk - Chalk friction angle value noted for the 0.4 μm interface. This suggests that damage at the interface may be filling the rough surface of the rougher steel samples and reducing their apparent interface roughness to that approaching the smoothest interface tested here, tending to φ_b (i.e. Chalk – Chalk interface friction angle). Significantly more damage was noticed in some samples tested at 700 kPa and 1000 kPa, where parts of the perimeter of the sample were chipped off (labeled as surface damage, SD in Table 7-1), or at the highest normal stress level (1000 kPa) resulted in complete tensile failure of the

sample (NI) as shown in Figure 7-8 (possibly influenced by the fact that the radial deformation increases with increasing distance from the center of the sample).

Figure 7-8. Tensile failure of a dry Chalk sample sheared at 1000 kPa

Therefore, in the case of Chalk the upper limit to the interface strength appears to be linked to the local surface strength of the material with potential for catastrophic disruption of the interface at higher normal stresses on approaching the tensile strength of the Chalk (T_0 = 0.96 to 1.1 MPa). Although, some of the samples tested at the higher stress of 1000 kPa were non - intact after removal of the sample from its clamp it is believed that the interface shearing behaviour remained valid as the clamping system maintained the integrity of the sample and shearing surface during testing. The reduced shear stress noted during testing at these stresses reflects the increased interface damage.

7.2 Comparison of Chalk and Sandstone interfaces

As mentioned earlier, the adoption of a linear failure envelope for Chalk does not seem appropriate for design purposes, since the interface friction angle is affected by the normal stress level. Although, in order to allow comparison, linear failure envelopes for peak and ultimate interface resistance were calculated. These are based upon the average peak or ultimate resistance determined over the range of effective stresses tested. To allow the effect of normal stress and potential for surface degradation and damage to be

represented the range of normalised friction angles obtained are denoted by vertical error bars as shown in Figure 7-9 (shown for Chalk peak values only for clarity).

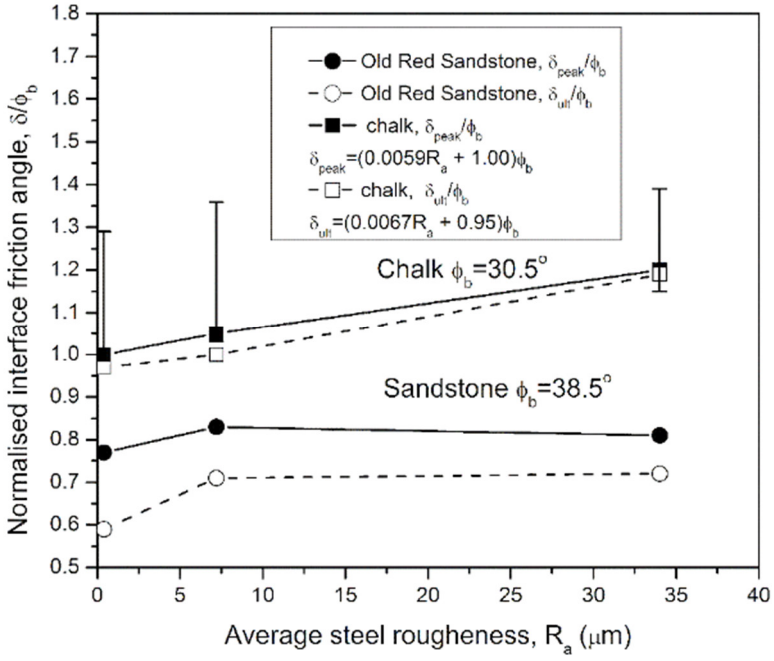

Figure 7-9. Variation of normalised friction angle with increasing steel roughness, for saturated Chalk samples and dry Sandstone

The results suggest that over the steel roughness range investigated (R_a = 0.4 – 34 μm), that on average interface becomes stronger as the steel roughness increases (as seen previously for Flagstone and Limestone interfaces), without reaching a “plateau” as seen in other studies (Ziogos et al., 2015b, Jardine et al., 1993) and as shown for Sandstone. Although when increasing normal stress is considered there appears to be a tendency for the Chalk - steel interfaces to tend towards the basic Chalk - Chalk interface properties.

7.3 Extended deformation tests

Results from the large displacement tests can be seen in Figure 7-10 compared with the result from a similar test undertaken on Sandstone.

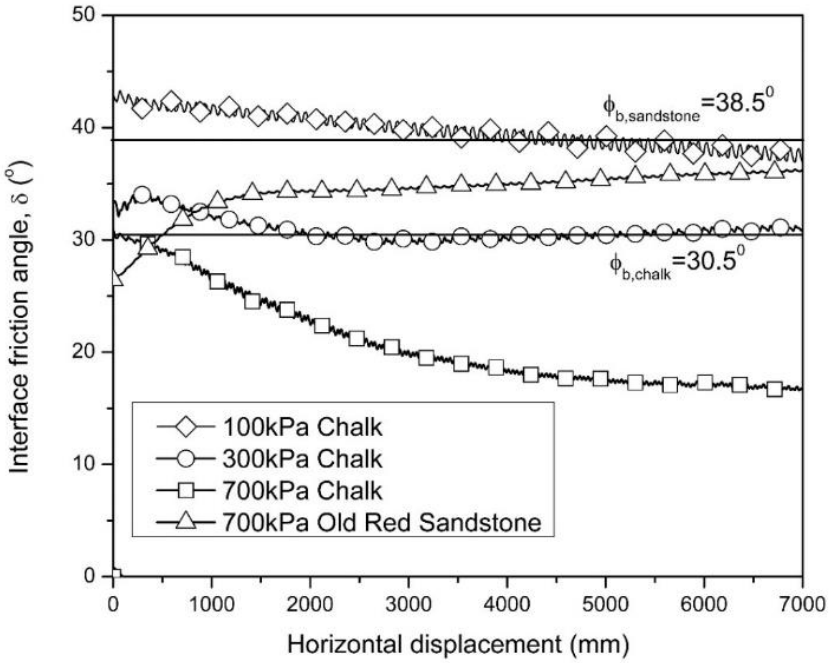

Figure 7-10. Interface friction angle plotted against horizontal displacement for saturated Chalk samples

It is clear from the tests on Chalk that there is continuous degradation of the shear surface throughout the test. At the lowest stress of 100 kPa the friction angle has fallen from an initial peak of 43° to 37° at 7.0 m with the rate of degradation appearing to reduce. At 300 kPa normal stress, reduced initial degradation is observed with a relatively constant interface friction angle of 30 – 31° being reached after 2.4 m of displacement which tends to the basic Chalk - Chalk interface friction angle which may be explained by the degradation behaviour described above for the low displacement tests. In contrast at a normal stress of 700 kPa there is a significant reduction in the interface friction angle below the basic Chalk - Chalk interface friction angle until reaching a relatively constant value of 17° (0.56 φ_b) at 6.5 m. Previous low displacement testing results shown earlier may have led to the recommendation of a lower safe bound design interface friction angle of approximately 29° (0.95 φ_b) which could be determined from the basic Chalk - Chalk interface friction angle. In the case of large displacement events this may be a suitable approach where the normal stresses do not exceed 300 kPa (0.31 T_0). Where this value is exceeded then a more conservative interface resistance must be assumed. The behaviour observed in Figure 7-10 for the

large displacement test on Sandstone show very different behaviour with increasing resistance with increasing displacement up to 1.7 m displacement and then a more gradual increase with increasing displacement which again appears to be tending to the Sandstone - Sandstone basic interface friction angle. This may be due to the removal of weak exposed Sandstone asperities (individual weakly cemented grains), which essentially “fil up” the steel roughness leading to essentially a Sandstone – Sandstone interface. What is apparent from the testing is that, unless normal stresses are high enough to cause significant interface and sample damage, that large deformation tests on steel (R_a = 7.2 μm) rock interfaces result in interface behaviour that tends to the basic low stress rock-rock interface behavior (for both Chalk and Sandstone - steel interfaces).

It should be noted that the testing regime here is constant normal stress and in the case of driven piles a constant normal stiffness regime may more adequately represent in-situ conditions leading to a reduced potential for tensile strength linked degradation. This assumes though that the Chalk in-situ is intact and well confined without faults or voids/low strength zones. In addition, constant normal stiffness conditions may lead to significantly higher in-situ stresses than those tested here which could result in a more rapid degradation with displacement and thus is an area for further investigation.

7.4 Results from Chalk – concrete interface testing

As per the other rock types examined in this study (results presented in Chapters 5 and 6), Chalk samples have also been tested against concrete using the IST. Normal stress levels of 16, 79, 159 and 316 kPa have been applied (unique normal stress per test) and the total shear deformation was 10 mm for each test. The results for both dry and saturated Chalk for against the concrete interface are shown in Figure 7-11 and Figure 7-12.

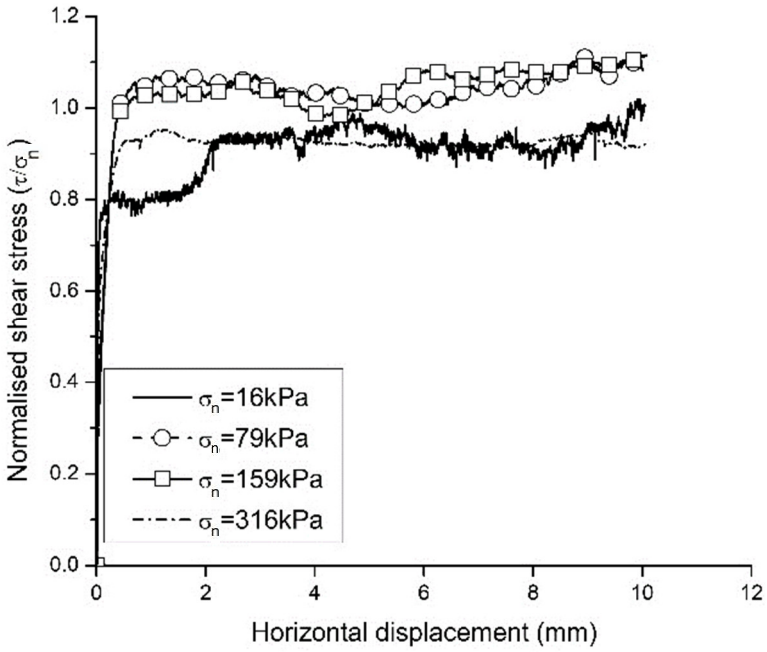

Figure 7-11. Results of IST testing Chalk-concrete interface for dry Chalk

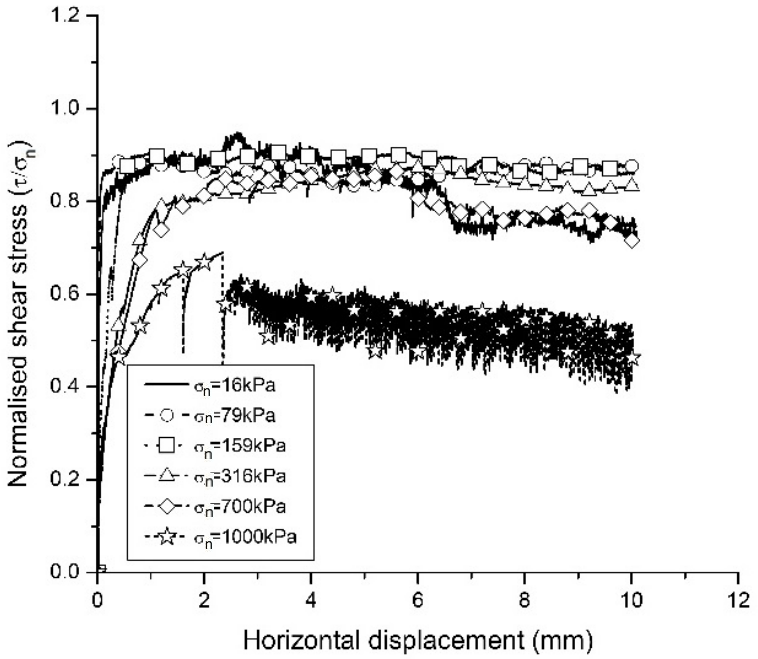

Figure 7-12. Results of IST testing Chalk-concrete interface for saturated Chalk

The results for the dry tests (Figure 7-11) show higher shear stress resistance during interface testing than the saturated tests (Figure 7-12). The normalised shear stress is relatively low at low normal stress and then appear to increase

with increasing normal stress up to 159 kPa (0.16 T_0) before reducing back down to lower levels with increasing normal stress. This matches the behaviour observed for Chalk – steel interfaces. Similar behavior is observed for the saturated tests but as the tests were taken to higher normal stresses (Figure 7-14) there appears to be some additional significant post-peak degradation associated with the 700 kPa (0.73 T_0) normal stress and a significant reduction in normalised shear stress when the normal stress reaches 1000 kPa (1.04 T_0). The variation of shear stress - displacement associated with this high normal stress test is also very “noisy” and displays significant low displacement drops in shear stress (Figure 7-12).

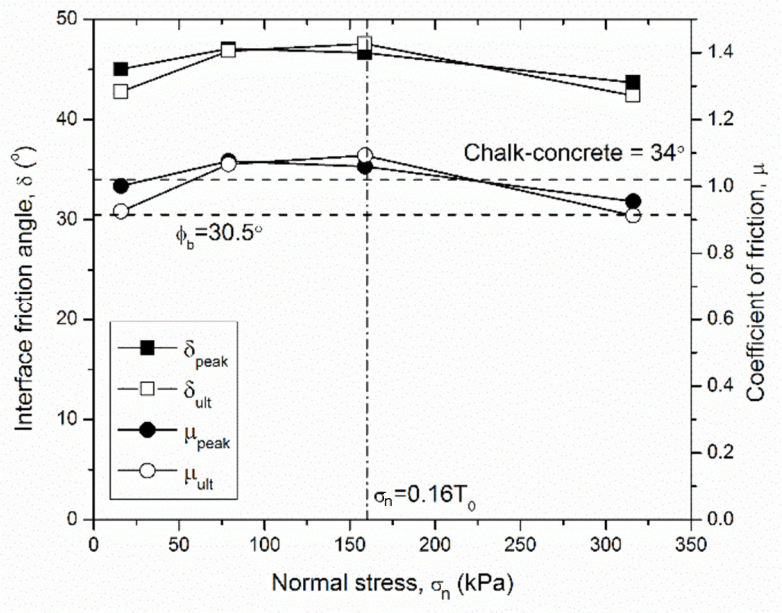

Figure 7-13. Summary of results for Chalk-concrete interface for dry Chalk

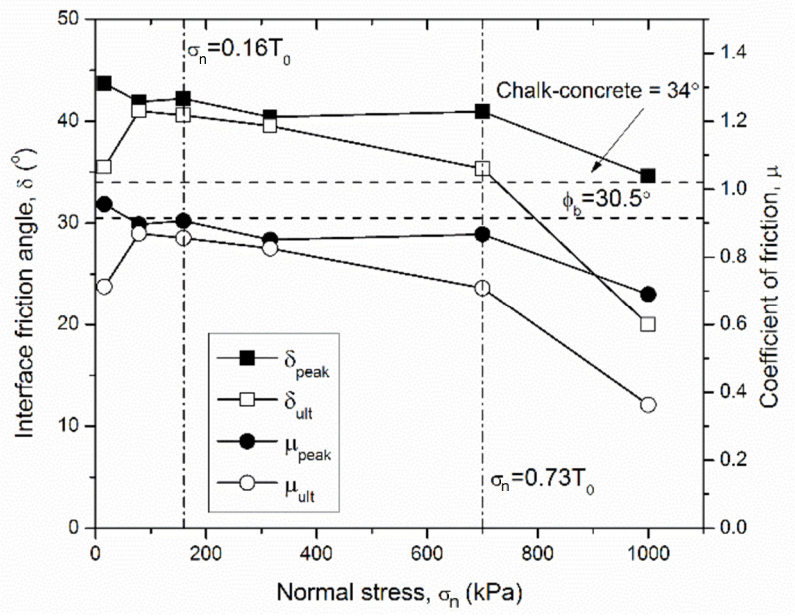

Figure 7-14. Summary of results for Chalk-concrete interface for saturated Chalk

For the dry Chalk average peak friction angles up to 45.6° are obtained (Figure 7-13) but these values are erratic and not sustained (Figure 7-11) thus design based upon ultimate values would seem more appropriate where these are actually very similar to the peak values. The ultimate values average at 44.9°, and some way above (1.47 φ_b) the Chalk - Chalk interface value from tilt table testing (φ_b = 30.5°) over the range of normal stresses tested. The peak interface angles obtained for saturated Chalk (39.2°, $\delta_{sat}/\delta_{dry}$ = 0.860) are lower as would be anticipated based upon the lower T_0 of Chalk ($T_{0,sat}/T_{0,dry}$= 0.873) when saturated (Table 3-4). The similarity in the drop in strength at the interface and in T_0 from dry to saturated suggests that T_0 is playing a direct role in interface shear strength. The ultimate friction angles are again higher than the basic friction angles for Chalk 1.28 (φ_b). Figure 7-14 suggests that at low normal stresses and at stresses not exceeding 0.73 T_0 that the simply measured Chalk-concrete friction angle may be used as a lower bound to design.

Figure 7-14 shows that if the normal stress exceeds 73% of the tensile strength of the Chalk that there is a significant drop in shear resistance. As noted in Table 7-2 on inspection of the Chalk samples after testing the samples tested at σ_n = 700 kPa showed marked surface damage (SD) in the form of Chalk

powder for dry samples and Chalk putty for saturated samples with perimeter chips in the round samples. For samples tested at σ_n = 1000 kPa where the tensile strength of the Chalk was exceeded the sample chipped and cracked through the full sample thickness (non-intact = NI). This behaviour is identical to that noticed for Chalk – steel interfaces. Based upon this behavior in constant normal stress testing the adoption of linear failure envelopes where cohesion values are referred to (Clayton & Saffari - Shooshtari, 1990) is not appropriate unless testing and application is limited to low stress levels.

Table 7-2. Summary of Chalk - concrete testing results

Normal stress (kPa)	Initial[1] sample state	Post test[2] sample condition	Peak shear stress (kPa)	Ultimate shear stress (kPa)
16	D	I	16.0	15.0
79	D	I	85.0	84.5
159	D	I	168.5	174.0
316	D	I	301.5	288.5
16	S	I	15.5	11.5
79	S	I	71.0	68.5
159	S	I	144.0	136.0
316	S	I	269.0	261.0
700	S	SD	607.0	496.5
1000	S	NI	690.0	363.0

[1]S, saturated, D, dry samples
[2]I, intact, SD, surface damage, NI, non-intact samples

Further comparison of the results with those presented for tests on Chalk - steel interfaces where the roughness of the steel was also varied between 0.4 to 34 μm show a marked difference. For the Chalk -steel interfaces the shear resistance always exceeds the basic friction angle for Chalk, even at high normal stress levels thus recommending the basic friction angle as a

lower bound design assumption even at normal stresses exceeding the tensile strength seemed appropriate for low displacement levels. Here the friction angle is lower for the Chalk – concrete at high normal stresses.

The interface friction angles of the Chalk – concrete interfaces have been normalised against the values of Chalk – steel R_a = 34 μm interfaces, as they seem to exhibit the higher interface friction angles and could be considered an upper limit for the Chalk – steel interfaces. Figure 7-15 and Figure 7-16 show the normalised data for dry and saturated samples respectively.

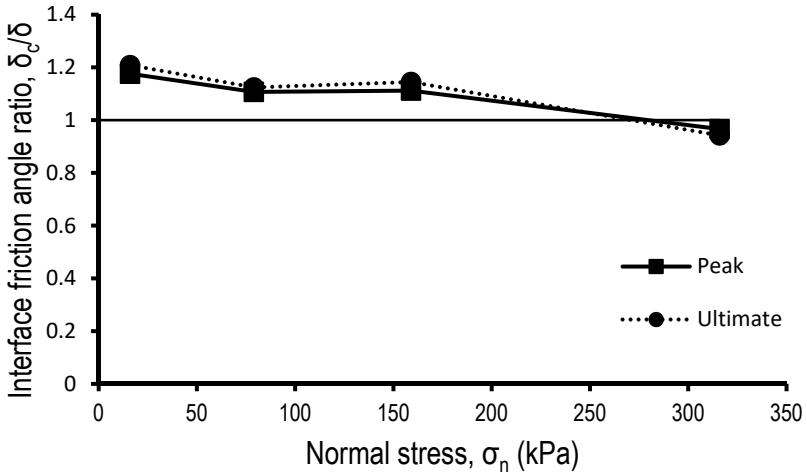

Figure 7-15. Normalised interface friction angles for Chalk - concrete interfaces over Chalk - steel (R_a = 34 μm) interfaces, considering dry samples

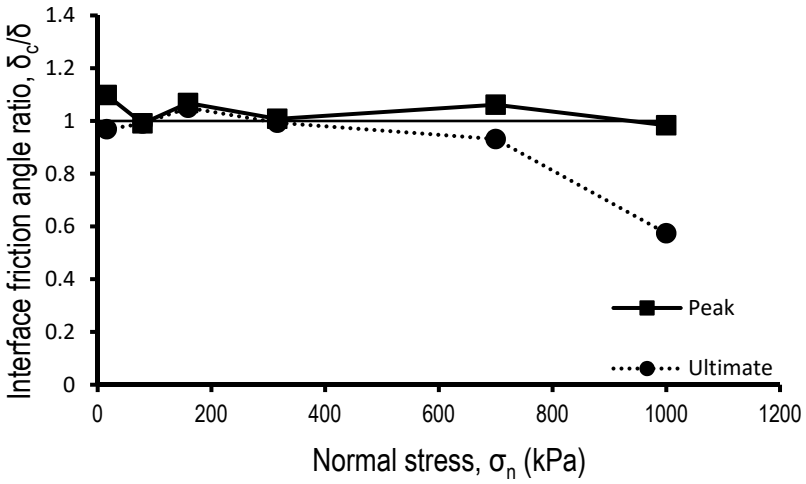

Figure 7-16. Normalised interface friction angles for Chalk - concrete interfaces over Chalk - steel (R_a = 34 μm) interfaces, considering dry samples

In Figure 7-15 it can be seen that dry Chalk – concrete interfaces exhibit higher (~15 – 20%) values of friction angle for normal stress up to 159 kPa, whereas at 316 kPa the friction angle is practically the same for Chalk – concrete and Chalk – steel interfaces. The relevant hardness ratio M, increases from 1.6 to 2 when steel (Mohs hardness of 4) is replaced by concrete (Mohs hardness of 5) and it is believed that this increases the ploughing during shear, thus increasing the shear strength. As mentioned earlier, the interface shear strength of both types of interfaces (i.e. rock and steel against Chalk) degrades for normal stress over 159 kPa, however it seems that the rate of degradation is higher for the Chalk – concrete interfaces (possibly due to higher M) and as a result the interface strength is very similar at normal stress of 316 kPa. Ploughing is believed to be beneficial for the shear strength of the interface, but for increasing normal stress, material chips were found on the Chalk samples indicating significant surface degradation and thus drop on the shear strength of the interface. The effect of degradation is more apparent when the ultimate values at normal stress of 700 and 1000 kPa are considered (Figure 7-16 for saturated samples).

7.5 Alpha factor design approach for Chalk interfaces

Alpha factor α design approach has already been introduced in the previous chapters and Figure 7-17 displays how the results from Chalk – steel interfaces compare with results of previous rock - steel interfaces.

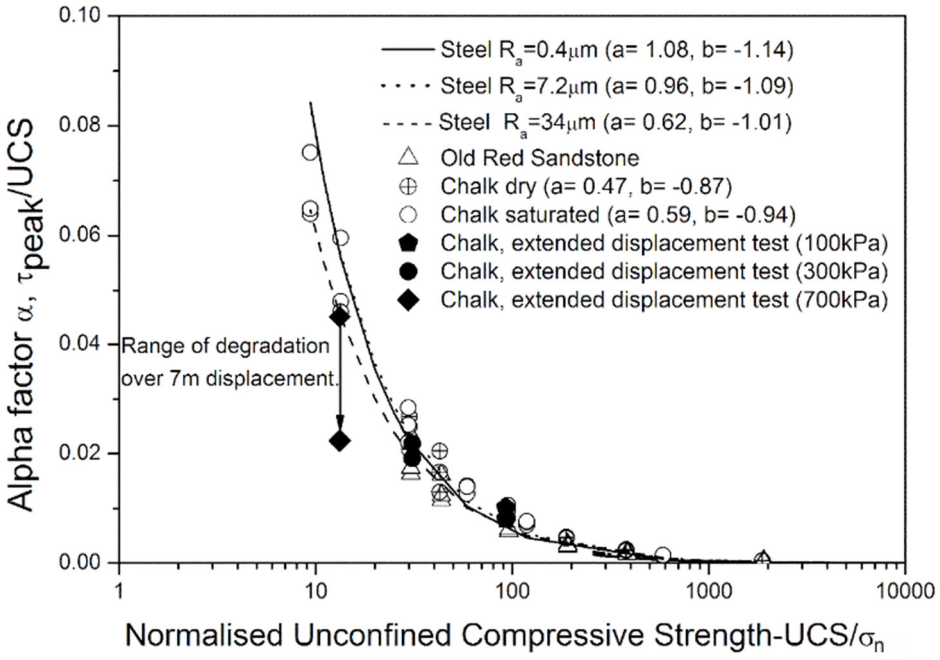

Figure 7-17. Alpha factors for Chalk-concrete compared with Chalk-steel and contours from data from rock –steel testing

The lines previously determined for various steel roughness levels (R_a from 0.4 to 34 μm and UCS from 31.5 to 192.7 MPa) have been extrapolated to cover the UCS/σ_n range of the Chalk – steel interface testing. Specific data points are also shown for the IST testing of Sandstone as way of comparison. It can be seen that the previously determined relationship for rocks of much higher UCS seems applicable for the much lower strength Chalk and offers an alternative approach to an interface friction angle based approach to design where low displacements occur (which could be attempted from the results in Table 7-1 or the lower bound basic friction angle). Additionally, the results are shown for the large displacement tests on Chalk (Figure 7-10) which suggests that the alpha factor approach should be used with caution for Chalk where large displacements may occur at an interface during installation or service. Similarly, prototype deployment of tidal stream generator, foundations are

likely to experience cyclic loading that has the potential to cause degradation at lower stress levels and lower displacements. The behaviour studied here and previously is only for monotonic loading and the behaviour when subject to cyclic loading would need to be studied before generic design guidance could be given in an offshore environment. The alpha factor ranges from 0.001 (σ_n= 16 kPa) to 0.07 (σ_n= 1000 kPa) for saturated Chalk samples. These values are relatively similar to the cohesion intercept/UCS ratio (ranges from 0.02 to 0.13) defined by Clayton and Saffari-Shooshtari (1990) from interface tests on bonded planar Chalk - concrete interfaces.

Figure 7-18 shows the alpha factors for Chalk – concrete interfaces and how they compare to Chalk –steel and other rock – concrete interfaces that have been presented earlier.

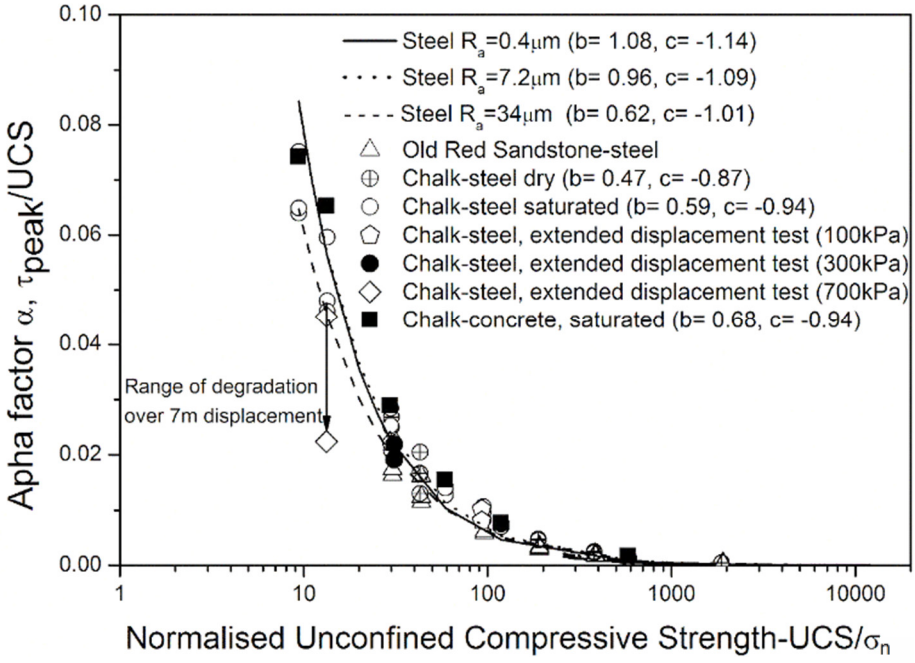

Figure 7-18. Alpha factors for Chalk-concrete compared with Chalk-steel and Sandstone-steel and contours from contours from data from rock –steel testing. (modified from Ziogos et al., 2017and Ziogos et al., 2018)

As per the Chalk – steel interfaces, it seems that the relationships previously derived for rocks of much higher UCS can be applied to the Chalk - concrete interfaces and offers an alternative approach to interface predictions where displacements are limited. As noted earlier though and shown previously in

Figure 7-17 caution needs to be exercised when larger displacement events occur especially where these are at normal stresses where degradation is likely to occur (degradation shown for 7 m events).

7.6 Summary

Results from interface testing of Chalk – steel and Chalk – concrete interfaces have been presented in this chapter and a summary of the findings is presented next.

1. Results revealed that saturated samples yield lower interface shear strength and it is believed that this is related to the decrease in tensile strength of Chalk.

2. For shear displacement up to 10 mm, interface strength of Chalk – steel interfaces tends to degrade when the applied normal stress exceeds 30 % of tensile strength of Chalk and tends towards the basic friction angle (i.e. Chalk – Chalk interface). When greater shear deformation is applied (up to 7 m in this study), the interface seems to degrade at lower normal stress and tends to values significantly lower than φ_b.

3. Shear strength of Chalk – steel interfaces increases with increasing steel roughness and this is in accordance with the behaviour of Flagstone – steel and Limestone – steel interfaces (i.e. rocks with lower Mohs hardness).

4. The shear strength of Chalk – steel interfaces and Chalk – concrete interfaces varies in a non – linear fashion with increasing normal stress, therefore a linear failure envelope is not suitable.

5. Chalk – concrete interfaces exhibit higher (~ 15 %) strength than the Chalk –steel interfaces for normal stress up to 159 kPa, possibly due to the higher relative hardness ratio M. Chalk – concrete interfaces seem to degrade more than the Chalk – steel ones during shear, resulting into

very low interface friction angle values, when the applied normal stress takes values greater than 316 kPa.

Chapter 8

8 Implications for industrial practice

This chapter presents the findings of the project that could be considered during the design process of GBS on rock for marine renewable applications.

Field trips at areas of interest (e.g. high energy potential) have been carried out at different stages of this project in order to collect samples for interface testing. Various methods have been used to characterise the test materials both in-situ or in the field and in the lab. Comparison of the results between the different test methods, revealed that under specific conditions, inexpensive test methods (e.g. tilt table test) can be utilised to determine design values for preliminary design. These findings are presented in more detail in this chapter.

8.1 Potential deployment issues

Observations of a wave cut platform at low tide of Old Red Sandstone 200 m north of John O' Groats (ND38299 73382) revealed a bedrock that could potentially complicate the deployment of generators in particular. The dip of the rock stratum (measured ~5^{o} in-situ) creates a saw - blade type structure with an elevated facade (0.60m high) in advance of a shielded zone (Figure 8-1). This geometry is repeated every 5.5 m approximately. No superficial sediment was noticed on the exposed rock but cobbles and boulders had collected in some shielded zones. A similar bedrock structure was found on the wave cut platform at Castletown beach (ND19305 68858) where the Caithness Flagstone group outcrops. The dip of the strata was slightly steeper (6-7^{o}) and the elevation of the facade was 0.40 m. The geometry was repeated every 3 m and 6 m alternately.

These outcrop structures suggest that the seabed might be undulating with steps, possibly filled with cobbles or boulders, making the positioning of the

support structures (and foundations) challenging and potentially restricting the size of the footings. Tidal generators should be as level as possible in order to be efficient, so seabed preparation techniques may be required (e.g. gravel beds and/or levelling foundation systems). Traditional methods (e.g. rock/gravel carpeting) can be considered but the cost increase and environmental impact would need to be considered. In both locations, no sediment was present on the exposed rock but cobble size rock units had collected in places on the John O'Groats beach. For this kind of seabed condition, a detailed seabed survey and bathymetry mapping would be required (e.g. utilising Side Scan and Multibeam Sonar plus visual/video inspection) to select the most appropriate location for deployment.

Figure 8-1. Old Red Sandstone wave cut platform at John O' Groats, UK. Zigzag line displays saw blade structure

8.2 Effect of weathering on UCS

The values of UCS for the various locations visited are summarised in Table 8-1 (more details about the process can be found in section 3.3.6).

Table 8-1. UCS values (determined in-situ) at various locations (modified Table 3-2)

Rock type	Location	UCS (MPa)*	Condition of rock	Strength classification+
Old Red Sandstone	John O' Groats Quarry (Disused)	82.2	Weathered	Strong
Old Red Sandstone	John O' Groats wave cut platform	86.3	Weathered	Strong
Catithness Flagstone	Achscrabster Quarry (Active)	157.2	Fresh	Very strong
Caithness Flagstone	Castletown wave cut platform	110.0	Weathered	Very strong
Middle Skateraw Limestone	Dunbar Quarry (Active)	115.8	Fresh	Very strong
Middle Skateraw Limestone	Barn Ness wave cut platform	45.0	Weathered	Medium strong

* after Kilic and Teymen (2008), + after BS5930:2015

Results indicate that the UCS of similar rock types may vary significantly depending on the location and the weathering conditions. The rock exposures at the quarries (Achscrabster and Dunbar) are significantly stronger compared to those of the wave cut platforms, Castletown (30% reduction) and Barn Ness (61% reduction). A possible explanation for this difference might be the effect of weathering. The wave cut platforms are exposed to repeated cycles of wetting and drying, while the quarry faces are renewed relatively frequently. No significant difference was noticed for Sandstone samples but this is reasonable, because the quarry appeared to have been disused for a long period of time.

Based on these findings it is proposed that where UCS is used as a design parameter allowance should be made for the differences between freshly

cored rock from ground investigation and exposed (and potentially weathered) rock on the seabed. A possible reduction factor might be considered for fresh cored samples in order to “capture” the weathering that a rock surface might have undergone.

8.3 Design Framework

The development of methodology to estimate the anticipated shear resistance of rock – steel interfaces has been presented in Chapter 5. It is noted that all the tests of this project were carried out on nominally flat surfaces with limited macro roughness (undulation), therefore the advice provided is limited to such surfaces. The advice provided is applicable to cases of monotonic loading and cases of cyclic loading would require further investigation.

Figure 8-2 presents a flowchart that describes the steps that can be followed in order to select the appropriate equations for the estimation of the shear strength of a given foundation – seabed combination. The steps are also outlined below:

Step 1: Identification of bathymetry and seabed topography in order to estimate the available area for the placement of the foundation.

Step 2: Identification of the rock type of the top layer of the seabed. This could ideally be done through seabed sampling or by referring to geological maps at the early stages of design (only if site specific access cannot be achieved and this could only then result in preliminary design with access and sampling required for Step 5).

Step 3 and 4: The configuration of the foundation (i.e. dimensions) and the applied load should be determined in order to calculate the average normal stress on the foundation seabed interface.

Step 5: Determination of the R_a (surface roughness of steel and rock), UCS (unconfined compressive strength of rock) and Mohs hardness of the seabed

and determination of the relative roughness R and relative hardness M ratios. This should be preferably done by lab testing or by adopting indicative values from the literature for preliminary design only (i.e. sampling and testing will be required at a later stage). If M ≤ 0.67 then Equation 5-2 and Equation 5-3 should be used for the calculation of the peak and ultimate values of b. The shear strength of the interface can then be calculated from Equation 5-6 and Equation 5-7. Otherwise, if 0.67 < M ≤ 1.33, Equation 5-4 and Equation 5-5 should be used for the calculation of the peak and ultimate values of b. The aforementioned equations shall not be used for M < 0.57 or M > 1.333 as these values would be outside of the range of M values used in this study.

For rock – concrete interfaces, the shear strength should be calculated from Equation 5-1 using the fitting constant values provided in Table 6-1 and Table 6-2 (one set of fitting curves were developed for rock – concrete interfaces due to the limited number of datapoints as discussed in Chapter 6). In general, rock – concrete interfaces seem to exhibit higher shear strength than the rock – steel interfaces, however only one type of concrete mix has been examined (due to time limitations), however, more types could be examined to allow optimisation.

The presence of granular material between the counterface materials (i.e. foundation and rock) has the potential to affect the shear strength as indicated in section 6.2. The shear strength of the interface could either increase or decrease (depending on the counterface materials, normal stress etc.); therefore, extra caution should be exercised when sediment is expected to be present.

For Chalk interfaces, the results presented in Table 7-1 and Table 7-2 along with the alpha type approach (section 7.5) could be used as a guidance of the anticipated shear strength depending on the interface (i.e. steel roughness, normal stress etc.).

Step 6: Comparison of the anticipated shear strength of the interface and the anticipated shear load. If the anticipated shear strength is not adequate to maintain stability, the properties of the foundation surface shall be modified and the steps 3 to 6 shall be repeated until the required shear strength is reached. If modifying the foundation cannot lead to the required capacity, then the dimensions of the foundation shall be changed.

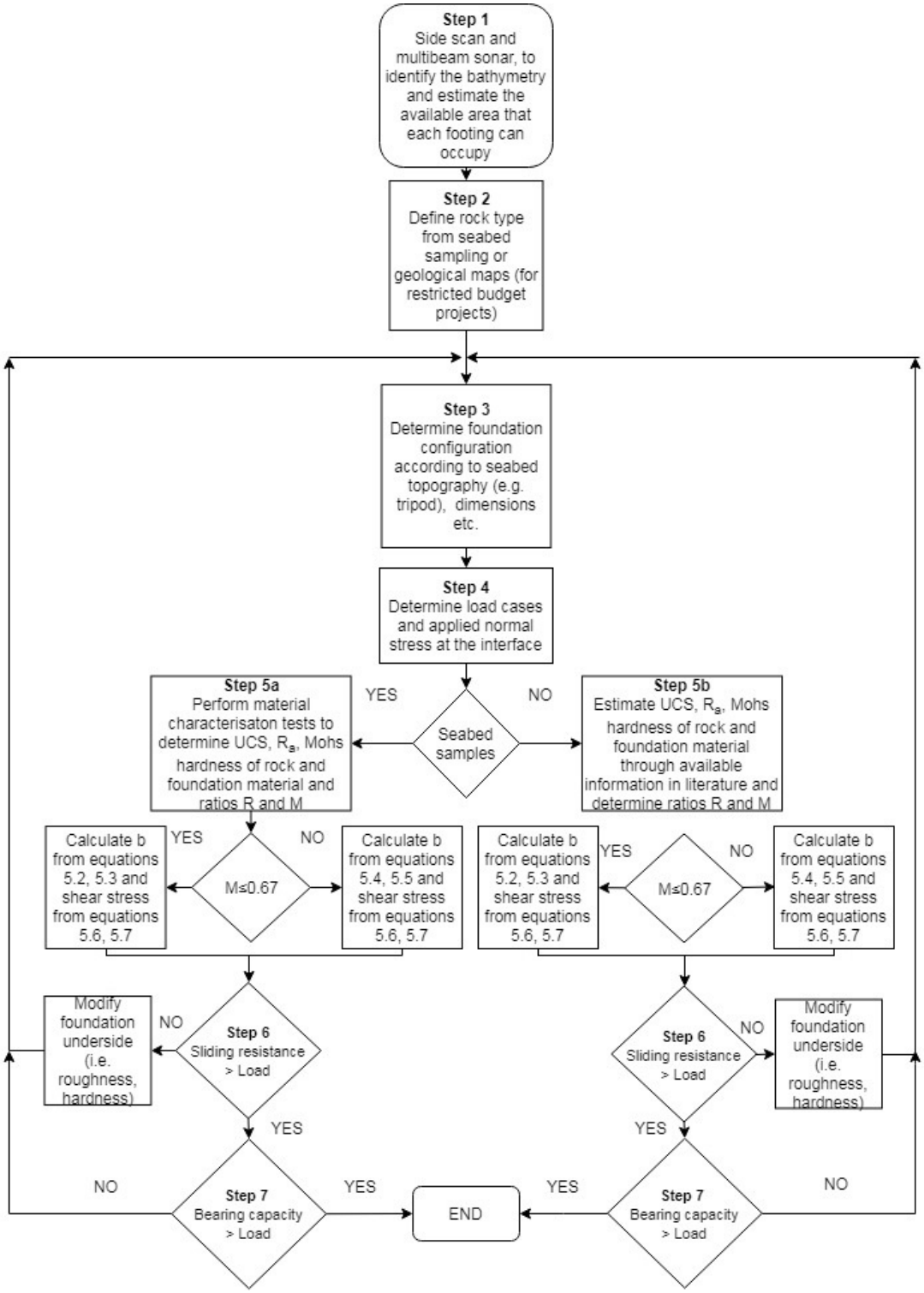

Figure 8-2. Flowchart for the estimation of the shear resistance of steel foundation – seabed interface. The flowchart shall not be used for values of M < 0.57 or M > 1.33

8.4 Utilisation of tilt table for simple interface characterisation

Table 8-2 - Table 8-6 present the results of interface testing using the tilt table along with those obtained from IST testing for the different rock types. The applied normal stress for a tilt table test is ~ 0.6 kPa (i.e. mass of sample over the area) and the tables display the peak friction angles (obtained from IST) for individual normal stress levels (16 - 316 kPa) along with the average peak and ultimate friction angles across this range, to allow comparison. It should be noted that the average values were calculated considering the coefficient of friction and not directly the friction angles, since tangent function is nonlinear.

Table 8-2. Comparison of results of Sandstone - steel interface testing utilising the tilt table and the IST device

		Interface		
		Sandstone-steel R_a=0.4μm	Sandstone-steel R_a=7.2μm	Sandstone-steel R_a=34μm
	σ_n (kPa)	Measured peak interface friction angle, δ_{peak} (°)		
Tilt table	~0.6	24.0	26.0	37.5
IST	16	37.5	40.5	41.0
IST	79	32.0	36.0	35.0
IST	159	29.5	34.0	31.5
IST	316	29.0	31.0	31.0
	Average peak interface friction angle for normal stress of 16 – 316 kPa			
IST	-	32.5	35.5	35.0
	Average ultimate interface friction angle for normal stress of 16 – 316 kPa			
IST		28.0	28.5	27.0

Table 8-3. Comparison of results of Flagstone - steel interface testing utilising the tilt table and the IST device

		Interface		
		Flagstone-steel R_a=0.4μm	Flagstone-steel R_a=7.2μm	Flagstone-steel R_a=34μm
	σ_n (kPa)	Measured peak interface friction angle, δ_{peak} (°)		
Tilt table	~0.6	18.0	27.5	30.0
IST	16	33.5	28.5	37.5
IST	79	23.5	21.5	36.5
IST	159	20.0	21.0	33.0
IST	316	18.0	17.5	32.5
	Average peak interface friction angle for normal stress of 16 – 316 kPa			
IST	-	24.0	22.5	35.0
	Average ultimate interface friction angle for normal stress of 16 – 316 kPa			
IST		16.0	15.0	23.5

Table 8-4. Comparison of results of Andesite - steel interface testing utilising the tilt table and the IST device

		Interface		
		Andesite-steel R_a=0.4μm	Andesite-steel R_a=7.2μm	Andesite-steel R_a=34μm
	σ_n (kPa)	Measured peak interface friction angle, δ_{peak} (°)		
Tilt table	~0.6	17.5	25.0	31.5
IST	16	27.5	35.5	38.5
IST	79	29.5	29.5	33.5
IST	159	26.5	26.5	29.5
IST	316	25.5	26.5	25.0
	Average peak interface friction angle for normal stress of 16 – 316 kPa			
IST	-	27.5	30.0	32.0
	Average ultimate interface friction angle for normal stress of 16 – 316 kPa			
IST		21.0	21.0	22.5

For Sandstone, Flagstone and Andesite interfaces, the results from both methods (tilt table test and IST) seem to have relative good agreement in most of the cases. As described before, the interface behaviour is affected significantly by the applied normal stress, which is something that unavoidably cannot be captured by the tilt table test. However, tilt table tests for rock against relatively smooth steel could provide a lower bound value for design as they are close to the minimum values obtained from IST tests.

Table 8-5. Comparison of results of Limestone - steel interface testing utilising the tilt table and the IST device

		Interface		
		Limestone-steel R_a=0.4μm	Limestone-steel R_a=7.2μm	Limestone-steel R_a=34μm
	σ_n (kPa)	Measured peak interface friction angle, δ_{peak} (°)		
Tilt table	~0.6	18.0	25.0	30.0
IST	16	17.0	33.0	30.0
IST	79	13.5	29.0	25.0
IST	159	13.0	17.5	26.5
IST	316	10.0	14.5	23.0
	Average peak interface friction angle for normal stress of 16 – 316 kPa			
IST	-	13.5	24.0	26.0
	Average ultimate interface friction angle for normal stress of 16 – 316 kPa			
IST		9.5	17.0	20.5

For Limestone – steel interfaces, the tilt table seems to “overestimate” the friction angle when compared to the average values obtained from IST testing. However, the values seem to have quite good agreement when the peak values for normal stress of 16 kPa are considered. Thus, the tilt table could potentially be used to characterise Limestone – steel interfaces when normal stress up to 16 kPa is anticipated.

Table 8-6. Comparison of results of Chalk - steel interface testing utilising the tilt table and the IST device

		Interface		
		Chalk-steel R_a=0.4μm	Chalk-steel R_a=7.2μm	Chalk-steel R_a=34μm
	σ_n (kPa)	Measured peak interface friction angle, δ_{peak} (°)		
Tilt table	~0.6	30.0	36.5	37.5
IST	16	36.0	39.5	40.5
IST	79	39.5	41.5	42.5
IST	159	37.0	40.0	39.5
IST	316	33.5	37.0	40.0
IST	700	32.5	31.5	38.5
IST	1000	31.0	31.5	35.0
	Average peak interface friction angle for normal stress of 16 – 316 kPa			
IST		36.5	39.5	40.5
	Average ultimate interface friction angle for normal stress of 16 – 316 kPa			
IST		34.0	35.5	39.0

It can be seen that there is good agreement between the peak interface friction angle measured in both types of test, especially for the rougher steel plates (R_a= 7.2 and 34 μm) and for σ_n up to 700 kPa. Therefore, it is felt that the tilt table can be used at the early stage of design in order to make an estimation of the anticipated peak friction angle depending on the rock type and the texture of the footing. It is obvious that for a more detailed design, friction parameters obtained through more sophisticated interface testing (e.g. direct shearbox or IST) may be required. Based upon the IST tests here for Chalk (Figure 7-5 - Figure 7-7), and the apparent tendency to degrade to low friction angles with increasing normal stress levels and interface degradation, tilt tables tests for Chalk against a relatively smooth interface may give a useful lower bound for design. For both the low and high displacements it would seem that the normal lower bound interface friction angle should be taken as the basic Chalk-Chalk friction angle from tilt table testing (φ_b) irrespective of the foundation material or roughness. For higher displacement tests though some caution has to be exercised when normal stress levels exceed 31% of tensile strength T_0.

8.5 Summary

1. Seabed surface could potentially be undulating (displaying a saw blade – like structure), making the deployment and positioning of the tidal stream generators challenging (Ziogos et al., 2015a). Detailed seabed survey is needed to identify the most appropriate positions for deployment and reveal possible topographical restraints. Employment of seabed preparation techniques might also be required, leading to cost increase.

2. UCS results obtained from rock samples of the same type can vary significantly depending on the degree of weathering. UCS has already been identified as a significant parameter affecting the shear behaviour of rock interfaces (Chapter 5) and is one of the independent variables in Equation 5-1 that estimates the shear strength of an interface. For this reasons it is very important for UCS values to be representative of the foundation (i.e. seabed) surface, meaning that a reduction factor might need to be applied on values obtained from fresh samples acquired beneath the seabed.

3. Tilt table test is an inexpensive method to characterise interfaces. Results appear to have a satisfactory agreement with IST testing for most of the rock types (apart from the case of Limestone where the tilt table values are higher) studied. If significant surface degradation is not expected, the values from tilt table test for smooth steel – rock interfaces can be used to determine a lower bound value for preliminary design purposes. In the case of Chalk, high surface degradation is expected for normal stress > 0.31 T_0 and in this case φ_b should be considered as lower bound. It should be noted that tilt table test is only appropriate for preliminary design and more complex interface testing (e.g. IST) should be utilised to determine parameters for detailed design.

Chapter 9

9 Conclusions and recommendations for further work

9.1 Introduction

Tidal stream generators are deployed in the offshore environment to harness the kinetic energy of the water masses that are set in motion during the tidal cycles. GBS seem like a promising foundation solution with distinct advantages. These devices are subjected to significant lateral forces making the sliding resistance of the foundation, critical. GBS maintain stability exclusively due to their own mass (i.e. no fixed connections), therefore, the friction characteristics of the foundation – seabed interface are crucial for the sliding resistance of the foundation. Laboratory element testing of various foundation – seabed anlogue interfaces has been carried out to obtain friction properties and obtain a better understanding of the shear behaviour of foundation – seabed interfaces. Test data was analysed and the conclusions are presented in this chapter along with recommendations for future research on the shear behaviour of offshore GBS upon rock.

9.2 Rock – steel and rock – concrete interfaces

The conclusions drawn from testing of rock – steel and rock concrete interfaces are presented here.

1. Normal stress affects the behaviour of rock – steel interfaces in a non linear manner and a linear failure envelope should not be used to describe this behaviour. For normal stress of 16 – 79 kPa dilation occurs leading to higher peak shear stresses. Dilation is suppressed (thus lower peak values are observed) and the behaviour is more linear for normal stress of 159 – 316 kPa.

2. Normal stress level of at least 159 kPa seems to be more desirable for design as the behaviour is more predictable in contrast to the “erratic” behaviour observed between 16 and 79 kPa.

3. Peak interface friction angle values drop to ultimate values within small shear displacement (8 - 10 mm). Therefore, it is felt that ultimate values should be preferably used for design.

4. The behaviour of two shearing surfaces could potentially be correlated with the relative scratch hardness of the counterface materials (Engelder and Scholz 1976, Abuel-Naga 2018). It appears to be that when the hardness of the two counterfaces (rock and steel) differs more than 50%, (i.e. the resulting relative hardness ratio M is significantly different to 1, e.g. 0.57 and 0.67 for Sandstone and Andesite interfaces respectively); the shearing consists of sliding and ploughing (irrespective of steel R_a) and the interfaces exhibit similar behaviour, albeit Andesite exhibits lower interface friction angles. On the contrary, when the Mohs hardness of the two counterface materials (rock and steel) differs less than 50% (i.e. the rock is of similar or lower hardness than the steel, e.g. 1.33 for Flagstone and 0.89 for Limestone interfaces); it is felt that higher localised stress is required for ploughing to occur, hence the interfaces seem to be affected by the roughness of the steel (higher R_a leads to higher localised stress due to fewer points of contact).

5. Increasing steel roughness seems to increase the interface shear strength, however this seems to be more apparent for the cases where M is closer to 1 (i.e. Flagstone and Limestone). When M is significantly different to 1 (i.e. Sandstone and Andesite), the effect of steel roughness is minimised as the normal stress level increases.

6. An alpha factor approach which is similar to the adhesion factor approach used for the calculation of the shaft friction of grouted pies has been developed for the calculation of the shear strength of the

interface. This approach is based on the UCS of the rock, the applied normal stress on the interface and the relative roughness and hardness of the counterface materials. The alpha factor approach seems to capture the behaviour of rock – steel interfaces and a power law function can be used to estimate the shear strength of interfaces within the UCS and normal stress range used in this study. Relative hardness ratio M appears to significantly affect the shear behaviour, thus two different sets of equations have been proposed depending on the value of M (Equation 5-2 - Equation 5-3 and Equation 5-4 - Equation 5-5).

7. Rock – concrete interfaces seem to yield higher shear resistance than rock - steel interfaces (with the exception of interfaces with Sandstone at normal stress of 16 – 79 kPa). This becomes more apparent for normal stress of 159 – 316 kPa.

8. The presence of a sand layer (simulating seabed sediment) on the interface changes the mode of shearing of the interface. For normal stress up to 79 kPa, the sand grains appear to roll on the interface thus reducing the shear strength (compared to the free of sediment interface). For higher normal stress over 79 kPa up to 316 kPa, rolling is suppressed and the relevant scratch hardness of the interface materials appears to influence the shear behaviour.

9. When the hardness (M) of the sand grains is higher than the steel and similar to the rock, then the interface friction angle is not affected by the steel - sand relative roughness ratio R_s ($R_s = R_{a,steel}/D_{50}$). In contrast when the sand grains are harder than the steel and the rock of the interface, the friction angle increases with increasing R_s.

9.3 Chalk - steel and Chalk – concrete interfaces

Chalk – steel and Chalk – concrete interfaces have been investigated separately to the rest of the rock types (due to the extraordinary behaviour of the Chalk) and the following conclusions were reached.

1. Saturated samples tend to yield lower interface shear strength and it is believed that this is related to the decrease in tensile strength of Chalk that occurs on saturation.

2. For shear displacement up to 10 mm, interface strength of Chalk – steel interfaces tends to degrade when the applied normal stress exceeds 30 % of tensile strength of Chalk and tends towards the basic friction angle (i.e. Chalk – Chalk interface). When longer shear deformation is applied (up to 7 m in this study), the interface seems to degrade at lower normal stress and tends to values significantly lower than φ_b.

3. Increasing steel roughness appears to increase the shear strength of Chalk – steel interfaces. This is in accordance with the behaviour of Flagstone – steel and Limestone – steel interfaces, which are interfaces where the rock is of similar or lower hardness than the steel, (M = 1.33 for Flagstone and 0.89 for Limestone interfaces) .

4. The shear strength of Chalk – steel interfaces and Chalk – concrete interfaces varies in a non – linear fashion with increasing normal stress, therefore a linear failure envelope is not considered appropriate.

5. Chalk – concrete interfaces exhibit higher (~ 15 %) strength than the Chalk –steel interfaces for normal stress up to 159 kPa, possibly due to the higher relative roughness ratio M. Chalk – concrete interfaces seem to degrade more than the Chalk – steel ones during shear, resulting into very low interface friction angle values, when the applied normal stress takes values greater than 316 kPa.

9.4 Considerations for design

1. The deployment and positioning of the tidal stream generators might be challenging if the seabed surface is undulating (displaying a saw blade – like structure), (Ziogos et al., 2015a). Detailed seabed survey is required to identify the most appropriate positions for deployment and reveal possible topographical restraints. Employment of seabed preparation techniques might also be required, leading to cost increase.

2. Weathering can affect the rock strength (UCS) results obtained from rock samples of the same type can vary significantly. UCS has already been identified as a parameter affecting the shear behaviour of rock interfaces (Chapter 5) and is one of the independent variables in Equation 5-1 that estimates the shear strength of an interface. Thus, it is important for UCS values to be representative of the foundation (i.e. seabed) surface. Therefore, a reduction factor might need to be applied to values obtained from fresh samples acquired beneath the seabed.

3. Tilt table results appear to have a satisfactory agreement with IST testing for most of the rock types (apart from the case of Limestone where the tilt table values are higher), thus tilt table test seems to be an inexpensive method to characterise interfaces. The values from tilt table test for smooth steel – rock interfaces can be used as a lower bound value for preliminary design purposes when significant surface degradation is not expected. In the case of Chalk, high surface degradation is expected for normal stress > 0.31 T_0 and in this case φ_b should be considered as lower bound. It should be noted that tilt table test is only appropriate for preliminary design and more complex interface testing (e.g. IST) should be utilised to determine parameters for detailed design.

9.5 Recommendations for further work

Recommendations for further work that have risen through the course of this research project are presented in this section.

1. The direction of the water currents is likely to vary throughout the day, therefore cycling loading might be induced at the foundation – seabed interface. Extended deformation (7 m) tests on Chalk – steel interfaces indicated that the shear strength might degrade with increasing shear deformation. Therefore, the effect of cyclic loading on the shear behaviour of rock – steel and rock – concrete interfaces requires further investigation.

2. 54 mm diameter disc shaped, saw cut rock samples with nominally flat surface have been used in this study. This allowed the investigation of the effect of micro roughness on the shear behaviour of the interface. Use of larger non - flat rock samples could be used to allow the effect of waviness (macro scale roughness) on the shear behaviour. The current setup of the IST can only accommodate nominally flat (saw cut) samples, therefore, modifications to the current setup or utilization of another apparatus (such as the 300 x 300 mm direct shear box, GDSLADS) will be required.

3. The surface degradation of the counterface materials (e.g. steel, rock) was visually examined post testing, however no measurable change on the surface roughness was captured by the contact stylus profilimeter used for the surface roughness characterisation. A non contact profilometer (e.g. 3D surface scanner) would possibly allow a more detailed evaluation of the surface roughness profile pre and post testing.

4. Five rock types (Sandstone, Flagstone, Andesite, Limestone and Chalk) have been tested in the current study as they can be found at

sites with tidal energy potential around the U.K.. A wider range of rock types would allow the research outcome to be applicable to other areas of offshore geotechnical engineering.

5. A thin (single grain) layer of HST 95 (silica) sand has been used to investigate the effect of seabed sediment on the foundation seabed interface. Silt and clay layers could be used to evaluate the influence of the soil type on the rock – sediment – steel interface. In reality, the foundation might embed into the sediment layer and passive forces might evolve during shearing. This behaviour could be investigated if a thicker soil layer was used. The IST should be modified in order to accommodate thicker sand layers, as with the current setup soil extrusion might occur during shear.

6. The Chalk samples have been tested both dry and saturated. It was assumed that the shearing rate was slow enough to prevent excess pore water pressure generation in the saturated samples, although pore pressure measurement was not available in order to confirm that. A pore pressure transducer could be mounted at the bottom of the Chalk sample to log the pore pressure during the tests. This would allow investigation of drainage rates during shearing, confirm drained testing and the study of rate effects.

7. In this study, one type of concrete mix was used to prepare saw cut concrete samples with R_a = 6.8 μm. Different types of concrete mix could be used to prepare samples to different levels of surface roughness (e.g. smoother and rougher) to allow further investigation of the effect of concrete composition and relative roughness ratio on the shear strength of rock – concrete interfaces. This would allow the development of an alpha type design framework similar to that of the rock - steel interfaces.

8. Sandstone, Flagstone, Andesite and Limestone sample samples were tested against steel and concrete foundation analogues at a normal

stress range of 16 – 316 kPa, as this is a range that covers (according to the literature review) the anticipated normal stress level for tidal stream GBS applications. The results revealed that the behaviour is different under lower (16 and 79 kPa) and higher (159 and 316 kPa) normal stress level, therefore tests at higher normal stress (e.g. 1000 kPa or more) would reveal any potential effect of normal stress above 316 kPa. The onset of surface damage could also investigated for the various interface combinations.

9. The interface tests performed in this study have been carried out under constant normal load (CNL) conditions as this case is applicable to the gravity based foundations. However, constant normal stiffness (CNS) testing could be performed to investigate the performance of other types of foundation (e.g. grouted piles in rock) that could be considered for marine energy applications.

References

Acar, Y.B., Durgunoglu, H.T. & Tumay M.T. (1982). Interface Properties of Sand. *Journal of Geotechnical and Geoenvironmental Engineering*, Vol. 108, Issue 4, pp. 648-654.

Abuel-Naga, H. M., Shaia, H. A. & Bouazza, A. (2018). Effect of Surface Roughness and Hardness of Continuum Materials on Interface Shear Strength of Granular Materials. *Journal of Testing and Evaluation*, Vol. 46, No. 2, 2018, pp. 826–831, https://doi.org/10.1520/JTE20160375. ISSN 0090-3973.

Alejano, L.R., Gonzalez, J. & Muralha, J. (2012). Comparison of Different Techniques of Tilt Testing and Basic Friction Angle Variability Assessment, *Rock Mech Rock Eng* (2012) 45:1023–1035.

Altindag, R. & Guney, A. (2010). Predicting the Relationships between Brittleness and Mechanical Properties (UCS, TS and SH) of Rocks. *In: Scientific Research and Essays* Vol. 5(16), pp. 2107 – 2118.

Aydin, A. (2009). ISRM Suggested method for determination of the Schmidt hammer rebound hardness: Revised version, *International Journal of Rock Mechanics & Mining Sciences*, Vol 46, pp 627-634

Barmpopoulos I.H., Ho T.Y.K., Jardine R.J. & Anh-Minh N. (2010). The large displacement shear characteristics of granular media against concrete and steel interfaces. *Research Symposium on the Characterization and Behavior of Interfaces (CBI)*, IOS Press, Amsterdam, Pages:17-24.

Barton, N.R. (1973). Review of a new shear-strength criterion for rock fractures. *Engineering geology*, Vol. 7, Nr. 4, pp. 287-332.

Barton, N.R. & Choubey, V. (1977). The shear strength of rock fractures in theory and practice. *Rock Mechanics*, Vol. 10, pp. 1-54.

Basu A. & Aydin A. (2004). A method for normalization of Schmidt hammer rebound values. *Int J Rock Mech Min Sci*;41:1211–4.

BMT Cordah (2009). Foundations and Moorings for Tidal Stream Sites available at:http://www.carbontrust.com/media/170419/foundations-and-moorings-tidal-systems.pdf .

Bolton, M.D. (1979). A guide to soil mechanics. *Macmillan, London*.

British Geological Survey (1989). British Regional Geology. The Northern Highlands. *Keyworth*, Nottingham.

British Regional Geology (1971). The South of Scotland. Her Majesty's Stationery Office, Edinburgh

British Standards Institution (1990). Methods of test for soils for civil engineering purposes. Classification tests. BS 1377-2:1990. London BSI

British Standards Institution. (2011). Composition, specifications and conformity criteria for common cements. BS EN 197-1:2011. London BSI

British Standards Institution (2015). Code of practice for ground investigations. BS 5930:2015. London BSI.

Brown, E.T. (1981). ISRM suggested methods – rock characterization, testing and monitoring. *Pergamon Press*, Oxford.

Bowden, F.P. & Tabor, D. (1964). The Friction and Lubrication of Solids. Vol. 2, p 544, *Clarendon Press*, Oxford.

Bryden, I.G. & Couch, S.J. (2006). ME1—marine energy extraction: tidal resource analysis. Renewable Energy, Elsevier, vol. 31(2), pp. 133-139.

Buckley, R.M., Jardine, R. J., Kontoe, S., Parker, D. & Schroeder, F.C. (2018). Ageing and cyclic behaviour of axially loaded piles driven in Chalk. *Géotechnique* 68:2, 146-161.

Carbon Trust (2005). Variability of UK marine resources. Environmental Change Institute. Available at: https://www.carbontrust.com/media/174017/eci-variability-uk-marine-energy-resources.pdf (accessed 05/06/2016).

Chan, D.L.H., Buckley, R.M., Liu, T. & Jardine, R.J., (2019), Laboratory investigation of interface shearing in Chalk, *E3S Web Conf*. 92 2019 13009.

Clayton, CRI and Saffari-Shooshtari N (1990) Constant normal stiffness direct shear testing of Chalk/concrete interfaces. *In Proceedings of the International Chalk Symposium*. Thomas Telford London, pp 233-238

Danyildiz, E. & Baykal, G., (2010), Use of manufactured pellet aggregates to study the effect of the aggregate crushing on strength and deformation behavior at the concrete-soil interface. *In: Chacterization and Behavior of Interfaces: Proceedings of Research Symposium on Characterization and Behavior of Interfaces*, 21 September 2008, Atlanta, Georgia, USA.

De Toledo, P.E.C. & De Freitas, M.H. (1993): Laboratory testing and parameters controlling the shear strength of filled rock joints. *Geotechnique* 42(1): 1-19.

Deere, D.U., Hendron, A.J., Patton, F.D. & Cording, E.J., (1967). Design of Surface and Near-Surface Construction in Rock:, Failure and Breakage of Rock, Proceedings of 8th U.S. Symposium of Rock Mechanics., ed. C., Fairhurst, N.Y., pp. 237-302.

Defence Nuclear Agency (1976). Measurements of dynamic friction between rock and steel.

Dietrich, J. & Kilgore, B., (1994). Direct Observation of Frictional Contacts: New Insights for State-dependent Properties, *Pageoph*, Vol. 143, pp 283-302.

Deitz, M. & Lings, J.D., (2010). Changes in surface roughness in multi-reverse sand-steel interface tests. In *Characterization and Behavior of Interfaces. Proceedings of the Research Symposium on Characterization and Behavior of Interfaces*. September 2008, Atlanta, Georgia, USA, IOS Press, 2010, Netherlands, pp 7-15.

Dove, J.E. & Frost, J.D., (1999). Peak friction behavior of smooth geomembrane–particle interfaces. *ASCE J Geotech Geoenviron Eng*;125(7):544–55.

EN 1992-1-1:2004 *Eurocode 2: Design of concrete structures*

Engelder, J.T. (1976). Effect of scratch hardness on frictional wear and stick-slip of Westerly granite and Cheshire Quartzite. *In: The Physics and Chemistry of Minerals and Rocks*. Strens, R.G.J. (ed.), Wiley 1976, pp. 139-150

Engelder, J.T. & Scholz, C.H. (1976). The role of asperity indentation and ploughing in rock friction,2: Influence of relative hardness and normal load, Int. jour. *Rock Mech. Min. Sci*. 13, 155-163.

Engelder, T. (1978). Aspects of Asperity-Surface Interaction and Surface Damage of Rocks during Experimental Frictional Sliding. *Pageoph* ,16: 705, , Birkhauser Verlag, Basel

Engineering and Design, (1994) Rock Foundations Department of the army. *U.S. Army Corps of Engineers.*

European Marine Energy Centre (EMEC). (2009). Guidelines for Design Basis of Marine Energy Conversion Systems: Marine Renewable Energy Guides.

European Marine Energy Centre (EMEC) (2012). Decommissioning Programme.

Fairley, I., Neill, S., Wrobelowski, T., Willis, M.R. & Masters, I. (2011). Potential Array Sites for Tidal Stream Electricity Generation off the Pembrokeshire Coast, *In*: *Proceedings of 9th European Wave and Tidal Energy Conference (EWTEC)*, Southampton, 2011.

Fioravante, V., Ghionna, V.N., Pedroni, S. & Porcino D. (1999). A constant normal stiffness direct shear box for soil – solid interface tests. *Rivisita Italiana di Geotecnica* Vol. 33, No. 3, pp. 7-22.

Fraenkel, P. (2002). Power From Marine Currents. Proceedings of the Institution of Mechanical Engineers, Part A: *Journal of Power and Energy*, 216(1), pp. 1–14.

Fraenkel, P. (2010). Practical Tidal Turbine Design Considerations: A Review of Technical Alternatives and Key Design Decisions Leading to the Development of the SeaGen 1.2MW Tidal Turbine *Proceedings – Fluid Machinery Group - Ocean Power Fluid Machinery Seminar*, London.

Fuggle, A.R. & Frost, J.D. (2010). Particle size effects on interface shear behavior and geomembrane wear. In *Characterization and Behavior of Interfaces. Proceedings of the Research Symposium on Characterization and Behavior of Interfaces*. September 2008, Atlanta, Georgia, USA, IOS Press, 2010, Netherlands, pp. 51-57.

Geological Survey of Scotland. (1914). The geology of Caithness, printed under the authority of *His Majesty's Stationery Office*, 1914.

Ghosh, A.K., (2010), Shear Strength of Dam-Foundations Rock Interface - A Case Study. *In: Proceedings of Indian Geotechnical Conference*, Bombay.

Goodman, R. E., (1980). Methods of Geological Engineering in Discontinuous Rock. *Wiley and Sons,* NY.

Goodman, R.E., Talyor R.L. & Brekke T.L., (1968). A model for the mechanics of fractureed rock. *Journal of the Soil Mechanics and Foundations Division*, Vol. 94, pp. 637-660.

Henderson, A.R. & Zaaijer, M.B., (2002). Hydrodynamic Loading of Compact Structures and the Effect on Foundation Design. *Marine Renewable Energy Conference (MAREC)*, Newcastle, U.K.

Ho, T.Y.K., Jardine, R.J. & Anh-Minh, N. (2011). Large-displacement interface shear between steel and granular media. *Geotechnique.* Vol 61, Issue 3, pp. 221-234.

Hoek, E. & Bray, J. W. (1981). Rock Slope Engineering. *The Institution of Mining and Metallurgy*. London, England.

Homand-Etienne F., Lefevre F., Belem, T. & Souley M. (1999). Rock joints behavior under cyclic direct shear tests*. In: Proceedings of 37th U.S. Rock Mechanics Symp., June 6-9, 1999*, Vail, Colorado, Balkema : Rotterdam, pp. 399-406.

Horvath, R.G. (1978). Field Load Test Data on Concrete to Rock Bond Strength. *University of Toronto*, Publication No. 78-07.

Horvath, R. G., Kenney, T. C., & Kozicki, P. (1983). Methods of Improving the Performance of Drilled Piers in Weak Rock. *Canadian Geotechnical Journal*, Vol. 20, No. 4, pp. 758-772.

Iscimen, M., Frost, J.D. (2010). Shearing behaviour of curved interfaces. In *Characterization and Behavior of Interfaces. Proceedings of the Research Symposium on Characterization and Behavior of Interfaces*. September 2008, Atlanta, Georgia, USA, IOS Press, 2010, Netherlands, pp. 35-43.

IS 7746:1991 –*Indian Standard Code on In Situ Shear Test on Rock (First revision), pp. 5-7.*

ISRM (2007). The Blue Book: The Complete ISRM Suggested Methods for Rock Characterization, Testing and Monitoring: 1974-2006. Edited by R. Ulusay and J.A. Hudson.

Jardine, R.J., Lehane, B.M. & Everton, S.J. (1993). Friction Coefficients for Piles in Sands and Silts. *In: Proceedings of Conference on Offshore Site Investigation and Foundation Behaviour*, Kluwer Academic Publ, pp. 661-677.

Johnstone, G.S. & Mykura, W. (1989). British Regional Geology, The Northern Highlands of Scotland. British Geological Survey, *Keyworth*, Nottingham, UK.

Johnstone, C.M., Nielsen, K., Lewis, T., Sarmento, A. & Lemonis, G. (2006). EC FPVI Coordinated Action on Ocean Energy: A European platform for sharing technical information and research outcomes in wave and tidal energy systems, *Renewable Energy International Journal, Elservier*, UK, , ISSN: 0960-1481.

Kılıc, A. & Teymen, A. (2008). Determination of mechanical properties of rocks using simple methods. *Bull Eng. Geol. Environ*., 67: 237–244.

Kishida, H. & Uesugi, M., (1987). Tests of the interface between sand and steel in the simple shear apparatus. *Geotechnique* 37(1), 45-52.

Li, C. & Hakansson, U. (1999). Performance of the Swellex bolt in hard and soft rocks. *Rock Support and Reinforcement Practice in Mining* (eds: E Villaescusa, C.R. Windsor & A.G. Thompson), pp. 103-108.

Lo, K.Y. & Grass, J.D (1994). Recent Experience with Safety Assessment of Concrete Dams on Rock Foundations. *In: Proceedings of Canadian Dam Safety Conference*, Winnipeg, Manitoba, October 1994, pp.231-250.

Lo, KY., Lukajic, B., Wang, S., Ogawa, T. & Tsui, K.K. (1990). Evaluation of Strength Parameters of Concrete-Rock Interface for Dam Safety Assessment. *In: Proceedings of Canadian Dam Safety Conference, Toronto, Ontario, September 1990*, W. 71-94.

Lo, K.Y., Ogawa, T., Lukajic, B., Smith, GF. & Tanh, J.H.K. (1991). The evaluation of stability of existing concrete dams on rock foundations and remedial measures. In: Proceedings of 17th International Congress on Large Dams.

Lord, J.A., Clayton, C.R. & Mortimore, R.N. (2002) Engineering in Chalk, *CIRIA Publication C574*, London, UK.

Matthews, M.C. & Clayton, C.R.I. (1993). Influence of intact porosity on the engineering properties of a weak rock. Geotechnical Engineering of hard soils – soft rocks (Anagnostopoulos A, Schlosser F, Kalteziotis N and Frank R (eds)). *AA Balkema*, Rotterdam, Netherlands vol. 1, pp. 693–702.

Menezes, P.L., Kishore, Kailas S. V. (2006). Effect of roughness parameter and grinding angle on coefficient of friction when sliding of Al-Mg alloy over EN8 steel. *Trans. Of the ASME: J. Tribol.* 128(4): 697-704

Najjar, S. S., Leidke, E. A., Gilbert, R. B. & McCarron, B. (2003). Tilt table tests for interface shear resistance between flowlines and soils. *American Society of Mechanical Engineers*, Volume 3, pp. 859-866.

Newson, T., Larkin, P. & Maynard, R. (2011). A review of founda-tion concepts for in-stream tidal turbine systems. *Proceedings :ASME 2011 30th International Conference on Ocean, Offshore and Arctic Engineering*, OMAE 2011,Rotterdam, Netherlands.

NVE, Norwegian Water Resources and Energy Directorate. (2005). *Retningslinje for betongdammer*.

Ocean Energy Systems (OES). Ocean Energy Systems: Annual Report. 2015.
Available online: https: //www.ocean-energy-systems.org/library/annual-reports/

Paikowsky, S.G., Player, C. M. & Connors, P. J. (1995). A Dual Interface Apparatus For Testing Unrestricted Friction of Soil Along Solid Surfaces. *ASTM, Geotechnical Testing Journal*, GTJODJ, Vol. 18, No. 2, pp. 168-193.

Patton, F.D., (1966). Multiple modes of shear failure in rock. pp. 509-513.

Pells, P.J.N, Rowe, R.K., Turner, R.M. (1980). An experimental investigation into side shear for socketed piles in sandstone. *In: Proceedings of the International Conference of Structural Foundations on Rock*, Sydney, 1980.

Peterson, M. S., Kulhawy, F. H., Nucci, L. R. & Wasil, B. A. (1976). Stress deformation behavior of soil-concrete interfaces. *Contract report B-49 to Niagara Mohawk Power Corporation*, Syracuse, NY.

Potyondy, J., G. (1961). Skin Friction Between Various Soils And Construction Materials. *Geotechnique*, (11): 339-355.

Puntel, E., Bolzon, G., Saouma, V.E. (2005). An experimental and numerical investigation of concrete dam joints. *In: Proceedings of 11th International Conference on Fracture (IFC)*, Turin, 2005.

Renewable Energy Policy Network for the 21st Century, “Renewables Global status Report 2012”.

Rosenberg, P., Journeaux, N.L. (1976). Friction and end bearing tests on bedrock for high capacity socket design. *Canadian Geotechnical Journal*, 13, 324-333.

Saada, A.S. & Townsend, F.C. (1981). State of the Art: Laboratory strength testing of soils Laboratory shear strength of soil. *ASTM STP 740. R.N. Young & F.C. Townsend, Eds,* ASTM, 1981: 7-77

Sandvik, K., Eie, R. & Advocaat, J.D (2004). Norway Offshore Structures—A new challenge. Acapulco: Aker Kvaerner Engineering & Technology AS, 2004. *XIV National Conference on Structural Engineering*.

Seidel, J.P. & Collingwood, B., (2001). A new socket roughness factor for prediction of rock socket saft resistance. *Canadian Geotechnical Journal*, 38:138-153.

Singh, R.N., Hassani, F.P. & Elkington, PAS. (1983). The application of strength and deformation index testing to the stability assessment of coal measures excavations. *In: Proceedings of 24th US symposium on rock mechanics*, Texas A & M Univ, AEG, 599–609.

Small, A.A., Cook, G.A. & Brown, M.J. (2014). The geotechnical challenges of tidal turbine projects. *Proc. ASME 2014 33rd Int. Conf. on Ocean, Offshore and Arctic Engineering (OMAE2014)* 8-13 June, 2014, San Francisco, USA.

Staheli K., Frost D. & Iscimen M. (2006). Studies of interface friction between jacking pipe materials and frictional soils and the impact on jacking forces. *North American Society for Trenchless Technology*.

Stegman A., de Andres A., Jeffrey H., Johanning L. & Bradley S. (2017). Exploring Marine Energy Potential in the UK Using a Whole Systems Modelling Approach. *12th European Wave and Tidal Energy Conference (EWTEC 2017)* 27th August – 1st September, 2017, Cork, Ireland.

Strabag Offshore Wind GMBH, Sea Turtle Tidal Test Project. http://www.strabagoffshore.com/fileadmin/Bilder/Presse/4S_SOW_SeaTurtle_0609pre.pdf

Tabor D. (1954). Mohs´ Hardness scale – a physical interpretation. *Proc. Phys. Soc*. 67, 249-257.

Tam, C.C.Y., Kwong, A.K.L. & Lee, P.K.K., (2008). Estimation of rock joint shear strength by 3D laser scanning. In: Brown, M.J., Bransby, M.F., Brennan, A.J. & Knappett, J.A. (2008) *Proceedings of the 2nd British Geotechnical Association International Conference on Foundations. ICOF'08*, Dundee, UK, 24-27th June 2008. IHS BRE Press, Bracknell, UK. 2 Volumes, EP95 & 96 of set EP93. ISBN-13: 978-1-84806-044-9.

The Crown Estate (2011). Wave and Tidal Energy in the Pentland Firth and Orkney Waters: How the Projects Could be Built. May 2011.

Tomlinson M.J., (2001). Foundation Design and Constructions. 7th Edition, Pearson Education Limited.

Uesugi, M. & Kishida, H. (1986a). Frictional resistance at yield between dry sand and mild steel. *Soils and Foundations* 26(4), 139-149.

Uesugi, M. & Kishida, H. (1986b). Influential factors of friction between steel and dry sands. *Soils and Foundations* 26(2), 33-46.

Uesugi, M., Kishida, H. & Uchikawa, Y. (1990). Friction between dry sand and concrete under monotonic and repeated loading. *Soils and Foundations* 30(1), 115-128.

USBR 6258: Procedure for Determining the Angle of Basic Fric-tion (Static) Using a Tilting Table Test.

Wei, Z., Xiaolin, C, Chuangbing, Z. & Xinghong, L., (2007). Failure analysis of high-concrete gravity dam based on strength reserve factor method. *Wuham University*, China.

Williams, J.A. (1996). Engineering tribology. New York: Oxford Science Publications.

Whitham, F. (1991). The stratigraphy of the Upper Cretaceous Ferriby, Welton and Burnham formations north of the Humber, north-east England. *Proceedings of the Yorkshire Geological Society* 48(3): 247–254.

Whitham, F. (1993). The stratigraphy of the Upper Cretaceous Flamborough Chalk Formation north of the Humber, north-east England. *Proceedings of the Yorkshire Geological Society* 49(3): 235–258.

Xue F.G., Julian P., Seidelnand, C. & Haberfield M. (2003). Direct Shear Test of Sandstone-Concrete Joints. *Int. J. Geomech.*, 3(1), 21–33. Technical Paper.

Yoshimi, Y. & Kishida, T. (1981). A Ring Torsion Apparatus for Evaluating Friction Between Soil and Metal Surfaces. Geotechnical Testing Journal 4, no. 4: 145-152.

Ziogos, A., Brown, M.J., Ivanovic, A. & Morgan N (2015a). Interface shear characteristics of Scottish rock samples from sites with tidal energy potential. *XVI European Conference on Soil Mechanics and Geotechnical Engineering*. ICE Publishing, London. pp. 1357-1362. DOI:10.1680/ecsmge.60678.

Ziogos, A., Brown, M.J., Ivanovic, A. & Morgan, N. (2015b). Investigation of rock-steel interface testing for gravity foundations for marine energy generators. *3rd International Symposium on Frontiers in Offshore Geotechnics (ISFOG)* (Meyer V (eds)). Taylor & Francis Group, London. pp. 1245-1250.

Ziogos, A., Brown, M.J., Ivanovic, A. & Morgan, N. (2017). Chalk-steel Interface testing for marine energy foundations. *Proc. Inst. of Civil Engineers: Geotechnical Engineering Journal*, Vol 170, GE 3. pp. 285-298. DOI:

10.1680/jgeen.16.00112. ISSN 1353-2618 | E-ISSN 1751-8563. Themed issue.

Ziogos, A., Brown, M.J., Ivanovic, A., & Morgan, N. (2018). Characterising chalk-concrete interfaces for offshore renewable energy foundations. *In J. A. Lawrence, M. Preene, U. L. Lawrence, & R. Buckley (Eds.),* Engineering in Chalk: Proceedings of the Chalk 2018 Conference (pp. 521-527). London: ICE Publishing. https://doi.org/10.1680/eiccf.64072.521.